

STATE OF NEW MEXICO

DEPARTMENT OF ENERGY, MINERALS, AND NATURAL RESOURCES
OIL CONSERVATION COMMISSION

APPLICATION OF THE NEW MEXICO OIL
CONSERVATION DIVISION TO ADOPT 19.15.27 NMAC
AND 19.15.28 NMAC, AND TO AMMEND 19.15.7 NMAC,
19.15.18 NMAC, AND 19.15.19 NMAC; STATEWIDE

CASE NO. 21528

ENVIRONMENTAL DEFENSE FUND'S LIST OF EXHIBITS – VOLUME II

22. Lyon, D. R. et. al, *Concurrent Variation in Oil and Gas Methane Emissions and Oil Price During the COVID-19 Pandemic*, ATMOS. CHEM. PHYS. DISCUSS. (in review) 2020, <https://doi.org/10.5194/acp-2020-1175>
23. Zhou, Xiaochi et al., *Mobile Measurement System for the Rapid and Cost-Effective Surveillance of Methane and Volatile Organic Compound Emissions from Oil and Gas Production Sites*, ENVIRON. SCI. TECHNOL., Dec. 14, 2020, <https://pubs.acs.org/doi/10.1021/acs.est.0c06545>
24. State of New Mexico Environment Department, *Embracing Innovation and Technology, the Environment Department Identifies Potential Emissions Violations* (Jan. 2020), <https://www.env.nm.gov/wp-content/uploads/2020/01/2020-01-14-Methane-Map-Updates-final.pdf>
25. *National Ambient Air Quality Standards*, 80 Fed. Reg. 65292, 65322 (Oct. 26, 2015)
26. New Mexico Environmental Improvement Board, Preamble (July 2020), <https://www.env.nm.gov/new-mexico-methanestrategy/wp-content/uploads/sites/15/2020/07/Draft-Ozone-Precursor-Rule-for-Oil-and-Natural-Gas-Sector-Version-Date-7.20.20.pdf>.
27. EDF analysis of 2017 design values.
28. *2021 Regional Haze Planning*, New Mexico Environment Department (accessed Dec. 15, 2020), <https://www.env.nm.gov/air-quality/reg-haze/>
29. *Waste Prevention, Production Subject to Royalties, and Resource Conservation*, 81 Fed. Reg. 83008, 83069 (Nov. 18, 2016).
30. *Health and Environmental Effects of Particulate Matter (PM)*, EPA (Apr. 13, 2020), <https://www.epa.gov/pm-pollution/health-and-environmental-effects-particulate-matter-pm>
31. *Health and Environmental Effects of Hazardous Air Pollutants*, EPA (Feb. 9, 2017), <https://www.epa.gov/haps/health-and-environmental-effects-hazardous-air-pollutants>
32. Schwartz, Joshua et al., *Black Carbon Emissions from the Bakken Oil and Gas Development Region*, 2, 10 ENVIRON. SCI. TECHNOL. LETT. 281-285 (Sept. 3, 2015), <https://pubs.acs.org/doi/abs/10.1021/acs.estlett.5b00225>
33. CIRES, *Emissions of Black Carbon from Flaring in the Bakken Oil and Gas Fields* (Sept. 9, 2015), <https://cires.colorado.edu/news/emissions-black-carbon-flaring-bakken-oil-and-gas-fields>

34. Ravikumar, Arvind P. et al., *Single-Blind Intercomparison of Methane Detection Technologies – Results from the Stanford/EDF Mobile Monitoring Challenge*, 7 ELEM. SCI. ANTH. 37, 2019, <https://online.ucpress.edu/elementa/article/doi/10.1525/elementa.373/112505>
35. Kemp, Chandler E. et al., *Comparing Natural Gas Leakage Detection Technologies Using an Open-Source “Virtual Gas Field” Simulator*, 50 ENVTL. SCI. TECHNOL. 4546-53, Mar. 23, 2016, <https://pubs.acs.org/doi/abs/10.1021/acs.est.5b06068>
36. EDF, *With Initial Data Showing Permian Flaring on the Rise Again, New Survey Finds Malfunctioning or Unlit Venting Unburned Methane into the Air 1 in 10 Flares* (July 22, 2020), <https://www.edf.org/media/initial-data-showing-permian-flaring-rise-again-new-survey-finds-1-10-flares-malfunctioning>
37. Chamberlain, Kendra, *NMED Discovers More Potential Methane Emissions Violations*, NM POLITICAL REPORT (Jan. 16, 2020), <https://nmpoliticalreport.com/2020/01/16/nmed-discovers-more-potential-methaneemission-violations/>.
38. Zhang, Yuzhong et al., *Quantifying Methane Emissions from the Largest Oil-Producing Basin in the United States from Space*, 6 SCI. ADVANCES, Apr. 22, 2020, <https://advances.sciencemag.org/content/6/17/eaaz5120>.
39. 5 C.C.R. 1001-9, Sections VI.D & XVII.C.1 (2020)
40. COGCC 900 Series Rules (2020)
41. Cardoso-Saldana, Felipe & Allen, David T., *Projecting the Temporal Evolution of Methane Emissions from Oil and Gas Production Sites*, 54, 22 ENVIRON. SCI. TECHNOL. 14172-81, Oct. 27, 2020, <https://pubs.acs.org/doi/10.1021/acs.est.0c03049>
42. *Permian Methane Analysis Project*, EDF, <https://www.permianmap.org/>
43. Resume of Tom Alexander

Exhibit 22



Concurrent variation in oil and gas methane emissions and oil price during the COVID-19 pandemic

David R. Lyon^{1*}, Benjamin Hmiel¹, Ritesh Gautam¹, Mark Omara¹, Kate Roberts¹, Zachary R. Barkley², Kenneth J. Davis², Natasha L. Miles², Vanessa C. Monteiro², Scott J. Richardson², Stephen Conley³,
5 Mackenzie L. Smith³, Daniel J. Jacob⁴, Lu Shen⁴, Daniel J. Varon⁴, Aijun Deng⁵, Xander Rudelis^{6,†},
Nikhil Sharma⁶, Kyle T. Story⁶, Adam R. Brandt⁷, Mary Kang⁸, Eric A. Kort⁹, Anthony J. Marchese¹⁰,
Steven P. Hamburg¹

¹Environmental Defense Fund, 301 Congress Ave., Suite 1300, Austin, TX, USA.

²The Pennsylvania State University, University Park, PA, USA.

10 ³Scientific Aviation, Boulder, CO, USA.

⁴Harvard University, Cambridge, MA, USA.

⁵Utopus Insights, Inc., Valhalla, NY, USA.

⁶Descartes Labs, Santa Fe, NM, USA.

⁷Stanford University, Palo Alto, CA, USA.

15 ⁸McGill University, Montreal, QB, Canada.

⁹University of Michigan, Ann Arbor, MI, USA.

¹⁰Colorado State University, Fort Collins, CO, USA.

[†] now at Google LLC, Mountain View, CA, USA.

Correspondence to: David R. Lyon (dlyon@edf.org)

20 **Abstract.** Methane emissions associated with the production, transport, and use of oil and natural gas increase the climatic
impacts of energy use; however, little is known about how emissions vary temporally and with commodity prices. We present
airborne and ground-based data, supported by satellite observations, to measure weekly to monthly changes in total methane
emissions in the United States' Permian Basin during a period of volatile oil prices associated with the COVID-19 pandemic.
As oil prices declined from ~\$60 to \$20 per barrel, emissions changed concurrently from 3.4% to 1.5% of gas production; as
25 prices partially recovered, emissions increased back to near initial values. Concurrently, total oil and natural gas production
only declined by a maximum of ~10% from the peak values seen in the months prior to the crash. Activity data indicate that a
rapid decline in well development and subsequent effects on associated gas flaring and midstream infrastructure throughput
are the likely drivers of temporary emission reductions. Our results, along with past satellite observations, suggest that under
more typical price conditions, the Permian Basin is in a state of overcapacity in which rapidly growing natural gas production
30 exceeds midstream capacity and leads to high methane emissions.



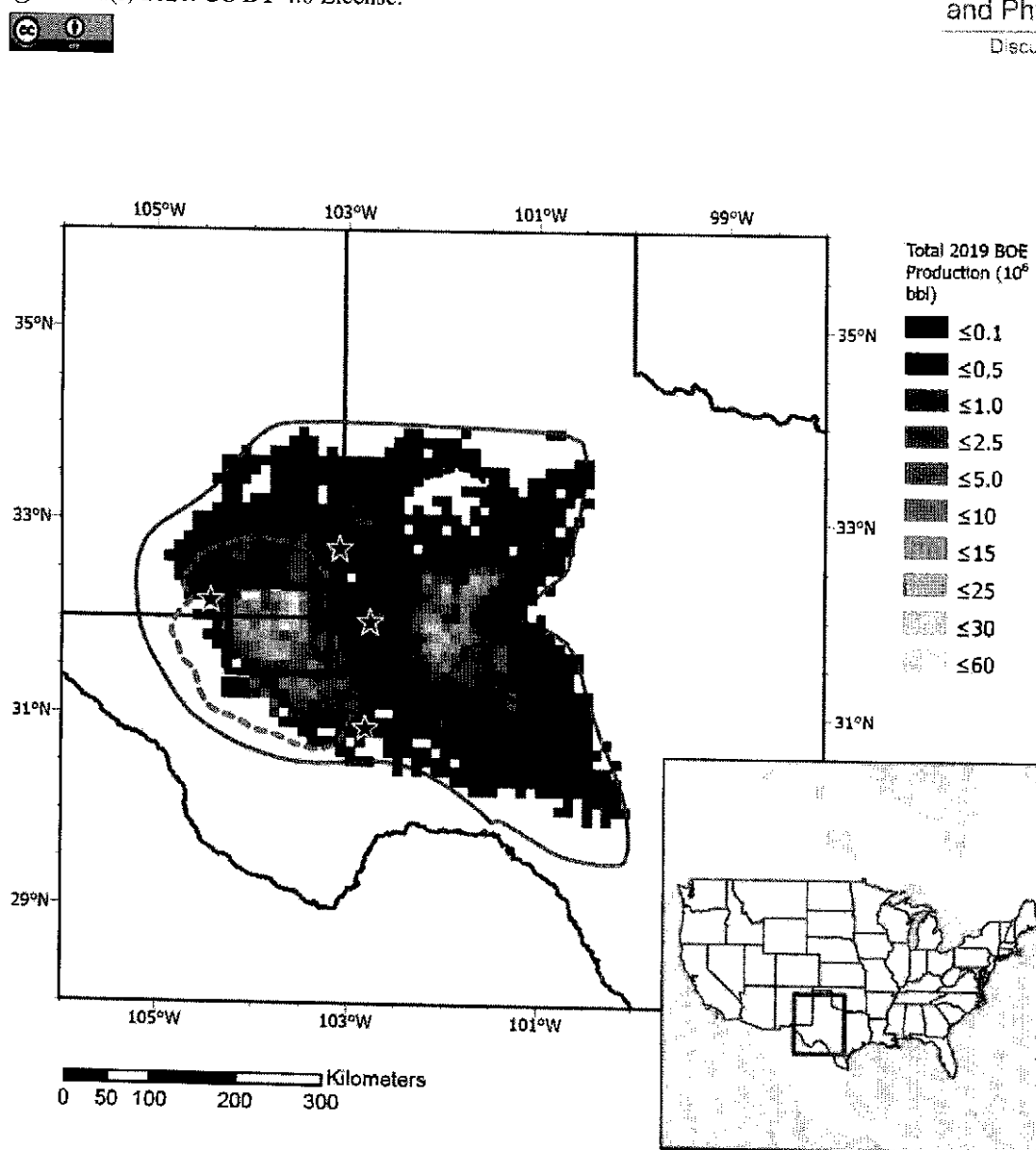
1 Introduction

Accurate quantification of methane (CH_4) emissions from the oil and natural gas (O&G) supply chain is critical for determining the climatic impact of O&G production and use (Alvarez et al., 2012). Alvarez et al. (2018) synthesized over 400 site- and basin-level measurements to estimate United States O&G supply chain emissions at 13 Tg CH_4 in 2015, equivalent to 2.3% of the nation's natural gas production and over 80% higher than the U.S. Environmental Protection Agency (USEPA)'s bottom-up estimate (USEPA, 2020a). There is growing evidence of systematic underestimation of O&G methane emissions when bottom-up methods such as emission factors and engineering equations are used rather than top-down, atmospheric measurements (Allen, 2014; Brandt et al., 2014; Zavala-Araiza et al., 2017). The Permian Basin (Fig. 1) is the largest oil producing basin in the U.S. and rivals the Ghawar Field in Saudi Arabia for the global record (Jacobs, 2019). Although the first oil well was drilled in the Permian Basin nearly 100 years ago, the basin has experienced rapid growth in recent years as directional drilling and hydraulic fracturing allowed production from unconventional reservoirs (Enverus, 2020). In 2019, the Permian Basin had ~600 new wells drilled per month and produced an average of 4.3 million barrels (bbl) oil and 15 billion cubic feet (Bcf) natural gas per day, more than double the 2016 average values (Enverus, 2020). The Permian Basin's limited midstream gathering and processing (G&P) infrastructure for delivering natural gas to market results in high rates of associated gas flaring relative to other U.S. basins. In 2019, average daily flared gas volumes were 0.8 Bcf, 5% of the basin's natural gas production (Appendix A). There is limited methane emissions data from the Permian beyond two recent studies (Zhang et al., 2020; Robertson et al., 2020). Zhang et al. (2020) used satellite observations from May 2018 – March 2019 in an atmospheric inversion to estimate total O&G related emissions in the Permian Basin of 2.7 Tg CH_4 annually, or 3.7% of regional gas production. Robertson et al. (2020) found higher well pad CH_4 emission rates in the Permian Basin compared to most other U.S. basins based on over 70 site-level measurements made in 2018. Alvarez et al. (2018), which pre-dates these studies, had assumed other U.S. basins were representative of the Permian; updating their estimate with the Permian Basin loss rate from Zhang et al. (2020) results in a roughly 10% increase in the U.S. supply chain estimate to 14.2 Tg CH_4 , or 2.5% of total gas production.

In January 2020, oil prices declined as the COVID-19 pandemic triggered a global slowdown in O&G consumption; in March, there was a rapid price drop when the oil oversupply was exacerbated by both the Organization of the Petroleum Exporting Countries (OPEC) failing to reach a deal to cut production and global oil storage capacity reaching its limit (Reed and Krauss, 2020). Spot prices for the U.S. oil benchmark, known as West Texas Intermediate-Cushing (WTI-Cushing), varied dramatically during this period; price per barrel was relatively stable at \$50–60 (USD) for most of 2019, declined to \$20 by late April 2020, briefly dropped below zero on April 20, then recovered to \$40 by early July (USEIA, 2020b). Natural gas spot prices (Henry Hub) were less volatile during this period (\$1.50–2.00 per million British Thermal Units), continuing a gradual downward trend since late 2018 (USEIA, 2020a). Lower commodity prices reduce investment in new well and infrastructure development; in the Permian Basin, the number of active drilling rigs, which had averaged over 400 from April 2019 to March 2020, dropped to approximately 300, 180, and 135 in April, May, and June 2020, respectively (Baker-Hughes, 2020) (Fig. 2).



We hypothesize that the rapid drop in oil price would be associated with a concomitant reduction in methane emissions due to lower rates of well development and a subsequent decline in O&G production. The postulated causal mechanism for this relationship is the effect of natural gas production from new wells on midstream infrastructure throughput. During periods of higher commodity prices, the rapid growth in natural gas production likely exceeds the capacity of the pipelines, compressor stations, and processing plants that deliver and process gas to market, leading to associated gas flaring and anomalous conditions that increase emissions. Such trends were observed in an earlier drilling slowdown in the Bakken, another U.S. unconventional oil formation (Enverus, 2020) (Fig. F1). However, this effect might have been countered in the Permian if lower profit margins led operators to allocate fewer resources to infrastructure maintenance and emissions mitigation, or similarly, restrictions due to COVID-19 reduced the number of field staff performing tasks such as leak detection and repair (LDAR) (Gould et al., 2020).



75

Figure 1. Regional map with outlines of the Permian Basin (orange), Delaware and Midland sub-basins (dashed green and purple) and the 100 km x 100 km study area (Black). Locations of the methane measurement tower sites are shown with red stars. A heatmap displays combined gas and oil production from 2019 expressed in barrels-of-oil equivalents (BOE) and gridded to $0.1^\circ \times 0.1^\circ$ resolution (Enverus, 2020).

80

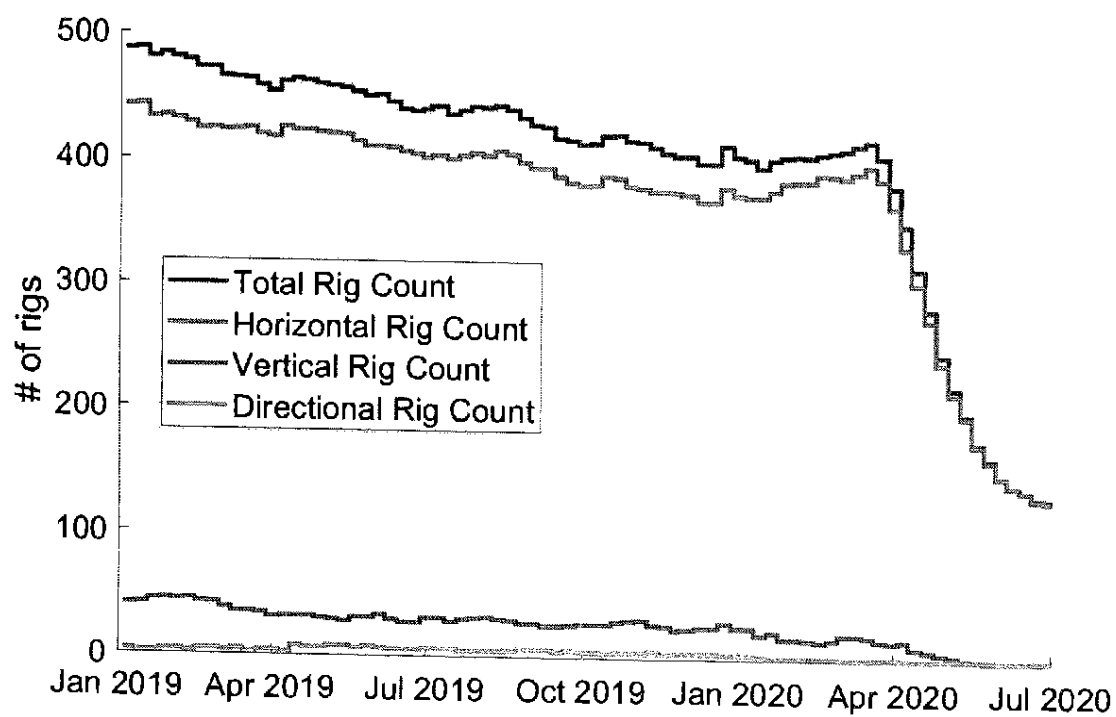


Figure 2. Weekly count of active drilling rigs by type in the Permian Basin between January 2019 and July 2020



2 Study Area and Methods

2.1 Study Area

In January 2020, we began quantifying O&G methane emissions at varying spatiotemporal scales within the Permian Basin with a concentrated effort within a 100 km x100 km area of the Delaware sub-basin along the Texas/New Mexico border (Fig. 1). The 10,000 km² study area includes ~11,000 active wells and accounts for 33% and 43% of the Permian Basin's oil and natural gas production in 2019, respectively (Enverus, 2020). The study area has a high density of midstream O&G infrastructure including 125 gathering and transmission compressor stations, 44 processing plants, and ~32,000 kilometers of gathering pipeline (Enverus, 2020). Based on spatially allocated USEPA inventory data, O&G sources accounted for >90% of methane emissions in the study area in 2012; other sources, dominated by agriculture and waste, were responsible for ~0.5 Mg CH₄ hr⁻¹ (Maasakkers et al., 2016). Since the non-O&G sources account for only a small fraction of total emissions and there have been no major changes in these activities over the past few years, we have assumed all study area emissions are attributable to O&G sources beyond the 0.5 Mg CH₄ hr⁻¹.

2.2 Methods

Between January and August 2020, we used two inversion approaches to quantify total methane emission flux from the study area at a weekly to monthly frequency. The first approach used aircraft-based instruments to measure atmospheric boundary layer (ABL) methane concentration ([CH₄]) along the study area perimeter during six daytime flights (January 22, March 9, March 25, May 4, May 21, and July 13; Sect. 2.22). The second approach continuously quantified [CH₄] from March through August 2020 using sensors installed at three tall towers and one mountaintop station located around the perimeter of the study area ((Richardson et al., 2017); Sect. 2.21). Both approaches estimated study area methane flux on a daily basis by optimizing a prior emissions inventory to minimize model-data differences between observed and simulated regional atmospheric [CH₄] ((Barkley et al., 2017); Sects. 2.21 and 2.23).

We also evaluated satellite-based remote sensing observations of column methane enhancement (ΔXCH_4) for evidence of basin-wide trends (Sect. 2.14). To provide insights about the contribution of natural gas flares to methane emissions, we qualitatively assessed over 300 flares across the basin in February, March, and June 2020 using helicopter-based infrared optical gas imaging (OGI) to visually detect combustion issues ((Lyon et al., 2016); Appendix B). We estimated flare-related methane emissions by applying combustion efficiency assumptions based on survey results to flared gas volume estimates based on satellite observations of flare radiant heat ((Elvidge et al., 2016); Appendix A).

2.2.1 Regional atmospheric [CH₄] reanalysis

An atmospheric reanalysis similar to the system used in previous studies (Barkley et al., 2019; Barkley et al., 2017) was used to create simulated regional atmospheric [CH₄] estimates. The modeling system used Weather Research and Forecasting (WRF) model coupled with Chemistry v3.6 (Skamarock et al., 2008) configured to simulate two domains, an outer 2600 km



x 2100 km domain with 9 km x 9 km horizontal resolution and 50 vertical levels, with about 30 of these levels in the lowest 3 km above ground level, and an inner 830 km x 830 km domain with 3 km x 3 km horizontal resolution and the same vertical layers. The outer domain is nudged to ERA5 wind, temperature and water vapor reanalyses, and the inner domain is nudged to regional observations including ~50 National Weather Service / World Meteorological Organization surface stations, five National Weather Service rawinsonde site soundings launched at 0 and 12 UT, and the meteorological measurements from commercial aircraft-ACARS. Our choice of parameterization schemes within WRF-Chem matches previous studies (Barkley et al., 2019; Barkley et al., 2017).

Only atmospheric $[\text{CH}_4]$ from emissions within the model domain are simulated, using techniques demonstrated previously (Barkley et al., 2019; Barkley et al., 2017). Preliminary estimates of surface fluxes of $[\text{CH}_4]$ within the domain are taken from the EPA 2012 gridded inventory (Maasakkers et al., 2016), save for the Permian Basin where an updated, production-based inventory is used. This updated inventory is described in detail by Zhang et al. (2020). Briefly, production site CH_4 emission factors were developed using methods in Zavala-Araiza et al. (2015) and based on measurements by Robertson et al. (2020), which accounted for complexity of well site infrastructure and their related CH_4 emissions. Total basin-wide CH_4 emissions were estimated using activity (Enverus, 2020) and disaggregated to individual sites based on their gas production. Additional facility-level CH_4 emissions for gathering and boosting stations, gathering pipelines and processing plants were estimated based on activity data (Enverus, 2020) and CH_4 emission factors from Marchese et al. (2015) and the EPA GHGI (USEPA, 2020a). For the transmission and storage stations, CH_4 emissions were taken from Maasakkers et al. (2016). For the Delaware basin, total CH_4 emissions were estimated at 1.2, 0.11, 0.04, and 0.01 Tg for production sites, gathering and boosting stations, gas processing plants and gas transmission and distribution stations, respectively. These O&G CH_4 emissions were then spatially allocated to a $0.1^\circ \times 0.1^\circ$ grid over the entire basin. This update within the Delaware Basin is important to account for the rapid development within the basin since 2012. Different $[\text{CH}_4]$ sources (e.g. oil and gas production, landfills, agriculture) and sources inside and outside the study domain are tagged as independent tracers in the model. Oil and gas emissions outside of the study domain are multiplied by 1.6 to match estimates from Alvarez et al. (2018) and to better account for development in the areas surrounding the study domain. This atmospheric reanalysis system enables us to create a first estimate of atmospheric $[\text{CH}_4]$ consistent with the regional meteorology and the preliminary estimate of sources within the outer model domain.

Note that the emissions magnitude from the preliminary $[\text{CH}_4]$ emissions estimates are not highly important since the emissions estimate is not a Bayesian inversion that assigns an uncertainty estimate to this preliminary estimate. The spatial pattern of emissions, however, including the relative change in these spatial patterns, is important for the estimate of fluxes. Our assumption that emissions are proportional to gas production should provide a reasonable estimate of the spatial pattern of emissions corresponding to well locations.



2.2.2 Aircraft based methane emission estimates

The total CH₄ emissions from the study area in the Permian Basin study area were determined using airborne data in conjunction with transport modeling. The airborne platform has been deployed and described previously (Conley et al., 2017; Conley et al., 2016; Karion et al., 2015; Smith et al., 2017). In brief, a single-engine Mooney aircraft is outfitted with a Picarro CRDS instrument (G2210-m) to measure in-situ atmospheric CH₄, CO₂, H₂O mole fractions, a differential GPS and aircraft data computer to enable computation of horizontal wind speeds and directions, and a Vaisala probe to measure ambient temperature and relative humidity.

On each flight day, two laps consisting of a box enclosing the 100 km x 100 km study area were flown at 1100 ± 100 ft above ground level (agl), with one complete lap taking ~ 2 h to complete. Two to three vertical profiles were also flown by the aircraft as pairs of ascents/descents between the lowest safe flight altitude (typically 200 to 500 ft agl) and the flight altitude at which significant changes are observed in measured species concentrations (e.g., CH₄, water vapor, relative humidity and potential temperature)- typically 3,000 to 10,000 ft agl. Plots of agl altitude versus these species are used to assess the mixing height of surface emissions. Both CH₄ concentrations along the flight path and the mixing height determined from the airborne vertical profiles are used in transport modeling to determine emissions from the entire study area.

[CH₄] emissions are computed from each complete circuit of the study area by the aircraft. This is done by comparing the observed and simulated [CH₄] enhancement, the increase in [CH₄] downwind of the study area relative to a background value, and adjusting emissions within the study area to minimize the absolute error between the simulated and observed ABL [CH₄]. The 10th percentile of [CH₄] observations in the circuit determines the background. This mole fraction value is subtracted from the observed [CH₄] observations, resulting in an estimate of [CH₄] enhancements. These observed enhancements are then compared to simulated [CH₄] enhancements by matching observation and model at the nearest gridpoints in space and time. Simulated enhancements are split into two categories: study domain enhancements and enhancements originating from outside the study domain. Enhancements associated with sources outside the study domain are subtracted from the observed [CH₄] enhancements, resulting in a set of observations whose enhancements can be directly attributed to emissions within the study domain. The simulated study domain enhancements are then compared to the observed study domain enhancement, and a scalar multiplier is applied to the simulated enhancements to minimize the absolute error between the two datasets. Because the emissions scale linearly with the simulated enhancements, this scalar multiplier, applied to the preliminary emissions estimate within the study area, provides a solution to the emissions within the study domain (Barkley et al., 2017). The solution for each circuit is merged into a single daily estimate.

To test the uncertainty of the emission rate solution for each flight day, a 1000-iteration Monte Carlo uncertainty assessment was performed, adjusting various parameters to test how they impacted the solution. Through the iterations we examine the impact of various possible sources of error, including uncertainty in the background, uncertainty in the assumed influence from sources outside the domain, and uncertainty in the atmospheric transport. For uncertainty in the background, we select a random



180 percentile between 5 and 15 to use as the methane background in a flight lap. For uncertainty in sources outside of the domain that are subtracted from the observations, we multiply the “other” enhancement tracer by a random factor between 0.5 and 1.5 to account for the possibility that regional emissions may be incorrect. For uncertainty in the transport, the time of the observations are adjusted by ± 30 minutes, creating perturbations to the model output timeframe used to compare to the observations. From the 1000 iterations, the 2.5th and 97.5th percentile of solutions are chosen to represent the 95% confidence
 185 interval.

2.2.3 Tower-based methane emissions estimates

Atmospheric mole fraction measurements of CH_4 and CO_2 were collected at five locations in the Permian Basin beginning 1 March 2020, using methods similar to those described in Richardson et al. (2017). A map of the measurement locations, along with oil and gas facilities in the Permian Basin, is shown in Fig. 1. Note that only four of the five planned measurement sites
 190 are used in this analysis and shown on Fig. 1 due to instrument malfunctions at the northernmost site. Of these measurement locations, three were on towers at measurement heights of 91 – 134 m agl and the westernmost site was at a mountaintop station on a rooftop 4 m agl. The measurements were made with wavelength-scanned cavity ring down spectroscopic instruments (Picarro, Inc., models G2301, G2401, G2204, and G2132-i). The air samples were dried using Nafion dryers (PermaPure, Inc.) in reflux mode, with an internal water vapor correction applied for the effects of the remaining water vapor
 195 ($< 1\%$). The instruments were calibrated in the laboratory prior to deployment and using quasi-daily field tanks traceable to the WMO X2004A scale (Dlugokencky et al., 2005; NOAA, 2015). The CH_4 measurement uncertainty (including instrument noise, uncertainty due to water vapor calibration and tank assignment uncertainty) for the four tower locations was 0.6 ppb (Carlsbad), 0.6 ppb (Fort Stockton), 3.4 ppb (Hobbs), and 5.4 ppb (Notress), with the differences being attributable to different instrument type and short Nafion dryer in the case of Hobbs, and laser aging (Notrees).

200 $[\text{CH}_4]$ emissions in the study domain were calculated for each day of tower observations using a similar technique as used with the aircraft observations. Daily afternoon $[\text{CH}_4]$ at each tower site averaged from 16Z (11 LST) through 22Z (17 LST) was computed from both the observations and the simulation. A background $[\text{CH}_4]$ value (both for the observations and the model) is selected based on the lowest measurement from the available tower sites. This background is subtracted from all tower sites to create an observed CH_4 enhancement. Simulated enhancements from sources outside of the domain are subtracted from the
 205 observed enhancements to produce an observed $[\text{CH}_4]$ enhancement associated with sources inside the study domain. A scalar multiplier is then applied to minimize the absolute error between the observed and modelled enhancements, and a daily emission rate is solved for in the study domain (Fig. 3).

Figure 4 presents the daily difference between the highest and lowest observed CH_4 measurement across the tower network. Although though the overall magnitude of the study area plume observed at the tower network can be affected by various
 210 meteorological factors (e.g. wind speed, direction, boundary layer height) large changes in the typical size of the observed plumes can be indicative of sudden shift in behavior of local emissions. From the tower network, we frequently observe large



enhancements >200 ppb in March and mid-April, after which point the enhancement rarely increases above 150 ppb for the remainder of the summer months. It should be noted that a slight decrease in the size of the enhancements would be expected during this period due to increased vertical mixing in a seasonally growing boundary layer; however, modelled results from this timespan exhibit a much smaller magnitude of change. Therefore, the dramatic rechange in behavior CH_4 enhancements coincident with the timing of the price crash is likely due to a change in the emissions rather than a change in the meteorology.

Unlike the aircraft mass balance observations, which are collected on days where meteorological conditions are ideal for measuring emissions from the study domain, the tower dataset is continuous and many days may not be suitable for calculating an emission rate from the study domain. The most useful tower observations for solving for emissions within the study domain are those whose enhancements are influenced primarily by sources within the study domain and contain minimal enhancements from sources outside of the domain. We select for these conditions by retaining days when >50% of the simulated downwind afternoon tower enhancements come from sources within the study domain. This filtering removes 85 of 184 available days, most of which have easterly winds and contain air masses heavily influenced by oil and gas basins in central and eastern Texas. For the remaining 99 days, we remove 5 days whose solutions are more than three median absolute deviations away from the median solution, presumably caused by issues in the model transport. In total, 94 days are used to calculate emissions and trends in the tower dataset between March 1st, 2020 and August 30th, 2020.

Figure 3 presents a timeseries of CH_4 emissions within the 100 x 100 km study area between March 1st, 2020 and June 30th, 2020. This timespan was chosen to focus discussion on the correlations between emissions and activity in the basin during a period of volatile oil prices; accurate activity data is only available through the month of June at the time of manuscript submission (Appendix E). Figure 4 extends the observation of the tower and aerial measurements from Fig. 3 through August 30th 2020 while also presenting monthly mean estimates and 95% CI of the combined results from aircraft and tower-based estimates (Table 1). The 95% CI ranges are derived from twice the standard error of all accepted estimates in each month. Extending the dataset reveals that the mean emissions decreased briefly in July before increasing in August to a similar level as observed in March 2020, albeit with larger uncertainty. Without production or other activity data to relate the observations, we do not have a mechanistic understanding of the reason for the decreased emissions in July, although we note the significant overlap in confidence intervals does not allow for statistically independent estimates between the months of June, July, and August.

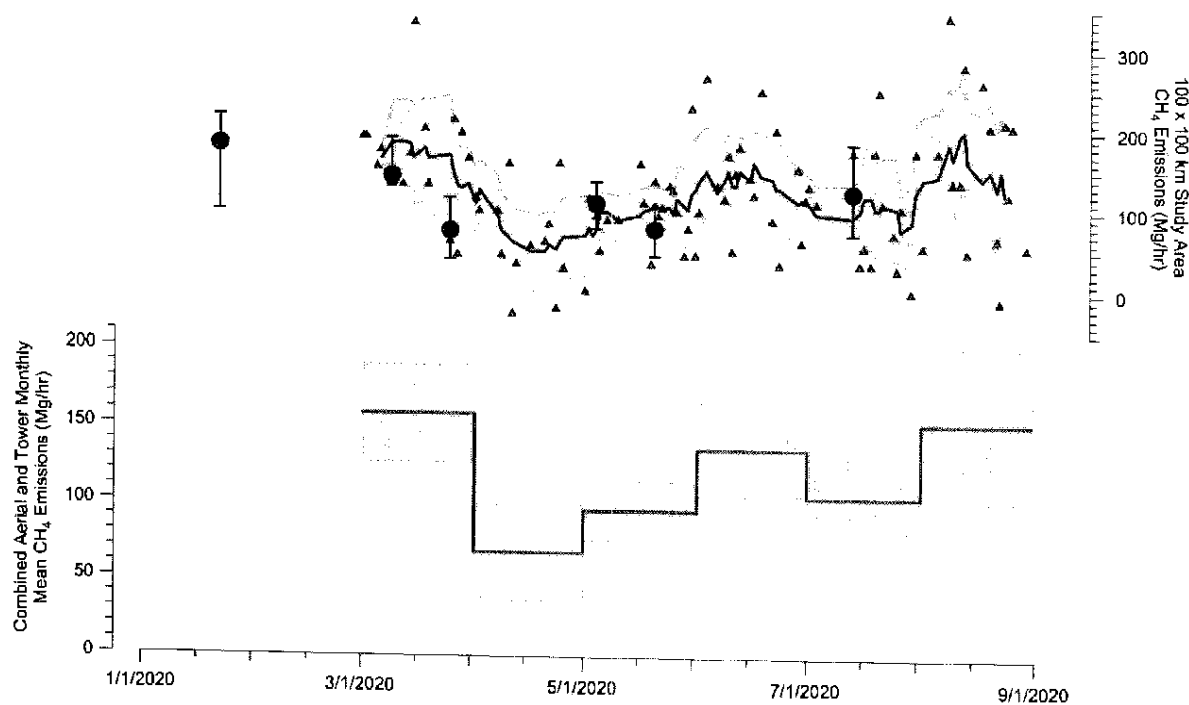


Figure 3. Tower and aerial emission estimates from the 100 x 100 km study area extended for the full available record through August 2020. Individual daily accepted estimates from the tower observations are shown in green triangles while red points represent the aerial estimate and 95% CI and Blue line and shading represent the 7-datapoint moving average of the tower estimates and 95% CI expressed as twice the 7-datapoint moving standard error. Brown line and shading on the lower plot represents the monthly mean estimate and 95% CI from the combination of aerial and tower-based methods.



245

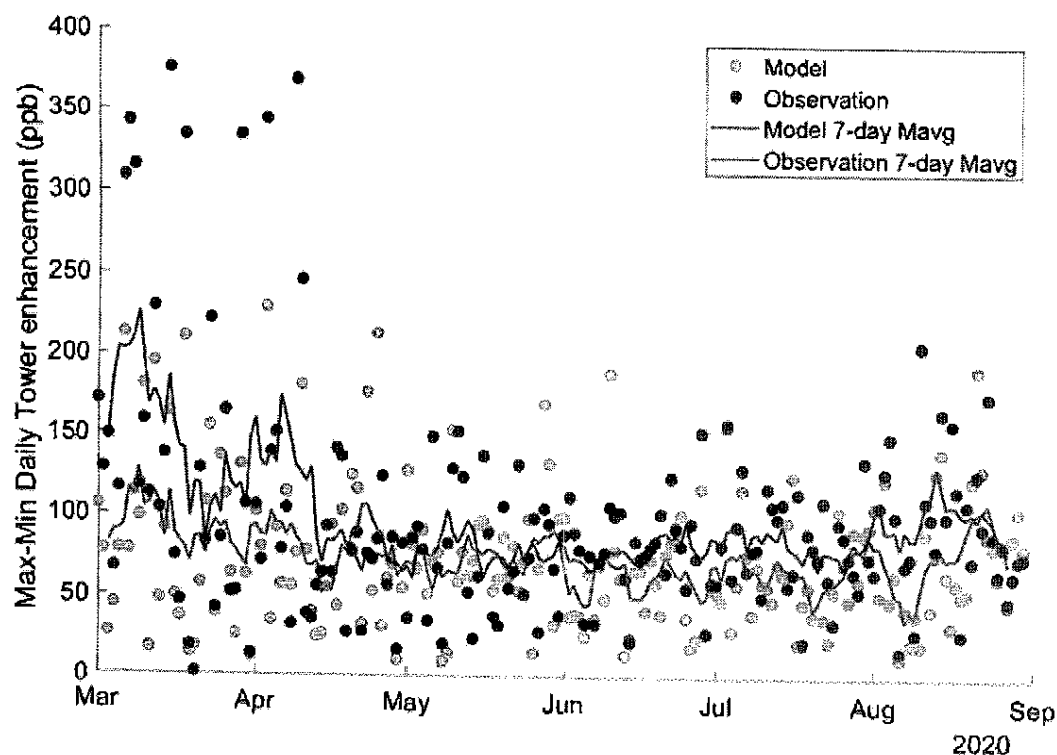


Figure 4. Comparison between modeled and observed differences in the maximum and minimum daily CH_4 enhancement across the tower network. Also shown are the 7-day moving averages of each trend.

250

255



Table 1. Numerical estimates of CH₄ flux from the 100 x 100 km study area derived from the combination of tower and aerial measurements across several temporal ranges.

Time Range	Mean Emissions (Mg/hr)	Standard Deviation (Mg/Hr)	Number of accepted daily tower and aerial measurements	Standard Error (Mg/hr)	95% CI Emission estimate
March 2020	157	66	17	16	126 - 189
April 2020	67	58	13	16	35 - 99
May 2020	95	47	22	10	75 - 115
June 2020	135	64	17	16	105 - 166
July 2020	104	69	15	18	69 - 139
August 2020	152	100	15	26	101 - 202
'Pre-Crash Period' Jan 22 - Mar 19 2020	176	59	12	17	142 - 209
'Emissions Minima' Apr 7 - May 1 2020	55	61	12	17	21 - 89



2.2.4 TROPOMI-derived column-averaged methane mixing ratios

We use column-averaged dry air methane mixing ratios (XCH_4) from the TROPOMI instrument from January to June 2020. TROPOMI was launched in October 2017 onboard the polar sun-synchronous Sentinel-5 Precursor satellite with an ~13:30 local overpass time. It provides daily global coverage with 7 km x 7 km pixel resolution at nadir (Hu et al., 2018); the pixel resolution has changed to ~7 km x 5.5 km at nadir since August 2019. The XCH_4 retrieval uses sunlight backscattered by the Earth's surface and atmosphere in the shortwave infrared (SWIR) spectral range and has near-unit sensitivity down to the surface (Hasekamp et al., 2019). Here we consider only higher-quality XCH_4 measurements (quality assurance value > 0.5).

Figures 5a and 5b show mean methane column enhancements over the Permian basin, observed by TROPOMI in (a) January-February 2020 and (b) April-May 2020. We calculate the daily methane enhancements over the Permian basin from topography-corrected XCH_4 , relative to a regional background column defined by the 10th percentile of XCH_4 across the full Permian domain (29-34°N, 100-106°W). The topography correction is based on a linear regression of XCH_4 against surface altitude (similar to the methodology presented in (Kort et al., 2014; Zhang et al., 2020), performed across the continental United States (25-48°N, 66-125°W). Enhancements over the Permian basin appear to be lower in April-May compared to January-February, as indicated by an ~18% reduction in the regional mean between those two periods. This reduction may be due in part to lower spatial coverage after February 2020, likely caused by the introduction in March of a different cloud mask product in the TROPOMI retrieval algorithm (Siddans, 2020). Considering TROPOMI retrievals with quality assurance values of 0.5 or greater, we obtain roughly 6,000-32,000 enhancement measurements per month from January to June 2020 over the full Permian Basin (Fig. 5c). The limited number of satellite observations over our 100 km x 100 km study area for tower and aircraft measurements (Fig. 3) precludes direct comparison with the suborbital measurements, and therefore we provide here an analysis of TROPOMI methane enhancement over the broader Permian Basin. Coverage is particularly sparse in March and June, so we neglect those two months in the TROPOMI analysis presented here.

Figure 5d shows frequency distributions of methane column enhancements observed by TROPOMI in January, February, April, and May 2020. For these monthly curves we restrict our attention to a smaller Permian domain that closely bounds the methane hotspots seen over the Delaware and Midland sub-basins (dashed lines in Figs. 5a,b; 31-34°N, 101.4-105.6°W). Roughly 5,000-14,000 TROPOMI observations are available per month across this domain, neglecting March and June (Fig. 5c). To mitigate the impact of reduced spatial coverage on our change analysis after February, we manually discard observations from days with little to no coverage of the Delaware and/or Midland sub-basins. Data from 20-40% of observation days in January, February, April, and May (depending on the month) are discarded in this way, but the total number of observations is reduced by only 5%. Permian basin methane enhancements as observed by TROPOMI appear to decrease in early 2020, reaching a minimum in April before beginning to rise again in May.

Repeating our analysis with the background defined at the 25th percentile level (rather than the 10th), we find that these trends are insensitive to the percentile value used. Furthermore, the trends are not explained by seasonal changes in wind speed across



the Permian. Higher winds could lead to lower enhancements, but data from the NASA GEOS-FP meteorological reanalysis
295 product indicate that the daily wind speed averaged over the full Permian basin domain, in the lowest 3 km of the atmosphere,
during the six hours closest to TROPOMI observation time (15:00-21:00 UTC) decreased from a mean of 7.02 m/s in January-
February to 5.48 m/s in April-May.

The trends we identify in TROPOMI methane enhancement analysis across the Permian Basin are broadly consistent with our
findings from tower and aircraft observations of reduced emissions particularly during April in our campaign domain of the
300 Delaware sub-basin, but large uncertainties remain due to the different spatial domains and the reduced satellite coverage after
February 2020. More data and/or more advanced analysis using inverse modelling techniques may be needed to reliably
characterize Permian basin methane emission trends using TROPOMI satellite observations.

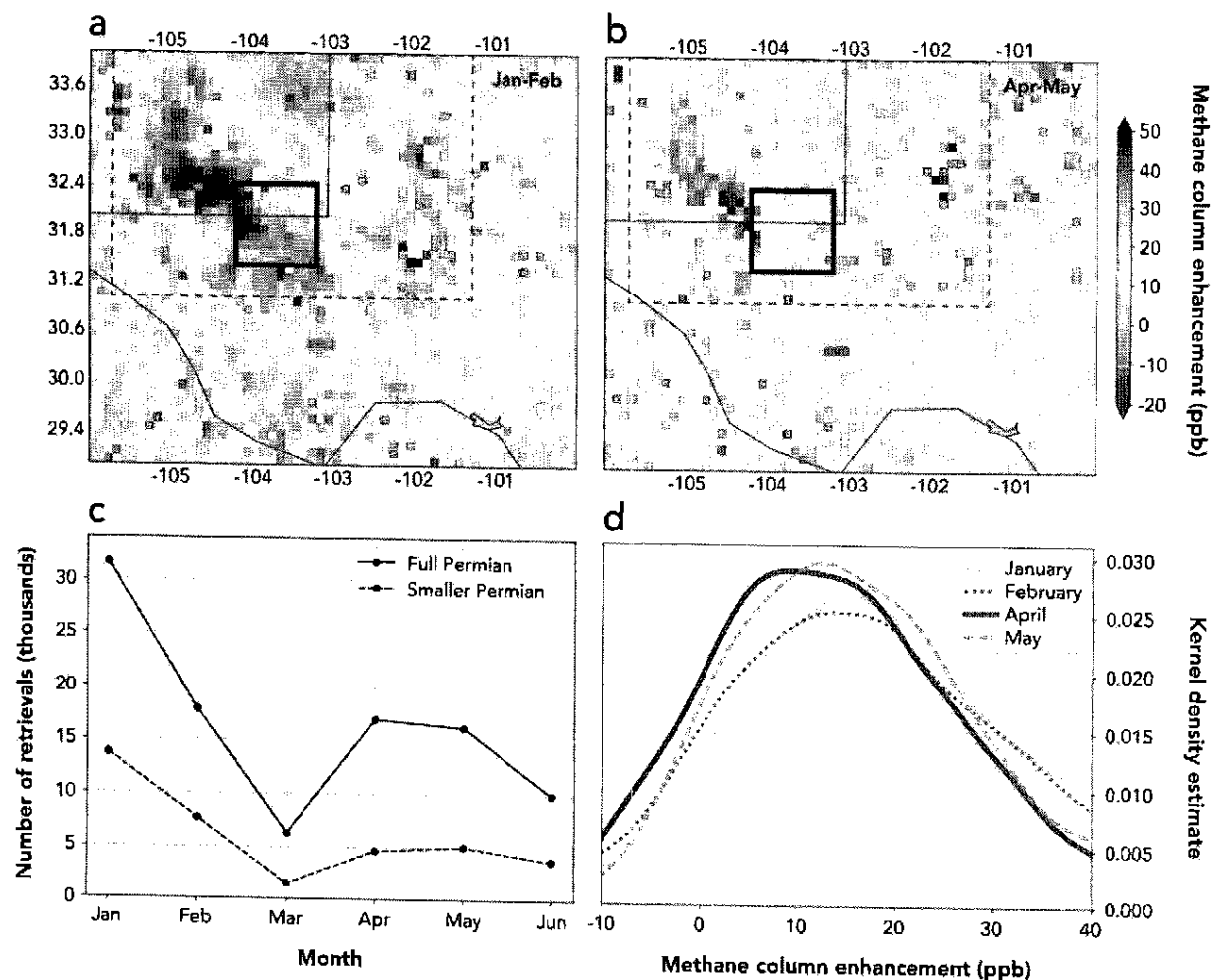


Figure 5. TROPOMI observations of topography-corrected methane column enhancements over the Permian basin, from January to June 2020. a-b: Mean methane column enhancements (ppb) over the Permian basin for the January-February and April-May 2020 time periods, gridded to $0.1^\circ \times 0.1^\circ$ resolution. The thin solid lines indicate state and national borders; the thick solid lines describe the $100 \text{ km} \times 100 \text{ km}$ tower and aircraft study region; and the dotted lines trace a smaller Permian domain that closely bounds the methane hotspots seen over the Delaware and Midland sub-basins. c: Number of TROPOMI column retrievals over the full Permian basin domain ($29\text{--}34^\circ\text{N}$, $100\text{--}106^\circ\text{W}$) and over the smaller Permian basin domain ($31\text{--}34^\circ\text{N}$, $101.4\text{--}105.6^\circ\text{W}$; dashed lines in panels a, b), by month in 2020. d: Frequency distribution plots of methane column enhancements over the smaller Permian domain, by month, after removal of days without coverage of the Delaware and/or Midland sub-basins (see text). The gray vertical line indicates the distribution maximum for January.

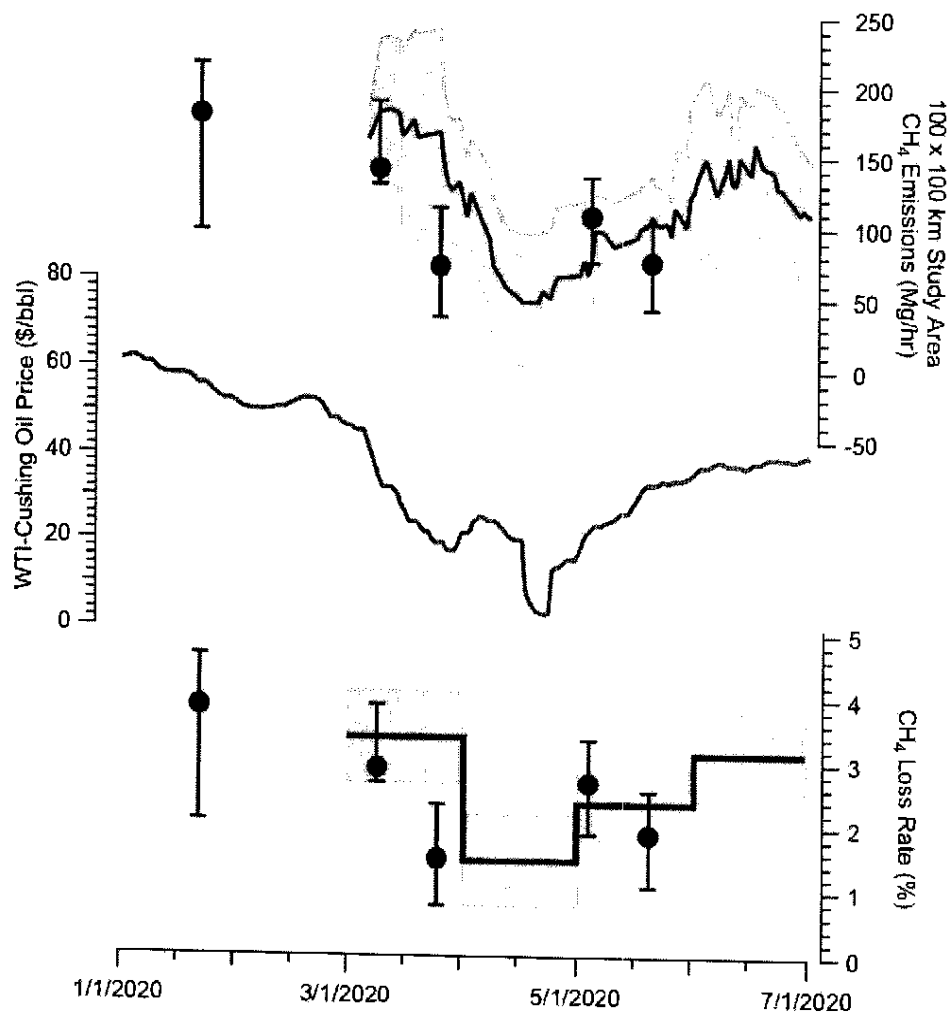


3 Results

Both aircraft and tower-based methane flux data show consistent trends of declining then rebounding methane emissions in our Permian Basin study area during March – June 2020 (Fig. 6). Between January 22 and March 19, 2020, Emissions were 176 Mg CH₄ hr⁻¹ (95% confidence interval range: 142 – 209 Mg CH₄ hr⁻¹). Following the rapid decrease in oil price, emissions between April 7 and May 1, 2020 reached a minimum of 55 Mg CH₄ hr⁻¹ (95% CI range: 21 – 89 Mg CH₄ hr⁻¹). After the oil price mostly recovered, emissions for the month of June had increased to 135 Mg CH₄ hr⁻¹ (95% CI range 105 – 166 Mg CH₄ hr⁻¹) and by August had recovered largely to pre-crash levels at, albeit with higher uncertainty (152 Mg CH₄ hr⁻¹; 95% CI range 101 – 202 Mg CH₄ hr⁻¹, Fig. 3). Combining the monthly tower estimates with reported gas production (Enverus, 2020), we calculate a March 2020 loss rate of 3.4% of total gas production (95% CI range: 2.7 – 4.1%), slightly lower but within the uncertainty of previously reported basin wide estimates from 2018 – 2019 (3.7 ± 0.7 (1 σ) %) (Zhang et al., 2020). The minimum loss rate calculated for April 2020 was 1.5% of gas production (95% CI range: 0.8 – 2.2%); the loss rate of later months is uncertain due to incomplete gas production data (Appendix E). In the full Permian Basin, orbital observations of XCH₄ indicate lower methane column enhancements in April – May versus January – February 2020, consistent with the aircraft and tower-based flux data (Fig. 5).

Well pad development in the study area proceeded at an average rate of 71 new sites per month between August 2019 and March 2020, then dropped to a monthly average of 24 sites between April and July 2020 (Appendix C, Fig. 7). The number of well completions per month declined from 134 to 53 between January and April 2020 (Enverus, 2020); completion counts are higher than well pad development rates due to multiple wells being located on a single pad. After rising steadily throughout 2019, oil and gas production peaked in March 2020 and then declined 9 and 8%, respectively, in April. Based on adjusted, incomplete production data for May and June, gas production stayed relatively steady after April while oil production dropped an additional 3% (Appendix E). The relative decline in O&G production between March and April 2020 was much greater among wells in the first two months of production, decreasing 50 and 45%, for oil and gas, respectively (Appendix E).

The three flare surveys between February and June 2020 consistently found that 11% of flares had combustion issues, with 5% unlit and emitting hydrocarbons. Even when using conservative assumptions of greater combustion efficiency, we estimate a basin-wide flare combustion efficiency of 93%, with the remaining gas (assuming 80% methane content) being emitted to the atmosphere (Appendix B). Satellite observations of radiant heat indicate that flared gas volumes were cut in half from 7.6 to 3.2 Bcf between January and April 2020 (Fig. 8).



345 **Figure 6.** Temporal variation in methane emissions and crude oil price. Top: Aerial (red circles with 95% CI error range) and tower based 7-point moving average and 95% CI (blue line and shading) atmospheric estimates of 100 km x 100 km study area CH_4 emissions. Middle: 7-day moving average of WTI-Cushing daily oil price. Bottom: Resulting CH_4 loss rate from aerial and monthly mean tower-based measurements utilizing published monthly gas production within the study area (Enverus, 2020).

350



355

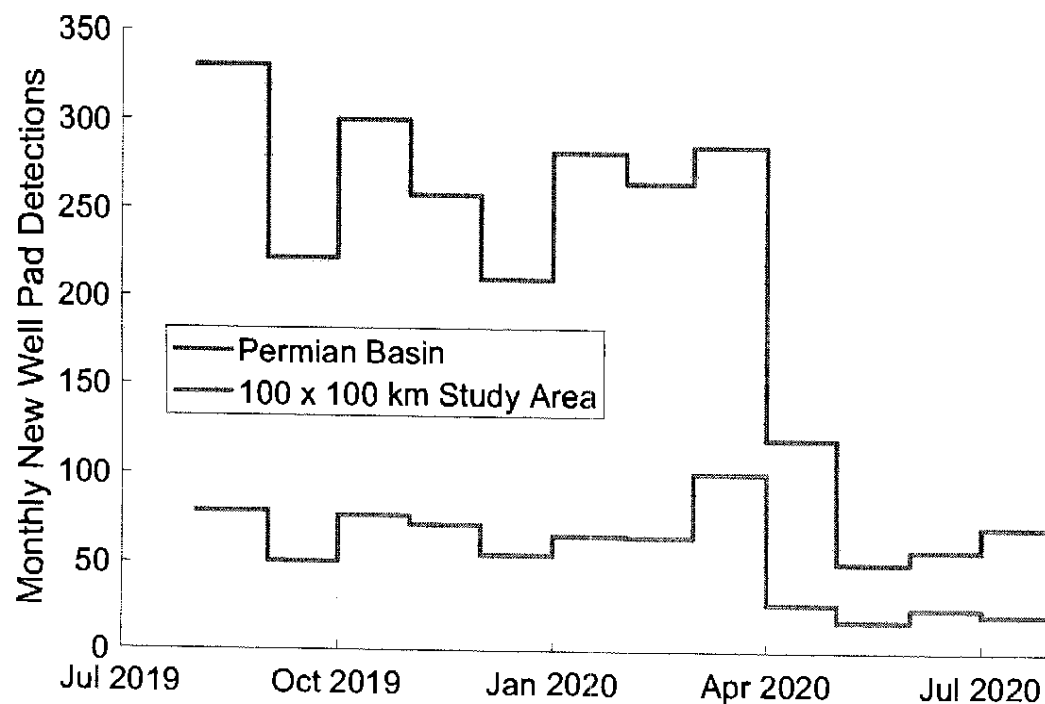
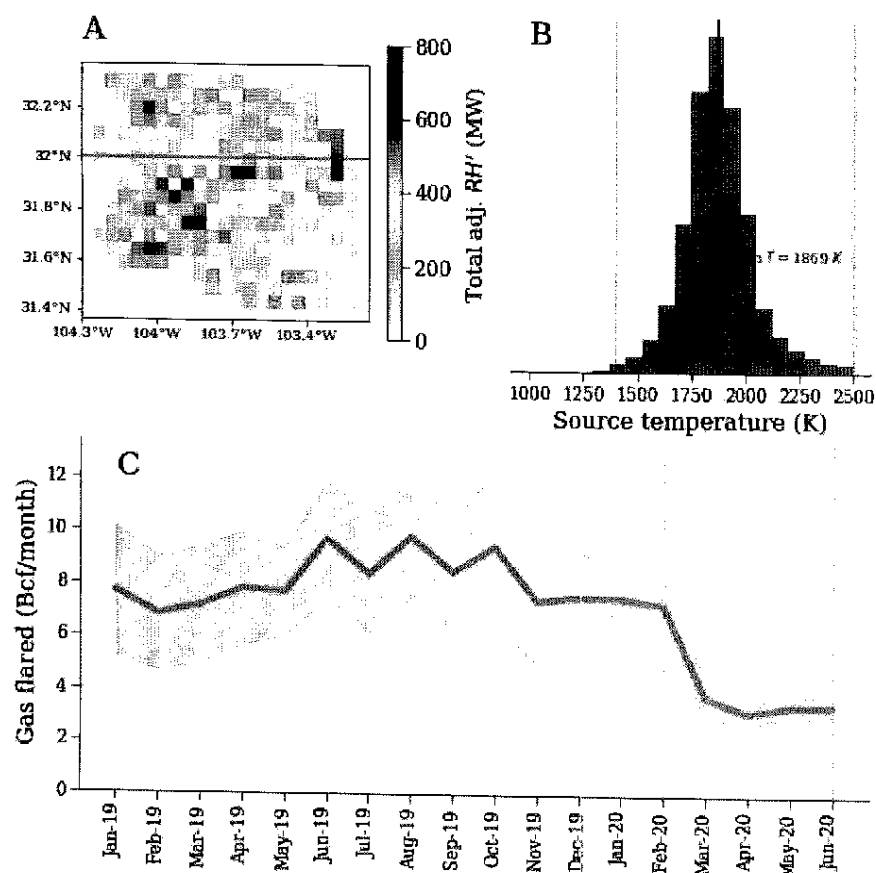


Figure 7. Number of new well pads constructed per month between August 1, 2019 and August 1, 2020.



360

Figure 8. VIIRS-derived gas flaring in the study region. (A) Spatial distribution of the cumulative adjusted radiant heat over the period between January 2019 and June 2020 aggregated over a $0.05 \times 0.05^\circ$ grid resolution. (B) Histogram of VIIRS-derived source temperatures. Dotted lines show the temperature regime characteristic of gas flaring sources (1400–2500 K). (C) Monthly trend in VIIRS-derived gas flared volumes. The mean estimate is shown in solid line and the 95% CI on the mean is shown in the shaded area.

365



4 Conclusions

The pandemic-related oil price crash provided an unexpected opportunity to assess temporal variability in methane emissions during a period of volatile oil prices and associated operational changes. In support of our hypothesis that methane emissions would decline with oil price, we observed a three-fold reduction in Permian Basin study area methane emissions that was strongly correlated to the average daily oil price. The relative decline in O&G production during this period was less than 10%; accordingly, loss rate temporarily decreased from 3.4% to 1.5% of gas production between January 22 – March 19 and April 7 – May 1, 2020 (Appendix E). It is important to note that even the minimum observed loss rate of 1.5% is several times higher than the performance targets committed to by major O&G companies accounting for about one-third of global oil production, including some with operations in the Permian Basin (OGCI, 2020). We hypothesize that total methane emissions are positively correlated with oil price due to three interrelated factors associated with well development: 1) well completion rates, 2) associated gas flaring volumes, and 3) indirect impacts of new gas production on the gathering and processing (G&P) system.

Lower oil prices directly led to reduced emissions by decreasing well development activities, as we observed for rig count, new site construction, and well completions following the price crash. Well development activities are an intermittent source of methane emissions, particularly completion flowback, the typically multi-day period following hydraulic fracturing when fluids, excess proppant, and entrained gas are expelled from the wellbore (Allen et al., 2013). We estimate that the ~80 fewer well completions in April versus January 2020 caused average potential flowback emissions in our study area to decline from 9 to 2 Mg CH₄ hr⁻¹ (Appendix D). At the time of the study, U.S. federal regulations mandated the use of reduced emission completions to control emissions in most situations; however, operator reported data suggest actual emissions (1 – 2.5 Mg CH₄ hr⁻¹) are of similar magnitude to our estimate of potential emissions. ((USEPA, 2019, 2020b); Appendix D).

The observed two-fold reduction in flared gas volumes between January and April 2020 was likely the result of the large drop in gas production from new wells. Unconventional wells tend to have high initial gas production followed by steep declines. With lower rates of well development and new gas production in the area, competition for limited gas pipeline capacity likely was abated, leading to less flaring of stranded associated gas. Assuming a combustion efficiency of 93%, we estimate flare-related methane emissions in our study area were approximately 8 and 3 Mg CH₄ hr⁻¹ in January and April 2020, respectively (Appendix A). Our combustion efficiency assumption, which is based on repeat observations of over 300 flares, is conservatively high and therefore our emission estimate represents a lower bound. However, even with worst-case assumptions of flare combustion efficiency it is unlikely that January and April flare-related emissions would have exceeded 20 and 7 Mg CH₄ hr⁻¹, respectively (Appendix B).

Our estimates of well completion and flare-related methane emissions account for less than 20% of the observed total reduction between pre-crash and minimum price conditions; therefore, we theorize that the primary driver of emission reductions is indirect improvements to G&P system performance resulting from reduced inputs of gas from new wells. This result suggests

that the high methane emission rate observed in the Permian Basin in recent years is in large part due to insufficient capacity of G&P infrastructure for handling and delivering rapidly growing rates of natural gas production (Zhang et al., 2020). The drastic decline in flared gas volumes during the oil price crash suggests that the reduction in new gas production relieved G&P capacity issues. A similar pattern was observed in the Bakken formation during the oil price decline of 2015-2016: price drops caused only a small decrease in total production but a large decrease in drilling and flaring rates (Appendix F). Our study provides the first direct evidence of reduced methane emissions resulting from an apparent abatement of infrastructure capacity limitations.

The high methane emission rate observed in the Permian Basin during periods of higher commodity prices is likely a consequence of associated gas production increasing at a faster rate than midstream infrastructure capacity, which leads to extensive flaring and anomalous conditions related to excess gas throughput (e.g. pressure relief venting). Our observations of emissions declining concurrently with new well development suggest that methane emissions could be mitigated in the Permian Basin and similar oil-producing fields by better aligning development rates of wells and midstream infrastructure. For example, regulations could prohibit the drilling of wells in areas without sufficient capacity to transport newly produced gas to market. Our findings suggest that policies which tie the maximum rate of well development to infrastructure capacity, in addition to other approaches such as requiring high frequency or continuous monitoring to detect large emission sources (Alvarez et al., 2018), can facilitate lower methane emissions that reduce the climatic impact of oil and gas production.

Appendix A. VIIRS-derived flared natural gas volumes

We assess the monthly trends in the volumes of natural gas flared in the study region using nighttime fire and flare data observed by the Visible Infrared Imaging Radiometer Suite (VIIRS) instrument onboard the Suomi National Polar-Orbiting Partnership satellite. Specifically, we use the VIIRS NightFire V3.0 data product to support our analysis (Elvidge et al., 2013). For the study region and for the period between January 2019 and June 2020, we retrieved 49,885 individual VIIRS detections for which it was possible to estimate flaring source temperatures based on Planck curve fitting of the source radiances Elvidge et al. (2013). During this period, the mean VIIRS-derived source temperature was 1869 K. The histogram of source temperatures is shown in Fig. 8b, indicating a strong gas flaring signal in the characteristic temperature regime of between 1400 and 2500 K. Elvidge et al. (2015) developed a correlation between the VIIRS-derived radiant heat and reported gas flared volumes and derived the relationship:

$$V_d = 0.0274 RH' (R^2 = 0.86)$$

where V_d is the annual volume of gas flared (in billion cubic meters) and RH' is the modified radiant heat for each individual flare, adjusted to account for the observed non-linear relationship between flared gas volume and radiant heat and was computed as: $RH' = \sigma T^4 S^{0.7}$, where σ is the Stefan-Boltzmann constant ($5.67 \times 10^{-8} \text{ W m}^{-2} \text{ K}^{-1}$), T and S are the source temperature and area, respectively, and the exponent (0.7) was empirically developed by Elvidge et al. (2015) to address non-



linearity. Figure 8a shows the spatial distribution of the cumulative RH' in the study region over the period between January 2019 and June 2020, as aggregated over a $0.05^\circ \times 0.05^\circ$ grid resolution. To estimate monthly gas flared volumes (V_m in billion cubic feet) for the study area, we modify equation the equation above, assuming the relationship holds over monthly intervals:

$$V_m = 0.0274 RH' \times \frac{1}{12} \times 35.315 \left[\frac{Bcf}{Bcm} \right]$$

We use the equation above to compute the mean monthly gas flared volumes (and 95% CI on the mean) in the study area based on the daily RH' aggregated from individual detected flares. The trend in the monthly gas flared volumes is shown in Fig. 8c.

The average flaring rate in 2019 was 8.2 ± 2.2 Bcf/month. From February 2020, a sharp decline in the mean gas flaring rate was observed, with the lowest estimated flaring rate of 3.2 ± 0.4 Bcf in April. Following a similar procedure for the entire Permian region, the estimated mean monthly flaring rate declined from a mean of 23 ± 5 Bcf/month in 2019 to 8.1 ± 1.7 Bcf in May 2020. Thus, the lowest estimated monthly gas flared volumes in 2020 were a factor of 2.6 and 2.8 times lower than the monthly mean observed in 2019 for the 100 km x 100 km study region and full Permian Basin, respectively.

Appendix B. Aerial flare performance survey

We compiled a list of potential locations of recently active flares in the Permian Basin (Delaware and Midland sub-Basins) based on a geospatial analysis of the SkyTruth Global Flaring Dataset, which is derived from heat sources detected by the Visible Infrared Imaging Radiometer Suite (VIIRS) instrument on the NOAA Suomi NPP satellite; SkyTruth has applied several filters to the VIIRS data including removing heat sources $<1,500^\circ\text{C}$ and with <3 detections per month (Skytruth, 2020). To account for spatial uncertainty of SkyTruth flare locations, we spatially joined their individual flare detections between October 1, 2019 and January 31, 2020 using a 100-meter buffer distance; the centroid latitude/longitude of the 1,014 joined detections were defined as likely locations of recently active O&G flares. Leak Surveys, Inc. (LSI), a leak detection company specializing in aerial optical gas imaging, was provided a list of 573 potential active flare locations from the original set of 1,014. The site selection methodology balanced representativeness and survey efficiency by defining one contiguous, high flare density area in each sub-basin that could be surveyed over the course of approximately five days. For the Delaware sub-Basin, we selected 323 locations located within our main study area (NW and SE corners are 32.325°N , 103.822°W and 31.417°N , 103.202°W , respectively). For the Midland sub-Basin, we selected 250 locations from the two counties (Midland and Martin) with the highest flare counts from the analysis of VIIRS data. LSI surveyed these locations with a custom infrared camera (IR) deployed in a R44 helicopter. Potential flare locations were identified with spatial coordinates and a unique flare ID.

LSI performed three surveys of the potential flare locations during the weeks of February 17, March 23, and June 22, 2020 (EDF, 2020). At each potential flare location, LSI determined if one or more flares was present at the spatial coordinates, and



465 if so, observed the flare(s) for operational status. For flares with apparent combustion issues, LSI recorded 30 – 60 seconds of
infrared and visual video footage of the flare plume to provide visual evidence of flare status. For each flare, LSI assigned a
qualitative assessment of the apparent flare status at the time of survey from four categories: inactive and unlit with no
emissions (inactive); active, lit, and operating properly (operational); active and lit but with operational issues such as
incomplete combustion or excessive smoke (malfunction); or active, unlit, and venting methane (unlit). For survey 1, LSI
470 observed 337 flares from the random selection of potential locations. For surveys 2 and 3, a random subset of the 337 flares
was selected for re-survey, prioritizing locations that had previously observed issues. We observed similar flare performance
in each of the three surveys: 11% of active flares had observed malfunctions, including 5% that were unlit and venting (Table
B1).

475 To estimate methane emissions from flaring, we used our qualitative flare performance data and conservatively high
assumptions about the combustion efficiency of operational, malfunctioning, and unlit flares to estimate overall combustion
efficiency, and then applied combustion efficiency to estimated flared volumes in 2019 based on an analysis of VIIRS data
(Appendix B). We assume that operational flares perform at the EPA default combustion efficiency of 98% (Regulations,
2016). The 5% of flares that were unlit and venting were assumed to have a combustion efficiency of 0%. The 6% of flares
480 that were lit with apparent combustion issues were assumed to have 90% combustion efficiency. If we assume flared gas
volumes are proportional to the observed fraction of flares by performance, then the overall combustion efficiency of active
flares in the Permian Basin is 93%, which means 7% of flared methane is emitted. Applying 93% combustion efficiency to the
280 Bcf of gas flared in the Permian in 2019 (assuming 80% CH₄ content) results in annual methane emissions of
approximately 300,000 Mg CH₄ from flaring in the Permian; unlit flares account for about 65% of these emissions, while
485 operational and poorly combusting flares account for about 15 and 10%, respectively. As a sensitivity analysis, we use
alternative combustion efficiency assumptions of 90%, 50%, and 0% for operational, malfunctioning, and unlit flares,
respectively; this leads to an overall combustion efficiency of 83% and 2.3x more flare-related methane emissions than our
conservatively low assumptions.

490 EPA publishes two separate estimates of Permian flaring methane emissions, which incorporates the 98% combustion
efficiency but different gas flared data. The 2020 Greenhouse Gas Inventory (USEPA, 2020a) reports 2018 Permian Basin
methane emissions of 12,100 Mg CH₄ from associated gas flaring, plus 8,500 and 4,600 Mg CH₄ from associated gas venting
and miscellaneous production flaring, respectively. The Greenhouse Gas Reporting Program (USEPA, 2020b) reports 18,800
Mg CH₄ from Permian Basin onshore production facilities.

495

Table B1. The operational performance of Permian Basin flares as observed during three helicopter-based infrared optical gas imaging surveys.

Surveyed Flares	Survey 1	Survey 2	Survey 3	Average
Operational	276	147	237	
Inactive	25	0	62	
Combustion Issue	23	9	18	
Unlit and Venting	13	10	12	
Total	337	166	329	
Malfunctioning (% of active)	11.5%	11.4%	11.2%	11.4%
Unlit and Venting (% of active)	4.2%	6.0%	4.5%	4.9%

500 Appendix C. Satellite imagery and machine learning based estimates of well pad development

We mapped new well pad construction in the Permian Basin using a two-step machine learning and remote sensing approach. First, well pad candidates were identified in satellite imagery with a convolutional neural network (CNN) model in individual scenes. The model predictions were then compared between the beginning and end of each month to identify the locations of newly constructed well pads. Second, by differencing before/after model outputs, persistent false-positives in the model were removed. The resulting model was deployed on imagery over the Permian Basin on a monthly cadence between August 1, 2019 and July 1, 2020.

We assessed the monthly trends in new well pad construction in the Permian Basin using a combination of satellite imagery from the European Space Agency Sentinel-2 satellite (ESA, 2020) and the National Aeronautics and Space Administration (NASA) Landsat-8 satellite (USGS, 2020). Imagery from Sentinel-2 has a pixel resolution of 10m, sufficient to clearly identify well pads, and is collected approximately once every 5 days for any location, providing an average of 6 collects per month. While this is generally sufficient for monthly monitoring, some areas experience high cloud cover in all the scenes, causing well pads to be missed. Imagery from Landsat-8 was used to fill in for such cloudy scenes. Despite the slower 16-day revisit rate and coarser (30m) pixel resolution of Landsat-8, well pads are still easily detectable. The combined use of these two satellites provided at least one cloud-free scene for all of the Permian Basin for each month within the time period we monitored. We use six spectral bands from both Sentinel-2 and Landsat-8: "red", "green", "blue", "NIR", "SWIR1", and "SWIR2".



520 New well pad construction was detected in a two-step approach. Well pad candidates were first identified with a convolutional neural network (CNN) model in individual scenes. The model predictions were compared between the beginning and end of each month, and new well pads were identified. Well pads were detected using a semantic segmentation approach. We used a UNet architecture with a six-band input layer with shape (*height*, *width*, 12) and output predicting the presence or absence of well pads in each pixel. Landsat-8 imagery was resampled to 10m to match the resolution of Sentinel-2 imagery.

525 The model was trained on a ground-truth dataset taken from well pads detected with a separate machine learning model run on high resolution (1.5m) imagery. We generated ~7000 training tiles, each of size 512 x 512 pixels and containing 0 to 400 well pads each. The dataset was split into sets with 70 % for training, 10% for validation, and 20% for testing. Examples of image-target pairs are shown in Fig. C1.

530 New well pads were detected by comparing model output heatmaps between the beginning and end of sequential monthly time periods (Fig. C2). Intuitively, pixel values in satellite imagery change frequently in irrelevant ways, so it is more effective to identify change in the model output. The heatmap from the earlier time was subtracted from the later time. A threshold operator followed by a morphological opening operation were applied to these difference maps. New well pad detections were identified in the resulting binary map as shown in Fig. C3.

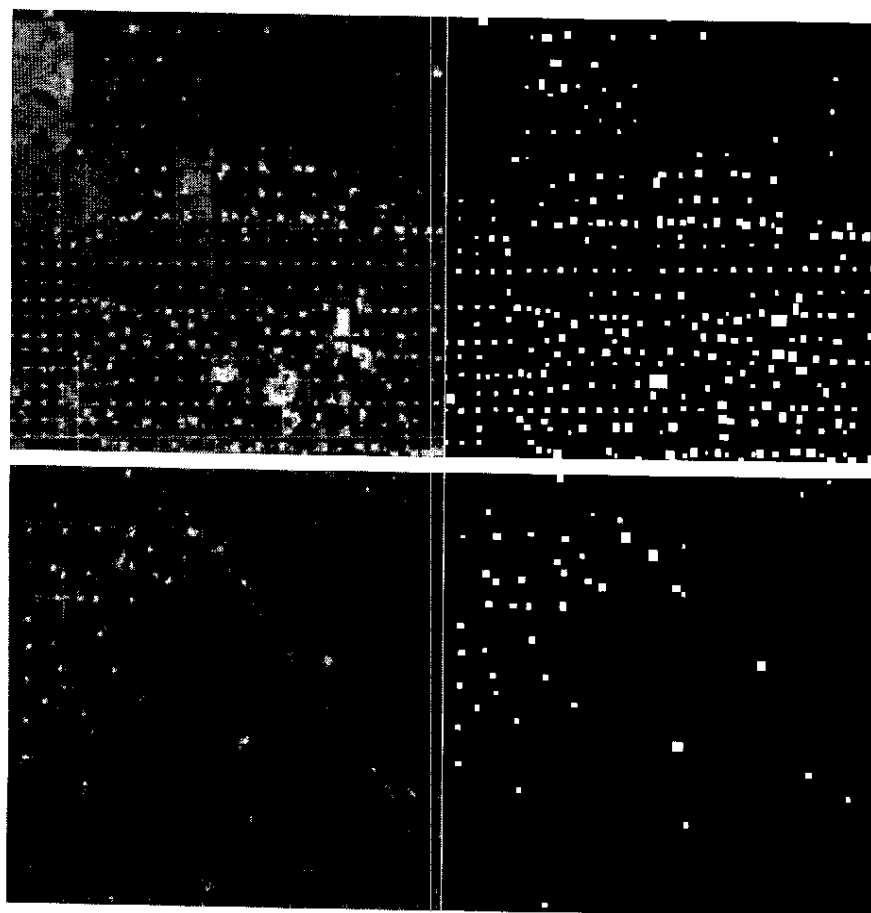
535 To further remove false positives, we require that new well pad candidates should not have existed in multiple months leading up to the construction date, and should continue to exist for several months after. We thus used the three months before and the two months after to remove candidates that fail this condition. While the 10m resolution of the imagery makes it difficult to confirm with certainty that candidates contain oil and gas infrastructure, we suspect that the Permian Basin region is unlikely to experience a high volume of unrelated ground clearing for development. We confirm this with manual inspection, see details below.

545 The CNN and change detection pipeline was run over the Permian Basin on monthly imagery composites between August 1, 2019 to July 1, 2020. The deployment was done using the Descartes Labs platform. Tiled imagery was drawn on-the-fly, model inference was performed in a cloud-native kubernetes infrastructure, and results were stored in the commercial cloud. Finally, the authors hand-verified the candidates for each month.

550 The change detection analysis has a precision of ~100%, since the final results have been hand-verified. It is infeasible to measure the model accuracy or recall directly, as these would require identifying a substantial number of newly constructed well pads as well as false negatives (newly constructed well pads that were missed by the model), which would require extensive hand-labeling; additionally, the model performance may vary across geographies, making a single metric less useful. Instead, we estimated the recall using a dataset of well pads identified with a separate machine learning model in high-

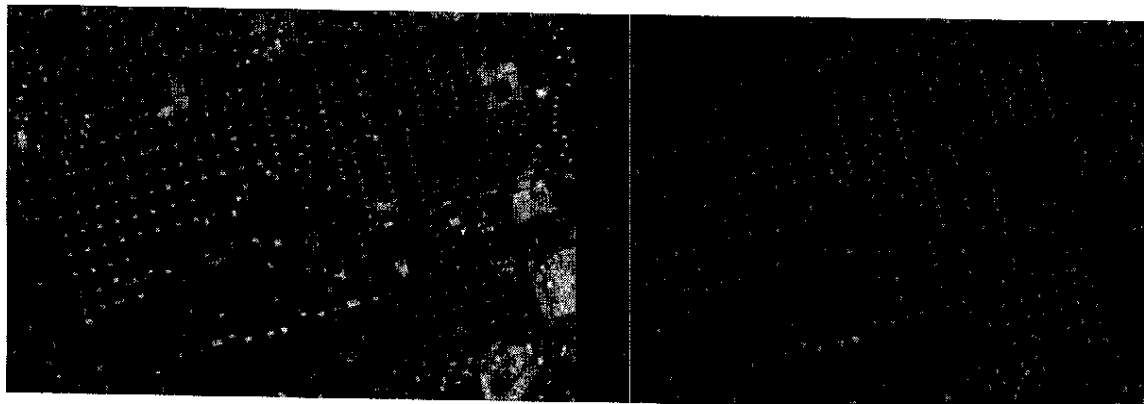


resolution imagery; we measured the fraction of these well pads that are detected as well pads by the UNet in single mosaics. Any well pads missed in this step will not be identified as new well pads. We measured this recall on four separate monthly
 555 mosaics, and found a recall of 90.0%, with a statistical uncertainty of less than a percent. Finally, the number of newly constructed well pads per month are shown in Fig. 7 with examples presented in Figs. C4 and C5.



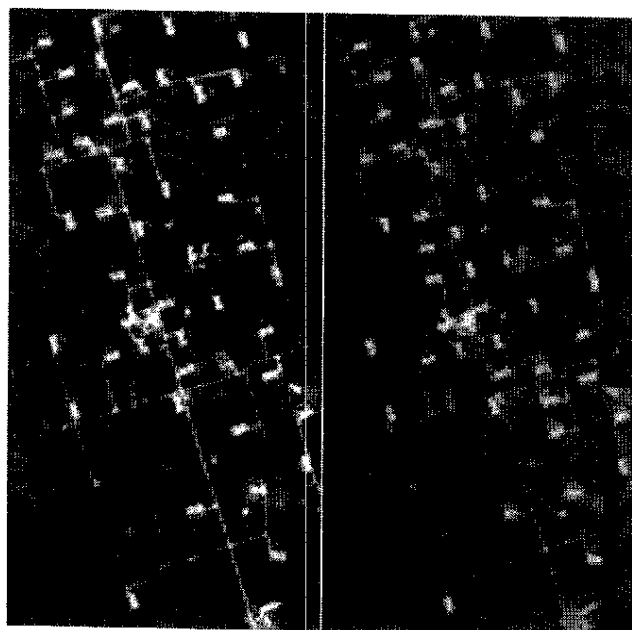
560

Figure C1. Examples of image-target pairs: (left) Sentinel-2 RGB imagery (ESA, 2020); (right) Ground truth



565

Figure C2. CNN model example, showing Sentinel-2 imagery (left; ESA, 2020) and model output heatmap over the same area (right).



570

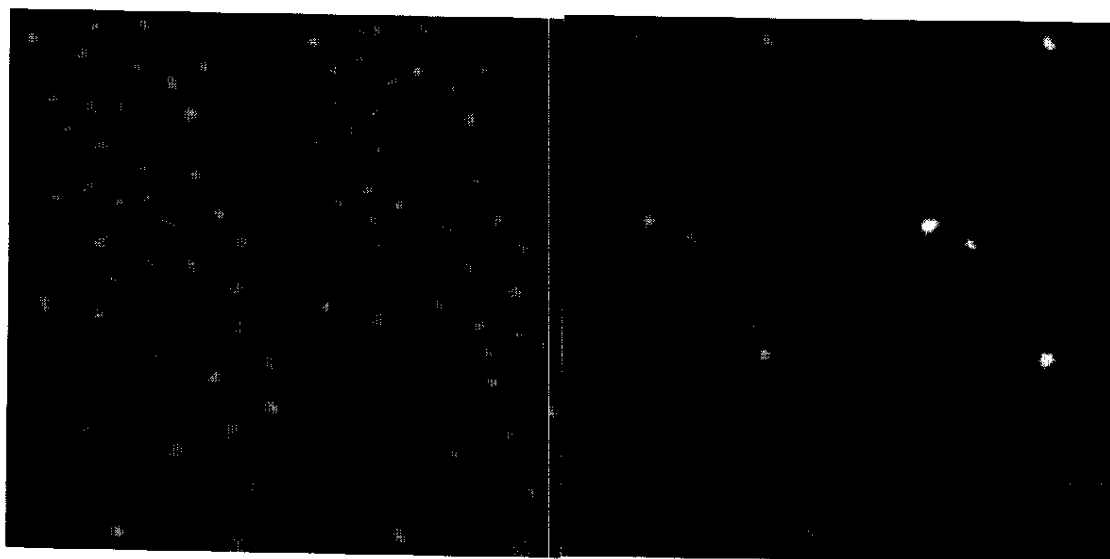
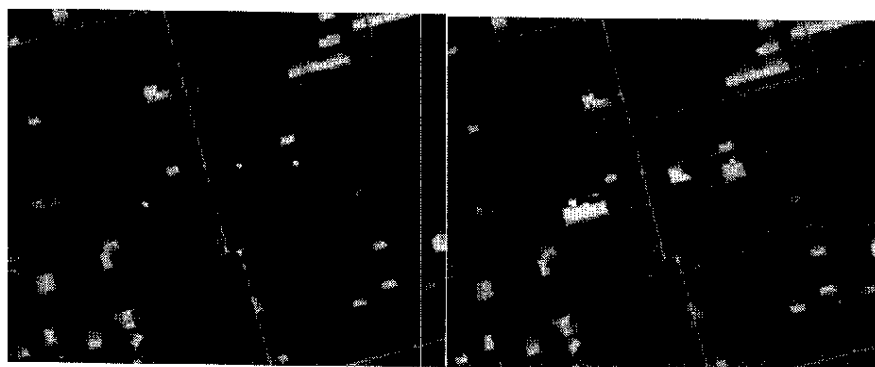
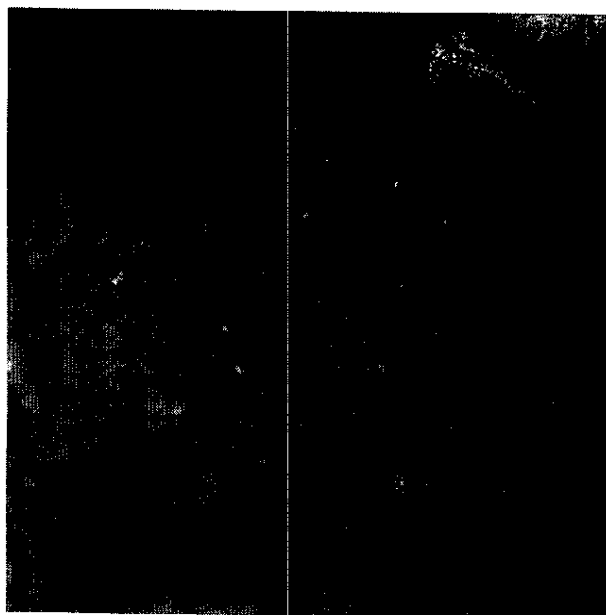


Figure C3. Before (top-left) and after (top-right) medium-resolution imagery (ESA, 2020). Same area in model output
 575 (bottom, left to right): 1. before, 2. after, 3. difference, 4. detected new well pads.



580 **Figure C4.** Example of an area where new development was found, before (top) and after (bottom) shown in Sentinel-2
 imagery (ESA, 2020). Points in yellow indicate the locations of new well pad development.



585 **Figure C5.** Number of new well pads constructed per month between August 1, 2019 and July 1, 2020 overlaid on Sentinel-2
 imagery over a subset of the Permian Basin (ESA, 2020).



Appendix D. Well completion emission estimates

Well completion flowback refers to the unconventional well development period following hydraulic fracturing in which water, proppant, and entrained natural gas flow out of the wellbore to prepare a well for production (Allen et al., 2013). As of 2015, U.S. federal regulations require all oil and gas wells except exploratory and low-pressure wells to utilize reduced emission completions (RECs), which separate the natural gas and send to a pipeline as soon as technically feasible (USEPA, 2019); occasionally, flaring or a combination of REC and flaring is used to partially control emissions. Previous research has demonstrated that RECs control flowback emissions by an average of 99% (Allen et al., 2013). To estimate monthly completion-related methane emissions within our 100 km x 100 km study area during the study period, we compiled a list of every well located within our study area with a completion date between January 1 and April 30, 2020 (Enverus, 2020) and applied two approaches to estimate potential and actual emissions. The first approach estimated actual emissions by applying an emission factor (total methane emitted per well completion) based on 2018 data from 3,359 completions in the Permian Basin reported to the EPA Greenhouse Gas Reporting Program, which operators estimate with a choice of measurements or engineering equations (USEPA, 2019, 2020b). To convert total emissions into an hourly emission rate, we assumed that completions emit at a constant rate over 4 days, the average duration from Allen et al. (2013). The second approach, which estimated potential emissions, assumes that wells emit their initial gas production for 4 days following the completion date; we assumed 80% methane content of natural gas and used the daily average production rate from the first complete month of gas production (referred to as PracIP by (Enverus, 2020)).

The number of well completions per month in the study area dropped from 134 in January to 53 in April 2020. Based on our first approach, January and April 2020 completion-related actual emissions were 2.5 and 1 Mg CH₄ h⁻¹, respectively, with an average emission factor of 19 kg CH₄ h⁻¹ per completion and 93% of completions utilizing a REC or REC plus flaring (Table D1). Based on the second approach, the average potential emission rate per completion was 61 kg CH₄ h⁻¹ in January and 23 kg CH₄ h⁻¹ in April 2020; this results in total study area completion-related emissions of 9.3 and 1.9 Mg CH₄ h⁻¹ in January and April, respectively (Table D2).



Table D1. Estimate of Permian Basin well completion emission factors based on US EPA Greenhouse Gas Reporting Program data.

	Permian Basin Annual Completions (#)	Total Methane Emissions (Mg CH ₄)	Average Emissions (Mg CH ₄ completion ⁻¹)	Average Emission Rate assuming 4 day duration (kg CH ₄ completion ⁻¹)
Reduced Emission Completion (REC)	1,162	376	0.3	3
REC & Flared	1,955	4,673	2.4	25
Uncontrolled	14	35	2.5	26
Flared	228	1,202	5.3	55
<i>Total</i>	3,359	6,287	1.9	19



625 **Table D2.** Estimate of average monthly potential completion-related emissions from our study area from January 2019 – April 2020 based on initial production data and the assumption of 4 day completion duration.

Year	Month	Average Ongoing Daily Well Completions (wells)	Average Aggregate Completion-Related Emissions (Mg CH ₄ h ⁻¹)
2019	1	435	7.1
2019	2	616	15.2
2019	3	570	12.3
2019	4	706	12.0
2019	5	595	11.0
2019	6	569	9.3
2019	7	762	14.7
2019	8	884	13.6
2019	9	492	12.1
2019	10	658	10.5
2019	11	720	14.6
2019	12	461	9.4
2020	1	505	9.3
2020	2	335	7.7
2020	3	259	3.7
2020	4	212	1.9



630 **Appendix E. Oil & Gas production data and assessment of database completeness**

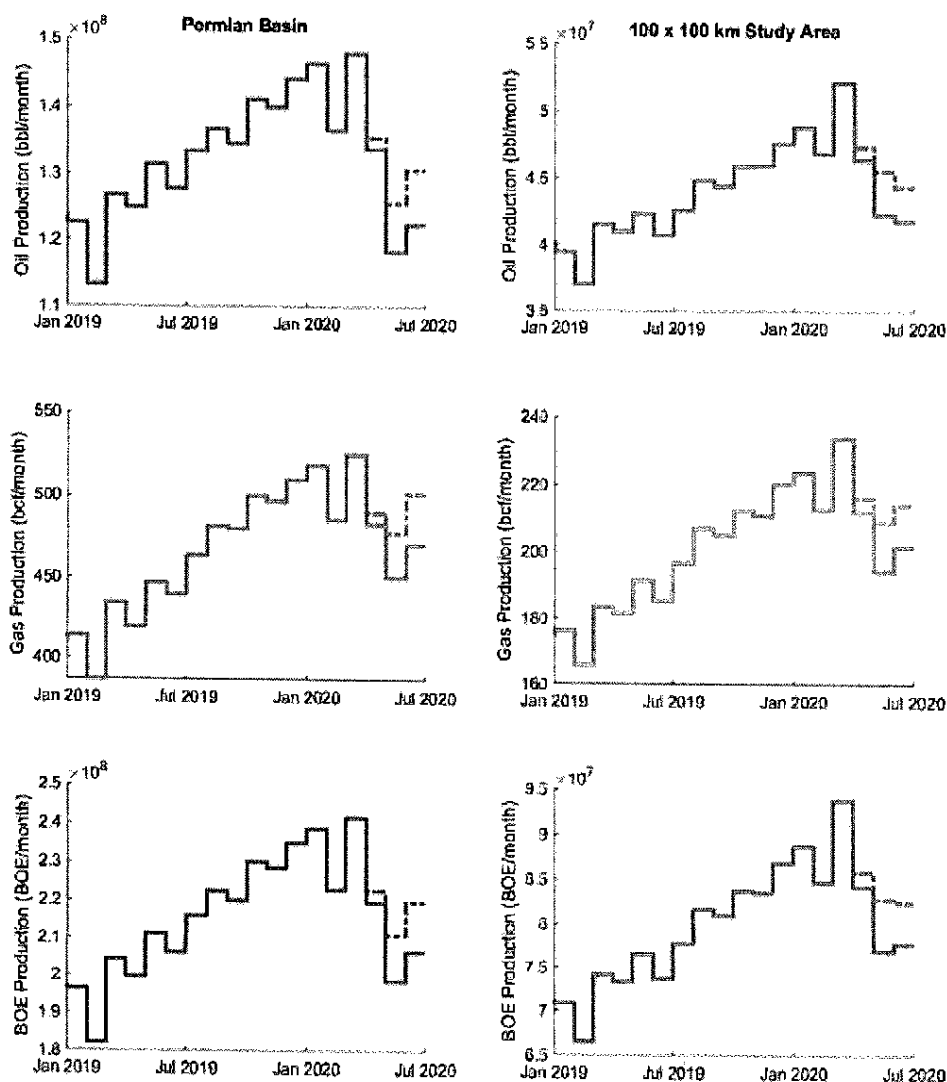
Production quantities of oil and gas from individual wells is reported to public state databases (RRC, 2020; NMOCD, 2020); however, the best results are achieved by analyses from an external database (Enverus, 2020) which filters and aggregates all of the publicly available datasets from all reporting agencies. Oil and Gas production data from New Mexico is updated on a monthly cadence, while data from Texas is updated twice each month but still only at monthly resolution. Timeseries of Oil,
 635 Gas and combined barrels-of-oil equivalent (BOE) production within the greater Permian basin and 100 x 100 km study area are presented in Fig. E1. Similarly, Fig. E2 presents a timeseries of the number wells reporting production each month within the basin and 100 x 100 km study area as well as timeseries of the number of wells exhibiting their first month of Oil and Gas production and their as their spud date: the date at which the subsurface drilling commences within the process of well development. The typical lag in data reporting is at least 3 months (Enverus, 2020) (e.g. O&G production during the month
 640 of June is available on or shortly after the 1st of September); however in practice reporting delays upwards of 6 months have been observed. We anticipate additional delays in the reporting of production data related to the global COVID-19 pandemic, thus here we attempt to broadly assess the incompleteness of the production dataset and its related impact on our estimates of the study area CH₄ loss rate.

645 The number of active wells reporting production was relatively constant in the Permian basin was relatively consistent through March 2020, only exhibiting a drop from the trend in April 2020 suggesting that new wells were coming online at roughly the same rate of older, depreciated wells being shut in. Alternatively, in the smaller 100 x 100 km study area which represents $7.4 \pm 0.3\%$ (1σ) of the total Permian basin active well count for January 2019 – March 2020, the number of wells reporting production each month was increasing at a rate of 102 ± 58 (1σ) wells per month between January 2019 and March 2020.
 650 During the same time span in the study area, the rate of new well production (168 ± 27 wells/month, 1σ) significantly outpaced the rate of depreciated wells being shut in by roughly a factor of 3.

Therefore, to estimate the complete dataset of total monthly production in the April-June 2020 under the timeframe of the observations of CH₄ emissions presented in Fig. 2, we extrapolate the average well count for January to March 2020 to the
 655 subsequent three months as the dotted line on the Orange and Red traces of Fig. E2. We assume the deficit in wells reported represent the same distribution of oil and gas reported from each well present in the database; therefore, we linearly scale the production upwards by this factor as shown in the dotted lines in Fig. E1. This assessment suggests that that production largely plateaued during the height of the COVID-19 pandemic, rather than the <10% decrease observed by the reported data at time of submission. Therefore, using the projected gas production estimates, we calculate a projected loss rate in the basin from
 660 both the monthly mean tower data and May aerial measurements the as the purple dotted line and yellow points respectively in Fig. E3.



665 This approach discussed above likely overestimates the oil and gas production due to the reduced activity observed from satellite well pad detection (Fig.7) and the reduced rate of new well development (Fig. E2). Therefore, we consider this to be an upper limit on the study area gas production and therefore a lower limit on the CH₄ loss rate, with the actual value likely falling between the two estimates. Regardless, the adjusted loss rate represents a minimal adjustment within the 95% CI estimate expressed by the aerial and tower data temporal and analytical uncertainty that we do not consider it to differ significantly from the reported result in Fig. 6.



670

Figure E1. Monthly Timeseries of monthly Oil, Gas and Barrels of Oil Equivalent production (Top, Middle and Bottom respectively) in both the Permian Basin (left) and 100 x 100 km Study Area (Right). Dotted lines for April-June 2020 represent adjusted production to assess incompleteness of the dataset.



675

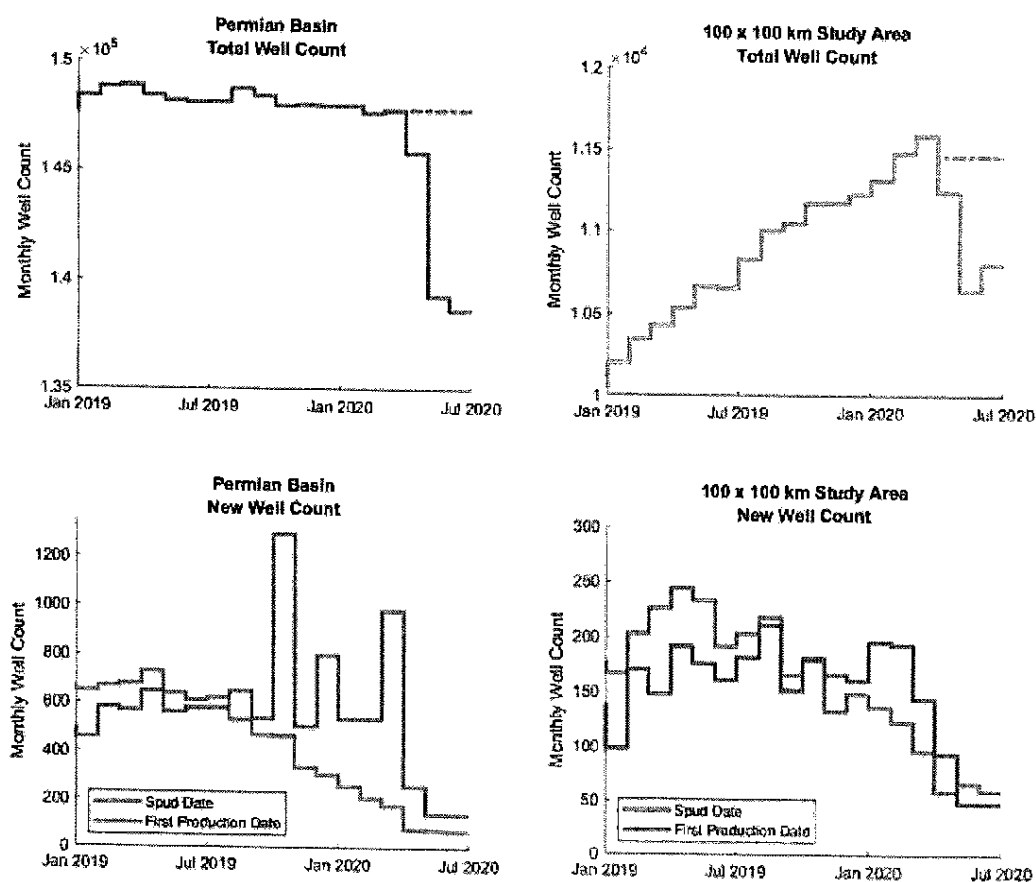


Figure E2. Monthly Timeseries of Active wells (top) and newly produced wells by spud date and month of first production (bottom) in both the Permian Basin (left) and 100 x 100 km Study Area (right). Dotted lines for April-June 2020 represent adjusted well counts to assess incompleteness of the dataset

680

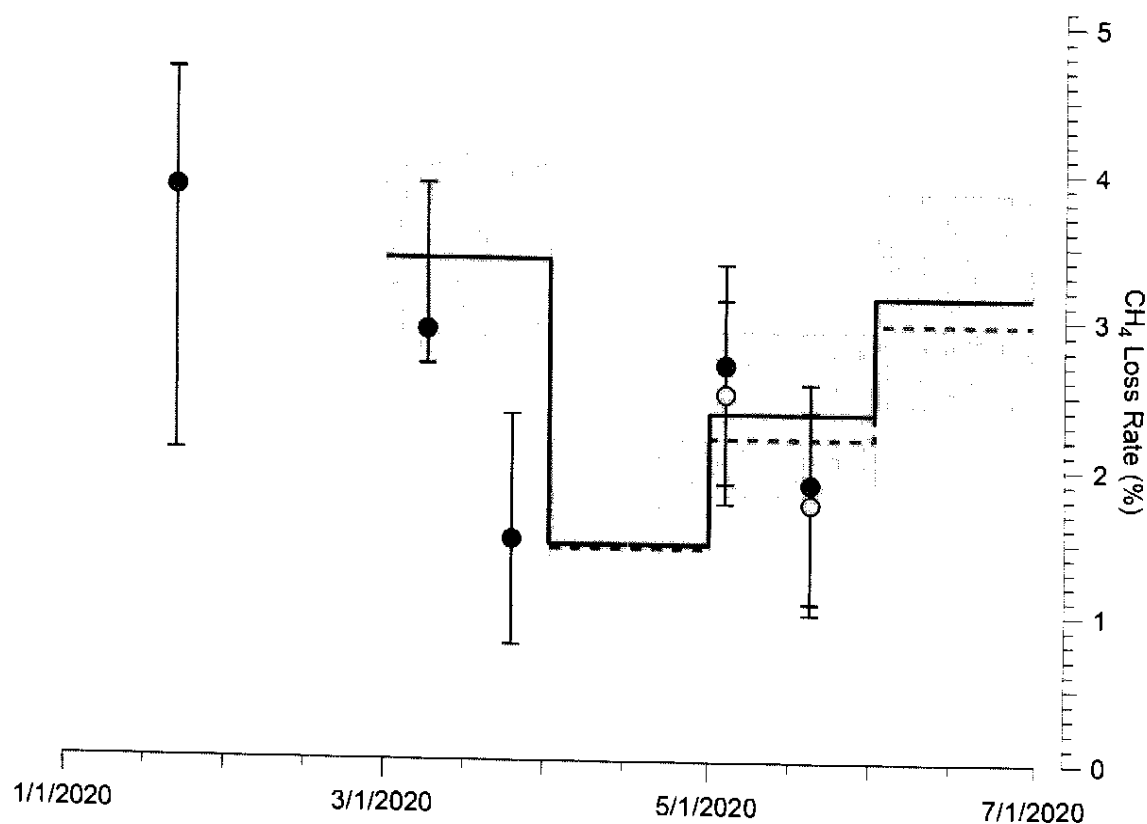
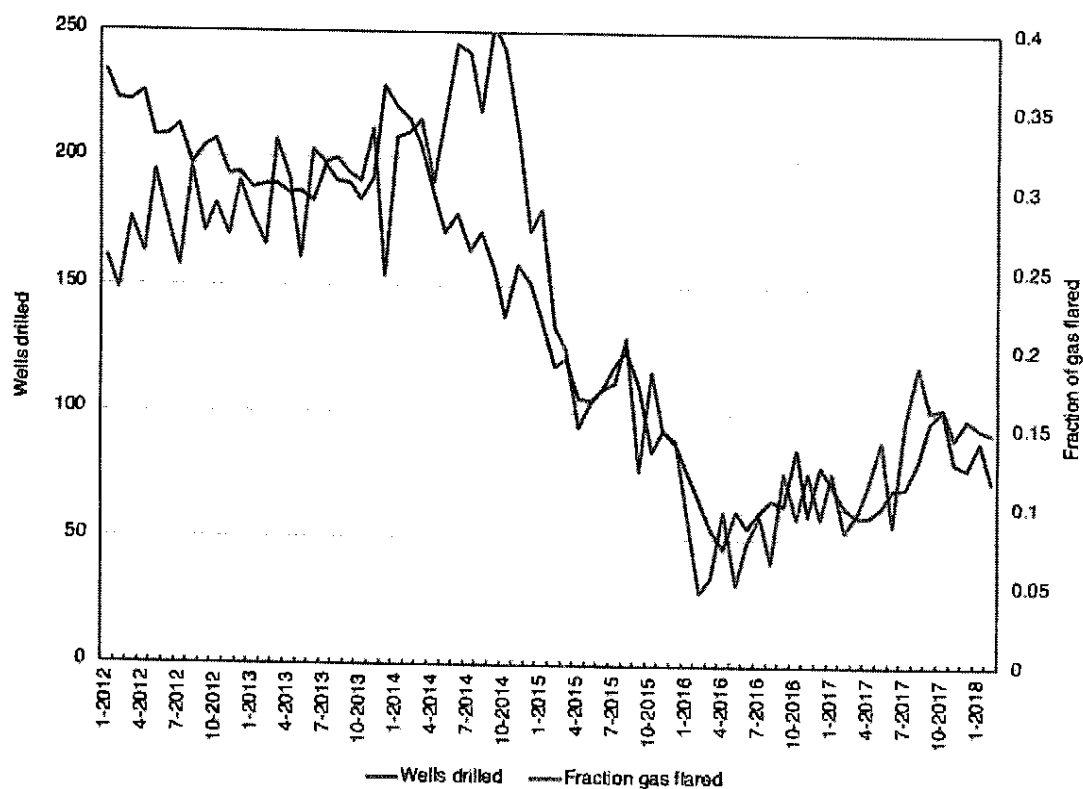


Figure E3. Gas production normalized loss rate in the 100 x 100 km study area following the same formatting as presented in Figure 6. Dotted purple line and yellow points reflect the adjusted tower and aerial based loss rates respectively after considering the incompleteness of the production database.

685



Appendix F. Supplementary data from Bakken Shale



690 **Figure F1.** Number of wells drilled versus fraction of total gas production flared in the Bakken region (North Dakota, U.S.A.) from 2012 - 2017. Similar to trends observed in the Permian, there was a strong correlation between wells drilled and fraction of gas flared with both values decreasing rapidly when oil prices crashed in 2014.



Data Availability

695 Data are available for download at <https://www.permianmap.org/>

Author Contribution

D.R.L., B.H., A.R.B., M.K., E.A.K., A.J.M., and S.P.H. contributed to study conceptualization. D.R.L., B.H., R.G., M.O., K.R., Z.R.B., K.J.D., N.L.M., V.C.M., S.J.R., S.C., M.L.S., D.J.J., L.S., D.V.V., A.D., X.R., N.S., and K.T.S. contributed to methods development and data analysis. D.R.L., B.H., M.O., Z.R.B., K.J.D., M.L.S., D.J.V., and K.T.S. wrote the original
700 draft and all authors reviewed and edited the manuscript

Competing Interests

A.R.B., E.A.K., M.K., and A.J.M. serve on the PermianMAP scientific advisory panel. Authors declare no other competing interests.

Acknowledgements

705 The authors thank Beth Trask, Colin Leyden, Jon Goldstein, Louise White, Caleb Berman, and the entire PermianMAP team for their contribution to the project. We are grateful to Ramon Alvarez, Maureen Lackner, Ricardo Esparza, Ilse Aben, and Johannes Maasackers for providing comments. We are grateful to Niall Armstrong for piloting the research aircraft and Leak Surveys, Inc. for performing the flare performance surveys. The PermianMAP project, which includes the aerial, tower, and flare survey data, is funded by Environmental Defense Fund; the work at Harvard University was supported by NASA Carbon
710 Monitoring System. Computations for this research were performed on The Pennsylvania State University's Institute for Computational and Data Sciences' Roar supercomputer.



References

- 715 Allen, D. T., Torres, V. M., Thomas, J., Sullivan, D. W., Harrison, M., Hendler, A., Herndon, S. C., Kolb, C. E., Fraser, M. P., Hill, A. D., Lamb, B. K., Miskimins, J., Sawyer, R. F., and Seinfeld, J. H.: Measurements of methane emissions at natural gas production sites in the United States, *Proceedings of the National Academy of Sciences*, 110, 17768-17773, 10.1073/pnas.1304880110, 2013.
- Allen, D. T.: Methane emissions from natural gas production and use: reconciling bottom-up and top-down measurements, *Current Opinion in Chemical Engineering*, 5, 78-83, 10.1016/j.coche.2014.05.004, 2014.
- 720 Alvarez, R. A., Pacala, S. W., Winebrake, J. J., Chameides, W. L., and Hamburg, S. P.: Greater focus needed on methane leakage from natural gas infrastructure, *Proceedings of the National Academy of Sciences*, 109, 6435-6440, 10.1073/pnas.1202407109, 2012.
- Alvarez, R. A., Zavala-Araiza, D., Lyon, D. R., Allen, D. T., Barkley, Z. R., Brandt, A. R., Davis, K. J., Herndon, S. C., Jacob, D. J., Karion, A., Kort, E. A., Lamb, B. K., Lauvaux, T., Maasakkers, J. D., Marchese, A. J., Omara, M., Pacala, S. W., Peischl, J., Robinson, A. L., Shepson, P. B., Sweeney, C., Townsend-Small, A., Wofsy, S. C., and Hamburg, S. P.: Assessment of methane emissions from the U.S. oil and gas supply chain, *Science*, 10.1126/science.aar7204, 2018.
- Baker-Hughes: North America Rig Count, Baker Hughes, 2020.
- Barkley, Z. R., Lauvaux, T., Davis, K. J., Deng, A., Miles, N. L., Richardson, S. J., Cao, Y., Sweeney, C., Karion, A., Smith, M., Kort, E. A., Schwietzke, S., Murphy, T., Cervone, G., Martins, D., and Maasakkers, J. D.: Quantifying methane emissions from natural gas production in north-eastern Pennsylvania, *Atmospheric Chemistry and Physics*, 17, 13941-13966, 10.5194/acp-17-13941-2017, 2017.
- 730 Barkley, Z. R., Lauvaux, T., Davis, K. J., Deng, A., Fried, A., Weibring, P., Richter, D., Walega, J. G., DiGangi, J., Ehrman, S. H., Ren, X., and Dickerson, R. R.: Estimating Methane Emissions From Underground Coal and Natural Gas Production in Southwestern Pennsylvania, *Geophysical Research Letters*, 46, 4531-4540, 10.1029/2019gl082131, 2019.
- 735 Brandt, A. R., Heath, G. A., Kort, E. A., O'Sullivan, F., Petron, G., Jordaan, S. M., Tans, P., Wilcox, J., Gopstein, A. M., Arent, D., Wofsy, S., Brown, N. J., Bradley, R., Stucky, G. D., Eardley, D., and Harriss, R.: Methane Leaks from North American Natural Gas Systems, *Science*, 343, 733-735, 10.1126/science.1247045, 2014.
- Conley, S., Franco, G., Faloona, I., Blake, D. R., Peischl, J., and Ryerson, T. B.: Methane emissions from the 2015 Aliso Canyon blowout in Los Angeles, CA, *Science*, 351, 1317-1320, 10.1126/science.aaf2348, 2016.
- 740 Conley, S., Faloona, I., Mehrotra, S., Suard, M., Lenschow, D. H., Sweeney, C., Herndon, S., Schwietzke, S., Pétron, G., Pifer, J., Kort, E. A., and Schnell, R.: Application of Gauss's theorem to quantify localized surface emissions from airborne measurements of wind and trace gases, *Atmos. Meas. Tech.*, 10, 3345-3358, 10.5194/amt-10-3345-2017, 2017.
- Glugokencky, E. J., Myers, R. C., Lang, P. M., Masarie, K. A., Crotwell, A. M., Thoning, K. W., Hall, B. D., Elkins, J. W., and Steele, L. P.: Conversion of NOAA atmospheric dry air CH₄ mole fractions to a gravimetrically prepared standard scale, *Journal of Geophysical Research: Atmospheres*, 110, 10.1029/2005jd006035, 2005.
- EDF: Permian Methane Analysis Project (PermianMAP), in, Environmental Defense Fund, 2020.
- Elvidge, C., Zhizhin, M., Hsu, F.-C., and Baugh, K.: VIIRS nightfire: Satellite pyrometry at night, *Remote Sensing*, 5, 4423-4449, 10.3390/rs5094423, 2013.
- 750 Elvidge, C. D., Zhizhin, M., Hsu, F.-C., Baugh, K., Khomarudin, M. R., Vetrina, Y., Sofan, P., and Hilman, D.: Long-wave infrared identification of smoldering peat fires in Indonesia with nighttime Landsat data, *Environmental Research Letters*, 10, 065002, 2015.
- Elvidge, C. D., Zhizhin, M., Baugh, K., Hsu, F.-C., and Ghosh, T.: Methods for Global Survey of Natural Gas Flaring from Visible Infrared Imaging Radiometer Suite Data, *Energies*, 9, 14, 2016.
- 755 Enverus: Drillinginfo, <https://www.enverus.com/>, 2020.
- ESA: Sentinel-2 data, European Space Agency, available at <https://sentinel.esa.int/web/sentinel/home>, last access: 31 7 2020
- Gould, T., McGlade, C., and Schulz, R.: Methane Emissions from Oil and Gas, International Energy Agency, 2020.
- Hasekamp, O. P., Gryspeerdt, E., and Quaas, J.: Analysis of polarimetric satellite measurements suggests stronger cooling due to aerosol-cloud interactions, *Nature Communications*, 10, 5405, 10.1038/s41467-019-13372-2, 2019.
- 760 Hu, H., Landgraf, J., Detmers, R., Borsdorff, T., Aan de Brugh, J., Aben, I., Butz, A., and Hasekamp, O.: Toward Global Mapping of Methane With TROPOMI: First Results and Intersatellite Comparison to GOSAT, *Geophysical Research Letters*, 45, 3682-3689, 10.1002/2018gl077259, 2018.



- Jacobs, T.: Ghawar vs. Permian Basin: Is There Even a Comparison?, in: *Journal of Petroleum Technology*, 2019.
- Karion, A., Sweeney, C., Kort, E. A., Shepson, P. B., Brewer, A., Cambaliza, M., Conley, S. A., Davis, K., Deng, A., Hardesty, M., Herndon, S. C., Lauvaux, T., Lavoie, T., Lyon, D., Newberger, T., Pétron, G., Rella, C., Smith, M., Wolter, S., Yacovitch, T. I., and Tans, P.: Aircraft-Based Estimate of Total Methane Emissions from the Barnett Shale Region, *Environmental Science & Technology*, 49, 8124-8131, 10.1021/acs.est.5b00217, 2015.
- Kort, E. A., Frankenberg, C., Costigan, K. R., Lindenmaier, R., Dubey, M. K., and Wunch, D.: Four corners: The largest US methane anomaly viewed from space, *Geophysical Research Letters*, 41, 6898-6903, 10.1002/2014gl061503, 2014.
- 770 Lyon, D. R., Alvarez, R. A., Zavala-Araiza, D., Brandt, A. R., Jackson, R. B., and Hamburg, S. P.: Aerial Surveys of Elevated Hydrocarbon Emissions from Oil and Gas Production Sites, *Environmental Science & Technology*, 50, 4877-4886, 10.1021/acs.est.6b00705, 2016.
- Maasakkers, J. D., Jacob, D. J., Sulprizio, M. P., Turner, A. J., Weitz, M., Wirth, T., Hight, C., DeFigueiredo, M., Desai, M., Schmeltz, R., Hockstad, L., Bloom, A. A., Bowman, K. W., Jeong, S., and Fischer, M. L.: Gridded National Inventory of U.S. Methane Emissions, *Environmental Science & Technology*, 50, 13123-13133, 10.1021/acs.est.6b02878, 2016.
- 775 Marchese, A. J., Vaughn, T. L., Zimmerle, D. J., Martinez, D. M., Williams, L. L., Robinson, A. L., Mitchell, A. L., Subramanian, R., Tkacik, D. S., Roscioli, J. R., and Herndon, S. C.: Methane Emissions from United States Natural Gas Gathering and Processing, *Environmental Science & Technology*, 49, 10718-10727, 10.1021/acs.est.5b02275, 2015.
- NMOCD: OCD Geographic Information Systems, in: New Mexico Oil Conservation Division, 2020.
- 780 Methane (CH₄) WMO Scale: https://www.esrl.noaa.gov/gmd/cc1/ch4_scale.html, 2015.
- Methane Intensity Target: <https://oilandgasclimateinitiative.com/action-and-engagement/provide-clean-affordable-energy/#methane-target>, 2020.
- Reed, S., and Krauss, C.: Too Much Oil: How a Barrel Came to Be Worth Less Than Nothing, in: *The New York Times*, 2020.
- Regulations, U. S. E. C. o. F.: eCFR Title 40 Section 98.233(n)(5), in, 2016.
- 785 Richardson, S. J., Miles, N. L., Davis, K. J., Lauvaux, T., Martins, D. K., Turnbull, J. C., McKain, K., Sweeney, C., and Cambaliza, M. O. L.: Tower measurement network of in-situ CO₂, CH₄, and CO in support of the Indianapolis FLUX (INFLUX) Experiment, *Elem Sci Anth*, 5, 59, 10.1525/elementa.140, 2017.
- Robertson, A., Edie, R., Field, R. A., Lyon, D. R., McVay, R., Omara, M., Zavala-Araiza, D., and Murphy, S. M.: New Mexico Permian Basin Well Pad Methane Emissions are a Factor of 6 – 13 Times Higher Than US EPA Estimates, *Environmental Science & Technology*, 2020.
- 790 RRC: Production Data, in, Railroad Commission of Texas, 2020.
- Siddans, R.: S5P Mission Performance Centre NPP Cloud [L2_NP_BDx] Readme, European Space Agency, 2020.
- Skamarock, W. C., Klemp, J. B., Dudhia, J., Gill, D. O., Barker, D. M., Duda, M. G., Huang, X.-Y., Wang, W., and Powers, J. G.: A description of the Advanced Research WRF version 3, NCAR Tech. Note NCAR/TN-475+ STR, 2008.
- 795 Skytruth: Global Flaring Map, in, 2020.
- Smith, M. L., Gvakharia, A., Kort, E. A., Sweeney, C., Conley, S. A., Faloona, I., Newberger, T., Schnell, R., Schwietzke, S., and Wolter, S.: Airborne Quantification of Methane Emissions over the Four Corners Region, *Environmental Science & Technology*, 51, 5832-5837, 10.1021/acs.est.6b06107, 2017.
- USEIA: Henry Hub Natural Gas Spot Price, United States Energy Information Administration, 2020a.
- 800 USEIA: Cushing, OK WTI Spot Price FOB, United States Energy Information Administration, 2020b.
- USEPA: Oil and Natural Gas Sector: Emission Standards for New, Reconstructed, and Modified Sources, in, 107, United States Environmental Protection Agency, 2019.
- USEPA: Inventory of U.S. Greenhouse Gas Emissions and Sinks: 1990-2018, United States Environmental Protection Agency, 2020a.
- 805 USEPA: GHG Reporting Program Data Sets, United States Environmental Protection Agency, 2020b.
- USGS: Landsat-8 data, United States Geological Survey, available at <https://www.usgs.gov/media/files/landsat-collection-1-level-1-product-definition>, last access: 31 7 2020
- Zavala-Araiza, D., Lyon, D., Alvarez, R. A., Palacios, V., Harriss, R., Lan, X., Talbot, R., and Hamburg, S. P.: Toward a Functional Definition of Methane Super-Emitters: Application to Natural Gas Production Sites, *Environmental Science & Technology*, 49, 8167-8174, 10.1021/acs.est.5b00133, 2015.
- 810



- Zavala-Araiza, D., Alvarez, R. A., Lyon, D. R., Allen, D. T., Marchese, A. J., Zimmerle, D. J., and Hamburg, S. P.: Super-emitters in natural gas infrastructure are caused by abnormal process conditions, *Nature Communications*, 8, 14012, 10.1038/ncomms14012, 2017.
- 815 Zhang, Y., Gautam, R., Pandey, S., Omara, M., Maasackers, J. D., Sadavarte, P., Lyon, D. R., Nesser, H., Sulprizio, M. P., Varon, D. J., Zhang, R., Houweling, S., Zavala-Araiza, D., Alvarez, R. A., Lorente, A., Hamburg, S. P., Aben, I., and Jacob, D. J.: Quantifying methane emissions from the largest oil-producing basin in the United States from space. *Science Advances*, 6, eaaz5120, 10.1126/sciadv.aaz5120, 2020.

Exhibit 23

Mobile Measurement System for the Rapid and Cost-Effective Surveillance of Methane and Volatile Organic Compound Emissions from Oil and Gas Production Sites

Xiaochi Zhou, Xiao Peng, Amir Montazeri, Laura E. McHale, Simon Gaßner, David R. Lyon, Azer P. Yalin, and John D. Albertson*



Cite This: <https://dx.doi.org/10.1021/acs.est.0c06545>



Read Online

ACCESS |



Metrics & More

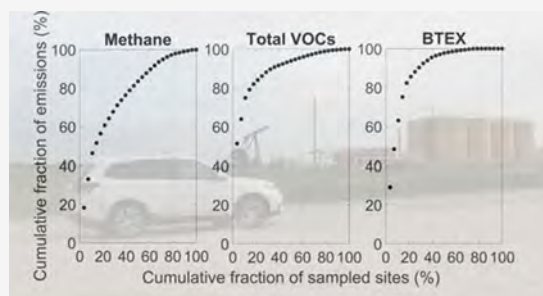


Article Recommendations



Supporting Information

ABSTRACT: In this study, a ground-based mobile measurement system was developed to provide rapid and cost-effective emission surveillance of both methane (CH_4) and volatile organic compounds (VOCs) from oil and gas (O&G) production sites. After testing in several controlled release experiments, the system was deployed in a field campaign in the Eagle Ford basin, TX. We found fat-tail distributions for both methane and total VOC (C4–C12) emissions (e.g., the top 20% sites ranked according to methane and total VOC (C4–C12) emissions were responsible for ~60 and ~80% of total emissions, respectively) and a good correlation between them (Spearman's $R = 0.74$). This result suggests that emission controls targeting relatively large emitters may help significantly reduce both methane and VOCs in oil and wet gas basins, such as the Eagle Ford. A strong correlation (Spearman's $R = 0.84$) was found between total VOC (C4–C12) emissions estimated using SUMMA canisters and data reported from a local ambient air monitoring station. This finding suggests that this system has the potential for rapid emission surveillance targeting relatively large emitters, which can help achieve emission reductions for both greenhouse gas (GHG) and air toxics from O&G production well pads in a cost-effective way.



1. INTRODUCTION

Methane is a potent greenhouse gas (GHG) and is the second most prevalent anthropogenic GHG after carbon dioxide.¹ In the United States, the oil and gas (O&G) sector is a large anthropogenic methane emission source, representing 28% of the total methane emissions in 2018.¹ A recent study found that methane emissions from the O&G sector were 60% higher than the United States Environmental Protection Agency (U.S. EPA) GHG inventory estimate, and the greatest discrepancy was in the O&G production segment with a 2-fold difference.² Meanwhile, the O&G sector is the largest industrial source of volatile organic compounds (VOCs) in the United States, contributing more than 3 million tons per year according to a 2014 estimate by the U.S. EPA.³ Some VOCs are hazardous air pollutants (e.g., benzene, toluene, ethylbenzene, and xylene, collectively known as BTEX) and may have direct health impacts for residents nearby O&G production sites.^{4–6} VOCs are also precursors of ground-level ozone.^{7–9} The U.S. EPA published the New Source Performance Standards (NSPS) in 2016, which included regulations for VOCs and methane from the production and processing segment of the O&G sector.¹⁰ In 2019, the U.S. EPA rescinded the methane requirement in the policy amendment, arguing that regulations for VOCs can simultaneously reduce methane emissions.¹¹ Some studies have found that methane and VOCs may originate from different sources onsite a O&G production well pad (e.g., separator and storage tank).^{12,13}

Therefore, the effectiveness of achieving methane and VOC emission reductions by only regulating VOC emissions remains to be examined from additional field measurements. Also, only regulating VOC emissions will be ineffective to reduce methane emissions from dry gas wells.

Considering the presence of the fat-tail distribution for both methane and VOC emissions^{13,14} and their spatiotemporal variability of emissions,^{15,16} routine emission surveillance that can quickly identify large emitters and prioritize mitigation can be a cost-effective way to achieve efficient overall emission reductions while providing complete coverage of all sites in a region of study. A robust and cost-effective measurement system with a short turnaround time is needed to perform such emission surveillance. Airborne- and ground-based measurement systems have been deployed to study methane and VOC emissions from O&G production well pads. Airplanes equipped with high-sensitivity real-time gas analyzers or imaging spectrometers can measure methane and/or VOC emissions.^{17–20} Constrained by

Received: September 28, 2020

Revised: November 20, 2020

Accepted: December 3, 2020



ACS Publications

© XXXX American Chemical Society

A

<https://dx.doi.org/10.1021/acs.est.0c06545>
Environ. Sci. Technol. XXXX, XXX, XXX–XXX

weather conditions and high operational cost, airborne measurements are often limited to deployment in ad hoc field campaigns. Drone-based systems are emerging as a relatively low-cost and rapidly deployable monitoring approach.^{21–24} However, their deployment can be limited by payload capacity as well as safety and regulatory-driven constraints on flight paths.

Leak detection and repair (LDAR) surveys following U.S. EPA Method 21²⁵ or using an optical gas imaging (OGI) camera²⁶ are ideal for component-level leak detection. However, they cannot provide leak quantification and are very time and resource intensive, thus tending to have infrequent return periods that open the possibility of long-duration problems prior to detection and mitigation. Ground-based mobile measurement systems have shown great potential for identifying and quantifying methane and VOC emissions from O&G production wells.^{27–29} Ground-based mobile measurements can host a wide range of equipment (from research grade to low-cost) and provide emission detection and quantification with high spatial resolution. The use of advanced real-time instruments for speciated VOC measurements requires dedicated personnel with specialized training,^{12,13,30} which becomes prohibitively expensive to operate routinely. A less expensive system was developed to make *stationary* downwind measurement using an advanced methane analyzer to trigger sampling of VOCs with SUMMA canisters.²⁹ Such a paired approach relies on favorable wind conditions and is most suited to situations where the methane and VOCs are emitted from the same source, which may not always apply to O&G production wells.^{12,13}

This study addresses the development and demonstration of a ground-based mobile measurement system that can perform rapid emission surveillance of both methane and VOCs from O&G well pads. Real-time measurements of methane and total nonspeciated VOCs were made by an advanced methane analyzer and a photoionization detector (PID), respectively. Two methods were proposed to supplement the nonspeciated PID measurements for VOC emission surveillance: one focuses on emission quantification using SUMMA canisters to sample air downwind from the individual well pads, the other one focuses on rapid surveillance of multiple well pads using data obtained from nearby ambient monitoring stations. Bayesian inference was applied to estimate emission rates using repeated downwind plume measurements.^{27,31,32} The system was first tested in a series of controlled release experiments and then deployed to measure O&G production well pads in the Eagle Ford basin, TX. The Eagle Ford basin is one of the largest oil fields in the United States; and the state of Texas emitted the largest amount of VOCs among all 50 states according to the 2014 National Emission Inventory.³ Several studies have quantified regional hydrocarbon emissions from the Eagle Ford basin using monitoring towers or airplane,^{33–35} while only a few studies estimated emissions from individual well pads.²⁹ Elevated ambient BTEX mixing ratios were observed near unconventional O&G production well pads in the Eagle Ford basin; however, BTEX emission rates were not quantified.³⁶ Here, we present methane and VOC emissions from well pads to test the ability of rapid and cost-effective emission surveillance for both methane and VOCs, to improve our understanding of emissions in this region, and to discuss the implication for reduction strategies for both methane and VOCs.

2. MATERIALS AND METHODS

A mobile measurement system was developed to measure methane and VOC emissions from O&G production well pads

using a dedicated methane analyzer and a photoionization detector (PID) supplemented by SUMMA canisters for VOCs. A sport utility vehicle (SUV) was utilized as the mobile measurement platform (MMP), outfitted with a roof-mounted GPS unit (Trimble Geo 7X handheld from Trimble Inc., Sunnyvale, CA) to track its real-time position. The GPS unit samples at 1 Hz frequency, with an accuracy of 5–15 cm for >98% data points after postprocessing.

Two high-precision methane analyzers were used in this study: a research-grade open-path analyzer^{37,38} was used in the controlled release experiment and for development of methods, while a commercial close-path analyzer was used in the subsequent field campaign (Picarro G2301 from Picarro Inc., Santa Clara, CA). Both analyzers employ the laser-based cavity ring-down spectroscopy (CRDS) technique, which is a laser absorption method that derives improved sensitivity from a high-finesse optical cavity. The research-grade open-path analyzer has been quantitatively validated against a reference instrument and has been successfully used in the field for hundreds of hours.³⁸ The commercial Picarro methane analyzer has been successfully deployed in many vehicle-based field studies with robust performance.^{31,39–41} A PID was used to measure VOCs at the ppb level (Falco from Ion Science, Cambridge, U.K.). PID is nonselective and therefore responds to a broad range of VOCs with different response factors.⁴² In this study, a 10.6 eV lamp was used, which is fairly robust and sensitive to many VOCs often found in O&G production sites.^{12,39,43} According to the manufacturer, the detector used by Falco (miniPID 2 PPB) has good linearity over its full range (0–50 ppm) and can operate across a wide range of relative humidity conditions (0–99%, noncondensing).⁴⁴ However, it is not responsive to ethane and propane, two commonly observed VOCs from O&G productions.

To supplement PID measurements, air samples were taken by 3.2 L SUMMA canisters to provide speciated mixing ratios of VOCs from plumes emitted from the upwind O&G well pads. For each sample, the field technician held the canister steady with its position above and upwind of his/her head and kept the valve open for approximately 1 min.³⁹ For each sampled site, mixing ratios of 61 nonmethane hydrocarbons (C2–C12) were analyzed from the SUMMA canister by a commercial analytical lab following the EPA's TO-3 method, with a sampling precision within $\pm 5\%$ and a sampling accuracy within $\pm 10\%$.⁴⁵ It should be noted that the reporting limits for C2–C12 VOCs are in the range of 0.5–3 ppb (Supplemental Information B), which are much higher than research grade labs (e.g., 3 ppt).^{39,46} Among others, it includes speciated C4–C12 alkanes and C6–C9 aromatics. These VOCs are selected since they are mostly oil and NG production-related compounds. A previous study analyzed 58 nonmethane VOCs (56 of 58 are included in this study) and found that the combined mixing ratio of unknown compounds is <5% of the sum of the 58 nonmethane VOC mixing ratios.²⁹ Emissions of another two common VOCs, formaldehyde and methanol, have been detected from O&G production well pads.^{12,39} However, they are not selected for lab analysis since they are not detectable by the PID using the 10.6 eV lamp. VOC mixing ratios from all of the SUMMA canisters are summarized and included in the Supplemental Information A (Table S1). For rapid emission surveillance, time-averaged VOC data reported by local ambient air monitoring stations using automated gas chromatography (auto-GC) was used when canister data were not available. Due to the difference in sampling strategies, data from the local stations are used to

understand regional VOC mixing ratios, whereas data from canister samples can better capture emissions from individual well pads. Time synchronization was performed to correct for sampling line delay of the methane analyzer and the PID.

Before the onset of the field campaign, 53 candidate well pads were selected following the criteria that they are less than 150 m upwind of public roads and more than 150 m from other potential emission sources (e.g., other well pads or processing stations) using Google Earth. In addition, we ensured good road access for all of the candidate well pads and scheduled field sampling based on daily meteorological and road conditions (e.g., well pads with accessible road on the east side would be sampled with the prevailing wind from west). For each candidate well pad, three downwind mobile passes were first performed with GPS located methane and PID signals recorded. The MMP drove as slow as 5 m/s to capture the spatial structure of the downwind plume.⁴⁷ The vehicle was moving almost perpendicular to the prevailing wind direction, which was visually determined by the windsocks installed on the well pads and later confirmed using wind data collected by the sonic anemometer. If elevated methane mixing ratios (>0.2 ppm above background) were detected during the first three passes, the well pad was then identified for further investigation. Out of the 53 candidate well pads, a total of 28 well pads were identified for further study. The identification process is designed to help locate relatively strong sources and to improve the detectability of speciated VOCs collected by the downwind canister samples. However, it certainly excludes candidate well pads with small emissions from further investigation and this must be considered in the statistical interpretations (e.g., sampling roughly the top half of the emitters).

For each of the 28 identified well pads, additional downwind passes (at least 10) were conducted and a representative air sample was taken using a SUMMA canister. Meanwhile, wind speed, wind direction, and air temperature were measured near the identified well pad using a two-dimensional (2D) sonic anemometer (WindSonic 60 from Gill Instruments, Hampshire, U.K.). The sonic anemometer was mounted on a portable meteorological tower (~1.6 m aboveground), which was installed in a relatively flat and open location near the identified well pad. In future applications, one could integrate the sonic anemometer onto the MMP to evaluate wind speed in real time and at the exact sensor location.⁴⁸

2.1. Emission Rate Estimation. A previously developed Bayesian inference approach was adopted to quantify the emission rates of methane and VOCs from the identified well pad.^{27,31,32} Following Bayes' theorem, the posterior probability density function (pdf) of the emission rate Q given the observation of C (either measured methane mixing ratio C_{CH_4} or inferred mixing ratio of the i th VOC, C_i) and the ancillary information including the prevailing meteorological conditions (I) is

$$P(Q|C_y, I) = \frac{P(Q|I)P(C_y|Q, I)}{P(C_y|I)} \quad (1)$$

where C_y [ppm × m] is the cross-plume integrated above-ambient mixing ratios. Practically, C_y can be estimated as $C_y = \sum C_a \Delta x$, where C_a is the above-ambient mixing ratios and Δx [m] is the distance between the geo-referenced mixing ratio data points corrected for nonperpendicular angle of traversal. C_a is calculated as: $C_a = C - C_b$, where C is the raw mixing ratios (C_{CH_4}

for methane and C_i for VOCs) and C_b is the background mixing ratios. C_b was estimated as the fifth percentile of the ranked time series of $C_{CH_4}(t)$ and $C_i(t)$ for methane and the i th VOC, respectively.^{27,28} Real-time methane mixing ratios, $C_{CH_4}(t)$, can be readily measured by the onboard methane analyzer. Time-resolved and speciated VOC mixing ratios can be inferred from fusing the real-time PID readings and the SUMMA canister sample, by assuming that the plume chemical composition remains unchanged during the mobile sampling period (~30 min), and most VOCs contributing to the elevated PID signal were analyzed from the SUMMA canisters

$$\frac{C_i(t)/RF_i}{CP(t)} = \frac{CC_i/RF_i}{\sum_i CC_i/RF_i} \quad (2)$$

where t is the time, $C_i(t)$ is the inferred mixing ratio for the i th VOC, $CP(t)$ is the total nonspeciated VOC mixing ratio reported by the PID, CC_i is the mixing ratio for the i th VOC in the SUMMA canister, and RF_i is the PID's response factor for the i th VOC provided by the manufacturer.⁴² RF_i of VOCs are referenced to isobutylene ($RF_i = 1$). The greater the RF_i is, the less sensitive the PID is to the particular VOC.

Assuming that the prior knowledge of Q is limited to its upper and lower bound (Q_{\max} and Q_{\min} , respectively), a uniform distribution is adopted for $P(Q|I)$ as a noninformative prior.³¹ After the first sensor pass (with a valid measurement of C_y), eq (1) is updated recursively such that $P(Q|I)$ is replaced each time by the posterior pdf $P(Q|C_y, I)$ derived from the previous sensor pass.

$$P(Q|I) = \begin{cases} 1/(Q_{\max} - Q_{\min}), & j = 1 \\ P(Q|C_y, I)_{j-1}, & j > 1 \end{cases} \quad (3)$$

where j is a counter for successive sensor passes.

A Gaussian form of the likelihood function is adopted following previous studies^{27,31,49}

$$P(C_y|Q, I) = \frac{1}{\sigma_e \sqrt{2\pi}} \exp \left(-\frac{1}{2} \left(\frac{C_y - C_y^M(Q)}{\sigma_e} \right)^2 \right) \quad (4)$$

where $C_y^M(Q)$ is the modeled C_y as a function of the candidate emission rate Q . σ_e is the "error scale" that represents a measure of the uncertainty when comparing the modeled $C_y^M(Q)$ against the measurement C_y . The parameterization of σ_e is detailed elsewhere.³¹ A simple passive scalar plume model is used for $C_y^M(Q) = Q/\bar{U}D_z$ ²⁷ where \bar{U} is the plume advection speed and D_z represents the plume vertical dispersion. D_z can be estimated using the semianalytical relation⁵⁰ $D_z = \frac{A}{\bar{z}} \exp \left[-\left(\frac{Bz}{\bar{z}} \right)^s \right]$, where z [m] is the height of the sensor inlet, \bar{z} [m] is the mean plume height, and A , B , and s are unitless empirical parameters of atmospheric stability and \bar{z} .

By updating the prior term $P(Q|I)$ with the posterior ($P(Q|C_y, I)$) derived from the previous sensor pass, $P(Q|C_y, I)$ is calculated recursively to incorporate data collected after each pass and reflect the total weight of the data collected up to that point in time. After the final sensor pass, the estimated leak rate and the associated uncertainty can be estimated by the mode (Q_e) and standard deviation (σ_Q) of $P(Q|C_y, I)$, respectively.³¹

Table 1. Summary of Controlled Release Experiments, Including the Experiment Number (Exp No.), Emission Source, Controlled Emission Rate ($Q_0 \pm \sigma_Q$), Mean Downwind Distance (x_m), Number of Downwind Mobile Passes (N_p), Averaged Meteorological Data Reported by Two Nearby Weather Stations, Including the Mean Wind Speed (\bar{U}), Mean Wind Direction (θ_m) Clockwise from the North, and the Estimated Emission Rate ($Q_e \pm \sigma_Q$)

exp no.	emission source	controlled emission rate ($Q_0 \pm \sigma_Q$), in scfh	mean downwind distance (x_m), in m	number of downwind passes (N_p)	mean wind speed (\bar{U}), in m/s	mean wind direction (θ_m), in deg	estimated emission rate ($Q_e \pm \sigma_Q$), in scfh
1	separator prv	18.57 \pm 1.79	103.5	10	1.97	131	21.5 \pm 4.6
2	separator prv	45.03 \pm 4.71	87.4	13	1.51	102	50.1 \pm 9.4
3	tank thief hatch	62.53 \pm 3.00	87.6	14	1.43	84	61.4 \pm 15.4
4	tank thief hatch	78.76 \pm 2.53	92.4	15	1.35	73	71.8 \pm 14.1

$$Q_e = \text{argmax}(P(Q|C_y, I))$$

$$(\sigma_Q)^2 = \int (Q - Q_{\text{Exp}})^2 \times P(Q|C_y, I) dQ \quad (5)$$

where $Q_{\text{Exp}} = \int Q \times P(Q|C_y, I) dQ$ is the expectation of the posterior pdf.

The emission rates of VOCs that are not detected by PID but are analyzed in the SUMMA canister air sample can be estimated using a ratio method^{29,40}

$$\frac{Q_{e,n}}{\sum_i Q_{e,i}} = \frac{CC_n * MW_n}{\sum_i CC_i * MW_i} \quad (6)$$

where MW is molecular weight and the subscript n denotes the n th VOC that was not detected by PID but was later found from the SUMMA canister sample. Although C2–C12 VOCs were analyzed by the SUMMA canister, C2–C3 were either not sensitive to PID (e.g., acetylene, ethane, and propane) or found to be below detection limit (i.e., propene) from all of the SUMMA canisters. Therefore, eq 6 will only be used to infer C4–C12 VOCs.

Some of the observed well pads are quite complex with pump jacks, separators, dehydrators, storage tanks, and flare stack, while others have much less equipment on site. When multiple O&G-related equipment were present on a well pad, they were geo-located using Google Earth (later confirmed by field notes) and $P(Q|C_y, I)$ were estimated individually. Following Zhou et al.,⁴⁷ the probability of emissions was assumed to be equal for each equipment group; the probability of emission rates for the identified well pad can be estimated by integrating the $P(Q|C_y, I)$ over all of the equipment groups.

2.2. Controlled Release Testing. The Methane Emission Technology Evaluation Center (METEC) at Colorado State University (CSU) was purpose-built to represent typical O&G facilities, such as production well pads, gathering facilities, and underground distribution pipelines.⁵¹ On-site equipment is outfitted with gas release point(s) to mimic real-world NG emission scenarios, such as vented emissions (e.g., pneumatic devices) and fugitive emissions (e.g., seals, fittings, flanges, etc.). A central control system manages flowrates at all release points allowing emissions to vary over time to meet the specification of the test. Considering the slow chemical reaction rate of VOCs and methane in ambient temperature and pressure compared to the travel time from source to sensor, both can be considered as conserved passive scalars during the downwind measurement periods (typically <half an hour). Since they follow the same principles of plume transport, we contend that the methodo-

logical performance for methane emission can be readily applied to that for VOC emissions.

Meteorological data were obtained from two nearby weather stations (both within 500 m from METEC) operated by the Colorado Agricultural Meteorological network (CoAgMet). More specifically, wind speed and direction were measured by a wind anemometer and a wind vane (Wind Sentry from R.M. Young Company, Traverse City, Michigan). The air temperature was measured by a temperature and relative humidity probe (HMP45C-L from Vaisala, Vantaa, Finland). Both stations report time-averaged meteorological data once every 5 min. To better represent meteorological conditions at METEC, the averaged meteorological data recorded by the two stations are used here.

On August 30, 2017, a series of six controlled release experiments were performed at METEC. Each experiment lasted about 20 min, with emissions from the pressure release valve (prv) of the separator and the thief hatch of the storage tank. Two experiments were excluded due to low wind speed (<1 m/s) and high turbulent intensity (the ratio of wind gust to mean wind speed >2).³² Consequently, four experiments are available for further analysis, and their experimental conditions are summarized in Table 1.

We first evaluate results obtained from the controlled release experiments. As shown in Table 1, emission rates estimated using the Bayesian inference (Q_e) are fairly close to the controlled emission rate (Q_0), with Q_0 within $Q_e \pm \sigma_Q$ for all four experiments. The percentage error (i.e., $(Q_e - Q_0)/Q_0$) ranged from −8 to 15% with an average of bias of 5%, suggesting a solid model performance. The relatively large uncertainty for Q_e is partly due to the low-resolution wind data (5 min acquisition frequency) that has increased the uncertainty in the plume modeling. The same approach has been tested in multiple controlled release experiments with simplified experimental settings and showed good performance with averaged percentage error <10%.^{27,32,47} A recent study showed a good agreement between methane emissions of several fertilizer plants measured by a MMP using the abovementioned Bayesian inference³¹ and airborne mass balance approach.⁵² Another study found that leaky well pads detected by an OGI camera, which could not quantify emission rates, were all identified by a MMP with emission rates quantified by the Bayesian inference approach.⁴⁷ The good agreements between the MMP and other methods (i.e., airborne and OGI camera) in field measurements further improve our confidence in the skills of the Bayesian inference approach.

2.3. Field Campaign. A 1 week field campaign was conducted from March 17 to 24, 2018, to characterize emissions

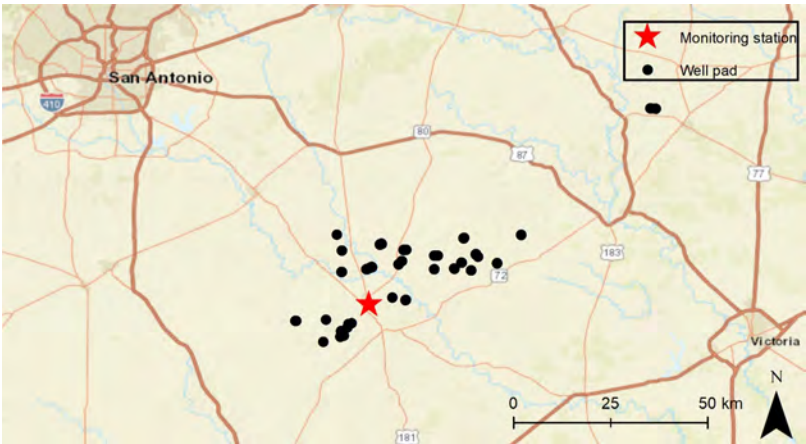


Figure 1. Map of the identified O&G well pads and the local ambient air monitoring station.

Table 2. Summary of Sampled Well-Pad ID, Sampling Date, Time, Mean Downwind Distance (x_m), Number of Downwind Mobile Passes (N_p), Mean Wind Speed (\bar{U}), and Mean Wind Direction Clockwise from the North (θ_m)^a

well-pad ID	date	local standard time	mean downwind distance (x_m), in m	number of downwind passes (N_p)	mean wind speed (\bar{U}), in m/s	Mean wind direction (θ_m), in deg
1	03/17/2018	12:45–13:21	125	16	2.7	164
2	03/17/2018	14:15–14:44	132	18	3.8	149
3	03/17/2018	14:44–15:13	165	17	3.7	144
4	03/17/2018	15:14–15:42	210	17	3.3	138
5	03/17/2018	16:52–17:27	118	23	3.3	122
6	03/17/2018	17:28–18:02	81	23	4.3	139
7	03/18/2018	15:28–15:45	137	11	2.9	143
8	03/18/2018	16:36–17:04	155	12	3.9	132
9	03/19/2018	10:43–11:15	107	18	4.6	339
10	03/19/2018	11:47–12:16	141	17	2.3	316
11	03/19/2018	14:55–15:20	97	21	3.1	321
12	03/19/2018	16:09–16:32	50	16	2.8	315
13	03/19/2018	16:55–17:20	51	16	2.5	327
14	03/20/2018	12:04–12:43	90	16	2.8	347
15	03/20/2018	12:04–12:43	107	16	2.8	347
16	03/21/2018	11:04–11:33	240	12	3.4	106
17	03/22/2018	10:20–10:44	85	10	4.9	153
18	03/22/2018	10:44–11:07	43	12	4.9	153
19	03/22/2018	13:07–13:57	149	15	4.3	152
20	03/22/2018	16:48–17:18	115	10	6.3	144
21	03/22/2018	16:48–17:18	128	10	6.3	144
22	03/23/2018	10:50–11:19	89	17	5.0	152
23	03/23/2018	12:43–13:03	80	15	4.1	145
24	03/23/2018	15:10–15:38	120	13	4.2	144
25	03/23/2018	17:13–17:46	104	11	5.0	150
26	03/23/2018	17:13–17:46	192	10	5.0	150
27	03/24/2018	07:37–08:00	171	10	1.7	161
28	03/24/2018	08:00–08:23	95	10	2.1	161

^a x_m , \bar{U} , and θ_m are averaged from data collected when sampling each well pad.

of methane and VOCs from active horizontally drilled O&G well pads located in Karnes and DeWitt County, which are part of the Eagle Ford Basin, TX (Figure 1). All of the identified well pads are in open and relatively flat shrubland/grassland. No other known methane and VOC emission sources, such as dairy farms, landfills, or non-O&G stationary combustion sources (e.g., boilers and heaters), were observed during the field campaign. In addition, all measurements were conducted in the absence of upwind mobile combustion sources (e.g., pick-up trucks) to avoid VOC emission interference.

Sampling conditions of the 28 identified active O&G well pads (out of the 53 candidate well pads) are provided in Table 2. No field experiments were excluded due to low wind speed and high turbulent intensity conditions since the mean wind speed (\bar{U}) > 1 m/s for all well pads in Table 2. A neutral atmospheric condition was assumed based on climatological analysis of a nearby flux tower, and sensitivity analysis showed that the estimated emission rates were only slightly affected (<5%) by typical variability of atmospheric stability in this region. For future application, measurements of local atmospheric stability

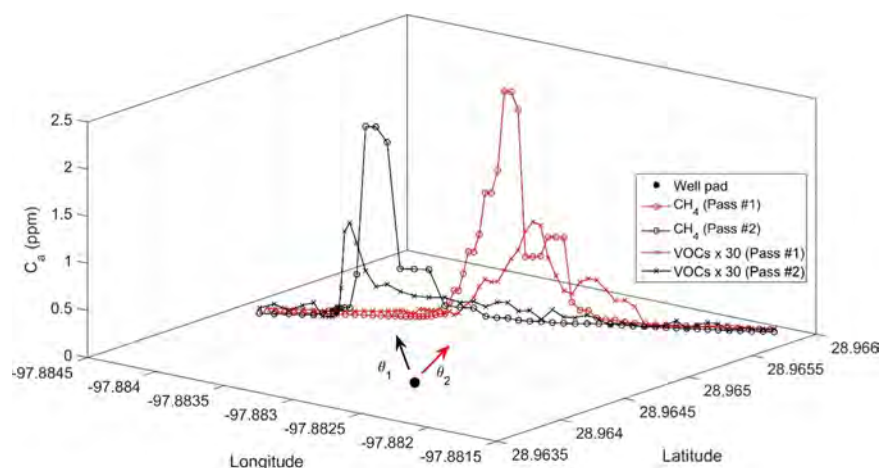


Figure 2. Examples of above-ambient mixing ratios (C_a) for methane and total nonspeciated VOCs measured by the PID (multiplied by a factor of 30 for visual interpretation) at 1 Hz sampling frequency. The vehicle drove from northeast to southwest (left to right on the figure) for Pass #1 at ~ 5.3 m/s and from southwest to northeast (right to left on the figure) for Pass #2 at ~ 5.7 m/s. Pass #1 and Pass #2 are collected on 03/17/2018, from 12:57:16 to 12:58:22 and from 13:10:20 to 13:11:21, respectively.

(i.e., using a three-dimensional (3D) sonic anemometer) would readily remove this aspect of the uncertainty related to plume dispersion modeling. Sometimes multiple well pads were located along the same road and were sampled sequentially in a single downwind mobile measurement (e.g., well pad #14 and #15 in Table 2). For each well pad, at least one whole air sample was collected using a 3.2 L SUMMA canister downwind from the target well pads. All of the SUMMA canister sample data are included in the Supplemental Information B.

To ensure the sensor performance, three-point calibrations were performed every other day during the field campaign. The isobutylene gas (1 and 10 ppm) was used to calibrate the PID as recommended by the manufacturer.⁴² We found consistent and satisfactory performance for the PID and the methane analyzer, with little drift and good accuracy ($<8\%$ for PID and $<1.5\%$ for methane analyzer at calibration points) during the field campaign. Linear regression curves were established for both sensors (with $R^2 > 0.95$) to postprocess the data.

Ambient VOC data was reported by an auto-GC in a local air monitoring station located in Karnes City, TX, which is within 50 km from most of the identified well pads (Figure 1). Hourly averaged mixing ratios of 46 nonmethane VOCs were measured at the station, 42 out of 46 were also analyzed by the SUMMA canisters, omitting propylene, 1,3-butadiene, isoprene, and *t*-2-butene from the overlap.⁵³

3. RESULTS AND DISCUSSION

For C4–C12 VOCs, around 70% (39 out of 56) can be detected by the PID with a measured response factor. The remaining 30% C4–C12 VOCs could not be accurately measured by the PID, and their emissions can only be inferred using canister data (eq 6). It was found that the combined mixing ratio of those nondetectable VOCs was $<2\%$ of the total C4–C12 mixing ratio averaged over all canister samples. This result supports the use of PID for VOC (C4–C12) measurements from the well pads in oil and wet gas basins such as the Eagle Ford.

The average background methane mixing ratio found throughout the study was 1.92 ± 0.02 ppm. In March 2018, the monthly average methane mixing ratio at Mauna Loa, Hawaii was 1.87 ± 0.02 ppm. The higher background methane mixing ratio measured in the field is partly caused by the regional enhancement, as found in previous studies.³⁹ This also applies to

the estimated background VOC mixing ratios, which were higher than the measured VOC mixing ratios from the local ambient air monitoring stations. To test the hypothesis that the plume VOC compositions remained relatively unchanged during the mobile sampling period (~ 30 min), multiple SUMMA canister samples were taken consecutively downwind from two well pads. It was found that the composition of various VOCs (represented as the percentage of total mixing ratios) sampled from the different canisters were very close (maximum difference $<5\%$), which provides support for the hypothesis. More details about the tests can be found in the Supplemental Information A (Section S2).

3.1. Emission Rate Estimation. We present an example of the measurements made on March 17, 2018 in Figure 2 (Well pad ID #1 from Table 2), showing the above-ambient mixing ratio of methane and total nonspeciated VOCs measured along two downwind passes. The start and end of the driving route were determined such that the measured mixing ratios were close to ambient mixing ratios, as shown in Figure 2. Methane and total nonspeciated VOC plumes were both observed during both passes, though plume centers were not entirely overlapped (i.e., the location of the peak methane and VOC mixing ratios were offset by 3 and 4 s for pass #1 and #2, respectively). We postulated that small offsets may be caused by the difference in response time (e.g., time to reach 90% of the actual mixing ratios or t_{90}) for the methane analyzer (<3 s) and the PID (<10 s). Due to the meandering of the wind (as suggested by the instantaneous wind directions θ_1 and θ_2 for passes 1 and 2, respectively), the plume shifted between passes.

The inferred emission rates for methane and two examples of VOCs (i.e., *i*-butane and toluene) are plotted in Figure 3. The results for all of the detectable VOCs are included in the Supplemental Information A (Section S3). For all three compounds, the posterior pdfs $P(Q|C_y, I)$ tend to “sharpen” with additional downwind passes, from a relatively broad pdf (e.g., the black dash lines representing the pdf after the first pass) to a narrower pdf (e.g., the solid red lines representing pdf after the final pass). Estimation uncertainty, which can be visually interpreted as the width of the pdf, was gradually reduced especially after the first several passes. This result clearly illustrates the capability of the recursive Bayesian inference

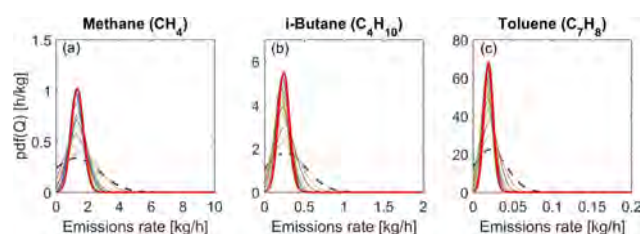


Figure 3. Posterior probability of emission rate Q , $P(Q|C_y, I)$, derived from the Bayesian inference for (a) methane, (b) *i*-butane, and (c) toluene. The black dash lines represent the $\text{pdf}(Q)$ after the first pass, and the red solid lines are the $\text{pdf}(Q)$ after the final pass.

model, which sharpens its lens on the underlying hidden variables as successive measurement passes are obtained.

We compared the emissions estimated using VOC mixing ratios obtained from the SUMMA canisters with those derived from directly adopting the local ambient air monitoring station mixing ratios (Figure 4). The station-based emissions were estimated by replacing the term CC_i (the mixing ratio for the i th VOC in the SUMMA canister) in eq 2 with the mixing ratio of the i th VOC reported by the local ambient air monitoring station. As expected, the station-based estimates differed somewhat from the canister-based estimates, since the latter fail to capture well pad-specific VOC mixing ratios. The canister-based emission estimates for VOCs will be used in the following analysis, as they certainly reflect more accurate and localized information. Considering the wide range of emissions for total VOCs (C4–C12) and BTEX, their correlations were evaluated using the Spearman's rank correlation coefficient (Spearman's R), which were less affected by the large values. A strong correlation was found between the station-based and canister-based emission estimates for C4–C12 total VOCs (Spearman's $R = 0.84$), while the correlation becomes weak for BTEX (Spearman's $R = 0.69$). This result indicates that VOC mixing ratios reported by local ambient air monitoring stations may be useful to identify relatively large VOC emitters, thus enable rapid surveillance for VOC emissions.

3.2. Emission Rate Distributions and Their Correlations. The emissions of methane, total VOCs (C4–C12), and BTEX from the 28 identified well pads are plotted in Figure 5. Due to the fat-tail distributions for the emission rates, both

arithmetic and geometric means are reported and their 95% confidence intervals (CIs) are calculated using bootstrapping.⁵⁴ Since the arithmetic means are more affected by the large values in the sample, it is generally higher than the geometric means as shown in Figure 5. The overall measured emissions showed variability ranging over several orders of magnitudes. Excluding the three outliers, the methane emissions range from 0.6 to 12.9 kg/h, which is comparable to the methane emissions of 0.4–10 kg/h estimated previously from a small number of well-pad measurements ($N = 4$) conducted in the Eagle Ford basin.²⁸ The three outliers (i.e., representing the largest emitters) are well within the measured outliers in other studies ranging from 10 to >300 kg/h, as summarized by Omara et al.⁵⁵ The arithmetic mean emissions (95% CI) of methane is 8.6 (5.3–12.9) kg/h, which is higher than the site-level emissions found in other O&G production basins in the United States, except for the Marcellus Basin (~9 kg/h).⁵⁵ This is likely caused by the fact that we only sampled the top ~50% of well pads with relatively large emissions (i.e., 28 out of the 53 candidate well pads), while missing well pads would be expected to have much lower emissions.

The total VOC (C4–C12) emissions exhibited the greatest intersite variability (compared to methane and BTEX), ranging from 0.1 to >100 kg/h. The geometric mean (95% CI) of the total VOC (C4–C12) emission is 2.8 (1.6–4.6) kg/h, which is close to the geometric mean emission of total VOCs (C2–C12) in Anadarko, Barnett, and Permian Basin (2.5–10.6 kg/h)⁵⁶ but higher than the geometric mean emission of total VOCs (C3–C12) found in the Barnett, Denver-Julesburg, and Pinedale Basins (0.2–0.9 kg/h).²⁹ Since C2–C3 VOCs are excluded from our analysis, the total VOC (C2–C12) emission is expected to be even higher considering that the averaged mixing ratios of C2–C3 combined is ~60% of the total mixing ratios in canister samples.

The median BTEX emission is estimated to be 0.05 kg/h, which is close to that found in Upper Green River Basin (UGRB) (~0.06 kg/h)¹³ and the Barnett Basin (0.05 kg/h).⁴⁰ The geometric mean (95% CI) of BTEX emissions is 0.1 (0.03–0.3) kg/h, which is also similar to the geometric mean (95% CI) of 0.05 (0.03–0.08) kg/h from several O&G Basins.²⁹ In contrast, the arithmetic mean (95% CI) of BTEX emission is 0.4 (0.1–0.6) kg/h, which is much higher than the arithmetic mean

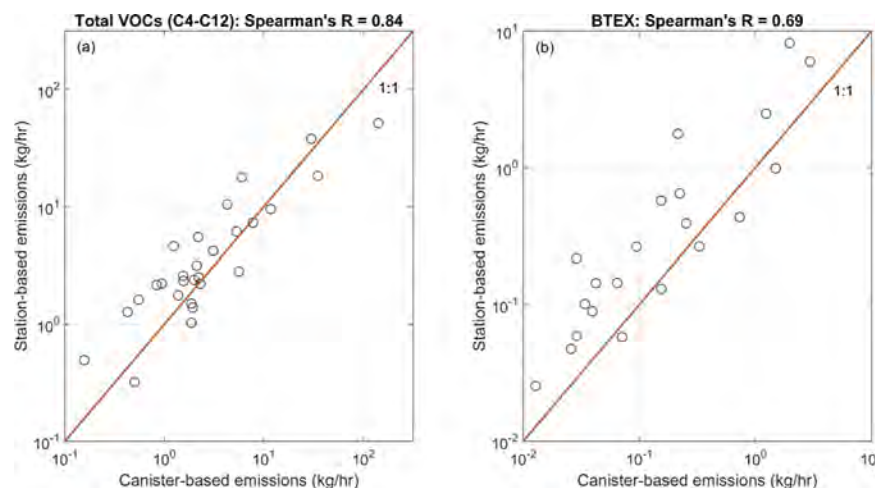


Figure 4. Estimated emission rates using SUMMA canisters and local ambient air monitoring stations for (a) total VOCs (C4–C12) and (b) BTEX. The Spearman's rank correlation coefficients (Spearman's R) are estimated. The red lines are the 1:1 line.

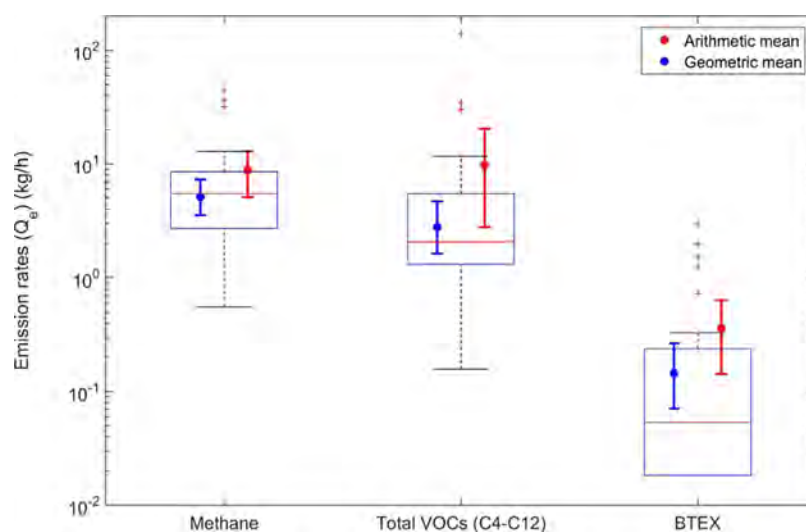


Figure 5. Estimated emission rates (Q_e) for methane, total VOCs (C4–C12), and BTEX across all of the sampled well pads. The results are presented as boxplots, with red lines indicating medians, and the bottom and top edges of the boxes indicating the 25th and 75th percentiles, respectively. The whiskers extend to the most extreme data points not considered as outliers, and the outliers are plotted as red crosses. The arithmetic means and geometric means of Q_e are shown in red and blue along with their 95% CIs, respectively.

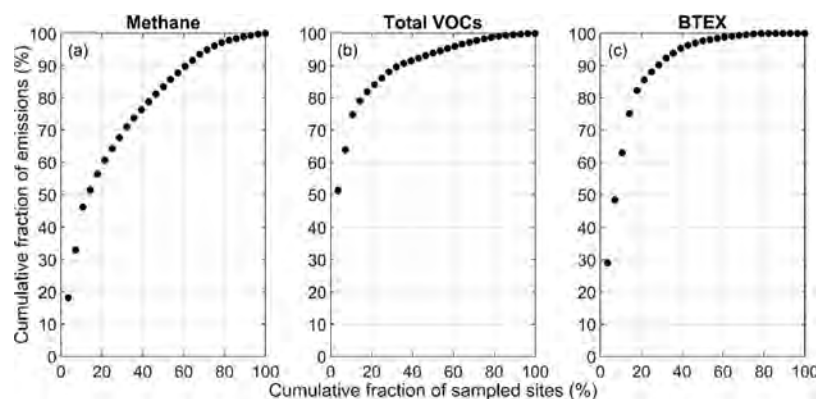


Figure 6. Cumulative fraction of emissions for (a) methane, (b) total VOCs (C4–C12), and (c) BTEX as a function of the cumulative fraction of the sampled well pads (rank ordered).

of 0.09 (0.003–0.38) kg/h found in UGRB.¹³ We hypothesize that the great discrepancy is partly caused by the presence of several large BTEX emitters found in this study since we focused on the top ~50% emitters. Previous work has found that the mean methane emissions (both absolute and production-normalized) were higher in the Eagle Ford Basin than that in the UGRB.⁵⁵ It is also possible that the variations between study areas relate to composition oil and gas and the O&G production for those well pads.

The cumulative fraction of total emissions was plotted as a function of the cumulative fraction of the sampled well pads, ranked from large to small emitters (Figure 6). For methane, the top 20% of the total number of sampled well pads were responsible for roughly 60% of total emissions. This is similar to studies in the Barnett and Marcellus basin, where 20% of sources were found to be responsible for 60–90% of emissions.^{57,58} A similar pattern is observed for VOCs and BTEX, such that the top 20% of the total number of sampled well pads represented roughly 80% of total emissions. This is slightly more skewed than the observed distribution in the UGRB, where the top 20% of sites were responsible for 67% of BTEX emissions.¹³ Again, the fact that this study focused on the top ~50% emitters would naturally reduce the skewness as compared to an unbiased

sampling. More importantly, an overlap was found between large emitters, such that the top 20% well pads ranked according to methane emissions were responsible for 79% of total VOCs (C4–C12), 78% BTEX, and 60% methane emissions. This finding showed that controlling the large emitters (i.e., the top 20%) could be a viable and cost-effective way to achieve emission reductions for both GHG and air toxics (e.g., BTEX) from O&G production well pads.

A good correlation was observed between methane and C4–C12 total VOCs (Spearman's $R = 0.74$), suggesting that emission controls may help reduce both methane and C4–C12 VOCs in oil and wet gas basin such as the Eagle Ford Basin. Relatively weak correlations were found between BTEX and methane (Spearman's $R = 0.47$) and between BTEX and total C4–C12 VOCs (Spearman's $R = 0.35$). We further explored the correlation between BTEX emission and others by introducing the combined C6–C10 VOCs, which are often considered to be gasoline range organics (GRO) or volatile petroleum hydrocarbons (VPH).⁵⁹ A correlation of Spearman's $R = 0.64$ was found between VPH and BTEX, which is superior to the correlations between BTEX and others shown in Table 3. Since VPH are often related to crude oil extraction processes, this

result indicates that BTEX emissions are likely caused by the oil production and processing on the well pads.

Table 3. Spearman's Rank Correlation Coefficient (Spearman's R) between Emissions of Methane, Total VOCs (C4–C12), and BTEX

	methane	total VOCs (C4–C12)	BTEX
methane	1	0.74	0.47
total VOCs (C4–C12)		1	0.35
BTEX			1

3.3. Sensitivity Analysis of Emissions Against Production Data. Well-pad level production statistics were obtained from the national database with data updated for the year 2018.⁵⁵ A sensitivity analysis was performed to explore the possible dependence of measured emission rates on daily NG production (in thousands of cubic feet per day or Mcf/d), daily liquid (combined oil and condensate) production (in barrels per day, or bbl/d), and daily produced water (in bbl/d). The results are included in Supplemental Information A (Section 4). Since all of the sampled well pads are fairly new (production age ranges from 0.9 to 8.3 years, with an average of 5.7 years), we do not expect any correlation between the age of well pads and the measured emissions. Little dependences were found between the emissions and production statistics, with all $R^2 < 0.1$. This result is consistent with previous studies^{12,28,60} and suggests that a considerable portion of emissions may be fugitive in nature.

4. DISCUSSION

A ground-based mobile measurement system was developed to detect and quantify methane and VOC emissions from O&G well pads using downwind plume measurements. The system was validated in controlled release experiments and successfully deployed to measure methane and VOC emissions from several O&G production well pads in the Eagle Ford basin, TX. A fat-tail distribution was found such that a small fraction of well pads were responsible for most emissions of methane and VOCs. Meanwhile, a good correlation was found between methane and total VOC (C4–C12) emissions (Spearman's $R = 0.74$). More importantly, ~60% methane emissions and ~80% VOC and BTEX emissions can be reduced by controlling the top 20% methane emitters. This finding showed that emission surveillance using the proposed mobile measurement system could be a cost-effective way to identify those large emitters and maximize emission reductions for both GHG and air toxics. It should be noted that the well-pad identification process excluded well pads with relatively small emissions from further investigation. Therefore, the measured emissions must be used with caution when attempting to assess regional or basin-wide emissions. Although total VOCs (C4–C12) emission rates estimated using canisters and auto-GC data were somewhat different, a strong correlation was found between them (Spearman's $R = 0.84$), suggesting that the local monitor data can be used for rapid and low-cost surveillance targeting on those large emitters. Such mobile surveillance could be used to trigger a focused follow-up investigation of high emitters with direct measurement techniques, such as an OGI camera, to directly guide repair efforts.

The system has shown a strong ability to detect and quantify emissions from O&G well pads, with the benefit of providing rigorous quantification but noted limitations. First, the measurements were conducted during a relatively short duration, which

limited its ability to capture temporal dynamics of emissions as observed in other basins.¹⁴ Second, the success of the mobile sampling approach depends on reasonable road access and favorable meteorological conditions. To improve sampling coverage to remote sites, other methods (e.g., airborne) may be needed to supplement the ground-based approach. Third, the system was tested in a limited number of controlled release experiments during a short duration. A more extensive testing program covering a full spectrum of environmental conditions (e.g., wind speed and temperature) and source complexity (single leak and multiple leak) is needed to fully evaluate the system performance. Fourth, the uncertainties of estimating speciated VOC mixing ratios by fusing the PID data and downwind canister samples were not quantified in this study. Future studies that compare the tracer gas releases or directly measured VOC mixing ratios (e.g., using the proton-transfer-reaction mass spectrometer or PTR-MS) and the PID-derived VOC mixing ratios will be useful to evaluate this uncertainty. Finally, the 10.6 eV lamp equipped with the PID is not sensitive to ethane and propane, two of the major VOCs emitted from the O&G production sites. Other types of methods or analyzers are needed to help quantify emissions of ethane and propane.

■ ASSOCIATED CONTENT

Supporting Information

The Supporting Information is available free of charge at <https://pubs.acs.org/doi/10.1021/acs.est.0c06545>.

VOCs analyzed in the SUMMA canister, VOC speciation from well pads with multiple SUMMA canister samples, and sensitivity analysis of VOC emissions against production data (PDF)

SUMMA canister data taken downwind from all of the identified well pads (XLSX)

■ AUTHOR INFORMATION

Corresponding Author

John D. Albertson – School of Civil and Environmental Engineering, Cornell University, Ithaca, New York 14853, United States; Phone: +1 (607)255-9671; Email: albertson@cornell.edu

Authors

Xiaochi Zhou – School of Civil and Environmental Engineering, Cornell University, Ithaca, New York 14853, United States; orcid.org/0000-0002-7123-3835

Xiao Peng – School of Civil and Environmental Engineering, Cornell University, Ithaca, New York 14853, United States; orcid.org/0000-0001-9402-2865

Amir Montazeri – School of Civil and Environmental Engineering and Sibley School of Mechanical and Aerospace Engineering, Cornell University, Ithaca, New York 14853, United States

Laura E. McHale – Department of Mechanical Engineering, Colorado State University, Fort Collins, Colorado 80523, United States

Simon Gaßner – Department of Mechanical Engineering, Colorado State University, Fort Collins, Colorado 80523, United States

David R. Lyon – Environmental Defense Fund, Austin, Texas 78701, United States; orcid.org/0000-0002-4400-1190

Azer P. Yalin – Department of Mechanical Engineering,
Colorado State University, Fort Collins, Colorado 80523,
United States

Complete contact information is available at:
<https://pubs.acs.org/10.1021/acs.est.0c06545>

Notes

The authors declare no competing financial interest.

ACKNOWLEDGMENTS

We thank Prof. Joe von Fischer from Colorado State University for the use of his Picarro G2301 GHG analyzer for the field campaign. We also thank Beth Trask from Environmental Defense Fund (EDF) San Francisco office to help coordinate the project and the funding, and Mario Bravo from EDF Austin office for help coordinating the field campaign. At Cornell University, the project was supported by the joint research program between EDF and the David R. Atkinson Center for a Sustainable Future (ACSF) at Cornell University, the DOE ARPA-E's Methane Observation Networks with Innovative Technology to Obtain Reductions (MONITOR) program under grant DE-AR0000749. At Colorado State University, the project was supported by an Advanced Industry grant from the Colorado Office of Economic Development and International Trade (award: POGG1 2016-0949).

REFERENCES

- (1) United States Environmental Protection Agency. Inventory of U.S. Greenhouse Gas Emissions and Sinks: 1990–2018. <https://www.epa.gov/ghgemissions/inventory-us-greenhouse-gas-emissions-and-sinks-1990-2018>.
- (2) Alvarez, R. A.; Zavala-Araiza, D.; Lyon, D. R.; Allen, D. T.; Barkley, Z. R.; Brandt, A. R.; Davis, K. J.; Herndon, S. C.; Jacob, D. J.; Karion, A.; Kort, E. A.; Lamb, B. K.; Lauvaux, T.; Maasakkers, J. D.; Marchese, A. J.; Omara, M.; Pacala, S. W.; Peischl, J.; Robinson, A. L.; Shepson, P. B.; Sweeney, C.; Townsend-Small, A.; Wofsy, S. C.; Hamburg, S. P. Assessment of Methane Emissions from the U.S. Oil and Gas Supply Chain. *Science* **2018**, *361*, 186–188.
- (3) United States Environmental Protection Agency. 2014 National Emission Inventory (NEI) Report, https://www.epa.gov/sites/production/files/2016-12/documents/nei2014v1_tsd.pdf (accessed Mar 6, 2020).
- (4) McKenzie, L. M.; Witter, R. Z.; Newman, L. S.; Adgate, J. L. Human Health Risk Assessment of Air Emissions from Development of Unconventional Natural Gas Resources. *Sci. Total Environ.* **2012**, *424*, 79–87.
- (5) Adgate, J. L.; Goldstein, B. D.; McKenzie, L. M. Potential Public Health Hazards, Exposures and Health Effects from Unconventional Natural Gas Development. *Environ. Sci. Technol.* **2014**, *48*, 8307–8320.
- (6) Tran, K. V.; Casey, J. A.; Cushing, L. J.; Morello-Frosch, R. Residential Proximity to Oil and Gas Development and Birth Outcomes in California: A Retrospective Cohort Study of 2006–2015 Births. *Environ. Health Perspect.* **2020**, *128*, No. 067001.
- (7) Schnell, R. C.; Oltmans, S. J.; Neely, R. R.; Endres, M. S.; Molenaar, J. V.; White, A. B. Rapid Photochemical Production of Ozone at High Concentrations in a Rural Site during Winter. *Nat. Geosci.* **2009**, *2*, 120–122.
- (8) Han, C.; Liu, R.; Luo, H.; Li, G.; Ma, S.; Chen, J.; An, T. Pollution Profiles of Volatile Organic Compounds from Different Urban Functional Areas in Guangzhou China Based on GC/MS and PTR-TOF-MS: Atmospheric Environmental Implications. *Atmos. Environ.* **2019**, *214*, No. 116843.
- (9) Luo, H.; Li, G.; Chen, J.; Lin, Q.; Ma, S.; Wang, Y.; An, T. Spatial and Temporal Distribution Characteristics and Ozone Formation Potentials of Volatile Organic Compounds from Three Typical Functional Areas in China. *Environ. Res.* **2020**, *183*, No. 109141.
- (10) United States Environmental Protection Agency. Oil and Natural Gas Sector: Emission Standards for New, Reconstructed, and Modified Sources, <https://www.govinfo.gov/content/pkg/FR-2016-06-03/pdf/2016-11971.pdf>.
- (11) United States Environmental Protection Agency. Proposed Policy Amendments 2012 and 2016 New Source Performance Standards for the Oil and Natural Gas Industry, <https://www.epa.gov/controlling-air-pollution-oil-and-natural-gas-industry/proposed-policy-amendments-2012-and-2016-new> (accessed Mar 6, 2020).
- (12) Warneke, C.; Geiger, F.; Edwards, P. M.; Dube, W.; Pétron, G.; Kofler, J.; Zahn, A.; Brown, S. S.; Graus, M.; Gilman, J. B.; Lerner, B. M.; Peischl, J.; Ryerson, T. B.; De Gouw, J. A.; Roberts, J. M. Volatile Organic Compound Emissions from the Oil and Natural Gas Industry in the Uintah Basin, Utah: Oil and Gas Well Pad Emissions Compared to Ambient Air Composition. *Atmos. Chem. Phys.* **2014**, *14*, 10977–10988.
- (13) Edie, R.; Robertson, A. M.; Soltis, J.; Field, R. A.; Snare, D.; Burkhart, M. D.; Murphy, S. M. Off-Site Flux Estimates of Volatile Organic Compounds from Oil and Gas Production Facilities Using Fast-Response Instrumentation. *Environ. Sci. Technol.* **2020**, *54*, 1385–1394.
- (14) Zavala-Araiza, D.; Alvarez, R. A.; Lyon, D. R.; Allen, D. T.; Marchese, A. J.; Zimmerle, D. J.; Hamburg, S. P. Super-Emitters in Natural Gas Infrastructure Are Caused by Abnormal Process Conditions. *Nat. Commun.* **2017**, *8*, No. 14012.
- (15) Vaughn, T. L.; Bell, C. S.; Pickering, C. K.; Schwietzke, S.; Heath, G. A.; Pétron, G.; Zimmerle, D. J.; Schnell, R. C.; Nummedal, D. Temporal Variability Largely Explains Top-down/Bottom-up Difference in Methane Emission Estimates from a Natural Gas Production Region. *Proc. Natl. Acad. Sci. U.S.A.* **2018**, *115*, 11712–11717.
- (16) Lavoie, T. N.; Shepson, P. B.; Cambaliza, M. O. L.; Stirr, B. H.; Conley, S.; Mehrotra, S.; Faloon, I. C.; Lyon, D. Spatiotemporal Variability of Methane Emissions at Oil and Natural Gas Operations in the Eagle Ford Basin. *Environ. Sci. Technol.* **2017**, *51*, 8001–8009.
- (17) Duren, R. M.; Thorpe, A. K.; Foster, K. T.; Rafiq, T.; Hopkins, F. M.; Yadav, V.; Bue, B. D.; Thompson, D. R.; Conley, S.; Colombi, N. K.; Frankenberg, C.; McCubbin, I. B.; Eastwood, M. L.; Falk, M.; Herner, J. D.; Croes, B. E.; Green, R. O.; Miller, C. E. California's Methane Super-Emitters. *Nature* **2019**, *575*, 180–184.
- (18) Karion, A.; Sweeney, C.; Pétron, G.; Frost, G.; Michael Hardesty, R.; Kofler, J.; Miller, B. R.; Newberger, T.; Wolter, S.; Banta, R.; Brewer, A.; Dlugokencky, E.; Lang, P.; Montzka, S. A.; Schnell, R.; Tans, P.; Trainer, M.; Zamora, R.; Conley, S. Methane Emissions Estimate from Airborne Measurements over a Western United States Natural Gas Field. *Geophys. Res. Lett.* **2013**, *40*, 4393–4397.
- (19) Halliday, H. S.; Thompson, A. M.; Wisthaler, A.; Blake, D. R.; Hornbrook, R. S.; Mikoviny, T.; Müller, M.; Eichler, P.; Apel, E. C.; Hills, A. J. Atmospheric Benzene Observations from Oil and Gas Production in the Denver-Julesburg Basin in July and August 2014. *J. Geophys. Res.: Atmos.* **2016**, *121*, 11,055–11,074.
- (20) Müller, M.; Mikoviny, T.; Feil, S.; Haidacher, S.; Hanel, G.; Hartungen, E.; Jordan, A.; Märk, L.; Mutschlechner, P.; Schottkowsky, R.; Sulzer, P.; Crawford, J. H.; Wisthaler, A. A Compact PTR-ToF-MS Instrument for Airborne Measurements of Volatile Organic Compounds at High Spatiotemporal Resolution. *Atmos. Meas. Tech.* **2014**, *7*, 3763–3772.
- (21) Zhou, X.; Aurell, J.; Mitchell, W.; Tabor, D.; Gullett, B. A Small, Lightweight Multipollutant Sensor System for Ground-Mobile and Aerial Emission Sampling from Open Area Sources. *Atmos. Environ.* **2017**, *154*, 31–41.
- (22) Golston, L. M.; Tao, L.; Brody, C.; Schäfer, K.; Wolf, B.; McSpirt, J.; Buchholz, B.; Caulton, D. R.; Pan, D.; Zondlo, M. A.; Yoel, D.; Kunstmann, H.; McGregor, M. Lightweight Mid-Infrared Methane Sensor for Unmanned Aerial Systems. *Appl. Phys. B Lasers Opt.* **2017**, *123*, No. 170.
- (23) Martinez, B.; Miller, T. W.; Yalin, A. P. Cavity Ring-down Methane Sensor for Small Unmanned Aerial Systems. *Sensors* **2020**, *20*, No. 454.

- (24) Barchyn, T. E.; Hugenholtz, C. H.; Fox, T. A. Plume Detection Modeling of a Drone-Based Natural Gas Leak Detection System. *Elem. Sci. Anthropocene* **2019**, *7*, 41.
- (25) United States Environmental Protection Agency. Method 21—Determination of Volatile Organic Compound Leak, https://www.epa.gov/sites/production/files/2017-08/documents/method_21.pdf.
- (26) United States Environmental Protection Agency. Alternative Work Practice To Detect Leaks From Equipment. <https://www.federalregister.gov/documents/2006/04/06/E6-5005/alternative-work-practice-to-detect-leaks-from-equipment> (accessed Mar 6, 2020).
- (27) Albertson, J. D.; Harvey, T.; Foderaro, G.; Zhu, P.; Zhou, X.; Ferrari, S.; Amin, M. S.; Modrak, M.; Brantley, H.; Thoma, E. D. A Mobile Sensing Approach for Regional Surveillance of Fugitive Methane Emissions in Oil and Gas Production. *Environ. Sci. Technol.* **2016**, *50*, 2487–2497.
- (28) Brantley, H. L.; Thoma, E. D.; Squier, W. C.; Guven, B. B.; Lyon, D. Assessment of Methane Emissions from Oil and Gas Production Pads Using Mobile Measurements. *Environ. Sci. Technol.* **2014**, *48*, 14508–14515.
- (29) Brantley, H. L.; Thoma, E. D.; Eisele, A. P. Assessment of Volatile Organic Compound and Hazardous Air Pollutant Emissions from Oil and Natural Gas Well Pads Using Mobile Remote and On-Site Direct Measurements. *J. Air Waste Manage. Assoc.* **2015**, *65*, 1072–1082.
- (30) Warneke, C.; Veres, P.; Murphy, S. M.; Soltis, J.; Field, R. A.; Graus, M. G.; Koss, A.; Li, S. M.; Li, R.; Yuan, B.; Roberts, J. M.; De Gouw, J. A. PTR-QMS versus PTR-TOF Comparison in a Region with Oil and Natural Gas Extraction Industry in the Uintah Basin in 2013. *Atmos. Meas. Tech.* **2015**, *8*, 411–420.
- (31) Zhou, X.; Passow, F. H.; Rudek, J.; Fisher, J. C. Von.; Hamburg, S. P.; Albertson, J. D. Estimation of Methane Emissions from the U. S. Ammonia Fertilizer Industry Using a Mobile Sensing Approach. *Elem. Sci. Anthropocene* **2019**, *7*, No. 19.
- (32) Zhou, X.; Montazeri, A.; Albertson, J. D. Mobile Sensing of Point-Source Gas Emissions Using Bayesian Inference: An Empirical Examination of the Likelihood Function. *Atmos. Environ.* **2019**, *218*, No. 116981.
- (33) Lavoie, T. N.; Shepson, P. B.; Cambaliza, M. O. L.; Stirr, B. H.; Conley, S.; Mehrotra, S.; Faloona, I. C.; Lyon, D. Spatiotemporal Variability of Methane Emissions at Oil and Natural Gas Operations in the Eagle Ford Basin. *Environ. Sci. Technol.* **2017**, *51*, 8001–8009.
- (34) Roest, G.; Schade, G. Quantifying Alkane Emissions in the Eagle Ford Shale Using Boundary Layer Enhancement. *Atmos. Chem. Phys.* **2017**, *17*, 11163–11176.
- (35) Peischl, J.; Eilerman, S. J.; Neuman, J. A.; Aikin, K. C.; de Gouw, J.; Gilman, J. B.; Herndon, S. C.; Nadkarni, R.; Trainer, M.; Warneke, C.; Ryerson, T. B. Quantifying Methane and Ethane Emissions to the Atmosphere From Central and Western U.S. Oil and Natural Gas Production Regions. *J. Geophys. Res.: Atmos.* **2018**, *123*, 7725–7740.
- (36) Hildenbrand, Z.; Phillip, M.; McBride, E.; Navid Dorreyat, M.; Taylor, J.; Carlton Jr, D.; Meik, J.; Fontenota, B.; Wrightg, K.; Schugae, K.; Verbeckc, G. Point Source Attribution of Ambient Contamination Events near Unconventional Oil and Gas Development. *Sci. Total Environ.* **2016**, *573*, 382–388.
- (37) McHale, L. E.; Hecobian, A.; Yalin, A. P. Open-Path Cavity Ring-down Spectroscopy for Trace Gas Measurements in Ambient Air. *Opt. Express* **2016**, *24*, 5523.
- (38) McHale, L. E.; Martinez, B.; Miller, T. W.; Yalin, A. P. Open-Path Cavity Ring-down Methane Sensor for Mobile Monitoring of Natural Gas Emissions. *Opt. Express* **2019**, *27*, 20084.
- (39) Townsend-Small, A.; Marrero, J. E.; Lyon, D. R.; Simpson, I. J.; Meinardi, S.; Blake, D. R. Integrating Source Apportionment Tracers into a Bottom-up Inventory of Methane Emissions in the Barnett Shale Hydraulic Fracturing Region. *Environ. Sci. Technol.* **2015**, *49*, 8175–8182.
- (40) Marrero, J. E.; Townsend-Small, A.; Lyon, D. R.; Tsai, T. R.; Meinardi, S.; Blake, D. R. Estimating Emissions of Toxic Hydrocarbons from Natural Gas Production Sites in the Barnett Shale Region of Northern Texas. *Environ. Sci. Technol.* **2016**, *50*, 10756–10764.
- (41) Rella, C. W.; Tsai, T. R.; Botkin, C. G.; Crosson, E. R.; Steele, D. Measuring Emissions from Oil and Natural Gas Well Pads Using the Mobile Flux Plane Technique. *Environ. Sci. Technol.* **2015**, *49*, 4742–4748.
- (42) Ion Science. Technical/Application Article 02, <https://www.ionscience.com/wp-content/uploads/2017/03/TA-02-Ion-Science-PID-Response-Factors-UK-V1.14.pdf> (accessed Aug 22, 2020).
- (43) Zheng, H.; Kong, S.; Xing, X.; Mao, Y.; Hu, T.; Ding, Y.; Li, G.; Liu, D.; Li, S.; Qi, S. Monitoring of Volatile Organic Compounds (VOCs) from an Oil and Gas Station in Northwest China for 1 Year. *Atmos. Chem. Phys.* **2018**, *18*, 4567–4595.
- (44) Ion Science. Ion Science. MiniPID 2 (3PIN) Instrument User Manual V1.2, <https://www.ionscience-usa.com/wp-content/uploads/2016/10/MiniPID-Manual-2-3-Pin-V1.2.pdf>.
- (45) United States Environmental Protection Agency. Method for the Determination of Volatile 697Organic Compounds in Ambient Air Using Cryogenic Preconcentration Techniques and 698Gas Chromatography with Flame Ionization and Electron Capture Detection, <https://www.epa.gov/sites/production/files/2019-11/documents/to-3.pdf>.
- (46) Marrero, J. E.; Townsend-Small, A.; Lyon, D. R.; Tsai, T. R.; Meinardi, S.; Blake, D. R. Estimating Emissions of Toxic Hydrocarbons from Natural Gas Production Sites in the Barnett Shale Region of Northern Texas. *Environ. Sci. Technol.* **2016**, *50*, 10756–10764.
- (47) Zhou, X.; Yoon, S.; Mara, S.; Falk, M.; Kuwayama, T.; Tran, T.; Cheadle, L.; Nyarady, J.; Croes, B.; Scheehle, E.; Herner, J. D.; Vijayan, A. Mobile Sampling of Methane Emissions from Natural Gas Well Pads in California. *Atmos. Environ.* **2021**, *244*, No. 117930.
- (48) Belušić, D.; H Lenschow, D.; Tapper, N. J. Performance of a Mobile Car Platform for Mean Wind and Turbulence Measurements. *Atmos. Meas. Tech.* **2014**, *7*, 1825–1837.
- (49) Yee, E. Bayesian Probabilistic Approach for Inverse Source Determination from Limited and Noisy Chemical or Biological Sensor Concentration Measurements, *Proceedings of SPIE*, 2007, 6554 (November), 65540W.
- (50) Gryning, S.; Ulden, A. P.; van Larsen, S. E. Dispersion from a Continuous Ground-Level Source Investigated by a K Model. *Q. J. R. Meteorol. Soc.* **1983**, *109*, 355–364.
- (51) Bell, C.; Vaughn, T.; Zimmerle, D. Evaluation of next Generation Emission Measurement Technologies under Repeatable Test Protocols. *Elem. Sci. Anth.* **2020**, *8*, 32.
- (52) Gvakharina, A.; Kort, E. A.; Smith, M. L.; Conley, S. Evaluating Cropland N₂O Emissions and Fertilizer Plant Greenhouse Gas Emissions With Airborne Observations. *J. Geophys. Res.: Atmos.* **2020**, *125*, No. e2020JD032815.
- (53) Texas Commission on Environmental Quality. Karnes County [36] Monthly Summary. https://www.tceq.texas.gov/cgi-bin/compliance/monops/agg_monthly_summary.pl.
- (54) Mooney, C. F.; Mooney, C. L.; Mooney, C. Z.; Duval, R. D.; Duval, R. *Bootstrapping: A Nonparametric Approach to Statistical Inference*; Sage, 1993.
- (55) Omara, M.; Zimmerman, N.; Sullivan, M. R.; Li, X.; Ellis, A.; Cesa, R.; Subramanian, R.; Presto, A. A.; Robinson, A. L. Methane Emissions from Natural Gas Production Sites in the United States: Data Synthesis and National Estimate. *Environ. Sci. Technol.* **2018**, *52*, 12915–12925.
- (56) Gidney, B.; Pena, S. Upstream Oil and Gas Storage Tank Project Flash Emissions Models Evaluation, <https://www.tceq.texas.gov/assets/public/implementation/air/am/contracts/reports/ei/20090716-ergi-UpstreamOilGasTankEIModels.pdf>. (accessed Mar 6, 2020).
- (57) Zavala-Araiza, D.; Lyon, D. R.; Alvarez, R. A.; Davis, K. J.; Harriss, R.; Herndon, S. C.; Karion, A.; Kort, E. A.; Lamb, B. K.; Lan, X.; Marchese, A. J.; Pacala, S. W.; Robinson, A. L.; Shepson, P. B.; Sweeney, C.; Talbot, R.; Townsend-Small, A.; Yacovitch, T. I.; Zimmerle, D. J.; Hamburg, S. P. Reconciling Divergent Estimates of Oil and Gas Methane Emissions. *Proc. Natl. Acad. Sci.* **2015**, *112*, 15597–15602.
- (58) Omara, M.; Sullivan, M. R.; Li, X.; Subramian, R.; Robinson, A. L.; Presto, A. A. Methane Emissions from Conventional and

Unconventional Natural Gas Production Sites in the Marcellus Shale Basin. *Environ. Sci. Technol.* **2016**, *50*, 2099–2107.

(59) United States Environmental Protection Agency. Nonhalogenated Organics by Gas Chromatography, <https://www.epa.gov/hw-sw846/sw-846-test-method-8015c-nonhalogenated-organics-gas-chromatography>.

(60) Allen, D.; Torres, V.; Thomas, J.; Sullivan, D.; et al. Measurements of Methane Emissions at Natural Gas Production Sites in the United States. *Proc. Natl. Acad. Sci. U.S.A.* **2013**, *110*, 17768–17773.

Exhibit 24



Environment Department

MICHELLE LUJAN GRISHAM, GOVERNOR

James C. Kenney, Cabinet Secretary

Jennifer J. Pruett, Deputy Secretary

NEWS RELEASE

For Immediate Release

Jan. 14, 2020

The Environment Department's mission is to protect and restore the environment and to foster a healthy and prosperous New Mexico for present and future generations.

Contact: Maddy Hayden, Communications Director
New Mexico Environment Department
505.231.8800 | maddy.hayden@state.nm.us

Embracing innovation and technology, the Environment Department identifies potential emissions violations

The New Mexico Environment Department (NMED) identified potential emission violations of methane and other air contaminants from oil and gas operations throughout the state using forward-looking infrared (FLIR) cameras. The FLIR video footage collection is now included on the Department's online interactive [methane map](#). NMED created and periodically updates this map to provide the public with information on how oil and gas operations directly impact their communities.

Footage available on the map now includes FLIR videos received from citizens the Department believes depict potential violations of existing state permits or regulations. The map also contains FLIR videos documenting significant emissions from the Department's recent flyover compliance inspections.

"The Department is addressing oil and natural gas emissions through innovative compliance assurance measures today as we invest in methane regulations for tomorrow," said NMED Cabinet Secretary James Kenney. "The emissions documented in many of these videos are unacceptable to this Department and pose significant health and safety risks to New Mexico communities and employees of these companies."

In response to footage received from citizens that may depict potential violations, NMED is sending written notices to oil and gas operators seeking an explanation for and correction to the documented emissions within 14 days. If the operator does not reply in writing to the notice or document the corrections made, the Department may launch an investigation or proceed directly to civil enforcement, which may include the assessment of penalties.

Also as part of NMED's ongoing compliance assurance activities, helicopter flyovers were conducted in conjunction with the U.S. Environmental Protection Agency (EPA) in September and October of 2019. Using FLIR cameras, leaks were identified from flares, tanks and other types of oil and gas equipment. The Department is reviewing the footage to determine if facilities are in compliance with applicable permits and regulations. Of the approximately 5,340 storage tanks observed, 111 were emitting methane and other pollutants at the time of the flyover. Of the approximately 530 flares observed, 13 were unlit and emitting methane and other pollutants.

NMED and EPA plan to conduct additional flyover inspections in the near future.

Emissions from oil and gas operations contribute to climate change as well as the formation of ground-level ozone. Several counties, including some in southeast New Mexico, are experiencing increased ozone levels. Aside from adverse public health effects, increasing ozone levels may result in more stringent federal sanctions, including more rigorous permitting requirements.

###

NMED does not discriminate on the basis of race, color, national origin, disability, age or sex in the administration of its programs or activities, as required by applicable laws and regulations. NMED is responsible for coordination of compliance efforts and receipt of inquiries concerning non-discrimination requirements implemented by 40 C.F.R. Parts 5 and 7, including Title VI of the Civil Rights Act of 1964, as amended; Section 504 of the Rehabilitation Act of 1973; the Age Discrimination Act of 1975, Title IX of the Education Amendments of 1972, and Section 13 of the Federal Water Pollution Control Act Amendments of 1972. If you have any questions about this notice or any of NMED's non-discrimination programs, policies or procedures, you may contact:

Kristine Yurdin, Non-Discrimination Coordinator | NMED | 1190 St. Francis Dr., Suite N4050 | P.O. Box 5469 | Santa Fe, NM 87502
(505) 827-2855 or nd.coordinator@state.nm.us

If you believe that you have been discriminated against with respect to a NMED program or activity, you may contact the Non-Discrimination Coordinator.

###

Exhibit 25

ENVIRONMENTAL PROTECTION AGENCY

40 CFR Parts 50, 51, 52, 53, and 58

[EPA-HQ-OAR-2008-0699; FRL-9933-18-OAR]

RIN 2060-AP38

National Ambient Air Quality Standards for Ozone

AGENCY: Environmental Protection Agency (EPA).

ACTION: Final rule.

SUMMARY: Based on its review of the air quality criteria for ozone (O₃) and related photochemical oxidants and national ambient air quality standards (NAAQS) for O₃, the Environmental Protection Agency (EPA) is revising the primary and secondary NAAQS for O₃ to provide requisite protection of public health and welfare, respectively. The EPA is revising the levels of both standards to 0.070 parts per million (ppm), and retaining their indicators (O₃), forms (fourth-highest daily maximum, averaged across three consecutive years) and averaging times (eight hours). The EPA is making corresponding revisions in data handling conventions for O₃ and changes to the Air Quality Index (AQI); revising regulations for the prevention of significant deterioration (PSD) program to add a transition provision for certain applications; and establishing exceptional events schedules and providing information related to implementing the revised standards. The EPA is also revising the O₃ monitoring seasons, the Federal Reference Method (FRM) for monitoring O₃ in the ambient air, Federal Equivalent Method (FEM) analyzer performance requirements, and the Photochemical Assessment Monitoring Stations (PAMS) network. Along with exceptional events schedules related to implementing the revised O₃ standards, the EPA is applying this same schedule approach to other future new or revised NAAQS and removing obsolete regulatory language for expired exceptional events deadlines. The EPA is making minor changes to the procedures and time periods for evaluating potential FRMs and equivalent methods, including making the requirements for nitrogen dioxide (NO₂) consistent with the requirements for O₃, and removing an obsolete requirement for the annual submission of Product Manufacturing Checklists by manufacturers of FRMs and FEMs for monitors of fine and coarse particulate matter. For a more detailed summary, see the Executive Summary below.

DATES: The final rule is effective on December 28, 2015.

ADDRESSES: EPA has established a docket for this action (Docket ID No. EPA-HQ-OAR-2008-0699) and a separate docket, established for the Integrated Science Assessment (ISA) (Docket No. EPA-HQ-ORD-2011-0050), which has been incorporated by reference into the rulemaking docket. All documents in the docket are listed on the www.regulations.gov Web site. Although listed in the docket index, some information is not publicly available, e.g., confidential business information or other information whose disclosure is restricted by statute. Certain other material, such as copyrighted material, is not placed on the Internet and may be viewed, with prior arrangement, at the EPA Docket Center. Publicly available docket materials are available either electronically in www.regulations.gov or in hard copy at the Air and Radiation Docket and Information Center, EPA/DC, WJC West Building, Room 3334, 1301 Constitution Ave., NW., Washington, DC. The Public Reading Room is open from 8:30 a.m. to 4:30 p.m., Monday through Friday, excluding legal holidays. The telephone number for the Public Reading Room is (202) 566-1744 and the telephone number for the Air and Radiation Docket and Information Center is (202) 566-1742. For additional information about EPA's public docket, visit the EPA Docket Center homepage at: <http://www.epa.gov/epahome/dockets.htm>.

FOR FURTHER INFORMATION CONTACT: Ms. Susan Lyon Stone, Health and Environmental Impacts Division, Office of Air Quality Planning and Standards, U.S. Environmental Protection Agency, Mail code C504-06, Research Triangle Park, NC 27711; telephone: (919) 541-1146; fax: (919) 541-0237; email: stone.susan@epa.gov.

SUPPLEMENTARY INFORMATION:

General Information

Availability of Related Information

A number of the documents that are relevant to this action are available through the EPA's Office of Air Quality Planning and Standards (OAQPS) Technology Transfer Network (TTN) Web site (http://www.epa.gov/ttn/naaqs/standards/ozone/s_o3_index.html). These documents include the *Integrated Science Assessment for Ozone* (U.S. EPA, 2013), available at http://www.epa.gov/ttn/naaqs/standards/ozone/s_o3_2008_isa.html; the *Health Risk and Exposure Assessment* and the *Welfare Risk and Exposure Assessment for Ozone*, Final

Reports (HREA and WREA, respectively; U.S. EPA, 2014a, 2014b), available at http://www.epa.gov/ttn/naaqs/standards/ozone/s_o3_2008_rea.html; and the *Policy Assessment for the Review of the Ozone National Ambient Air Quality Standards* (PA; U.S. EPA, 2014c), available at http://www.epa.gov/ttn/naaqs/standards/ozone/s_o3_2008_pa.html. These and other related documents are also available for inspection and copying in the EPA docket identified above.

Table of Contents

The following topics are discussed in this preamble:

Executive Summary

I. Background

- A. Legislative Requirements
- B. Related Control Programs
- C. Review of Air Quality Criteria and Standards for O₃
- D. Ozone Air Quality
- E. Summary of Proposed Revisions to the O₃ Standards
- F. Organization and Approach to Decisions in This O₃ NAAQS Review

II. Rationale for Decision on the Primary Standard

A. Introduction

1. Overview of Health Effects Evidence
2. Overview of Human Exposure and Health Risk Assessments

B. Need for Revision of the Primary Standard

1. Basis for Proposed Decision
2. Comments on the Need for Revision
3. Administrator's Conclusions on the Need for Revision

C. Conclusions on the Elements of a Revised Primary Standard

1. Indicator
2. Averaging Time
3. Form
4. Level

D. Decision on the Primary Standard

III. Communication of Public Health Information

A. Proposed Revisions to the AQI

B. Comments on Proposed Revisions to the AQI

C. Final Revisions to the AQI

IV. Rationale for Decision on the Secondary Standard

A. Introduction

1. Overview of Welfare Effects Evidence
2. Overview of Welfare Exposure and Risk Assessment

B. Need for Revision of the Secondary Standard

1. Basis for Proposed Decision
2. Comments on the Need for Revision
3. Administrator's Conclusions on the Need for Revision

C. Conclusions on Revision of the Secondary Standard

1. Basis for Proposed Revision
2. Comments on Proposed Revision
3. Administrator's Conclusions on Revision
- D. Decision on the Secondary Standard

V. Appendix U: Interpretation of the Primary and Secondary NAAQS for O₃

current primary and secondary standards for O₃. With regard to the primary standard, the Administrator proposed to revise the level from 75 ppb to a level within a range from 65 to 70 ppb. The EPA proposed to revise the AQI for O₃, consistent with revision to the primary standard.

With regard to the secondary standard, the Administrator proposed to revise the level of the current secondary standard to within the range of 0.065 to 0.070 ppm, which air quality analyses indicate would provide cumulative, seasonal air quality or exposure values, in terms of 3-year average W126 index values, at or below a range of 13–17 ppm-hours.

The EPA also proposed to make corresponding revisions in data handling conventions for O₃; to revise regulations for the PSD permitting program to add a provision grandfathering certain pending permits from certain requirements with respect to the proposed revisions to the standards; and to convey schedules and information related to implementing any revised standards. In conjunction with proposing exceptional event schedules related to implementing any revised O₃ standards, the EPA also proposed to extend the new schedule approach to other future NAAQS revisions and to remove obsolete regulatory language associated with expired exceptional event deadlines for historical standards for both O₃ and other pollutants for which NAAQS have been established. The EPA also proposed to make minor changes to the procedures and time periods for evaluating potential FRMs and equivalent methods, including making the requirements for NO₂ consistent with the requirements for O₃, and removing an obsolete requirement for the annual submission of documentation by manufacturers of certain particulate matter monitors.

F. Organization and Approach to Decisions in This O₃ NAAQS Review

This action presents the Administrator's final decisions in the current review of the primary and secondary O₃ standards. The final decisions addressing standards for O₃ are based on a thorough review in the ISA of scientific information on known and potential human health and welfare effects associated with exposure to O₃ at levels typically found in the ambient air. These final decisions also take into account the following: (1) Staff assessments in the PA of the most policy-relevant information in the ISA as well as a quantitative health and welfare exposure and risk assessments

based on that information; (2) CASAC advice and recommendations, as reflected in its letters to the Administrator and its discussions of drafts of the ISA, REAs, and PA at public meetings; (3) public comments received during the development of these documents, both in connection with CASAC meetings and separately; and (4) extensive public comments received on the proposed rulemaking.

The primary standard is addressed in section II. Corresponding changes to the AQI are addressed in section III. The secondary standard is addressed in section IV. Related data handling conventions and exceptional events are addressed in section V. Updates to the monitoring regulations are addressed in section VI. Implementation activities, including PSD-related actions, are addressed in sections VII and VIII. Section IX addresses applicable statutory and executive order reviews.

II. Rationale for Decision on the Primary Standard

This section presents the Administrator's final decisions regarding the need to revise the existing primary O₃ standard and the appropriate revision to the level of that standard. Based on her consideration of the full body of health effects evidence and exposure/risk analyses, the Administrator concludes that the current primary standard for O₃ is not requisite to protect public health with an adequate margin of safety. In order to increase public health protection, she is revising the level of the primary standard to 70 ppb, in conjunction with retaining the current indicator, averaging time and form. The Administrator concludes that such a revised standard will be requisite to protect public health with an adequate margin of safety. As discussed more fully below, the rationale for these final decisions draws from the thorough review in the ISA (U.S. EPA, 2013) of the available scientific evidence, generally published through July 2011, on human health effects associated with the presence of O₃ in the ambient air. This rationale also takes into account: (1) Analyses of O₃ air quality, human exposures to O₃, and O₃-associated health risks, as presented and assessed in the HREA (U.S. EPA, 2014a); (2) the EPA staff assessment of the most policy-relevant scientific evidence and exposure/risk information in the PA (U.S. EPA, 2014c); (3) CASAC advice and recommendations, as reflected in discussions of drafts of the ISA, REA, and PA at public meetings, in separate written comments, and in CASAC's letters to the Administrator; (4) public

input received during the development of these documents, either in connection with CASAC meetings or separately; and (5) public comments on the proposal notice.

Section II.A below summarizes the information presented in the proposal regarding O₃-associated health effects, O₃ exposures, and O₃-attributable health risks. Section II.B presents information related to the adequacy of the current primary O₃ standard, including a summary of the basis for the Administrator's proposed decision to revise the current standard, public comments received on the adequacy of the current standard, and the Administrator's final conclusions regarding the adequacy of the current standard. Section II.C presents information related to the elements of a revised primary O₃ standard, including information related to each of the major elements of the standard (*i.e.*, indicator, averaging time, form, level). Section II.D summarizes the Administrator's final decisions on the primary O₃ standard.

A. Introduction

As discussed in section II.A of the proposal (79 FR 75243–75246, December 17, 2014), the EPA's approach to informing decisions on the primary O₃ standard in the current review builds upon the general approaches used in previous reviews and reflects the broader body of scientific evidence, updated exposure/risk information, and advances in O₃ air quality modeling now available. This approach is based most fundamentally on using the EPA's assessment of the available scientific evidence and associated quantitative analyses to inform the Administrator's judgments regarding a primary standard for O₃ that is "requisite" (*i.e.*, neither more nor less stringent than necessary) to protect public health with an adequate margin of safety. Specifically, it is based on consideration of the available body of scientific evidence assessed in the ISA (U.S. EPA, 2013), exposure and risk analyses presented in the HREA (U.S. EPA, 2014a), evidence- and exposure-/risk-based considerations and conclusions presented in the PA (U.S. EPA, 2014c), advice and recommendations received from CASAC (Frey, 2014a, c), and public comments.

Section II.A.1 below summarizes the information presented in the proposal regarding O₃-associated health effects. Section II.A.2 summarizes the information presented in the proposal regarding O₃ exposures and O₃-attributable health risks.

1. Overview of Health Effects Evidence

The health effects of O₃ are described in detail in the ISA (U.S. EPA, 2013). Based on its assessment of the health effects evidence, the ISA determined that a “causal” relationship exists between short-term exposure to O₃ in ambient air and effects on the respiratory system¹⁵ and that a “likely to be causal” relationship exists between long-term exposure to O₃ in ambient air and respiratory effects¹⁶ (U.S. EPA, 2013, pp. 1–6 to 1–7). The ISA summarizes the longstanding body of evidence for O₃ respiratory effects as follows (U.S. EPA, 2013, p. 1–5):

The clearest evidence for health effects associated with exposure to O₃ is provided by studies of respiratory effects. Collectively, a very large amount of evidence spanning several decades supports a relationship between exposure to O₃ and a broad range of respiratory effects (see Section 6.2.9 and Section 7.2.8). The majority of this evidence is derived from studies investigating short-term exposures (*i.e.*, hours to weeks) to O₃, although animal toxicological studies and recent epidemiologic evidence demonstrate that long-term exposure (*i.e.*, months to years) may also harm the respiratory system.

Additionally, the ISA determined that the relationships between short-term exposures to O₃ in ambient air and both total mortality and cardiovascular effects are likely to be causal, based on expanded evidence bases in the current review (U.S. EPA, 2013, pp. 1–7 to 1–8). The ISA determined that the currently available evidence for additional endpoints is “suggestive” of causal relationships with short-term (central nervous system effects) and long-term exposures (cardiovascular effects, reproductive and developmental effects, central nervous system effects and total mortality) to ambient O₃.

Consistent with emphasis in past reviews on O₃ health effects for which the evidence is strongest, in this review the EPA places the greatest emphasis on studies of health effects that have been determined in the ISA to be caused by, or likely to be caused by, O₃ exposures (U.S. EPA, 2013, section 2.5.2). This preamble section summarizes the evidence for health effects attributable to O₃ exposures, with a focus on respiratory morbidity and mortality

effects attributable to short- and long-term exposures, and cardiovascular system effects (including mortality) and total mortality attributable to short-term exposures (from section II.B in the proposal, 79 FR 75246–75271).

The information highlighted here is based on the assessment of the evidence in the ISA (U.S. EPA, 2013, Chapters 4 to 8) and consideration of that evidence in the PA (U.S. EPA, 2014c, Chapters 3 and 4) on the known or potential effects on public health which may be expected from the presence of O₃ in the ambient air. This section summarizes: (1) Information available on potential mechanisms for health effects associated with exposure to O₃ (II.A.1.a); (2) the nature of effects that have been associated directly with both short- and long-term exposure to O₃ and indirectly with the presence of O₃ in ambient air (II.A.1.b); (3) considerations related to the adversity of O₃-attributable health effects (II.A.1.c); and (4) considerations in characterizing the public health impact of O₃, including the identification of “at risk” populations (II.A.1.d).

a. Overview of Mechanisms

This section briefly summarizes the characterization of the key events and pathways that contribute to health effects resulting from O₃ exposures, as discussed in the proposal (79 FR 75247, section II.B.1) and in the ISA (U.S. EPA, 2013, section 5.3).

Experimental evidence elucidating modes of action and/or mechanisms contributes to our understanding of the biological plausibility of adverse O₃-related health effects, including respiratory effects and effects outside the respiratory system (U.S. EPA, 2013, Chapters 6 and 7). Evidence indicates that the initial key event is the formation of secondary oxidation products in the respiratory tract (U.S. EPA, 2013, section 5.3). This mainly involves direct reactions with components of the extracellular lining fluid (ELF). Although the ELF has inherent capacity to quench (based on individual antioxidant capacity), this capacity can be overwhelmed, especially with exposure to elevated concentrations of O₃ (U.S. EPA 2014c, at 3–3, 3–9). The resulting secondary oxidation products transmit signals to the epithelium, pain receptive nerve fibers and, if present, immune cells involved in allergic responses. The available evidence indicates that the effects of O₃ are mediated by components of ELF and by the multiple cell types in the respiratory tract. Oxidative stress is an implicit part of this initial key event.

Secondary oxidation products initiate numerous responses at the cellular, tissue, and whole organ level of the respiratory system. These responses include the activation of neural reflexes which leads to lung function decrements; initiation of pulmonary inflammation; alteration of barrier epithelial function; sensitization of bronchial smooth muscle; modification of lung host defenses; airways remodeling; and modulation of autonomic nervous function which may alter cardiac function (U.S. EPA, 2013, section 5.3, Figure 5–8).

Persistent inflammation and injury, which are observed in animal models of chronic and quasi-continuous exposure to O₃, are associated with airways remodeling (see section 7.2.3 of the ISA, U.S. EPA, 2013). Chronic quasi-continuous exposure to O₃ has also been shown to result in effects on the developing lung and immune system. Systemic inflammation and vascular oxidative/nitrosative stress are also key events in the toxicity pathway of O₃ (U.S. EPA, 2013, section 5.3.8). Extrapulmonary effects of O₃ occur in numerous organ systems, including the cardiovascular, central nervous, reproductive, and hepatic systems (U.S. EPA, 2013, sections 6.3 to 6.5 and sections 7.3 to 7.5).

Responses to O₃ exposure are variable within the population. Studies have shown a large range of pulmonary function (*i.e.*, spirometric) responses to O₃ among healthy young adults, while responses within an individual are relatively consistent over time. Other responses to O₃ have also been characterized by a large degree of interindividual variability, including airways inflammation. The mechanisms that may underlie the variability in responses seen among individuals are discussed in the ISA (U.S. EPA, 2013, section 5.4.2). Certain functional genetic polymorphisms, pre-existing conditions or diseases, nutritional status, lifestyles, and co-exposures can contribute to altered risk of O₃-induced effects. Experimental evidence for such O₃-induced changes contributes to our understanding of the biological plausibility of adverse O₃-related health effects, including a range of respiratory effects as well as effects outside the respiratory system (*e.g.*, cardiovascular effects) (U.S. EPA, 2013, Chapters 6 and 7).

b. Nature of Effects

This section briefly summarizes the information presented in the proposal on respiratory effects attributable to short-term exposures (II.A.1.b.i), respiratory effects attributable to long-

¹⁵ In determining that a causal relationship exists for O₃ with specific health effects, the EPA has concluded that “[e]vidence is sufficient to conclude that there is a causal relationship with relevant pollutant exposures” (U.S. EPA, 2013, p. lxiv).

¹⁶ In determining a “likely to be causal” relationship exists for O₃ with specific health effects, the EPA has concluded that “[e]vidence is sufficient to conclude that a causal relationship is likely to exist with relevant pollutant exposures, but important uncertainties remain” (U.S. EPA, 2013, p. lxiv).

term exposures (II.A.1.b.ii), cardiovascular effects attributable to short-term exposures (II.A.1.b.iii), and premature mortality attributable to short-term exposures (II.A.1.b.iv) (79 FR 75247, section II.B.2).

i. Respiratory Effects—Short-term Exposure

Controlled human exposure, animal toxicological, and epidemiologic studies available in the last review provided clear, consistent evidence of a causal relationship between short-term O₃ exposure and respiratory effects (U.S. EPA, 2006a). Recent studies evaluated since the completion of the 2006 AQCD support and expand upon the strong body of evidence available in the last review (U.S. EPA, 2013, section 6.2.9).

Key aspects of this evidence are discussed below with regard to (1) lung function decrements; (2) pulmonary inflammation, injury, and oxidative stress; (3) airway hyperresponsiveness; (4) respiratory symptoms and medication use; (5) lung host defense; (6) allergic and asthma-related responses; (7) hospital admissions and emergency department visits; and (8) respiratory mortality.¹⁷

Lung Function Decrements

Lung function decrements are typically measured by spirometry and refer to reductions in the maximal amount of air that can be forcefully exhaled. Forced expiratory volume in 1 second (FEV₁) is a common index used to assess the effect of O₃ on lung function. The ISA summarizes the currently available evidence from multiple controlled human exposure studies evaluating changes in FEV₁ following 6.6-hour O₃ exposures in young, healthy adults engaged in moderate levels of physical activity¹⁸ (U.S. EPA, 2013, section 6.2.1.1, Figure 6-1). Exposures to an average O₃ concentration of 60 ppb results in group mean decrements in FEV₁ ranging from 1.8% to 3.6% (Adams, 2002; Adams, 2006;¹⁹ Schelegle et al., 2009;²⁰ Kim et

al., 2011). The weighted average group mean decrement was 2.7% from these studies. In some analyses, these group mean decrements in lung function were statistically significant (Brown et al., 2008; Kim et al., 2011), while in other analyses they were not (Adams, 2006; Schelegle et al., 2009).²¹ Prolonged exposure to an average O₃ concentration of 72 ppb results in a statistically significant group mean decrement in FEV₁ of about 6% (Schelegle et al., 2009).²² There is a smooth dose-response curve without evidence of a threshold for exposures between 40 and 120 ppb O₃ (U.S. EPA, 2013, Figure 6-1). When these data are taken together, the ISA concludes that “mean FEV₁ is clearly decreased by 6.6-hour exposures to 60 ppb O₃ and higher concentrations in [healthy, young adult] subjects performing moderate exercise” (U.S. EPA, 2013, p. 6-9).

As described in the proposal (79 FR 75250), the ISA focuses on individuals with >10% decrements in FEV₁ because (1) it is accepted by the American Thoracic Society (ATS) as an abnormal response and a reasonable criterion for assessing exercise-induced bronchoconstriction, and (2) some individuals in the Schelegle et al. (2009) study experienced 5–10% FEV₁ decrements following exposure to filtered air. The proportion of healthy adults experiencing FEV₁ decrements >10% following prolonged exposures to 80 ppb O₃ while at moderate exertion ranged from 17% to 29% and following exposures to 60 ppb O₃ ranged from 3% to 20%. The weighted average proportion (*i.e.*, based on numbers of subjects in each study) of young, healthy adults with >10% FEV₁ decrements is 25% following exposure to 80 ppb O₃ and 10% following exposure to 60 ppb O₃, for 6.6 hours at moderate exertion (U.S. EPA, 2013, page 6-18 and 6-19).²³ Responses within an

individual tend to be reproducible over a period of several months, reflecting differences in intrinsic responsiveness. Given this, the ISA concludes that “[t]hrough group mean decrements are biologically small and generally do not attain statistical significance, a considerable fraction of exposed individuals [in the clinical studies] experience clinically meaningful decrements in lung function” when exposed for 6.6 hours to 60 ppb O₃ during quasi-continuous, moderate exertion (U.S. EPA, 2013, section 6.2.1.1, p. 6-20).

This review has marked an advance in the ability to make reliable quantitative predictions of the potential lung function response to O₃ exposure, and, thus, to reasonably predict the degree of interindividual response of lung function to that exposure. McDonnell et al. (2012) and Schelegle et al. (2012) developed models, described in more detail in the proposal (79 FR 75250), that included mathematical approaches to simulate the potential protective effect of antioxidants in the ELF at lower ambient O₃ concentrations, and that included a dose threshold below which changes in lung function do not occur. The resulting empirical models can estimate the frequency distribution of individual responses and summary measures of the distribution such as the mean or median response and the proportions of individuals with FEV₁ decrements >10%, 15%, and 20%.²⁴ The predictions of the models are consistent with the observed results from the individual controlled human exposure studies of O₃-induced FEV₁ decrements (79 FR 75250–51, see also U.S. EPA, 2013, Figures 6-1 and 6-3). CASAC agreed that these models mark a significant technical advance over the exposure-response modeling approach used for the lung function risk assessment in the last review and explicitly found that “[t]he MSS model to be scientifically and biologically defensible” (Frey, 2014a, pp. 8, 2). CASAC also stated that “the comparison of the MSS model results to those obtained with the exposure-response model is of tremendous importance. Typically, the MSS model gives a result about a factor of three higher . . . for school-age children, which is expected because the MSS model includes

¹⁷ CASAC concurred that these were “the kinds of identifiable effects on public health that are expected from the presence of ozone in the ambient air” (Frey 2014c, p. 3).

¹⁸ Table 6-1 of the ISA includes descriptions of the activity levels evaluated in controlled human exposure studies (U.S. EPA, 2013).

¹⁹ Adams (2006); (2002) both provide data for an additional group of 30 healthy subjects that were exposed via facemask to 60 ppb O₃ for 6.6 hours with moderate exercise. These subjects are described on page 133 of Adams (2006) and pages 747 and 761 of Adams (2002). The facemask exposure is not expected to affect the FEV₁ responses relative to a chamber exposure.

²⁰ For the 60 ppb target exposure concentration, Schelegle et al. (2009) reported that the actual mean exposure concentration was 63 ppb.

²¹ Adams (2006) did not find effects on FEV₁ at 60 ppb to be statistically significant. In an analysis of the Adams (2006) data, Brown et al. (2008) addressed the more fundamental question of whether there were statistically significant differences in responses before and after the 6.6 hour exposure period and found the average effect on FEV₁ at 60 ppb to be small, but highly statistically significant using several common statistical tests, even after removal of potential outliers. Schelegle et al. (2009) reported that, compared to filtered air, the largest change in FEV₁ for the 60 ppb protocol occurred after the sixth (and final) exercise period.

²² As noted above, for the 70 ppb exposure group, Schelegle et al. (2009) reported that the actual mean exposure concentration was 72 ppb.

²³ The ISA notes that by considering responses uncorrected for filtered air exposures, during which lung function typically improves (which would increase the size of the change, pre- and post-exposure), 10% is an underestimate of the proportion of healthy individuals that are likely to

experience clinically meaningful changes in lung function following exposure for 6.6 hours to 60 ppb O₃ during quasi-continuous moderate exertion (U.S. EPA, 2012, section 6.2.1.1).

²⁴ One of these models, the McDonnell-Stewart-Smith (MSS) model (McDonnell et al. 2012) was used to estimate the occurrences of lung function decrements in the HREA.

responses for a wider range of exposure protocols" (Frey, 2014a, pp. 8, 2).

Epidemiologic studies have consistently linked short-term increases in ambient O₃ concentrations with lung function decrements in diverse populations and lifestyles, including children attending summer camps, adults exercising or working outdoors, and groups with pre-existing respiratory diseases such as asthmatic children (U.S. EPA, 2013, section 6.2.1.2). Some of these studies reported O₃-associated lung function decrements accompanied by respiratory symptoms²⁵ in asthmatic children. In contrast, studies of children in the general population have reported similar O₃-associated lung function decrements but without accompanying respiratory symptoms (79 FR 75251; U.S. EPA, 2013, section 6.2.1.2). As noted in the PA (EPA, 2014c, pp. 4–70 to 4–71), additional research is needed to evaluate responses of people with asthma and healthy people in the 40 to 70 ppb range. Further epidemiologic studies and meta-analyses of the effects of O₃ exposure on children will help elucidate the concentration-response functions for lung function and respiratory symptom effects at lower O₃ concentrations.

Several epidemiologic panel studies²⁶ reported statistically significant associations with lung function decrements at relatively low ambient O₃ concentrations. For outdoor recreation or exercise, associations were reported in analyses restricted to 1-hour average O₃ concentrations less than 80 ppb, down to less than 50 ppb. Among outdoor workers, Brauer et al. (1996) found a robust association with daily 1-hour max O₃ concentrations less than 40 ppb. Ulmer et al. (1997) found a robust association in schoolchildren with 30-minute maximum O₃ concentrations less than 60 ppb. For 8-hour average O₃ concentrations, associations with lung function decrements in children with asthma were found to persist at concentrations less than 80 ppb in a U.S. multicity study (Mortimer et al., 2002) and less than 51 ppb in a study conducted in the Netherlands (Gielen et al., 1997).

As described in the proposal (79 FR 75251), several epidemiologic panel studies provided information on potential confounding by copollutants and most O₃ effect estimates for lung function were robust to adjustment for temperature, humidity, and copollutants

such as particulate matter with mass median aerodynamic diameter less than or equal to 2.5 micrometers (PM_{2.5}), particulate matter with mass median aerodynamic diameter less than or equal to 10 micrometers (PM₁₀), NO₂, or sulfur dioxide (SO₂) (Hoppe et al., 2003; Brunekreef et al., 1994; Hoek et al. 1993; U.S. EPA, 2013, pp. 6–67 to 6–69). Although examined in only a few epidemiologic studies, O₃ also remained associated with decreases in lung function with adjustment for pollen or acid aerosols (79 FR 75251; U.S. EPA, 2013, section 6.2.1.2).

Pulmonary Inflammation, Injury and Oxidative Stress

As described in detail in section II.B.2.a.ii of the proposal (79 FR 75252), O₃ exposures can result in increased respiratory tract inflammation and epithelial permeability. Inflammation is a host response to injury, and the induction of inflammation is evidence that injury has occurred. Oxidative stress has been shown to play a key role in initiating and sustaining O₃-induced inflammation. As noted in the ISA (U.S. EPA, 2013, section 6.2.3), O₃ exposures can initiate an acute inflammatory response throughout the respiratory tract that has been reported to persist for at least 18–24 hours after exposure.

Inflammation induced by exposure of humans to O₃ can have several potential outcomes, ranging from resolving entirely following a single exposure to becoming a chronic inflammatory state, as described in detail in section II.B.2.a.ii of the proposal (79 FR 75252) and in the ISA (U.S. EPA, 2013, section 6.2.3). Continued cellular damage due to chronic inflammation "may alter the structure and function of pulmonary tissues" (U.S. EPA, 2013, p. 6–161). Lung injury and the resulting inflammation provide a mechanism by which O₃ may cause other more serious morbidity effects (e.g., asthma exacerbations) (U.S. EPA, 2013, section 6.2.3).²⁷

Building on the last review, recent studies continue to support the evidence for airway inflammation and injury with new evidence for such effects following exposures to lower concentrations than had been evaluated previously. These studies include recent controlled human exposure and epidemiologic studies and are discussed more below.

An extensive body of evidence from controlled human exposure studies, described in section II.B.2.a.ii of the proposal, indicates that short-term exposures to O₃ can cause pulmonary inflammation and increases in polymorphonuclear leukocyte (PMN) influx and permeability following 80–600 O₃ ppb exposures, eosinophilic inflammation following exposures at or above 160 ppb, and O₃-induced PMN influx following exposures of healthy adults to 60 ppb O₃, the lowest concentration that has been evaluated for inflammation. A meta-analysis of 21 controlled human exposure studies (Mudway and Kelly, 2004) using varied experimental protocols (80–600 ppb O₃ exposures; 1–6.6 hours exposure duration; light to heavy exercise; bronchoscopy at 0–24 hours post-O₃ exposure) reported that PMN influx in healthy subjects is linearly associated with total O₃ dose.

As with FEV₁ responses to O₃, inflammatory responses to O₃ are generally reproducible within individuals, with some individuals experiencing more severe O₃-induced airway inflammation than indicated by group averages. Unlike O₃-induced decrements in lung function, which are attenuated following repeated exposures over several days, some markers of O₃-induced inflammation and tissue damage remain elevated during repeated exposures, indicating ongoing damage to the respiratory system (79 FR 75252). Most controlled human exposure studies have reported that asthmatics experience larger O₃-induced inflammatory responses than non-asthmatics.²⁸

In the previous review (U.S. EPA, 2006a), the epidemiologic evidence of O₃-associated changes in airway inflammation and oxidative stress was limited (79 FR 75253). Since then, as a result of the development of less invasive test methods, there has been a large increase in the number of studies assessing ambient O₃-associated changes in airway inflammation and oxidative stress, the types of biological samples collected, and the types of indicators. Most of these recent studies have evaluated biomarkers of inflammation or oxidative stress in exhaled breath, nasal lavage fluid, or induced sputum (U.S. EPA, 2013, section 6.2.3.2). These recent studies form a larger database to establish coherence with findings from controlled human exposure and animal

²⁵ Reversible loss of lung function in combination with the presence of symptoms meets ATS criteria for adversity (ATS, 2000a).

²⁶ Panel studies include repeated measurements of health outcomes, such as respiratory symptoms, at the individual level (U.S. EPA, 2013, p. 1x).

²⁷ CASAC also addressed this issue: "The CASAC believes that these modest changes in FEV₁ are usually associated with inflammatory changes, such as more neutrophils in the bronchoalveolar lavage fluid. Such changes may be linked to the pathogenesis of chronic lung disease" (Frey, 2014a p. 2).

²⁸ When evaluated, these studies have also reported O₃-induced respiratory symptoms in asthmatics. Specifically, Scannell et al. (1996), Basha et al. (1994), and Vagaggini et al. (2001, 2007) reported increased symptoms in addition to inflammation.

studies that have measured the same or related biological markers. Additionally, results from these studies provide further biological plausibility for the associations observed between ambient O₃ concentrations and respiratory symptoms and asthma exacerbations.

Airway Hyperresponsiveness (AHR)

A strong body of controlled human exposure and animal toxicological studies, most of which were available in the last review of the O₃ NAAQS, report O₃-induced AHR after either acute or repeated exposures (U.S. EPA, 2013, section 6.2.2.2). People with asthma often exhibit increased airway responsiveness at baseline relative to healthy control subjects, and asthmatics can experience further increases in responsiveness following exposures to O₃. Studies reporting increased airway responsiveness after O₃ exposure contribute to a plausible link between ambient O₃ exposures and increased respiratory symptoms in asthmatics, and increased hospital admissions and emergency department visits for asthma (section II.B.2.a.iii, 79 FR 75254; U.S. EPA, 2013, section 6.2.2.2).

Respiratory Symptoms and Medication Use

Respiratory symptoms are associated with adverse outcomes such as limitations in activity, and are the primary reason for people with asthma to use quick relief medication and to seek medical care. Studies evaluating the link between O₃ exposures and such symptoms allow a direct characterization of the clinical and public health significance of ambient O₃ exposure. Controlled human exposure and toxicological studies have described modes of action through which short-term O₃ exposures may increase respiratory symptoms by demonstrating O₃-induced AHR (U.S. EPA, 2013, section 6.2.2) and pulmonary inflammation (U.S. EPA, 2013, section 6.2.3).

The link between subjective respiratory symptoms and O₃ exposures has been evaluated in both controlled human exposure and epidemiologic studies, and the link with medication use has been evaluated in epidemiologic studies. In the last review, several controlled human exposure studies reported respiratory symptoms following exposures to O₃ concentrations at or above 80 ppb. In addition, one study reported such symptoms following exposures to 60 ppb O₃, though the increase was not statistically different from filtered air controls. Epidemiologic studies reported associations between ambient O₃ and

respiratory symptoms and medication use in a variety of locations and populations, including asthmatic children living in U.S. cities (U.S. EPA, 2013, pp. 6–1 to 6–2). In the current review, additional controlled human exposure studies have evaluated respiratory symptoms following exposures to O₃ concentrations below 80 ppb and recent epidemiologic studies have evaluated associations with respiratory symptoms and medication use (U.S. EPA, 2013, sections 6.2.1, 6.2.4).

As noted in section II.B.2.a.iv in the proposal (79 FR 75255), the findings for O₃-induced respiratory symptoms in controlled human exposure studies, and the evidence integrated across disciplines describing underlying modes of action, provide biological plausibility for epidemiologic associations observed between short-term increases in ambient O₃ concentration and increases in respiratory symptoms (U.S. EPA, 2013, section 6.2.4).

Most epidemiologic studies of O₃ and respiratory symptoms and medication use have been conducted in children and/or adults with asthma, with fewer studies, and less consistent results, in non-asthmatic populations (U.S. EPA, 2013, section 6.2.4). The 2006 AQCD (U.S. EPA, 2006a; U.S. EPA, 2013, section 6.2.4) concluded that the collective body of epidemiologic evidence indicated that short-term increases in ambient O₃ concentrations are associated with increases in respiratory symptoms in children with asthma. A large body of single-city and single-region studies of asthmatic children provides consistent evidence for associations between short-term increases in ambient O₃ concentrations and increased respiratory symptoms and asthma medication use in children with asthma (U.S. EPA, 2013, Figure 6–12, Table 6–20, section 6.2.4.1). Methodological differences, described in section II.B.2.a.iv of the proposal, among studies make comparisons across recent multicity studies of respiratory symptoms difficult.

Available evidence indicates that O₃-associated increases in respiratory symptoms are not confounded by temperature, pollen, or copollutants (primarily PM) (U.S. EPA, 2013, section 6.2.4.5; Table 6–25). However, identifying the independent effects of O₃ in some studies was complicated due to the high correlations observed between O₃ and PM or different lags and averaging times examined for copollutants. Nonetheless, the ISA noted that the robustness of associations in some studies of individuals with

asthma, combined with findings from controlled human exposure studies for the direct effects of O₃ exposure, provide substantial evidence supporting the independent effects of short-term ambient O₃ exposure on respiratory symptoms (U.S. EPA, 2013, section 6.2.4.5).

In summary, both controlled human exposure and epidemiologic studies have reported respiratory symptoms attributable to short-term O₃ exposures. In the last review, the majority of the evidence from controlled human exposure studies in young, healthy adults was for symptoms following exposures to O₃ concentrations at or above 80 ppb. Although studies that have become available since the last review have not reported increased respiratory symptoms in young, healthy adults following exposures with moderate exertion to 60 ppb, one recent study did report increased symptoms following exposure to 72 ppb O₃. As was concluded in the last review, the collective body of epidemiologic evidence indicates that short-term increases in ambient O₃ concentration are associated with increases in respiratory symptoms in children with asthma (U.S. EPA, 2013, section 6.2.4). Recent studies of respiratory symptoms and medication use, primarily in asthmatic children, add to this evidence. In a smaller body of studies, increases in ambient O₃ concentration were associated with increases in respiratory symptoms in adults with asthma.

Lung Host Defense

The mammalian respiratory tract has a number of closely integrated defense mechanisms that, when functioning normally, provide protection from the potential health effects of exposures to a wide variety of inhaled particles and microbes. Based on toxicological and human exposure studies, in the last review EPA concluded that available evidence indicates that short-term O₃ exposures have the potential to impair host defenses in humans, primarily by interfering with alveolar macrophage function. Any impairment in alveolar macrophage function may lead to decreased clearance of microorganisms or nonviable particles. Compromised alveolar macrophage functions in asthmatics may increase their susceptibility to other O₃ effects, the effects of particles, and respiratory infections (U.S. EPA, 2006a).

Relatively few studies conducted since the last review have evaluated the effects of O₃ exposures on lung host defense. As presented in section II.B.2.a.v of the proposal (79 FR 75256),

when the available evidence is taken as a whole, the ISA concludes that acute O₃ exposures impair the host defense capability of animals, primarily by depressing alveolar macrophage function and perhaps also by decreasing mucociliary clearance of inhaled particles and microorganisms. Coupled with limited evidence from controlled human exposure studies, this suggests that humans exposed to O₃ could be predisposed to bacterial infections in the lower respiratory tract.

Allergic and Asthma Related Responses

Evidence from controlled human exposure and epidemiologic studies available in the last review indicates that O₃ exposure skews immune responses toward an allergic phenotype and could also make airborne allergens more allergenic, as discussed in more detail in the proposal (79 FR 75257). Evidence from controlled human exposure and animal toxicology studies available in the last review indicates that O₃ may also increase AHR to specific allergen triggers (75 FR 2970, January 19, 2010). When combined with NO₂, O₃ has been shown to enhance nitration of common protein allergens, which may increase their allergenicity (Franze et al., 2005).

Hospital Admissions and Emergency Department Visits

The 2006 AQCD concluded that “the overall evidence supports a causal relationship between acute ambient O₃ exposures and increased respiratory morbidity resulting in increased emergency department visits and [hospital admissions] during the warm season”²⁹ (U.S. EPA, 2006a). This conclusion was “strongly supported by the human clinical, animal toxicologic[al], and epidemiologic evidence for [O₃-induced] lung function decrements, increased respiratory symptoms, airway inflammation, and airway hyperreactivity” (U.S. EPA, 2006a).

The results of recent studies largely support the conclusions of the 2006 AQCD (U.S. EPA, 2013, section 6.2.7). Since the completion of the 2006 AQCD, relatively fewer studies, conducted in the U.S., Canada, and Europe, have evaluated associations between short-term O₃ concentrations and respiratory hospital admissions and emergency department visits, with a growing

number of studies conducted in Asia. This epidemiologic evidence is discussed in detail in the proposal (79 FR 75258) and in the ISA (U.S. EPA, 2013, section 6.2.7).³⁰

In considering this body of evidence, the ISA focused primarily on multicity studies because they examine associations with respiratory-related hospital admissions and emergency department visits over large geographic areas using consistent statistical methodologies (U.S. EPA, 2013, section 6.2.7.1). The ISA also focused on single-city studies that encompassed a large number of daily hospital admissions or emergency department visits, included long study durations, were conducted in locations not represented by the larger studies, or examined population-specific characteristics that may impact the risk of O₃-related health effects but were not evaluated in the larger studies (U.S. EPA, 2013, section 6.2.7.1). When examining the association between short-term O₃ exposure and respiratory health effects that require medical attention, the ISA distinguishes between hospital admissions and emergency department visits because it is likely that a small percentage of respiratory emergency department visits will be admitted to the hospital; therefore, respiratory emergency department visits may represent potentially less serious, but more common outcomes (U.S. EPA, 2013, section 6.2.7.1).

The collective evidence across studies indicates a mostly consistent positive association between O₃ exposure and respiratory-related hospital admissions and emergency department visits. Moreover, the magnitude of these associations may be underestimated to the extent members of study populations modify their behavior in response to air quality forecasts, and to the extent such behavior modification increases exposure misclassification (U.S. EPA, 2013, Section 4.6.6). Studies examining the potential confounding effects of copollutants have reported that O₃ effect estimates remained relatively robust upon the inclusion of PM and gaseous pollutants in two-pollutant models (U.S. EPA, 2013, Figure 6–20, Table 6–29). Additional studies that conducted copollutant analyses, but did not present quantitative results, also support these conclusions (Strickland et al., 2010; Tolbert et al., 2007; Medina-Ramon et

al., 2006; U.S. EPA, 2013, section 6.2.7.5).³¹

In the last review, studies had not evaluated the concentration-response relationship between short-term O₃ exposure and respiratory-related hospital admissions and emergency department visits. As described in the proposal in section II.B.2.a.vii (79 FR 75257) and in the ISA (U.S. EPA, 2013, section 6.2.7.2), a preliminary examination of this relationship in studies that have become available since the last review found no evidence of a deviation from linearity when examining the association between short-term O₃ exposure and asthma hospital admissions (Silverman and Ito, 2010; Strickland et al., 2010). In addition, an examination of the concentration-response relationship for O₃ exposure and pediatric asthma emergency department visits found no evidence of a threshold at O₃ concentrations as low as 30 ppb (for daily maximum 8-hour concentrations) (U.S. EPA, 2013, section 6.2.7.3). However, in these studies there is uncertainty in the shape of the concentration-response curve at the lower end of the distribution of O₃ concentrations due to the low density of data in this range. Further studies at low-level O₃ exposures might reduce this uncertainty.

Respiratory Mortality

Evidence from experimental studies indicates multiple potential pathways of respiratory effects from short-term O₃ exposures, which support the continuum of respiratory effects that could potentially result in respiratory-related mortality in adults (U.S. EPA, 2013, section 6.2.8).³² The evidence in the last review was inconsistent for associations between short-term O₃ concentrations and respiratory mortality (U.S. EPA, 2006a). New epidemiologic evidence for respiratory mortality is discussed in detail in the ISA (U.S. EPA, 2013, section 6.6) and summarized below. The majority of recent multicity studies have reported positive associations between short-term O₃ exposures and respiratory mortality, particularly during the summer months (U.S. EPA, 2013, Figure 6–36).

²⁹ Epidemiologic associations for O₃ are more robust during the warm season than during cooler months (e.g., smaller measurement error, less potential confounding by copollutants). The rationale for focusing on warm season epidemiologic studies for O₃ can be found at 72 FR 37838–37840.

³⁰ The consideration of ambient O₃ concentrations in the locations of these epidemiologic studies are discussed in sections II.D.1.b and II.E.4.a below, for the current standard and for alternative standards, respectively.

³¹ The ISA concluded that “[o]verall, recent studies provide copollutant results that are consistent with those from the studies evaluated in the 2006 O₃ AQCD [U.S. EPA, 2006(a)], Figure 7–12, page 7–80 of the 2006 O₃ AQCD], which found that O₃ respiratory hospital admissions risk estimates remained robust to the inclusion of PM in copollutant models (U.S. EPA, 2013, pp. 6–152 to 6–153).

³² Premature mortality is discussed in more detail below in section II.A.1.b.iv.

Recent multicity studies from the U.S. (Zanobetti and Schwartz, 2008), Europe (Samoli et al., 2009), Italy (Stafoggia et al., 2010), and Asia (Wong et al., 2010), as well as a multi-continent study (Katsouyanni et al., 2009), reported associations between short-term O₃ concentrations and respiratory mortality (U.S. EPA, 2013, Figure 6–37, page 6–259). With respect to respiratory mortality, summer-only analyses were consistently positive and most were statistically significant. All-year analyses had more mixed results, but most were positive.

Of the studies evaluated, only two studies analyzed the potential for copollutant confounding of the O₃-respiratory mortality relationship (Katsouyanni et al., (2009); Stafoggia et al., (2010)). Based on the results of these analyses, the O₃ respiratory mortality risk estimates appear to be moderately to substantially sensitive (e.g., increased or attenuated) to inclusion of PM₁₀. However, in the APHENA study (Katsouyanni et al., 2009), the mostly every-6th-day sampling schedule for PM₁₀ in the Canadian and U.S. datasets greatly reduced their sample size and limits the interpretation of these results (U.S. EPA, 2013, sections 6.2.8 and 6.2.9).

The evidence for associations between short-term O₃ concentrations and respiratory mortality has been strengthened since the last review, with the addition of several large multicity studies. The biological plausibility of the associations reported in these studies is supported by the experimental evidence for respiratory effects.

ii. Respiratory Effects—Long-Term Exposure

Since the last review, the body of evidence indicating the occurrence of respiratory effects due to long-term O₃ exposure has been strengthened. This evidence is discussed in detail in the ISA (U.S. EPA, 2013, Chapter 7) and summarized below for new-onset asthma and asthma prevalence, asthma hospital admissions, pulmonary structure and function, and respiratory mortality.

Asthma is a heterogeneous disease with a high degree of temporal variability. The onset, progression, and symptoms can vary within an individual's lifetime, and the course of asthma may vary markedly in young children, older children, adolescents, and adults. In the previous review, longitudinal cohort studies that examined associations between long-term O₃ exposures and the onset of asthma in adults and children indicated

a direct effect of long-term O₃ exposures on asthma risk in adults and effect modification by O₃ in children. Since then, additional studies have evaluated associations with new onset asthma, further informing our understanding of the potential gene-environment interactions, mechanisms, and biological pathways associated with incident asthma.

In children, the relationship between long-term O₃ exposure and new-onset asthma has been extensively studied in the Children's Health Study (CHS), a long-term study that was initiated in the early 1990's which has evaluated effects in several cohorts of children. For this review, recent studies from the CHS provide evidence for gene-environment interactions in effects on new-onset asthma by indicating that the lower risks associated with specific genetic variants are found in children who live in lower O₃ communities. Described in detail in the proposal (79 FR 75259) and in the ISA (U.S. EPA, 2013, section 7.2.1), these studies indicate that the risk for new-onset asthma is related in part to genetic susceptibility, as well as behavioral factors and environmental exposure. Cross-sectional studies by Akinbami et al. (2010) and Hwang et al. (2005) provide further evidence relating O₃ exposures with asthma prevalence. Gene-environment interactions are discussed in detail in Section 5.4.2.1 in the ISA (U.S. EPA, 2013).

In the 2006 AQCD (U.S. EPA, 2006a), studies on O₃-related hospital discharges and emergency department visits for asthma and respiratory disease mainly looked at short-term (daily) metrics. Recent studies continue to indicate that there is evidence for increases in both hospital admissions and emergency department visits in children and adults related to all respiratory outcomes, including asthma, with stronger associations in the warm months.

In the 2006 AQCD (U.S. EPA, 2006a), few epidemiologic studies had investigated the effect of chronic O₃ exposure on pulmonary function. As discussed in the proposal, epidemiologic studies of long-term exposures in both children and adults provide mixed results about the effects of long-term O₃ exposure on pulmonary function and the growth rate of lung function.

Long-term studies in animals allow for greater insight into the potential effects of prolonged exposure to O₃ that may not be easily measured in humans, such as structural changes in the respiratory tract. Despite uncertainties, epidemiologic studies observing associations of O₃ exposure with

functional changes in humans can attain biological plausibility in conjunction with long-term toxicological studies, particularly O₃-inhalation studies performed in non-human primates whose respiratory systems most closely resemble that of the human. An important series of studies, discussed in section 7.2.3.2 of the ISA (U.S. EPA, 2013), have used nonhuman primates to examine the effect of O₃ alone, or in combination with an inhaled allergen, house dust mite antigen, on morphology and lung function. Animals exhibit the hallmarks of allergic asthma defined for humans (NHLBI, 2007). These studies and others have demonstrated changes in pulmonary function and airway morphology in adult and infant nonhuman primates repeatedly exposed to environmentally relevant concentrations of O₃ (U.S. EPA, 2013, section 7.2.3.2). As discussed in more detail in the proposal, the studies provide evidence of an O₃-induced change in airway resistance and responsiveness and provide biological plausibility of long-term exposure, or repeated short-term exposures, to O₃ contributing to the effects of asthma in children.

Collectively, evidence from animal studies strongly suggests that chronic O₃ exposure is capable of damaging the distal airways and proximal alveoli, resulting in lung tissue remodeling and leading to apparent irreversible changes. Potentially, persistent inflammation and interstitial remodeling play an important role in the progression and development of chronic lung disease. Further discussion of the modes of action that lead to O₃-induced morphological changes and the mechanisms involved in lifestage susceptibility and developmental effects can be found in the ISA (U.S. EPA, 2013, section 5.3.7, section 5.4.2.4). The findings reported in chronic animal studies offer insight into potential biological mechanisms for the suggested association between seasonal O₃ exposure and reduced lung function development in children as observed in epidemiologic studies (U.S. EPA, 2013, section 7.2.3.1). Further research could help fill in the gaps in our understanding of the mechanisms involved in lifestage susceptibility and developmental effects in children of seasonal or long-term exposure to O₃.

A limited number of epidemiologic studies have assessed the relationship between long-term exposure to O₃ and mortality in adults. The 2006 AQCD concluded that an insufficient amount of evidence existed "to suggest a causal relationship between chronic O₃ exposure and increased risk for

mortality in humans" (U.S. EPA, 2006a). Though total and cardio-pulmonary mortality were considered in these studies, respiratory mortality was not specifically considered.

In a recent follow-up analysis of the American Cancer Society cohort (Jerrett et al., 2009), cardiopulmonary deaths were separately subdivided into respiratory and cardiovascular deaths, rather than combined as in the Pope et al. (2002) work. Increased O₃ exposure was associated with the risk of death from respiratory causes, and this effect was robust to the inclusion of PM_{2.5}. Additionally, a recent multicity time series study (Zaubetti and Schwartz, 2011), which followed (from 1985 to 2006) four cohorts of Medicare enrollees with chronic conditions that might predispose to O₃-related effects, observed an association between long-term (warm season) exposure to O₃ and elevated risk of mortality in the cohort that had previously experienced an emergency hospital admission due to chronic obstructive pulmonary disease (COPD). A key limitation of this study is the inability to control for PM_{2.5}, because data were not available in these cities until 1999.

iii. Cardiovascular Effects—Short-Term Exposure

A relatively small number of studies have examined the potential effect of short-term O₃ exposure on the cardiovascular system. The 2006 AQCD (U.S. EPA, 2006a, p. 8–77) concluded that "O₃ directly and/or indirectly contributes to cardiovascular-related morbidity," but added that the body of evidence was limited. This conclusion was based on a controlled human exposure study that included hypertensive adult males; a few epidemiologic studies of physiologic effects, heart rate variability, arrhythmias, myocardial infarctions, and hospital admissions; and toxicological studies of heart rate, heart rhythm, and blood pressure.

More recently, the body of scientific evidence available that has examined the effect of O₃ on the cardiovascular system has expanded. There is an emerging body of animal toxicological evidence demonstrating that short-term exposure to O₃ can lead to autonomic nervous system alterations (in heart rate and/or heart rate variability) and suggesting that proinflammatory signals may mediate cardiovascular effects. Interactions of O₃ with respiratory tract components result in secondary oxidation product formation and subsequent production of inflammatory mediators, which have the potential to penetrate the epithelial barrier and to

initiate toxic effects systemically. In addition, animal toxicological studies of long-term exposure to O₃ provide evidence of enhanced atherosclerosis and ischemia/reperfusion (I/R) injury, corresponding with development of a systemic oxidative, proinflammatory environment. Recent experimental and epidemiologic studies have investigated O₃-related cardiovascular events and are summarized in the ISA (U.S. EPA, 2013, section 6.3).

Controlled human exposure studies discussed in previous reviews have not demonstrated any consistent extrapulmonary effects. In this review, evidence from controlled human exposure studies suggests cardiovascular effects in response to short-term O₃ exposure (U.S. EPA, 2013, section 6.3.1) and provides some coherence with evidence from animal toxicology studies. Controlled human exposure studies also support the animal toxicological studies by demonstrating O₃-induced effects on blood biomarkers of systemic inflammation and oxidative stress, as well as changes in biomarkers that can indicate the potential for increased clotting following O₃ exposures. Increases and decreases in high frequency heart rate variability (HRV) have been reported. These changes in cardiac function observed in animal and human studies provide preliminary evidence for O₃-induced modulation of the autonomic nervous system through the activation of neural reflexes in the lung (U.S. EPA, 2013, section 5.3.2).

Overall, the ISA concludes that the available body of epidemiologic evidence examining the relationship between short-term exposures to O₃ concentrations and cardiovascular morbidity is inconsistent (U.S. EPA, 2013, section 6.3.2.9).

Despite the inconsistent evidence for an association between O₃ concentration and cardiovascular disease (CVD) morbidity, mortality studies indicate a consistent positive association between short-term O₃ exposure and cardiovascular mortality in multicity studies and in a multi-continent study. When examining mortality due to CVD, epidemiologic studies consistently observe positive associations with short-term exposure to O₃. Additionally, there is some evidence for an association between long-term exposure to O₃ and mortality, although the association between long-term ambient O₃ concentrations and cardiovascular mortality can be confounded by other pollutants (U.S. EPA, 2013). The ISA (U.S. EPA, 2013, section 6.3.4) states that taken together, the overall body of evidence across the animal and human

studies is sufficient to conclude that there is likely to be a causal relationship between relevant short-term exposures to O₃ and cardiovascular system effects.

iv. Premature Mortality—Short-Term Exposure

The 2006 AQCD concluded that the overall body of evidence was highly suggestive that short-term exposure to O₃ directly or indirectly contributes to nonaccidental and cardiopulmonary-related mortality in adults, but additional research was needed to more fully establish underlying mechanisms by which such effects occur (U.S. EPA, 2006a; U.S. EPA, 2013, p. 2–18). In building on the evidence for mortality from the last review, the ISA states (U.S. EPA, 2013, p. 6–261):

The evaluation of new multicity studies that examined the association between short-term O₃ exposures and mortality found evidence that supports the conclusions of the 2006 AQCD. These new studies reported consistent positive associations between short-term O₃ exposure and all-cause (nonaccidental) mortality, with associations persisting or increasing in magnitude during the warm season, and provide additional support for associations between O₃ exposure and cardiovascular and respiratory mortality.

The 2006 AQCD reviewed a large number of time-series studies of associations between short-term O₃ exposures and total mortality including single- and multicity studies, and meta-analyses. Available studies reported some evidence for heterogeneity in O₃ mortality risk estimates across cities and across studies. Studies that conducted seasonal analyses reported larger O₃ mortality risk estimates during the warm or summer season. Overall, the 2006 AQCD identified robust associations between various measures of daily ambient O₃ concentrations and all-cause mortality, which could not be readily explained by confounding due to time, weather, or copollutants. With regard to cause-specific mortality, consistent positive associations were reported between short-term O₃ exposure and cardiovascular mortality, with less consistent evidence for associations with respiratory mortality. The majority of the evidence for associations between O₃ and cause-specific mortality were from single-city studies, which had small daily mortality counts and subsequently limited statistical power to detect associations. The 2006 AQCD concluded that "the overall body of evidence is highly suggestive that O₃ directly or indirectly contributes to nonaccidental and cardiopulmonary-related mortality" (U.S. EPA, 2013, section 6.6.1).

Recent studies have strengthened the body of evidence that supports the association between short-term O₃ concentrations and mortality in adults. This evidence includes a number of studies reporting associations with nonaccidental as well as cause-specific mortality. Multi-continent and multicity studies have consistently reported positive and statistically significant associations between short-term O₃ concentrations and all-cause mortality, with evidence for larger mortality risk estimates during the warm or summer months (79 FR 75262; U.S. EPA, 2013 Figure 6-27; Table 6-42). Similarly, evaluations of cause-specific mortality have reported consistently positive associations with O₃, particularly in analyses restricted to the warm season (79 FR 75262; U.S. EPA, 2013 Fig. 6-37; Table 6-53).

In the previous review, multiple uncertainties remained regarding the relationship between short-term O₃ concentrations and mortality, including the extent of residual confounding by copollutants; characterization of the factors that modify the O₃-mortality association; the appropriate lag structure for identifying O₃-mortality effects; and the shape of the O₃-mortality concentration-response function and whether a threshold exists. Many of the studies, published since the last review, have attempted to address one or more of these uncertainties and are described in more detail in the proposal (79 FR 75262 and in the ISA (U.S. EPA, 2013, section 6.6.2)).

In particular, recent studies have evaluated different statistical approaches to examine the shape of the O₃-mortality concentration-response relationship and to evaluate whether a threshold exists for O₃-related mortality. These studies are detailed in the proposal (79 FR 75262) and in the ISA (U.S. EPA, 2013, p. 2-32). The ISA reaches the following overall conclusions that the epidemiologic studies identified in the ISA indicated a generally linear C-R function with no indication of a threshold but that there is a lack of data at lower O₃ concentrations and therefore, less certainty in the shape of the C-R curve at the lower end of the distribution (U.S. EPA, 2013, p. 2-32).

c. Adversity of Effects

In making judgments as to when various O₃-related effects become regarded as adverse to the health of individuals, in previous NAAQS reviews, the EPA has relied upon the guidelines published by the ATS and the advice of CASAC. In 2000, the ATS published an official statement on

"What Constitutes an Adverse Health Effect of Air Pollution?" (ATS, 2000a), which updated and built upon its earlier guidance (ATS, 1985). The earlier guidance defined adverse respiratory health effects as "medically significant physiologic changes generally evidenced by one or more of the following: (1) Interference with the normal activity of the affected person or persons, (2) episodic respiratory illness, (3) incapacitating illness, (4) permanent respiratory injury, and/or (5) progressive respiratory dysfunction," while recognizing that perceptions of "medical significance" and "normal activity" may differ among physicians, lung physiologists and experimental subjects (ATS, 1985). The more recent guidance concludes that transient, reversible loss of lung function in combination with respiratory symptoms should be considered adverse.³³ However, the committee also recommended "that a small, transient loss of lung function, by itself, should not automatically be designated as adverse" (ATS, 2000a, p. 670).

There is also a more specific consideration of population risk in the 2000 guidance. Specifically, the committee considered that a shift in the risk factor distribution, and hence the risk profile of the exposed population, should be considered adverse, even in the absence of the immediate occurrence of frank illness (ATS, 2000a, p. 668). For example, a population of asthmatics could have a distribution of lung function such that no individual has a level associated with clinically important impairment. Exposure to air pollution could shift the distribution to lower levels of lung function that still do not bring any individual to a level that is associated with clinically relevant effects. However, this would be considered to be adverse because individuals within the population would already have diminished reserve function, and therefore would be at increased risk to further environmental insult (ATS, 2000a, p. 668).

The ATS also concluded in its guidance that elevations of biomarkers such as cell numbers and types, cytokines, and reactive oxygen species may signal risk for ongoing injury and more serious effects or may simply represent transient responses, illustrating the lack of clear boundaries that separate adverse from nonadverse events. More subtle health outcomes also may be connected mechanistically

to health effects that are clearly adverse, so that small changes in physiological measures may not appear clearly adverse when considered alone, but may be part of a coherent and biologically plausible chain of related health outcomes that include responses that are clearly adverse, such as mortality (U.S. EPA, 2014c, section 3.1.2.1).

Application of the ATS guidelines to the least serious category of effects³⁴ related to ambient O₃ exposures, which are also the most numerous and, therefore, are also important from a public health perspective, involves judgments about which medical experts on CASAC panels and public commenters have in the past expressed diverse views. To help frame such judgments, in past reviews, the EPA has defined gradations of individual functional responses (e.g., decrements in FEV₁ and airway responsiveness) and symptomatic responses (e.g., cough, chest pain, wheeze), together with judgments as to the potential impact on individuals experiencing varying degrees of severity of these responses. These gradations were used by the EPA in the 1997 O₃ NAAQS review and slightly revised in the 2008 review (U.S. EPA, 1996b, p. 59; U.S. EPA, 2007, p. 3-72; 72 FR 37849, July 11, 2007). These gradations and impacts are summarized in Tables 3-2 and 3-3 in the 2007 O₃ Staff Paper (U.S. EPA, 2007, pp. 3-74 to 3-75).

For the purpose of estimating potentially adverse lung function decrements in active healthy people, the CASAC panel in the 2008 O₃ NAAQS review indicated that a focus on the mid to upper end of the range of moderate levels of functional responses is most appropriate (e.g., FEV₁ decrements ≥15% but <20%) (Henderson, 2006; U.S. EPA, 2007, p. 3-76). In this review, CASAC reiterated that the "[e]stimation of FEV₁ decrements of ≥15% is appropriate as a scientifically relevant surrogate for adverse health outcomes in active healthy adults" (Frey, 2014c, p. 3).

For the purpose of estimating potentially adverse lung function decrements in people with lung disease, the CASAC panel in the 2008 O₃ NAAQS review indicated that a focus on the lower end of the range of moderate levels of functional responses is most appropriate (e.g., FEV₁ decrements ≥10%) (Henderson, 2006; U.S. EPA, 2007, p. 3-76). In their letter

³³ "In drawing the distinction between adverse and nonadverse reversible effects, this committee recommended that reversible loss of lung function in combination with the presence of symptoms should be considered as adverse" (ATS, 2000a).

³⁴ These include, for example, the transient and reversible effects demonstrated in controlled human exposure studies, such as lung function decrements or respiratory symptoms.

advising the Administrator on the reconsideration of the 2008 final decision, CASAC stated that “[a] 10% decrement in FEV₁ can lead to respiratory symptoms, especially in individuals with pre-existing pulmonary or cardiac disease. For example, people with chronic obstructive pulmonary disease have decreased ventilatory reserve (*i.e.*, decreased baseline FEV₁) such that a ≥ 10% decrement could lead to moderate to severe respiratory symptoms” (Samet, 2011). In this review, CASAC provided similar advice, stating that “[a]n FEV₁ decrement of ≥ 10% is a scientifically relevant surrogate for adverse health outcomes for people with asthma and lung disease”, and that such decrements “could be adverse for people with lung disease” (Frey, 2014c, pp. 3, 7).

In judging the extent to which these impacts represent effects that should be regarded as adverse to the health status of individuals, in previous NAAQS reviews, the EPA has also considered whether effects were experienced repeatedly during the course of a year or only on a single occasion (U.S. EPA, 2007). While some experts would judge single occurrences of moderate responses to be a “nuisance,” especially for healthy individuals, a more general consensus view of the adversity of such moderate responses emerges as the frequency of occurrence increases. In particular, not every estimated occurrence of an O₃-induced FEV₁ decrement will be adverse.³⁵ However, repeated occurrences of moderate responses, even in otherwise healthy individuals, may be considered to be adverse since they could set the stage for more serious illness (61 FR 65723). The CASAC panel in the 1997 NAAQS review expressed a consensus view that these “criteria for the determination of an adverse physiological response were reasonable” (Wolff, 1995). In the review completed in 2008, as in the current review (II.B, II.C below), estimates of repeated occurrences continued to be an important public health policy factor in judging the adversity of moderate lung function decrements in healthy and asthmatic people (72 FR 37850, July 11, 2007).

d. Ozone-Related Impacts on Public Health

The currently available evidence expands the understanding of populations that were identified to be at greater risk of O₃-related health effects

at the time of the last review (*i.e.*, people who are active outdoors, people with lung disease, children and older adults and people with increased responsiveness to O₃) and supports the identification of additional factors that may lead to increased risk (U.S. EPA, 2006a, section 6.3; U.S. EPA, 2013, Chapter 8). Populations and lifestyles may be at greater risk for O₃-related health effects due to factors that contribute to their susceptibility and/or vulnerability to O₃. The definitions of susceptibility and vulnerability have been found to vary across studies, but in most instances “susceptibility” refers to biological or intrinsic factors (*e.g.*, lifestyle, sex, preexisting disease/conditions) while “vulnerability” refers to non-biological or extrinsic factors (*e.g.*, socioeconomic status (SES)) (U.S. EPA, 2013, p. 8–1; U.S. EPA, 2010, 2009b). In some cases, the terms “at-risk” and “sensitive” have been used to encompass these concepts more generally. In the ISA, PA, and proposal, “at-risk” is the all-encompassing term used to define groups with specific factors that increase their risk of O₃-related health effects.

There are multiple avenues by which groups may experience increased risk for O₃-induced health effects. A population or lifestyle³⁶ may exhibit greater effects than other populations or lifestyles exposed to the same concentration or dose, or they may be at greater risk due to increased exposure to an air pollutant (*e.g.*, time spent outdoors). A group with intrinsically increased risk would have some factor(s) that increases risk through a biological mechanism and, in general, would have a steeper concentration-risk relationship, compared to those not in the group. Factors that are often considered intrinsic include pre-existing asthma, genetic background, and lifestyle. A group of people could also have extrinsically increased risk, which would be through an external, non-biological factor, such as socioeconomic status (SES) and diet. Some groups are at risk of increased internal dose at a given exposure concentration, for example, because of breathing patterns. This category would include people who work or exercise outdoors. Finally, there are those who might be placed at increased risk for experiencing greater exposures by being exposed to higher O₃ concentrations. This would include, for example, groups of people with greater exposure

to ambient O₃ due to less availability or use of home air conditioners such that they are more likely to be in locations with open windows on high O₃ days. Some groups may be at increased risk of O₃-related health effects through a combination of factors. For example, children tend to spend more time outdoors when O₃ levels are high, and at higher levels of activity than adults, which leads to increased exposure and dose, and they also have biological, or intrinsic, risk factors (*e.g.*, their lungs are still developing) (U.S. EPA, 2013, Chapter 8). An at-risk population or lifestyle is more likely to experience adverse health effects related to O₃ exposures and/or, develop more severe effects from exposure than the general population. The populations and lifestyles identified by the ISA (U.S. EPA, 2013, section 8.5) identified that have “adequate” evidence for increased O₃-related health effects are people with certain genotypes, people with asthma, younger and older age groups, people with reduced intake of certain nutrients, and outdoor workers. These at-risk populations and lifestyles are described in more detail in section II.B.4 of the proposal (79 FR 75264–269).

One consideration in the assessment of potential public health impacts is the size of various population groups for which there is adequate evidence of increased risk for health effects associated with O₃-related air pollution exposure (U.S. EPA, 2014c, section 3.1.5.2). The factors for which the ISA judged the evidence to be “adequate” with respect to contributing to increased risk of O₃-related effects among various populations and lifestyles included: Asthma; childhood and older adulthood; diets lower in vitamins C and E; certain genetic variants; and working outdoors (U.S. EPA, 2013, section 8.5). No statistics are available to estimate the size of an at-risk population based on nutritional status or genetic variability.

With regard to asthma, Table 3–7 in the PA (U.S. EPA, 2014c, section 3.1.5.2) summarizes information on the prevalence of current asthma by age in the U.S. adult population in 2010 (Schiller et al. 2012; children—Bloom et al., 2011). Individuals with current asthma constitute a fairly large proportion of the population, including more than 25 million people. Asthma prevalence tends to be higher in children than adults. Within the U.S., approximately 8.2% of adults have reported currently having asthma (Schiller et al., 2012) and 9.5% of

³⁵ As noted above, the ATS recommended “that a small, transient loss of lung function, by itself, should not automatically be designated as adverse” (ATS, 2000a, p. 670).

³⁶ Lifestyles, which in this case includes childhood and older adulthood, are experienced by most people over the course of a lifetime, unlike other factors associated with at-risk populations.

children have reported currently having asthma (Bloom et al., 2011).³⁷

With regard to lifestages, based on U.S. census data from 2010 (Howden and Meyer, 2011), about 74 million people, or 24% of the U.S. population, are under 18 years of age and more than 40 million people, or about 13% of the U.S. population, are 65 years of age or older. Hence, a large proportion of the U.S. population (*i.e.*, more than a third) is included in age groups that are considered likely to be at increased risk for health effects from ambient O₃ exposure.

With regard to outdoor workers, in 2010, approximately 11.7% of the total number of people (143 million people) employed, or about 16.8 million people, worked outdoors one or more days per week (based on worker surveys).³⁸ Of these, approximately 7.4% of the workforce, or about 7.8 million people, worked outdoors three or more days per week.

While it is difficult to estimate the total number of people in groups that are at greater risk from exposure to O₃, due to the overlap in members of the different at-risk population groups, the proportion of the total population at greater risk is large. The size of the at-risk population combined with the estimates of risk of different health outcomes associated with exposure to O₃ can give an indication of the magnitude of O₃ impacts on public health.

2. Overview of Human Exposure and Health Risk Assessments

To put judgments about health effects into a broader public health context, the EPA has developed and applied models to estimate human exposures to O₃ and O₃-associated health risks. Exposure and risk estimates that are output from such models are presented and assessed in the HREA (U.S. EPA, 2014a). Section II.C of the proposal discusses the quantitative assessments of O₃ exposures and O₃-related health risks that are presented in the HREA (79 FR

75270). Summaries of these discussions are provided below for the approach used to adjust air quality for quantitative exposure and risk analyses in the HREA (II.A.2.a), the HREA assessment of exposures to ambient O₃ (II.A.2.b), and the HREA assessments of O₃-related health risks (II.A.2.c).

a. Air Quality Adjustment

As discussed in section II.C.1 of the proposal (79 FR 75270), the HREA uses a photochemical model to estimate sensitivities of O₃ to changes in precursor emissions in order to estimate ambient O₃ concentrations that would just meet the current and alternative standards (U.S. EPA, 2014a, Chapter 4).³⁹ For the 15 urban study areas evaluated in the HREA,⁴⁰ this model-based adjustment approach estimates hourly O₃ concentrations at each monitor location when modeled U.S. anthropogenic precursor emissions (*i.e.*, NO_x, VOC)⁴¹ are reduced. The HREA estimates air quality that just meets the current and alternative standards for the 2006–2008 and 2008–2010 periods.⁴²

As discussed in Chapter 4 of the HREA (U.S. EPA, 2014a), this approach to adjusting air quality models the physical and chemical atmospheric processes that influence ambient O₃ concentrations. Compared to the quadratic rollback approach used in previous reviews, it provides more realistic estimates of the spatial and temporal responses of O₃ to reductions in precursor emissions. Because ambient NO_x can contribute both to the formation and destruction of O₃ (U.S. EPA, 2014a, Chapter 4), the response of ambient O₃ concentrations to reductions in NO_x emissions is more variable than

indicated by the quadratic rollback approach. This improved approach to adjusting O₃ air quality is consistent with recommendations from the National Research Council of the National Academies (NRC, 2008). In addition, CASAC strongly supported the new approach as an improvement and endorsed the way it was utilized in the HREA, stating that “the quadratic rollback approach has been replaced by a scientifically more valid Higher-order Decoupled Direct Method (HDDM)” and that “[t]he replacement of the quadratic rollback procedure by the HDDM procedure is important and supported by the CASAC” (Frey, 2014a, pp. 1 and 3).

Within urban study areas, the model-based air quality adjustments show reductions in the O₃ levels at the upper ends of ambient concentrations and increases in the O₃ levels at the lower ends of those distributions (U.S. EPA, 2014a, section 4.3.3.2, Figures 4–9 and 4–10).⁴³ Seasonal means of daily O₃ concentrations generally exhibit only modest changes upon model adjustment, reflecting the seasonal balance between daily decreases in relatively higher concentrations and increases in relatively lower concentrations (U.S. EPA, 2014a, Figures 4–9 and 4–10). The resulting compression in the seasonal distributions of ambient O₃ concentrations is evident in all of the urban study areas evaluated, though the degree of compression varies considerably across areas (U.S. EPA, 2014a, Figures 4–9 and 4–10).

As discussed in the PA (U.S. EPA, 2014c, section 3.2.1), adjusted patterns of O₃ air quality have important implications for exposure and risk estimates in urban case study areas. Estimates influenced largely by the upper ends of the distribution of ambient concentrations (*i.e.*, exposures of concern and lung function risk estimates, as discussed in sections 3.2.2 and 3.2.3.1 of the PA) will decrease with model-adjustment to the current and alternative standards. In contrast, seasonal risk estimates influenced by the full distribution of ambient O₃ concentrations (*i.e.*, epidemiology-based risk estimates, as discussed in section 3.2.3.2 of the PA) either increase or decrease in response to air quality adjustment, depending on the balance between the daily decreases in high O₃

³⁷ As noted below (II.C.3.a.ii), asthmatics can experience larger O₃-induced respiratory effects than non-asthmatic, healthy adults. The responsiveness of asthmatics to O₃ exposures could depend on factors that have not been well-evaluated such as asthma severity, the effectiveness of asthma control, or the prevalence of medication use.

³⁸ The O*NET program is the nation's primary source of occupational information. Central to the project is the O*NET database, containing information on hundreds of standardized and occupation-specific descriptors. The database, which is available to the public at no cost, is continually updated by surveying a broad range of workers from each occupation. <http://www.onetcenter.org/overview.html>, http://www.onetonline.org/find/descriptor/browse/Work_Context/4.C.2/.

³⁹ The HREA uses the Community Multi-scale Air Quality (CMAQ) photochemical model instrumented with the higher order direct decoupled method (HDDM) to estimate O₃ concentrations that would occur with the achievement of the current and alternative O₃ standards (U.S. EPA, 2014a, Chapter 4).

⁴⁰ The urban study areas assessed are Atlanta, Baltimore, Boston, Chicago, Cleveland, Dallas, Denver, Detroit, Houston, Los Angeles, New York, Philadelphia, Sacramento, St. Louis, and Washington, DC.

⁴¹ Exposure and risk analyses for most of the urban study areas focus on reducing U.S. anthropogenic NO_x emissions alone. The exceptions are Chicago and Denver. Exposure and risk analyses for Chicago and Denver are based on reductions in emissions of both NO_x and VOC (U.S. EPA, 2014a, section 4.3.3.1; Appendix 4D).

⁴² These estimates thus reflect design values—8 hour values using the form of the NAAQS that meet the level of the current or alternative standards. These simulations are illustrative and do not reflect any consideration of specific control programs designed to achieve the reductions in emissions required to meet the specified standards. Further, these simulations do not represent predictions of when, whether, or how areas might meet the specified standards.

⁴³ It is important to note that sensitivity analyses in the HREA indicate that the increases in low O₃ concentrations are smaller when NO_x and VOC emissions are reduced than when only NO_x emissions are reduced (U.S. EPA, 2014a, Appendix 4–D, section 4.7).

concentrations and increases in low O₃ concentrations.⁴⁴

To evaluate uncertainties in air quality adjustments, the HREA assessed the extent to which the modeled O₃ response to reductions in NO_x emissions appropriately represent the trends observed in monitored ambient O₃ following actual reductions in NO_x emissions, and the extent to which the O₃ response to reductions in precursor emissions could differ with emissions reduction strategies that are different from those used in HREA to generate risk estimates.

To evaluate the first issue, the HREA conducted a national analysis evaluating trends in monitored ambient O₃ concentrations during a time period when the U.S. experienced large-scale reductions in NO_x emissions (*i.e.*, 2001 to 2010). Analyses of trends in monitored O₃ indicate that over such a time period, the upper end of the distribution of monitored O₃ concentrations (*i.e.*, indicated by the 95th percentile) generally decreased in urban and non-urban locations across the U.S. (U.S. EPA, 2014a, Figure 8–29). During this same time period, median O₃ concentrations decreased in suburban and rural locations, and in some urban locations. However, median concentrations increased in some large urban centers (U.S. EPA, 2014a, Figure 8–28). As discussed in the HREA, these increases in median concentrations likely reflect the increases in relatively low O₃ concentrations that can occur near important sources of NO_x upon reductions in NO_x emissions (U.S. EPA, 2014a, section 8.2.3.1). These patterns of monitored O₃ during a period when the U.S. experienced large reductions in NO_x emissions are qualitatively consistent with the modeled responses of O₃ to reductions in NO_x emissions.

To evaluate the second issue, the HREA assessed the O₃ air quality response to reducing both NO_x and VOC emissions (*i.e.*, in addition to assessing reductions in NO_x emissions alone) for a subset of seven urban study areas. As discussed in the PA (U.S. EPA, 2014c, section 3.2.1), the addition of VOC reductions generally resulted in larger decreases in mid-range O₃ concentrations (25th to 75th percentiles) (U.S. EPA, 2014a, Appendix 4D, section 4.7).⁴⁵ In addition, in all seven of the

urban study areas evaluated, the increases in low O₃ concentrations were smaller for the NO_x/VOC scenarios than the NO_x alone scenarios (U.S. EPA, 2014a, Appendix 4D, section 4.7). This was most apparent for Denver, Houston, Los Angeles, New York, and Philadelphia. Given the impacts on total risk estimates of increases in low O₃ concentrations (discussed below), these results suggest that in some locations optimized emissions reduction strategies could result in larger reductions in O₃-associated mortality and morbidity than indicated by HREA estimates.

b. Exposure Assessment

As discussed in section II.C.2 of the proposal, the O₃ exposure assessment presented in the HREA (U.S. EPA, 2014a, Chapter 5) provides estimates of the number and percent of people exposed to various concentrations of ambient O₃ while at specified exertion levels. The HREA estimates exposures in the 15 urban study areas for four study groups, all school-age children (ages 5 to 18), asthmatic school-age children, asthmatic adults (ages 19 to 95), and all older adults (ages 65 to 95), reflecting the evidence indicating that these populations are at increased risk for O₃-attributable effects (U.S. EPA, 2013, Chapter 8; II.A.1.d, above). An important purpose of these exposure estimates is to provide perspective on the extent to which air quality adjusted to just meet the current O₃ NAAQS could be associated with exposures to O₃ concentrations reported to result in respiratory effects.⁴⁶ These analyses of exposure assessment incorporate behavior patterns, including estimates of physical exertion, which are critical in assessing whether ambient concentrations of O₃ may pose a public health risk.⁴⁷ In particular, exposures to

(U.S. EPA, 2014a, Appendix 4–D, section 4.7). In this analysis, emissions of NO_x and VOC were reduced by equal percentages, a scenario not likely to reflect the optimal combination for reducing risks. In most of the urban study areas the inclusion of VOC emissions reductions did not alter the NO_x emissions reductions required to meet the current or alternative standards. The exceptions are Chicago and Denver, for which the HREA risk estimates are based on reductions in both NO_x and VOC (U.S. EPA, 2014a, section 4.3.3.1).

⁴⁶ In addition, the range of modeled personal exposures to ambient O₃ provide an essential input to the portion of the health risk assessment based on exposure-response functions (for lung function decrements) from controlled human exposure studies. The health risk assessment based on exposure-response information is discussed below (II.C.3).

⁴⁷ See 79 FR 75269 “The activity pattern of individuals is an important determinant of their exposure. Variation in O₃ concentrations among various microenvironments means that the amount of time spent in each location, as well as the level

ambient or near-ambient O₃ concentrations have only been shown to result in potentially adverse effects if the ventilation rates of people in the exposed populations are raised to a sufficient degree (*e.g.*, through physical exertion) (U.S. EPA, 2013, section 6.2.1.1). Estimates of such “exposures of concern” provide perspective on the potential public health impacts of O₃-related effects, including effects that cannot currently be evaluated in a quantitative risk assessment.⁴⁸

The HREA estimates 8-hour exposures at or above benchmark concentrations of 60, 70, and 80 ppb for individuals engaged in moderate or greater exertion (*i.e.*, to approximate conditions in the controlled human exposure studies on which benchmarks are based). Benchmarks reflect exposure concentrations at which O₃-induced respiratory effects are known to occur in some healthy adults engaged in moderate, quasi-continuous exertion, based on evidence from controlled human exposure studies (U.S. EPA, 2013, section 6.2; U.S. EPA, 2014c, section 3.1.2.1). The amount of weight to place on the estimates of exposures at or above specific benchmark concentrations depends in part on the weight of the scientific evidence concerning health effects associated with O₃ exposures at those benchmark concentrations. It also depends on judgments about the importance, from a public health perspective, of the health effects that are known or can reasonably be inferred to occur as a result of exposures at benchmark concentrations (U.S. EPA, 2014c, sections 3.1.3, 3.1.5).

In considering estimates of O₃ exposures of concern at or above benchmarks of 60, 70, and 80 ppb, the PA focuses on modeled exposures for school-age children (ages 5–18), including asthmatic school-age children, which are key at-risk populations identified in the ISA (U.S. EPA, 2014c, section 3.1.5). The percentages of children estimated to experience exposures of concern are considerably larger than the percentages estimated for adult populations (*i.e.*, approximately 3-fold larger across urban

of activity, will influence an individual's exposure to ambient O₃. Activity patterns vary both among and within individuals, resulting in corresponding variations in exposure across a population and over time” (internal citations omitted).

⁴⁸ In this review, the term “exposure of concern” is defined as a personal exposure, while at moderate or greater exertion, to 8-hour average ambient O₃ concentrations at and above specific benchmark levels. As discussed below, these benchmark levels represent exposure concentrations at which O₃-induced health effects are known to occur, or can reasonably be anticipated to occur, in some individuals.

⁴⁴ In addition, because epidemiology-based risk estimates use “area-wide” average O₃ concentrations, calculated by averaging concentrations across multiple monitors in urban case study areas (section 3.2.3.2 below), risk estimates on a given day depend on the daily balance between increasing and decreasing O₃ concentrations at individual monitors.

⁴⁵ This was the case for all of the urban study areas evaluated, with the exception of New York

study areas)⁴⁹ (U.S. EPA, 2014a, section 5.3.2 and Figures 5–5 to 5–8). The larger exposure estimates for children are due primarily to the larger percentage of children estimated to spend an extended period of time being physically active outdoors when O₃ concentrations are elevated (U.S. EPA, 2014a, sections 5.3.2 and 5.4.1).

Although exposure estimates differ between children and adults, the patterns of results across the urban study areas and years are similar among all of the populations evaluated (U.S. EPA, 2014a, Figures 5–5 to 5–8). Therefore, while the PA highlights estimates in children, including asthmatic school-age children, it also

notes that the patterns of exposures estimated for children represent the patterns estimated for adult asthmatics and older adults.

Table 1 of the proposal (79 FR 75272 to 75273) summarizes key results from the exposure assessment. This table is reprinted below.

TABLE 1—SUMMARY OF ESTIMATED EXPOSURES OF CONCERN IN ALL SCHOOL-AGE CHILDREN FOR THE CURRENT AND ALTERNATIVE O₃ STANDARDS IN URBAN STUDY AREAS

Benchmark concentration	Standard level (ppb)	Average % children exposed ⁵⁰	Average number of children exposed [average number of asthmatic children] ⁵¹	% Children—worst year and worst area
One or more exposures of concern per season				
≥ 80 ppb	75	0–0.3 (0.1)	27,000 [3,000]	1.1
	70	0–0.1 (0)	3,700 [300]	0.2
	65	0 (0)	300 [0]	0
	60	0 (0)	100 ⁵² [0]	0
≥ 70 ppb	75	0.6–3.3 (1.9)	362,000 [40,000]	8.1
	70	0.1–1.2 (0.5)	94,000 [10,000]	3.2
	65	0–0.2 (0.1)	14,000 [2,000]	0.5
	60	0 (0)	1,400 [200]	0.1
≥ 60 ppb	75	9.5–17 (12.2)	2,316,000 [246,000]	25.8
	70	3.3–10.2 (6.2)	1,176,000 [126,000]	18.9
	65	0–4.2 (2.1)	392,000 [42,000]	9.5
	60	0–1.2 (0.4)	70,000 [8,000]	2.2
Two or more exposures of concern per season				
≥ 80 ppb	75	0 (0)	600 [100]	0.1
	70	0 (0)	0 [0]	0
	65	0 (0)	0 [0]	0
	60	0 (0)	0 [0]	0
≥ 70 ppb	75	0.1–0.6 (0.2)	46,000 [5,000]	2.2
	70	0–0.1 (0)	5,400 [600]	0.4
	65	0 (0)	300 [100]	0
	60	0 (0)	0 [0]	0
≥ 60 ppb	75	3.1–7.6 (4.5)	865,000 [93,000]	14.4
	70	0.5–3.5 (1.7)	320,000 [35,000]	9.2
	65	0–0.8 (0.3)	67,000 [7,500]	2.8
	60	0–0.2 (0)	5,100 [700]	0.3

Uncertainties in exposure estimates are summarized in section II.C.2.b of the proposal (79 FR 75273). For example, due to variability in responsiveness, only a subset of individuals who experience exposures at or above a benchmark concentration can be expected to experience health effects.⁵³ In addition, not all of these effects will

be adverse. Given the lack of sufficient exposure-response information for most of the health effects that informed benchmark concentrations, estimates of the number of people likely to experience exposures at or above benchmark concentrations generally cannot be translated into quantitative estimates of the number of people likely

to experience specific health effects.⁵⁴ The PA views health-relevant exposures as a continuum with greater confidence and less uncertainty about the existence of adverse health effects at higher O₃ exposure concentrations, and less confidence and greater uncertainty as one considers lower exposure concentrations (e.g., U.S. EPA, 2014c,

⁴⁹ HREA exposure estimates for all children and asthmatic children are virtually indistinguishable, in terms of the percent estimated to experience exposures of concern (U.S. EPA, 2014a, Chapter 5). Consistent with this, HREA analyses indicate that activity data for people with asthma is generally similar to non-asthmatic populations (U.S. EPA, 2014a, Appendix 5G, Tables 5G2-to 5G-5).

⁵⁰ Estimates for each urban case study area were averaged for the years evaluated in the HREA (2006 to 2010). Ranges reflect the ranges across urban study areas. Estimates smaller than 0.05% were rounded downward to zero (from U.S. EPA, 2014a, Tables 5–11 and 5–12). Numbers in parentheses

reflect averages across urban study areas, as well as over the years evaluated in the HREA.

⁵¹ Numbers of children exposed in each urban case study area were averaged over the years 2006 to 2010. These averages were then summed across urban study areas. Numbers were rounded to nearest thousand unless otherwise indicated. Estimates smaller than 50 were rounded downward to zero (from U.S. EPA, 2014a, Appendix 5F Table 5F-5).

⁵² As discussed in section 4.3.3 of the HREA, the model-based air quality adjustment approach used to estimate exposures and lung function decrements associated with the current and alternative standards was unable to estimate the distribution of

ambient O₃ concentrations in New York City upon just meeting an alternative standard with a level of 60 ppb. Therefore, for the 60 ppb standard level, the numbers of children and asthmatic children, and the ranges of percentages, reflect all of the urban study areas except New York.

⁵³ As noted below (II.C.3.e.ii), in the case of asthmatics, responsiveness to O₃ could depend on factors that have not been well-evaluated, such as asthma severity, the effectiveness of asthma control, or the prevalence of medication use.

⁵⁴ The exception to this is lung function decrements, as discussed below (and in U.S. EPA, 2014c, section 3.2.3.1).

sections 3.1 and 4.6). This view draws from the overall body of available health evidence, which indicates that as exposure concentrations increase, the incidence, magnitude, and severity of effects increases.

Another important uncertainty is that there is very limited evidence from controlled human exposure studies, which provided the basis for health benchmark concentrations for both exposures of concern and lung function decrements, related to clinical responses in at-risk populations. Compared to the healthy young adults included in the controlled human exposure studies, members of at-risk populations could be more likely to experience adverse effects, could experience larger and/or more serious effects, and/or could experience effects following exposures to lower O₃ concentrations.⁵⁵

There are also uncertainties associated with the exposure modelling. These are described most fully, and their potential impact characterized, in section 5.5.2 of the HREA (U.S. EPA, 2013, pp. 5–72 to 5–79). These include interpretation of activity patterns set forth in diaries which do not typically distinguish the basis for activity patterns and so may reflect averting behavior,⁵⁶ and whether the HREA underestimates exposures for groups spending especially large proportion of time being active outdoors during the O₃ season (outdoor workers and especially active children).

c. Quantitative Health Risk Assessments

As discussed in section II.C.3 of the proposal (79 FR 75274), for some health endpoints, there is sufficient scientific evidence and information available to support the development of quantitative estimates of O₃-related health risks. In the current review, for short-term O₃ concentrations, the HREA estimates lung function decrements; respiratory symptoms in asthmatics; hospital admissions and emergency department visits for respiratory causes; and all-cause mortality (U.S. EPA, 2014a). For long-term O₃ concentrations, the HREA estimates respiratory mortality (U.S. EPA, 2014a).⁵⁷ Estimates of O₃-induced lung function decrements are based on exposure modeling using the MSS model (see section II.1.b.i.(1) above, and 79 FR 75250), combined with exposure-response relationships from controlled human exposure studies (U.S. EPA, 2014a, Chapter 6). Estimates of O₃-associated respiratory symptoms, hospital admissions and emergency department visits, and mortality are based on concentration-response relationships from epidemiologic studies (U.S. EPA, 2014a, Chapter 7). As with the exposure assessment discussed above, O₃-associated health risks are estimated for recent air quality and for ambient concentrations adjusted to just meet the current and alternative O₃ standards, based on 2006–2010 air quality and adjusted precursor emissions. The following sections summarize the discussions from the

proposal on the lung function risk assessment (II.A.2.c.i) and the epidemiology-based morbidity and mortality risk assessments (II.A.2.c.ii).

i. Lung Function Risk Assessment

The HREA estimates risks of lung function decrements in school-aged children (ages 5 to 18), asthmatic school-aged children, and the general adult population for the 15 urban study areas. The results presented in the HREA are based on an updated dose-threshold model that estimates FEV₁ responses for individuals following short-term exposures to O₃ (McDonnell et al., 2012), reflecting methodological improvements since the last review (II.B.2.a.i (1), above; U.S. EPA, 2014a, section 6.2.4). The impact of the dose threshold is that O₃-induced FEV₁ decrements result primarily from exposures on days with average ambient O₃ concentrations above about 40 ppb (U.S. EPA, 2014a, section 6.3.1, Figure 6–9).⁵⁸

Table 2 in the proposal (79 FR 75275), and reprinted below, summarizes key results from the lung function risk assessment. Table 2 presents estimates of the percentages of school-aged children estimated to experience O₃-induced FEV₁ decrements >10, 15, or 20% when air quality was adjusted to just meet the current and alternative 8-hour O₃ standards. Table 2 also presents the numbers of children, including children with asthma, estimated to experience such decrements.

TABLE 2—SUMMARY OF ESTIMATED O₃-INDUCED LUNG FUNCTION DECREMENTS FOR THE CURRENT AND POTENTIAL ALTERNATIVE O₃ STANDARDS IN URBAN CASE STUDY AREAS

Lung function decrement	Alternative standard level	Average % children ⁵⁹	Number of children (5 to 18 years) [number of asthmatic children] ⁶⁰	% Children worst year and area
One or more decrements per season				
≥10%	75	14–19	3,007,000 [312,000]	22
	70	11–17	2,527,000 [261,000]	20
	65	3–15	1,896,000 [191,000]	18
	60	5–11	1,404,000 [139,000]	13
≥15%	75	3–5	766,000 [80,000]	7
	70	2–4	562,000 [58,000]	5
	65	0–3	356,000 [36,000]	4
	60	1–2	225,000 [22,000]	3
≥20%	75	1–2	285,000 [30,000]	2.8
	70	1–2	189,000 [20,000]	2.1
	65	0–1	106,000 [11,000]	1.4
	60	0–1	57,000 [6,000]	0.9

⁵⁵ “The CASAC further notes that clinical studies do not address sensitive subgroups, such as children with asthma, and that there is a scientific basis to anticipate that the adverse effects for such subgroups are likely to be more significant at 60 ppb than for healthy adults” (Frey 2014a, p. 7).

⁵⁶ See EPA 2014a pp. 5–53 to 54 describing EPA’s sensitivity analysis regarding impacts of potential averting behavior for school-age children on the

exposure and lung function decrement estimate, and see also section B.2.a.i below.

⁵⁷ Estimates of O₃-associated respiratory mortality are based on the study by Jerrett *et al.* (2009). This study used seasonal averages of 1-hour daily maximum O₃ concentrations to estimate long-term concentrations.

⁵⁸ Analysis of this issue in the HREA is based on risk estimates in Los Angeles for 2006 unadjusted air quality. The HREA shows that more than 90% of daily instances of FEV₁ decrements ≥10% occur when 8-hr average ambient concentrations are above 40 ppb for this modeled scenario. The HREA notes that the distribution of responses will be different for different study areas, years, and air quality scenarios (U.S. EPA, 2014c, Chapter 6).

TABLE 2—SUMMARY OF ESTIMATED O₃-INDUCED LUNG FUNCTION DECREMENTS FOR THE CURRENT AND POTENTIAL ALTERNATIVE O₃ STANDARDS IN URBAN CASE STUDY AREAS—Continued

Lung function decrement	Alternative standard level	Average % children ⁵⁹	Number of children (5 to 18 years) [number of asthmatic children] ⁶⁰	% Children worst year and area
Two or more decrements per season				
≥10%	75	7.5–12	1,730,000 [179,000]	14
	70	5.5–11	1,414,000 [145,000]	13
	65	1.3–8.8	1,023,000 [102,000]	11
≥15%	60	2.1–6.4	741,000 [73,000]	7.3
	75	1.7–2.9	391,000 [40,000]	3.8
	70	0.9–2.4	276,000 [28,000]	3.1
≥20%	65	0.1–1.8	168,000 [17,000]	2.3
	60	0.2–1.0	101,000 [10,000]	1.4
	75	0.5–1.1	128,000 [13,000]	1.5
	70	0.3–0.8	81,000 [8,000]	1.1
	65	0–0.5	43,000 [4,000]	0.8
	60	0–0.2	21,000 [2,000]	0.4

Uncertainties in estimates of lung function risks are summarized in section II.C.3.a.ii of the proposal (79 FR 75275). In addition to the uncertainties noted for exposure estimates, an uncertainty which impacts lung function risk estimates stems from the lack of exposure-response information in children. In the near absence of controlled human exposure data for children, risk estimates are based on the assumption that children exhibit the same lung function response following O₃ exposures as healthy 18 year olds (*i.e.*, the youngest age for which controlled human exposure data is generally available) (U.S. EPA, 2014a, section 6.5.3). This assumption is justified in part by the findings of McDonnell et al. (1985), who reported that children (8–11 years old) experienced FEV₁ responses similar to those observed in adults (18–35 years old) (U.S. EPA, 2014a, p. 3–10). In

addition, as discussed in the ISA (U.S. EPA, 2013, section 6.2.1), summer camp studies of school-aged children reported O₃-induced lung function decrements similar in magnitude to those observed in controlled human exposure studies using adults. In extending the risk model to children, the HREA thus fixes the age term in the model at its highest value, the value for age 18. Notwithstanding the information just summarized supporting this approach, EPA acknowledges the uncertainty involved, and notes that the approach could result in either over- or underestimates of O₃-induced lung function decrements in children, depending on how children compare to the adults used in controlled human exposure studies (U.S. EPA, 2014a, section 6.5.3).

A related source of uncertainty is that the risk assessment estimates of O₃-induced decrements in asthmatics used the exposure-response relationship developed from data collected from healthy individuals. Although the evidence has been mixed (U.S. EPA, 2013, section 6.2.1.1), several studies have reported statistically larger, or a tendency toward larger, O₃-induced lung function decrements in asthmatics than in non-asthmatics (Kreit et al., 1989; Horstman et al., 1995; Jorres et al., 1996; Alexis et al., 2000). On this issue, CASAC noted that “[a]sthmatic subjects appear to be at least as sensitive, if not more sensitive, than non-asthmatic subjects in manifesting O₃-induced pulmonary function decrements” (Frey, 2014c, p. 4). To the extent asthmatics experience larger O₃-induced lung function decrements than the healthy adults used to develop exposure-response relationships, the HREA could underestimate the impacts of O₃ exposures on lung function in

asthmatics, including asthmatic children. The implications of this uncertainty for risk estimates remain unknown at this time (U.S. EPA, 2014a, section 6.5.4), and could depend on a variety of factors that have not been well-evaluated, including the severity of asthma and the prevalence of medication use. However, the available evidence shows responses to O₃ increase with severity of asthma (Horstman et al., 1995) and corticosteroid usage does not prevent O₃ effects on lung function decrements or respiratory symptoms in people with asthma (Vagaggini et al., 2001, 2007).

ii. Mortality and Morbidity Risk Assessments

As discussed in section II.C.3.b of the proposal (79 FR 75276), the HREA estimates O₃-associated risks in 12 urban study areas⁶² using concentration-response relationships drawn from epidemiologic studies. These concentration-response relationships are based on “area-wide” average O₃ concentrations.⁶³ The HREA estimates risks for the years 2007 and 2009 in order to provide estimates of risk for a year with generally higher O₃

⁵⁹ Estimates in each urban case study area were averaged for the years evaluated in the HREA (2006 to 2010). Ranges reflect the ranges across urban study areas.

⁶⁰ Numbers of children estimated to experience decrements in each study urban case study area were averaged over 2006 to 2010. These averages were then summed across urban study areas. Numbers are rounded to nearest thousand unless otherwise indicated.

⁶¹ As discussed in section 4.3.3 of the HREA, the model-based air quality adjustment approach used to estimate risks associated with the current and alternative standards was unable to estimate the distribution of ambient O₃ concentrations in New York City upon just meeting an alternative standard with a level of 60 ppb. Therefore, for the 60 ppb standard level, the numbers of children and asthmatic children experiencing decrements, and the ranges of percentages of such children across study areas, reflect all of the urban study areas except New York City. Because of this, in some cases (*i.e.*, when New York City provided the smallest risk estimate), the lower end of the ranges in Table 2 are higher for a standard level of 60 ppb than for a level of 65 ppb.

⁶² The 12 urban areas evaluated are Atlanta, Baltimore, Boston, Cleveland, Denver, Detroit, Houston, Los Angeles, New York, Philadelphia, Sacramento, and St. Louis.

⁶³ In the epidemiologic studies that provide the health basis for HREA risk assessments, concentration-response relationships are based on daytime O₃ concentrations, averaged across multiple monitors within study areas. These daily averages are used as surrogates for the spatial and temporal patterns of exposures in study populations. Consistent with this approach, the HREA epidemiologic-based risk estimates also utilize daytime O₃ concentrations, averaged across monitors, as surrogates for population exposures. In this notice, we refer to these averaged concentrations as “area-wide” O₃ concentrations. Area-wide concentrations are discussed in more detail in section 3.1.4 of the PA (U.S. EPA, 2014c).

concentrations (2007) and a year with generally lower O₃ concentrations (2009) (U.S. EPA, 2014a, section 7.1.1).

In considering the epidemiology-based risk estimates, the proposal focuses on mortality risks associated with short-term O₃ concentrations. The proposal considers estimates of total risk (*i.e.*, based on the full distributions of ambient O₃ concentrations) and estimates of risk associated with O₃ concentrations in the upper portions of ambient distributions. Both estimates are discussed to provide information that considers risk estimates based on concentration-response relationships being linear over the entire distribution of ambient O₃ concentrations, and thus have the greater potential for morbidity and mortality to be affected by changes in relatively low O₃ concentrations, as well as risk estimates that are associated with O₃ concentrations in the upper portions of the ambient distribution, thus focusing on risk from higher O₃ concentrations and placing greater weight on the uncertainty associated with the shapes of concentration-response curves for O₃ concentrations in the lower portions of the distribution. These results for O₃-associated mortality risk are summarized in Table 3 in the proposal (79 FR 75277).

Important uncertainties in epidemiology-based risk estimates, based on their consideration in the HREA and PA, are discussed in section II.C.3.b.ii of the proposal (79 FR 75277). Compared to estimates of O₃ exposures of concern and estimates of O₃-induced lung function decrements (discussed above), the HREA conclusions reflect lower confidence in epidemiologic-based risk estimates (U.S. EPA, 2014a, section 9.6). In particular, the HREA highlights the heterogeneity in effect estimates between locations, the potential for exposure measurement errors, and uncertainty in the interpretation of the shape of concentration-response functions at lower O₃ concentrations (U.S. EPA, 2014a, section 9.6). The HREA also concludes that lower confidence should be placed in the results of the assessment of respiratory mortality risks associated with long-term O₃, primarily because that analysis is based on only one study, though that study is well-designed, and because of the uncertainty in that study about the existence and identification of a potential threshold in the concentration-response function (U.S. EPA, 2014a, section 9.6).^{64,65} This section further

discusses some of the key uncertainties in epidemiologic-based risk estimates, as summarized in the PA (U.S. EPA, 2014c, section 3.2.3.2), with a focus on uncertainties that can have particularly important implications for the Administrator's consideration of epidemiology-based risk estimates.

The PA notes that reducing NO_x emissions generally reduces O₃-associated mortality and morbidity risk estimates in locations and time periods with relatively high ambient O₃ concentrations and increases risk estimates in locations and time periods with relatively low concentrations (II.A, above). When evaluating uncertainties in epidemiologic risk estimates, the PA considered (1) the extent to which the modeled O₃ response to reductions in NO_x emissions appropriately represents the trends observed in monitored ambient O₃ following actual reductions in NO_x emissions, (2) the extent to which the O₃ response to reductions in precursor emissions could differ with emissions reduction strategies that are different from those used in HREA to generate risk estimates, and (3) the extent to which estimated changes in risks in urban study areas are representative of the changes that would be experienced broadly across the U.S. population. The first two of these issues are discussed in section II.A.2.c above. The third issue is discussed below.

The HREA conducted national air quality modeling analyses that estimated the proportion of the U.S. population living in locations where seasonal averages of daily O₃ concentrations are estimated to decrease in response to reductions in NO_x emissions, and the proportion living in locations where such seasonal averages are estimated to increase. Given the close relationship between changes in seasonal averages of daily O₃ concentrations and changes in seasonal mortality and morbidity risk estimates, this analysis informs consideration of the extent to which the risk results in urban study areas represent the U.S. population as a whole. This "representativeness analysis" indicates that the majority of the U.S. population lives in locations where reducing NO_x emissions would be expected to result in decreases in warm season averages of

mortality response, the estimated number of premature deaths avoidable for long-term exposure reductions for several levels need to be viewed with caution" (Frey, 2014a, p. 3).

⁶⁵ There is also uncertainty about the extent to which mortality estimates based on the long-term metric used in the study by Jerrett et al. (2009) (*i.e.*, seasonal average of 1-hour daily maximum concentrations) reflects associations with long-term average O₃ versus repeated occurrences of elevated short-term concentrations.

daily maximum 8-hour ambient O₃ concentrations. Because the HREA urban study areas tend to underrepresent the populations living in such areas (*e.g.*, suburban, smaller urban, and rural areas), risk estimates for the urban study areas are likely to understate the average reductions in O₃-associated mortality and morbidity risks that would be experienced across the U.S. population as a whole upon reducing NO_x emissions (U.S. EPA, 2014a, section 8.2.3.2).

Section 7.4 of the HREA also highlights some additional uncertainties associated with epidemiologic-based risk estimates (U.S. EPA, 2014a). This section of the HREA identifies and discusses sources of uncertainty and presents a qualitative evaluation of key parameters that can introduce uncertainty into risk estimates (U.S. EPA, 2014a, Table 7-4). For several of these parameters, the HREA also presents quantitative sensitivity analyses (U.S. EPA, 2014a, sections 7.4.2 and 7.5.3). Of the uncertainties discussed in Chapter 7 of the HREA, those related to the application of concentration-response functions from epidemiologic studies can have particularly important implications for consideration of epidemiology-based risk estimates, as discussed below.

An important uncertainty is the shape of concentration-response functions at low ambient O₃ concentrations (U.S. EPA, 2014a, Table 7-4).⁶⁶ In recognition of the ISA's conclusion that certainty in the shape of O₃ concentration-response functions decreases at low ambient concentrations, the HREA provides estimates of epidemiology-based mortality risks for entire distributions of ambient O₃ concentrations, as well as estimates of total mortality associated with various ambient O₃ concentrations. The PA considers both types of risk estimates, recognizing greater public health concern for adverse O₃-attributable effects at higher ambient O₃ concentrations (which drive higher exposure concentrations, section 3.2.2 of the PA (U.S. EPA, 2014c)), as compared to lower concentrations.

A related consideration is associated with the public health importance of the increases in relatively low O₃ concentrations following air quality adjustment. There is uncertainty that relates to the assumption that the concentration response function for O₃ is linear, such that total risk estimates are equally influenced by decreasing

⁶⁴ The CASAC also concluded that "[i]n light of the potential nonlinearity of the C-R function for long-term exposure reflecting a threshold of the

⁶⁵ A related uncertainty is the existence, or not, of a threshold. The HREA addresses this issue for long-term O₃ by evaluating risks in models that include potential thresholds (II.D.2.c).

high concentrations and increasing low concentrations, when the increases and decreases are of equal magnitude. Even on days with increases in relatively low area-wide average concentrations, resulting in increases in estimated risks, some portions of the urban study areas could experience decreases in high O₃ concentrations. To the extent adverse O₃-attributable effects are more strongly supported for higher ambient concentrations (which, as noted above, are consistently reduced upon air quality adjustment), the impacts on risk estimates of increasing low O₃ concentrations reflect an important source of uncertainty. In addition to the uncertainties discussed above, the proposal also notes uncertainties related to (1) using concentration-response relationships developed for a particular population in a particular location to estimate health risks in different populations and locations; (2) using concentration-response functions from epidemiologic studies reflecting a particular air quality distribution to adjusted air quality necessarily reflecting a different (simulated) air quality distribution; (3) using a national concentration-response function to estimate respiratory mortality associated with long-term O₃; and (4) unquantified reductions in risk that could be associated with reductions in the ambient concentrations of pollutants other than O₃, resulting from control of NO_x (79 FR 75277 to 75279).

B. Need for Revision of the Primary Standard

The initial issue to be addressed in the current review of the primary O₃ standard is whether, in view of the advances in scientific knowledge and additional information, it is appropriate to revise the existing standard. This section presents the Administrator's final decision on whether it is "appropriate" to revise the current standard within the meaning of section 109 (d)(1) of the CAA. Section II.B.1 contains a summary discussion of the basis for the proposed conclusions on the adequacy of the primary standard. Section II.B.2 discusses comments received on the adequacy of the primary standard. Section II.B.3 presents the Administrator's final conclusions on the adequacy of the current primary standard.

1. Basis for Proposed Decision

In evaluating whether it is appropriate to retain or revise the current standard, the Administrator's considerations build upon those in the 2008 review, including consideration of the broader body of scientific evidence and

exposure and health risk information now available, as summarized in sections II.A to II.C (79 FR 75246–75279) of the proposal and section II.A above.

In developing conclusions on the adequacy of the current primary O₃ standard, the Administrator takes into account both evidence-based and quantitative exposure- and risk-based considerations. Evidence-based considerations include the assessment of evidence from controlled human exposure, animal toxicological, and epidemiologic studies for a variety of health endpoints. The Administrator focuses on health endpoints for which the evidence is strong enough to support a "causal" or a "likely to be causal" relationship, based on the ISA's integrative synthesis of the entire body of evidence. The Administrator's consideration of quantitative exposure and risk information draws from the results of the exposure and risk assessments presented in the HREA.

The Administrator's consideration of the evidence and exposure/risk information is informed by the considerations and conclusions presented in the PA (U.S. EPA, 2014c). The purpose of the PA is to help "bridge the gap" between the scientific and technical information assessed in the ISA and HREA, and the policy decisions that are required of the Administrator (U.S. EPA, 2014c, Chapter 1); see also *American Farm Bureau Federation*, 559 F. 3d at 516, 521 ("[a]lthough not required by the statute, in practice EPA staff also develop a Staff Paper, which discusses the information in the Criteria Document that is most relevant to the policy judgments the EPA makes when it sets the NAAQS"). The PA's evidence-based and exposure-/risk-based considerations and conclusions are briefly summarized below in sections II.B.1.a (evidence-based considerations), II.B.1.b (exposure- and risk-based considerations), and II.B.1.c (PA conclusions on the current standard). Section II.B.1.d summarizes CASAC advice to the Administrator and public commenter views on the current standard. Section II.B.1.e presents a summary of the Administrator's proposed conclusions concerning the adequacy of the public health protection provided by the current standard, and her proposed decision to revise that standard.

a. Evidence-Based Considerations From the PA

In considering the available scientific evidence, the PA evaluates the O₃ concentrations in health effects studies (U.S. EPA, 2014c, section 3.1.4).

Specifically, the PA characterizes the extent to which health effects have been reported for the O₃ exposure concentrations evaluated in controlled human exposure studies, and effects occurring over the distributions of ambient O₃ concentrations in locations where epidemiologic studies have been conducted. These considerations, as they relate to the adequacy of the current standard, are presented in detail in section 3.1.4 of the PA (U.S. EPA, 2014c) and are summarized in the proposal (79 FR 75279–75287). The PA's considerations are summarized briefly below for controlled human exposure, epidemiologic panel studies, and epidemiologic population-based studies.

Section II.D.1.a of the proposal discusses the PA's consideration of the evidence from controlled human exposure and panel studies. This evidence is assessed in section 6.2 of the ISA (U.S. EPA, 2013) and is summarized in section 3.1.2 of the PA (U.S. EPA, 2014c). A large number of controlled human exposure studies have reported lung function decrements, respiratory symptoms, air inflammation, airway hyperresponsiveness, and/or impaired lung host defense in young, healthy adults engaged in moderate quasi-continuous exertion, following 6.6-hour O₃ exposures. These studies have consistently reported such effects following exposures to O₃ concentrations of 80 ppb or greater. In addition to lung function decrements, available studies have evaluated respiratory symptoms or airway inflammation following exposures to O₃ concentrations below 75 ppb. Table 3–1 in the PA highlights the group mean results of individual controlled human exposure studies that evaluated exposures to O₃ concentrations below 75 ppb. These studies observe the combination of lung function decrements and respiratory symptoms following exposures to O₃ concentrations as low as 72 ppb, and lung function decrements and airway inflammation following exposures to O₃ concentrations as low as 60 ppb (based on group means).

Based on this evidence, the PA notes that controlled human exposure studies have reported a variety of respiratory effects in young, healthy adults following exposures to a wide range of O₃ concentrations for 6.6 hours, including exposures to concentrations below 75 ppb. In particular, the PA further notes that a recent controlled human exposure study reported the combination of lung function decrements and respiratory symptoms in healthy adults engaged in quasi-

Exhibit 26

Rule Preamble: The New Mexico Environment Department has developed the following draft regulation pursuant to the directives of Section 74-2-5.3 of the New Mexico Air Quality Control Act. The objective of the proposed rule is to establish emissions standards for volatile organic compounds (VOC) and nitrogen oxides (NOx) for oil and gas production and processing sources located in areas of the State within the Environmental Improvement Board's jurisdiction where ozone concentrations are exceeding 95% of the national ambient air quality standard.

This is a preliminary draft being released for public input in advance of the Department filing a formal rulemaking petition with the Board and requesting a public hearing. The purpose of this initial, pre-petition comment period is to foster transparency and facilitate continued engagement from stakeholders, members of the public, and other interested parties. Specifically, the Department is seeking public input on the proposed rule language to assist in identifying potential regulatory and technical issues, and areas that require additional clarification or modification. Additional opportunities for public input and changes to the draft rule will occur through the formal rule-making process following the filing of the rulemaking petition. This initial, pre-petition process will help ensure that major issues or problematic areas are identified and can be addressed prior to the initiation of the formal process.

NMED is soliciting specific review and public input on a number of proposed provisions and concepts in the draft rule. In particular, for the equipment standards section, NMED requests feedback on the following:

1. The proposed definitions of stripper wells and marginal wells under the draft rule and the regulatory requirements that would apply to those wells under Section 20.2.50.25 NMAC;
2. Examples of technologies or regulatory programs utilizing non-combustion emission control technologies, like fuel cells, as a means of reducing or eliminating emissions for inclusion in Section 20.2.50.15 NMAC;
3. Specific regulatory language regarding criteria necessary to demonstrate equivalency of alternative equipment leak monitoring plans in Section 20.2.50.16(C) NMAC;
4. Specific regulatory language to establish a pre-approved equipment leak monitoring plan in 20.2.50.16(C) NMAC;
5. For leak detection and repair requirements under Section 20.2.50.16 NMAC, specific standards to be used by NMED to determine if certain new or existing technologies (real-time remote fence line and aerial surveillance, for example) or proposals are enforceable, effective, and equivalent. Specific feedback on data capture requirements, quality assurance, error rates, calibration requirements, training and certification, interference issues, quantification methods, and pollutant identification will assist the Department in exploring this option further;
6. Regulatory requirements for oil and gas evaporative ponds in Section 20.2.50.26 NMAC, including whether to establish emission standards based on the pond's potential to emit or throughput; and
7. Opportunities for greater transparency.

Comments or input on the draft rules may be submitted electronically to nm.methanestrategy@state.nm.us or via hardcopy to Liz Bisbey-Kuehn, NMED Air Quality Bureau, 525 Camino de los Marquez, Santa Fe, NM 87505 by 5 p.m. Aug. 20, 2020.

Exhibit 27

Ozone Areas of Concern Counties

Red Zones	Total Production (MMBtu)	# Wells
San Juan	382634160.8	168813
Bernalillo	0	0
Lea	857778290.1	160027
Eddy	763690957.3	150014
Dona Ana	0	0

Yellow Zones		
Rio Arriba	240968443.4	134663
Sandoval	20267048.26	4028
Valencia	0	0
Roosevelt	3225335.854	1688
Chaves	20256435.67	19407

Red Counties		% of total state
Production (MMBtu)	2.00E+09	83.4%
Number of Wells	478,854	
Emissions (metric tons)	120,110	

Red and Yellow Counties		% of total state
Production (MMBtu)	2.29E+09	95.2%
Number of Wells	638,640	
Emissions (metric tons)	137,174	

Red Counties	
Percentage of state wells	72.9%
Red and Yellow Counties	
Percentage of state wells	97.2%

County/Parish	Production Year	Oil	Gas	Wells	Total Production (MMBtu)
CHAVES (NM)	2017	1023197	14013594	19407	20256435.7
COLFAX (NM)	2017	0	19530551	9858	19960223.1
EDDY (NM)	2017	67739955	362817239	150014	763690957
HARDING (NM)	2017	0	45172035	3713	46165819.8
LEA (NM)	2017	94997343	300189531	160027	857778290
MCKINLEY (NM)	2017	13476	107370	361	187892.94
RIO ARriba (NM)	2017	1428412	227674808	134663	240968443
ROOSEVELT (NM)	2017	251914	1726257	1688	3225335.85
SAN JUAN (NM)	2017	5018129	345918799	168813	382634161
SANDOVAL (NM)	2017	1363107	12094939	4028	20267048.3
UNION (NM)	2017	0	47074150	4128	48109781.3
Total				656700	2.40E+09

Exhibit 28

2021 Regional Haze Planning

Summer 2020 Announcements:

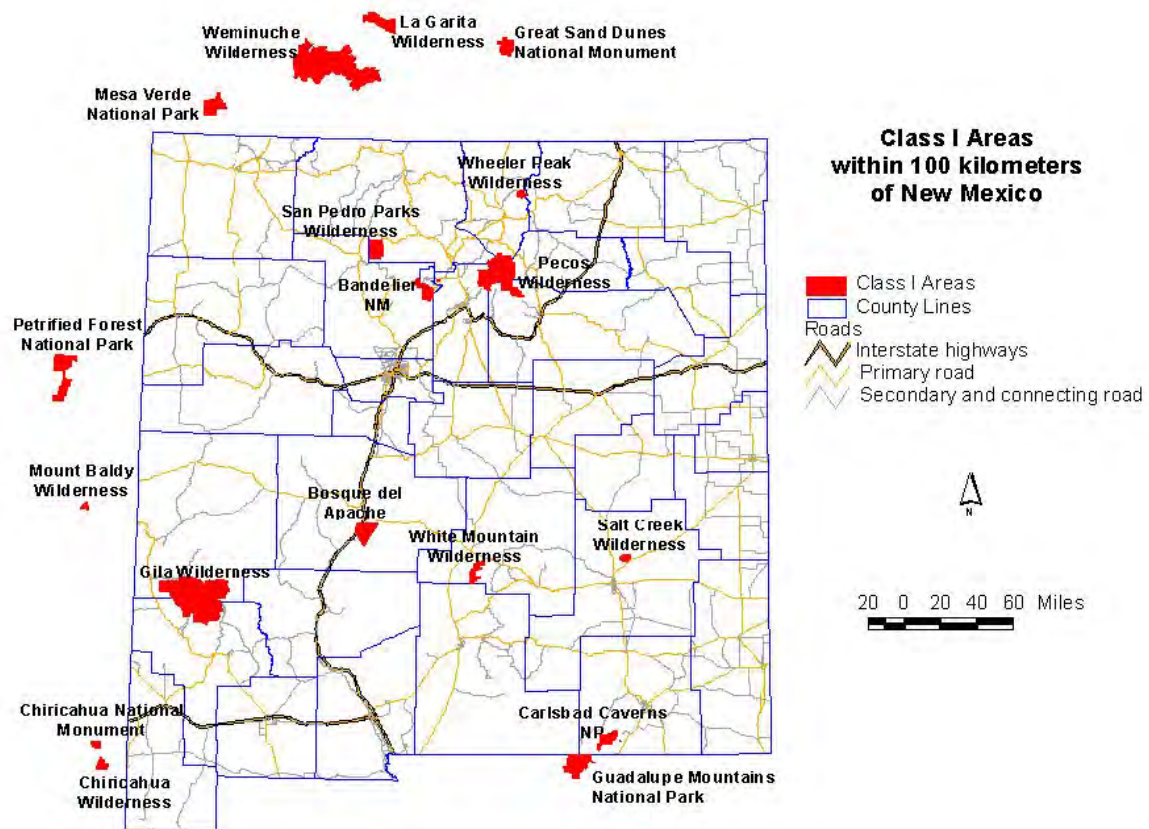
- The **2nd NMED and EHD Regional Haze Stakeholder Outreach Meeting** will be August 25, 2020 starting at 10:00 A.M. Mountain Daylight Time.
 - Meeting link: <https://nmed-oit.webex.com/nmed-oit/j.php?MTID=m14765658d0a21e1782b714236415695c>
 - Meeting number: 133 382 9774
 - Password: kAZbdtDH532
 - Stakeholder Outreach webinar (8/25/2020): [Webinar Slides](#)
- Input on New Mexico's Regional Haze Planning can be sent to nm.regionalhaze@state.nm.us or sent to Mark Jones at mark.jones@state.nm.us

VISIBILITY & REGIONAL HAZE IN NEW MEXICO

The blue skies and scenic vistas of New Mexico are considered some of the most beautiful in the United States. While New Mexico's residents and visitors frequently enjoy good visibility, air pollutants and natural phenomena interfering with light transmission can impose limitations on aesthetic appreciation of scenery. Visibility is the term used to characterize physical limitations in the atmosphere that affect our ability to see clearly. Human-caused pollution of varied concentrations and sizes in the atmosphere can, along with natural events like dust storms and wildfires, impair or reduce visibility. Widespread visibility impairment caused by anthropogenic pollutants from a variety of sources and activities over a broad geographic area is known as regional haze.

EPA Requirements on Regional Haze

EPA's Regional Haze program addresses reduced visibility in **national parks and wilderness areas** <https://www.epa.gov/visibility/list-areas-protected-regional-haze-program>. The map and table below show the areas that are protected in NM and some in neighboring states near NM's border. EPA refers to these areas as "Class I Areas." There are 156 of these, 116 of which are in Western states.



New Mexico has 9 mandatory federal Class I Areas (CIAs):

- Bandelier Wilderness Area
- Bosque del Apache Wilderness Area
- Carlsbad Caverns National Park
- Gila Wilderness Area
- Pecos Wilderness Area
- Salt Creek Wilderness Area
- San Pedro Parks Wilderness Area
- Wheeler Peak Wilderness Area
- White Mountain Wilderness Area



Bosque del Apache (photo by Rhett Zyla)



Bandelier National Monument
(photo by Rhett Zyla)

Visibility-reducing haze is caused by natural and anthropogenic sources. Some haze-causing particles are emitted directly into the air, such as dust and soot. Others, however, form from chemical reactions of other gases emitted into the air. States must address visibility impairment that can be caused by such pollutants as particulate matter (PM), sulfur dioxide (SO₂) and nitrogen oxides (NO_x). Pollutants that cause haze may also form ground-level ozone. The Clean Air Act sets a goal of returning to “natural conditions” of visibility, by remedying human-caused visibility impairment from Class I Areas by 2064. The United States Environmental Protection Agency’s (U.S. EPA) original 2003 *Guidance for Tracking Progress Under the Regional Haze Rule* was based on the removal of anthropogenic impairment on the 20% of days each year with the highest total haze (natural and anthropogenic). In the western United States, these days regularly include large amounts of haze from wildfire smoke and windblown dust. Meeting the Clean Air Act goals of addressing human-caused haze by focusing on days dominated by sources that are not practically controllable is problematic.

EPA rule revisions and guidance published from 2016 and 2018 propose a new approach to track progress under the Regional Haze Rule. The method selects 20% of the sample days from each year that have the highest anthropogenic impairment. These represent the days each year that have the largest apparent change in visibility from what would have existed with no anthropogenic haze and that are expected to be most sensitive to emissions control programs.

In the eastern United States, there is generally little difference between the haziest and most impaired days, with similar temporal trends for both metrics. In the West, sites with insignificant or increased trends in the haziest days metric show modest but steady reductions in haze with the impairment metric.

Visibility trends at New Mexico’s Class 1 Areas, using the new impairment metric, are shown in a series of graphs: [2000-2017 trends in NM](#). Visibility trends in the Western states, using both the new and old metrics, are available via links at the bottom of this page.

EPA’s Regional Haze Rule requires states to make reasonable progress over time toward the long-term goal of natural visibility conditions. To make such progress, EPA requires submittal of Regional Haze State Implementation Plans (SIPs) approximately once every ten years.

Introduction to Regional Planning Group

Because of the harm that regional haze does to visibility in Class I Areas, many efforts to control and reduce man-made haze – and the air pollutants that cause it – are under way through national laws and regional collaboration. Such a collaboration is the Western Regional Air Partnership (**WRAP** <https://www.wrapair2.org/>), under the auspices of the **Western Governors’ Association** <http://www.westgov.org/>. WRAP is a voluntary partnership of states, tribes, federal land managers, local air agencies and the US EPA. Its purpose is to understand current and evolving regional air quality issues in the West and assist states in addressing those issues. New Mexico participates in the WRAP.



WRAP States

The WRAP develops the technical and policy tools needed by the western states and tribes to comply with the EPA's Regional Haze regulations. WRAP activities are conducted by a network of forums and committees composed of members and stakeholders who represent a wide range of viewpoints; public involvement is an integral part of the Partnership. The purpose of the WRAP Regional Haze Planning Work Group (RHPWG) (<https://www.wrapair2.org/RHPWG.aspx>) is to prepare the framework to support regional planning for the 15 western states, so that needed elements will be available for submission of plans to EPA by the July 2021 deadline, as explained further on this page and in the documents linked below.

NM Planning Process and Guiding Principles

New Mexico is required to develop and submit to EPA its own regional haze plans by July 31, 2021. To this end, the New Mexico Environment Department (NMED) is cooperating with the City of Albuquerque Environmental Health Department (EHD), which implements air quality regulations in Albuquerque and Bernalillo County. Because NMED and EHD are separate jurisdictions, they will submit separate Regional Haze SIPs to EPA. But the two agencies will develop two SIPs that function as an integrated whole, addressing regional haze for the entire state of New Mexico.

If New Mexico fails to develop its own regional haze plans, it will face the potential imposition of a Federal Implementation Plan (FIP) by EPA. A FIP could entail emissions limitations for certain sources with less input provided by New Mexico stakeholders.

Western regional haze issues differ significantly from eastern issues with natural events such as wildfires, high-wind dust storms and international emission sources contributing to haze in western Class I Areas more often and more significantly than in eastern Class I Areas. All visitors to Class I Areas deserve the beautiful vistas for which New Mexico can boast. Lack of careful planning and decision making for a Regional Haze SIP revision could endanger the experience that visitors expect and deserve. Additionally, many of the same pollutants that cause haze also have a health standard, so regulating these pollutants benefits New Mexicans' health.

NM has developed a set of guiding principles and a timeline for satisfying the EPA requirements. Guiding Principles and the timeline are available at the following links:

- [Guiding Principles](#)
- [Regional Haze 2021 State Implementation Plan timeline](#)

For inquiries related to the development of the NM Regional Haze SIP, contact Mark Jones at (505) 566-9746 or mark.jones@state.nm.us. For inquiries related to the Albuquerque – Bernalillo County Regional Haze SIP, contact Ed Merta of the City of Albuquerque at (505) 768-2660 or emerta@cabq.gov.

If you or someone you know is interested in participating in or following the Regional Haze planning process, please go to <https://public.govdelivery.com/accounts/NMED/subscriber/new> and register for the new AQB Regional Haze Announcements topic. Although NMED is in the early stages of planning, announcements will begin soon and this email alert system will be the best way to stay abreast of current events regarding Regional Haze.

Links to other information

- Outreach:
 - New Mexico Environment Department outreach webinar on Regional Haze Planning was held on October 2, 2019 from 10:30 a.m.-noon. [Presentation Slides](#)
 - [WRAP Overview of Regional Haze Planning \(draft\)](#)
 - [Stakeholder Comments Page](#)
- 4-factor analysis resources:
 - [Recommended Format for Four Factor Analysis \(8.16.19\)](#)
 - [WRAP Reasonable Progress Source Identification and Analysis Protocol](#)
 - [EPA Air Pollution Cost Control Manual 6th ed](#)
 - [EPA Assessment of non-EGU NOx Emission Controls](#)
 - [RACT/BACT/LAER clearinghouse](#)
 - List of facilities screened for Four-Factor Analysis ([facility list 7.23.2019](#))
 - [Example Four Factor Request letter](#)
 - [New Mexico Four Factor Analysis Submittals](#)
- EPA's Regional Haze web page <https://www.epa.gov/visibility>.
 - The above web page provides access to extensive regulatory text and guidance, including the August 20,2019 updated Regional Haze Rule.
 - EPA has released their most current update on Regional Haze Planning Guidelines available at the link: [Guidance on Regional Haze State Implementation Plans for Second Implementation Period 8-20-2019](#).
[additional webinar slides on guidance [webinar_rh_slides_9_10_19](#)]
- Class I Area visibility trends <http://views.cira.colostate.edu/tssv2>
- 2018 Regional SO2 Emissions and Milestone Report ([2018 Regional SO2 Emissions and Milestone Report](#))
- NMED Regional Haze planning web page for the first implementation period: [/air-quality/reg-haze/](#)
- WRAP Regional Haze Planning Workgroup: <https://www.wrapair2.org/RHPWG.aspx>

The Regional Haze archives page can be found here: [/air-quality/reg-haze-archive/](#)

Exhibit 29

DEPARTMENT OF THE INTERIOR

Bureau of Land Management

43 CFR Parts 3100, 3160 and 3170

[17X.LLWO310000.L13100000.PP0000]

RIN 1004-AE14

Waste Prevention, Production Subject to Royalties, and Resource Conservation

AGENCY: Bureau of Land Management, Interior.

ACTION: Final rule.

SUMMARY: The Bureau of Land Management (BLM) is promulgating new regulations to reduce waste of natural gas from venting, flaring, and leaks during oil and natural gas production activities on onshore Federal and Indian (other than Osage Tribe) leases. The regulations also clarify when produced gas lost through venting, flaring, or leaks is subject to royalties, and when oil and gas production may be used royalty-free on-site. These regulations replace the existing provisions related to venting, flaring, and royalty-free use of gas contained in the 1979 Notice to Lessees and Operators of Onshore Federal and Indian Oil and Gas Leases, Royalty or Compensation for Oil and Gas Lost (NTL-4A), which are over 3 decades old.

DATES: The final rule is effective on January 17, 2017.

FOR FURTHER INFORMATION CONTACT: Timothy Spisak at the BLM Washington Office, 20 M Street SE., Room 2134LM, Washington, DC 20003, or by telephone at 202-912-7311. For questions relating to regulatory process issues, contact Faith Bremner at 202-912-7441.

Persons who use a telecommunications device for the deaf (TDD) may call the Federal Relay Service (FRS) at 1-800-877-8339 to contact these individuals during normal business hours. FRS is available 24 hours a day, 7 days a week to leave a message or question with these individuals. You will receive a reply during normal business hours.

SUPPLEMENTARY INFORMATION:

I. Table of Contents

II. Executive Summary

- A. Background
- B. Summary of Rule
 1. Venting and Flaring
 2. Leaks
 3. Reducing Venting from Equipment and Practices
 4. Royalty Provisions Governing New Competitive Leases
 5. Unavoidable Versus Avoidable Losses of Gas

6. Interaction With EPA and State Regulations
7. Other Provisions
8. Summary of Costs and Benefits
- III. Background
 - A. Impacts of Waste and Loss of Gas
 - B. Purpose of the Rule
 1. Overview
 2. Issues Addressed by Rule
 3. Relationship to Other Federal, State, and Industry Activities
 - C. Legal Authority
 - D. Stakeholder Outreach
- IV. Summary of Final Rule
- V. Major Changes From Proposed Rule
 - A. Venting Prohibition and Capture Targets
 1. Venting Prohibition
 2. Capture Targets
 - B. Leak Detection and Repair
 1. Requirements of Final Rule
 2. Changes From Proposed Rule
 - C. Significant Comments
 3. Liquids Unloading at New Wells
 - D. Requirements of Final Rule and Changes From Proposed Rule
 1. Requirements of Final Rule
 2. Significant Comments
 3. Variances Related to State and Tribal Regulations
 1. Requirements of Final Rule
 2. Changes From Proposed Rule
 3. Significant Comments
- VI. Additional Significant Comments and Responses
 - A. Interaction With EPA Regulations
 - B. Authority to Require Flaring of Gas
 - C. "Avoidably Lost" Oil or Gas
 - D. Application to Units and Communitized Areas
 - E. ROW Permitting
 - F. Planning
- VII. Section by Section
 - Part 3100
 - Section 3103.3-1 Royalty on production
 - Section 3160.0-5 Definitions
 - Section 3162.3-1 Drilling applications and plans
 - Subpart 3178—Royalty-Free Use of Lease Production
 - Section 3178.1 Purpose
 - Section 3178.2 Scope of This Subpart
 - Section 3178.3 Production on Which Royalty is not due
 - Section 3178.4 Uses of Oil or Gas on a Lease, Unit, or Communitized Area That do not Require Prior Written BLM Approval for Royalty-Free Treatment of Volumes Used
 - Section 3178.5 Uses of Oil or Gas on a Lease, Unit, or Communitized Area That Require Prior Written BLM Approval for Royalty-Free Treatment of Volumes Used
 - Section 3178.6 Uses of Oil or Gas Moved off the Lease, Unit, or Communitized Area That do not Require Prior Written Approval for Royalty-Free Treatment of Volumes Used
 - Section 3178.7 Uses of Oil or Gas Moved off the Lease, Unit, or Communitized Area That Require Prior Written Approval for Royalty-Free Treatment of Volumes Used
 - Section 3178.8 Measurement or Estimation of Volumes of Oil or Gas That are Used Royalty-Free
 - Section 3178.9 Requesting Approval of Royalty-Free Treatment When Approval is Required

- Section 3178.10 Facility and Equipment Ownership
- Subpart 3179—Waste Prevention and Resource Conservation
 - Section 3179.1 Purpose
 - Section 3179.2 Scope
 - Section 3179.3 Definitions and Acronyms
 - Section 3179.4 Determining When the Loss of Oil or Gas is Avoidable or Unavoidable
 - Section 3179.5 When Lost Production is Subject to Royalty
 - Section 3179.6 Venting and Flaring From Gas Wells and Venting Prohibition
 - Section 3179.7 Gas Capture Requirement
 - Section 3179.8 Alternative Capture Requirement
 - Section 3179.9 Measuring and Reporting Volumes of Gas Vented and Flared
 - Section 3179.10 Determinations Regarding Royalty-Free Flaring
 - Section 3179.11 Other Waste Prevention Measures
 - Section 3179.12 Coordination With State Regulatory Authority
 - Section 3179.101 Well Drilling
 - Section 3179.102 Well Completion and Related Operations
 - Section 3179.103 Initial Production Testing
 - Section 3179.104 Subsequent Well Tests
 - Section 3179.105 Emergencies
 - Section 3179.201 Equipment Requirements for Pneumatic Controllers
 - Section 3179.202 Requirements for Pneumatic Diaphragm Pumps
 - Section 3179.203 Storage Vessels
 - Section 3179.204 Downhole Well Maintenance and Liquids Unloading
 - Section 3179.301 Operator Responsibility
 - Section 3179.302 Approved Instruments and Methods
 - Section 3179.303 Leak Detection Inspection Requirements for Natural Gas Wellhead Equipment and Other Equipment
 - Section 3179.304 Repairing Leaks
 - Section 3179.305 Leak Detection Inspection, Recordkeeping and Reporting
 - Section 3179.401 State or Tribal Requests for Variances From the Requirements of This Subpart
- VIII. Analysis of Impacts
 - A. Description of the Regulated Entities
 1. Potentially Affected Entities
 2. Affected Small Entities
 - B. Impacts of the Requirements
 1. Overall Costs of the Rule
 2. Overall Benefits of the Rule
 3. Net Benefits of the Rule
 4. Distributional Impacts
- IX. Procedural Matters
 - A. Executive Order 12866, Regulatory Planning and Review
 - B. Regulatory Flexibility Act and Small Business Regulatory Enforcement Fairness Act of 1996
 - C. Unfunded Mandates Reform Act of 1995
 - D. Executive Order 12630, Governmental Actions and Interference with Constitutionally Protected Property Rights (Takings)
 - E. Executive Order 13132, Federalism
 - F. Executive Order 12988, Civil Justice Reform

G. Executive Order 13175, Consultation and Coordination with Indian Tribal Governments

H. Paperwork Reduction Act

I. National Environmental Policy Act

J. Executive Order 13211, Actions Concerning Regulations That Significantly Affect Energy Supply, Distribution, or Use

K. Executive Order 13563, Improving Regulation and Regulatory Review

X. Authors

II. Executive Summary

A. Background

This final regulation aims to reduce the waste of natural gas from mineral leases administered by the BLM. This gas is lost during oil and gas production activities through venting or flaring of the gas, and through equipment leaks. While oil and gas production technology has advanced dramatically in recent years, the BLM's rules to minimize waste of gas have not been updated in over 30 years. The Mineral Leasing Act of 1920 (MLA) requires the BLM to ensure that lessees "use all reasonable precautions to prevent waste of oil or gas developed in the land," 30 U.S.C. 225, and that leases include "a provision that such rules . . . for the prevention of undue waste as may be prescribed by [the] Secretary shall be observed," *id.* at § 187. The BLM believes there are economical, cost-effective, and reasonable measures that operators can take to minimize gas waste. These measures will enhance our nation's natural gas supplies, boost royalty receipts for American taxpayers, tribes, and States, reduce environmental damage from venting, flaring, and leaks of gas, and ensure the safe and responsible development of oil and gas resources.

The BLM's onshore oil and gas management program is a major contributor to our nation's oil and gas production. The BLM manages more than 245 million acres of land and 700 million acres of subsurface estate, making up nearly a third of the nation's mineral estate. Domestic production from 96,000 Federal onshore oil and gas wells accounts for 11 percent of the Nation's natural gas supply and 5 percent of its oil. In Fiscal Year (FY) 2015, operators produced 183.4 million barrels (bbl) of oil, 2.2 trillion cubic feet (Tcf) of natural gas, and 3.3 billion gallons of natural gas liquids (NGLs) from onshore Federal and Indian oil and gas leases. The production value of this oil and gas exceeded \$20.9 billion and generated over \$2.3 billion in royalties, which were shared with tribes, Indian

allottee owners, and States.¹ Over the past decade, the United States has experienced a dramatic increase in oil and natural gas production due to technological advances, such as hydraulic fracturing combined with directional drilling. Yet the American public has not benefited from the full potential of this increased production, due to venting, flaring, and leaks of significant quantities of gas during the production process. Federal and Indian onshore lessees and operators reported to the Office of Natural Resources Revenue (ONRR) that they vented or flared 462 billion cubic feet (Bcf) of natural gas between 2009 and 2015—enough gas to serve about 6.2 million households for a year, assuming 2009 usage levels.²

Venting, flaring, and leaks waste a valuable resource that could be put to productive use, and deprive American taxpayers, tribes, and States of royalty revenues. In addition, the wasted gas may harm local communities and surrounding areas through visual and noise impacts from flaring, and contribute to regional and global air pollution problems of smog, particulate matter, and toxics (such as benzene, a carcinogen). Finally, vented or leaked gas contributes to climate change, because the primary constituent of natural gas is methane, an especially powerful greenhouse gas (GHG), with climate impacts roughly 25 times those of carbon dioxide (CO₂), if measured over a 100-year period, or 86 times those of CO₂, if measured over a 20-year period.³ Thus, measures to conserve gas and avoid waste may significantly benefit local communities, public health, and the environment.

Congress has directed the BLM to oversee Federal and Indian oil and gas activities under multiple laws, including the MLA, the Mineral Leasing Act for Acquired Lands of 1947 (MLAAL), the Federal Oil and Gas

Royalty Management Act (FOGRMA), the Federal Land Policy and Management Act of 1976 (FLPMA), the Indian Mineral Leasing Act of 1938 (IMLA), the Indian Mineral Development Act of 1982 (IMDA), and the Act of March 3, 1909.⁴ In particular, the MLA requires the BLM to ensure that lessees "use all reasonable precautions to prevent waste of oil or gas developed in the land."⁵ Leases issued by BLM must ensure that operations are conducted with "reasonable diligence, skill, and care" and that lessees comply with rules "for the prevention of undue waste."⁶

Advancing those mandates, this rule replaces the BLM's decades-old NTL-4A requirements related to venting and flaring, and to royalty-free use of oil and gas production; amends the BLM's oil and gas regulations at 43 CFR part 3160 to include requirements for a waste minimization plan; and adds new subparts 3178 and 3179 to 43 CFR part 3170 that address royalty-free use of lease production (subpart 3178) and waste prevention through reduction of venting, flaring and leaks (subpart 3179). This rule will apply to all Federal and Indian (other than Osage Tribe) onshore oil and gas leases as well as leases and business agreements entered into by tribes (including IMDA agreements), as consistent with those agreements and with principles of Federal Indian law.⁷

This rule implements recommendations from several oversight reviews, including reviews by the Office of the Inspector General of the Department of the Interior (OIG) and the Government Accountability Office (GAO). These reviews raised concerns about waste of gas from Federal and Indian production, found that the BLM's existing requirements regarding venting and flaring are insufficient and outdated, and expressed concerns about the "lack of price flexibility in royalty

¹ Office of Natural Resources Revenue, Statistical Information, <http://statistics.onrr.gov/ReportTool.aspx> using Sales Year—FY 2015—Federal Onshore—All States Sales Value and Revenue for Oil, Natural Gas Liquids (NGL), and Gas products as of September 7, 2016.

² BLM analysis of ONRR Oil and Gas Operations Report Part B (OGOR-B) data provided for 2009–2015; see Energy Information Administration (EIA), *Trends in U.S. Residential Natural Gas Consumption*, http://www.eia.gov/pub/oil_gas/natural_gas/feature_articles/2010/ngtrendsresidcon/ngtrendsresidcon.pdf (reporting that in 2009, U.S. residential consumption was approximately 74 Mcf per household with natural gas service).

³ See Intergovernmental Panel on Climate Change, *Climate Change 2013: The Physical Science Basis*, Chapter 8, *Anthropogenic and Natural Radiative Forcing*, at 714 (Table 8.7), available at https://www.ipcc.ch/pdf/assessment-report/ar5/wg1/WG1AR5_Chapter08_FINAL.pdf.

⁴ Mineral Leasing Act, 30 U.S.C. 188–287; Mineral Leasing Act for Acquired Lands, 30 U.S.C. 351–360; Federal Oil and Gas Royalty Management Act, 30 U.S.C. 1701–1758; Federal Land Policy and Management Act of 1976, 43 U.S.C. 1701–1785; Indian Mineral Leasing Act of 1938, 25 U.S.C. 396a–g; Indian Mineral Development Act of 1982, 25 U.S.C. 2101–2108; Act of March 3, 1909, 25 U.S.C. 396.

⁵ 30 U.S.C. 225.

⁶ 30 U.S.C. 187.

⁷ Key statutes underpinning this proposed regulation contain exceptions for the Osage Tribe. Specifically, the Osage Tribe is exempted from the application of both the Indian Mineral Leasing Act and the Federal Oil and Gas Royalty Management Act, 25 U.S.C. 396f; 43 U.S.C. 1702(3), 1702(4). The leasing of Osage Reservation lands for oil and gas mining is subject to special Bureau of Indian Affairs regulations contained in 25 CFR part 226.

Exhibit 30

An official website of the United States government.



Health and Environmental Effects of Particulate Matter (PM)

Health Effects

The size of particles is directly linked to their potential for causing health problems. Small particles less than 10 micrometers in diameter pose the greatest problems, because they can get deep into your lungs, and some may even get into your bloodstream.

Exposure to such particles can affect both your lungs and your heart. Numerous scientific studies have linked particle pollution exposure to a variety of problems, including:

- premature death in people with heart or lung disease
- nonfatal heart attacks
- irregular heartbeat
- aggravated [asthma](#)
- decreased lung function
- increased respiratory symptoms, such as irritation of the airways, coughing or difficulty breathing.

People with heart or lung diseases, children, and older adults are the most likely to be affected by particle pollution exposure.

- [AirNow](#) can help you monitor air quality near you, and protect yourself and your family from elevated PM levels.

Environmental Effects

Visibility impairment

Fine particles (PM_{2.5}) are the main cause of reduced visibility (haze) in parts of the United States, including many of our treasured national parks and wilderness areas. [Learn more about visibility and haze](#)

Environmental damage

Particles can be carried over long distances by wind and then settle on ground or water. Depending on their chemical composition, the effects of this settling may include:

- making lakes and streams acidic
- changing the nutrient balance in coastal waters and large river basins

- depleting the nutrients in soil
- damaging sensitive forests and farm crops
- affecting the diversity of ecosystems
- contributing to [acid rain effects](#).

Materials damage

PM can stain and damage stone and other materials, including culturally important objects such as statues and monuments. Some of these effects are related to [acid rain effects on materials](#).

Further Reading

[Particle Pollution and Your Health \(PDF\)](#) (2 pp, 320 K, [About PDF](#)):

Learn who is at risk from exposure to particle pollution, what health effects you may experience as a result of particle exposure, and simple measures you can take to reduce your risk.

[How Smoke From Fires Can Affect Your Health](#): It is important to limit your exposure to smoke -- especially if you may be susceptible.

[EPA research on airborne particulate matter](#): EPA supports research that provides the critical science on PM and other air pollutants to develop and implement Clean Air Act regulations that protect the quality of the air we breathe.

LAST UPDATED ON APRIL 13, 2020

Exhibit 31

An official website of the United States government.



Health and Environmental Effects of Hazardous Air Pollutants

People exposed to toxic air pollutants at sufficient concentrations and durations may have an increased chance of getting cancer or experiencing other serious health effects. These health effects can include damage to the immune system, as well as neurological, reproductive (e.g., reduced fertility), developmental, respiratory and other health problems. In addition to exposure from breathing air toxics, some toxic air pollutants such as mercury can deposit onto soils or surface waters, where they are taken up by plants and ingested by animals and are eventually magnified up through the food chain. Like humans, animals may experience health problems if exposed to sufficient quantities of air toxics over time.

Health and ecological effects resources

- The [Health Effects Notebook for Hazardous Air Pollutants](#) - Detailed information about the health effects of hazardous air pollutants (HAPs) is available in separate fact sheets, for nearly every HAP specified in the Clean Air Act Amendments of 1990.
- [Mercury](#) - Learn more about mercury and what is being done to protect your health.
- [Risk Assessment](#) - Learn about EPA Risk Assessments

LAST UPDATED ON FEBRUARY 9, 2017

Exhibit 32

Black Carbon Emissions from the Bakken Oil and Gas Development Region

Joshua P. Schwarz,^{*,†} John S. Holloway,^{†,‡} Joseph M. Katich,^{†,‡} Stuart McKeen,[†] Eric A. Kort,[§] Mackenzie L. Smith,[§] Thomas B. Ryerson,[†] Colm Sweeney,^{||} and Jeff Peischl^{†,‡}

[†]NOAA ESRL Chemical Sciences Division, Boulder, Colorado 80305, United States

[‡]Cooperative Institute for Research in the Environmental Sciences, University of Colorado, Boulder, Colorado 80309, United States

[§]University of Michigan, Ann Arbor, Michigan 48109, United States

^{||}NOAA ESRL Global Monitoring Division, Boulder, Colorado 80305, United States

S Supporting Information

ABSTRACT: Black carbon (BC) emission rates from the Bakken oil-producing region of North Dakota have been quantified with a NOAA airborne single-particle soot photometer (SP2). Flights in May 2014 led to six measurements of the BC emission rate in the region. Oil and gas operations (associated flaring, diesel engines associated with pumping and drilling, and oil production-related transport), limited agricultural burning, and sparse urban/transport sector activity contribute to these emissions. The BC emission rate was $1400 \pm 360 \text{ t year}^{-1}$, implying that Bakken production activities are unlikely to contribute to large-scale biases in estimates of BC emissions. An upper limit on the BC emission factor from flaring based on these observations is $0.57 \pm 0.14 \text{ g/m}^{-3}$. Flaring BC was not associated with optically significant internally mixed non-BC material or with significant emissions of non-BC-containing primary aerosol. BC in the outflow from the region was also generally externally mixed.



INTRODUCTION

The Bakken region extending over northwestern North Dakota and southeast Saskatchewan hosts extensive fossil-fuel extraction activities, including both shale and tight-sand extraction of crude oil and associated petroleum (natural) gas. Gas and oil development in the region continues to see dramatic increases initiated in the past decade. For example, between May 2013 and May 2014, the number of wells and the amount of oil and gas production in the region increased by 30%.¹ At present, the mining activities in the region have outpaced the development of typical infrastructure, and thus, there is considerable associated flaring of gas. In May 2014, flaring consumed 28%¹ of the total gas produced from operations.

The large-scale nature of development raises questions about the emission of black carbon (BC), a product of incomplete combustion that is a major anthropogenic forcer of climate² and a focus for possible mitigation efforts to permit short-term reductions in climate forcing and for health co-benefits.³ Modeling efforts suggest that flaring BC can have large impacts on climate,⁴ but the emissions inventories they use are not yet well constrained with measurements in the ambient atmosphere.

Here we present the results of black carbon measurements made as part of a NOAA initiative to quantify oil production emissions. The TOPDOWN 2014 (Twin Otter Projects: Defining Oil/gas Well emissionNs) mission was based out of

Minot, one of two central cities in the Bakken region of North Dakota, and involved flights in United States airspace. Figure 1 shows a map of the region in which the northwest corner of North Dakota abuts the southern Canadian and eastern Montana borders. Active oil and gas wells are shown with small black dots.¹ During the mission, in May 2014, some periods of steady high wind provided an excellent opportunity to evaluate the emission rate of black carbon from the area indicated by cross-hatching, which contains 80% by number of all ND wells. A single-particle soot photometer (SP2, Droplet Measurement Technology Inc., Boulder, CO) quantified black carbon atmospheric concentrations and also provided information about the microphysical state of this aerosol material. [Experimental Methods](#) describes the instrumentation, analysis, and relevant flight details of the mission, while the observations and contextual comparison to existing emissions inventories are provided in [Results and Discussion](#). The [Supporting Information](#) provides relevant details.

EXPERIMENTAL METHODS

The SP2, its data products, and its operation have been described extensively in the literature.^{5,6} Briefly, the SP2, as

Received: April 24, 2015

Accepted: September 3, 2015

Published: September 3, 2015

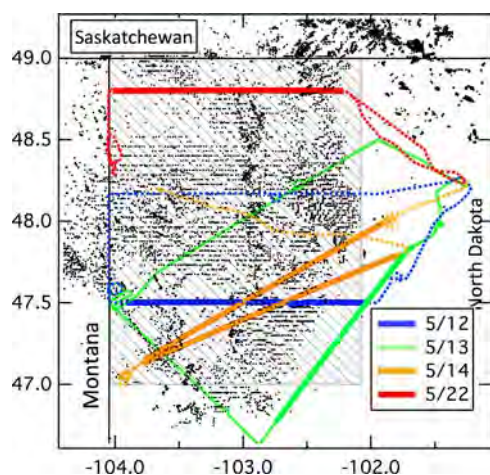


Figure 1. Map of the Bakken region, showing (hatched area) the region integrated in the NEI emissions inventory. The flight tracks on May 12 (blue), 13 (green), 14 (orange), and 22 (red), with mass balance transects in solid and other portions of the flights in dotted lines, and the location of oil and gas wells (black dots). Winds were from the north and northwest for May 12–14 and from the south for May 22.

configured for TOPDOWN, quantifies the refractory black carbon (rBC) content of individual aerosol particles in the mass range of ~ 0.7 – 160 fg [corresponding to an 80–550 nm volume-equivalent diameter (VED) assuming 1 g/cm^3 void-free density]. The SP2 also measures the total optical size of rBC-containing particles with 3–8 fg of rBC mass content,^{5,7} thus allowing estimation of the amount of non-rBC material in an individual particle.⁶ The size distribution of rBC observed here was fit with a log-normal function to evaluate the fraction of the accumulation mode rBC mass detected by the SP2. On the basis of this analysis, the observed mass mixing ratios were corrected upward to better represent the total accumulation mode rBC mass in the air. The correction ranged from 15% on most days to 30% on May 22. rBC in either smaller or larger sized modes would not be reflected in the corrected SP2 measurement; there was no indication of significant mass in such modes in the data set.

The SP2 was calibrated following community recommendations.⁸ “rBC” is the accepted term for the material quantified by the SP2,⁹ and this material has been shown to be equivalent to elemental carbon (EC), as measured under conditions minimizing possible biases, at the level of 15%.¹⁰ “EC” is the term associated with BC measurements performed with a thermal decomposition technique that is often used for

emissions inventories.⁹ Details of the calibration, aircraft inlet, and sampling line configuration are provided in the [Supporting Information](#).

RESULTS AND DISCUSSION

rBC mass emission rate from primarily the North Dakota portion of the basin was calculated for flights on days with very steady and relatively high winds (May 12–14 and 22). On these days, the Twin-Otter flew in the boundary layer, with occasional climbs well above the top of the mixed layer and into the free troposphere to allow identification of the mixed layer height, and to evaluate how well mixed the boundary layer was. Mixed layer height was determined from analysis of vertical profiles of high-signal tracers, including methane, water vapor, ethane, ozone, and potential temperature, which were consistent with a well-mixed layer, including a discernible transition to the free troposphere. All flights reported here occurred in the afternoons after the boundary layer had been well established. Figure 1 shows the flight tracks for these flights; on May 22, the wind was out of the south (with two transects at different altitudes overlaid on the map), on May 12 out of the north, and on all other flights out of the north–northwest. The heavy portions of the tracks indicate the transects used here to determine BC emission rates; sampling on different days with different winds provides confidence that sources outside of the region explored are not strongly contributing to the emission rates calculated here (two transects on May 22 overlaid each other). Transects were oriented within a small angle α from orthogonally to wind direction, and the average wind direction and wind speed (S_W) were averaged for each leg. Flight tracks were extended beyond the areas influenced by outflow from the basin to allow estimation of the mass flux that can be attributed to background air (i.e., the mass flux of rBC into the basin from more distant sources). The net rBC emission rate in the basin from each transect (F_{rBC}) was calculated using established mass balance techniques,^{11,12} here presented in a simplified formulation:

$$F_{\text{rBC}} = S_W \cos(\alpha) \times l h \beta (C_O - C_{\text{BG}}) \quad (1)$$

where l is the length of the flight track influenced by basin emissions, C_O is the average ambient concentration of rBC in the outflow of that track length, C_{BG} is the average concentration of rBC in the background air not influenced by local emissions, and h is the height over which emissions are mixed. Hence, $S_W \cos(\alpha) \times l h$ is the volume of air containing the emissions that is swept over the region per unit time, and $C_O - C_{\text{BG}}$ is the enhanced concentration of rBC in that volume. β is a correction factor to account for nonuniform mixing in the

Table 1. Relevant Parameters for Six Transects Obtained with the NOAA Twin-Otter Aircraft^a

2014 date	local time (pm)	transect altitude (m)	α (rad)	S_W (m s^{-1})	l (km)	h (m)	C_O (ng m^{-3})	C_{BG} (ng m^{-3})	β	F_{rBC} (g s^{-1})
May 12	5:45	1200	0.33	15.2	128	2308	30.4	18.1	0.89	49.5
May 13	3:30	1020	0.20	13.1	144	2271	50.1	35.7	0.91	58.2
May 14	4:10	1050	0.16	7.6	167	1956	65.5	46.5	0.96	47.5
May 14	5:30	1350	0.14	8.1	168	2022	65.9	46.1	0.97	47.0
May 22	4:45	1710	0.14	7.7	133	2112	80.1	49.5	0.91	39.2
May 22	3:30	1140	0.08	7.1	132	2068	63.9	46.1	0.92	36.9
mean									0.93	45.8 ± 3.5

^aThe central columns provide parameters used in the mass emission rate calculation. The mean value of the rBC emission rate from the region is shown at the bottom of the table, with its statistical uncertainty. The ground level varied over ~ 600 – 800 m altitude. BC concentrations are corrected to represent average ambient pressure and temperature in the mixed layer.

transition from the fully mixed layer to the free troposphere (further discussed in the [Supporting Information](#)). Here it averaged 0.93. [Table 1](#) shows the values of the various parameters for the six transects suitable for emission analysis.

Observations of methane (a clear tracer of oil/gas production) during the climbs to the free troposphere mentioned above indicate that the layer was homogeneously mixed vertically up to a transition layer with <10% variability; hence, we simply use the average value observed in each track, corrected for temperature and pressure, to reflect the concentration throughout the layer, with the correction (β) mentioned above to address the transition to air free of these emissions. Flight tracks conducted at different altitudes within the mixed layer (as shown in [Table 1](#)) produce very consistent estimates for the emission rate.

On the first transect for May 22 shown in the table, the contributions of a single exceptional burning source encountered were excluded from contributing to the average observed rBC concentrations. The rBC particles in this plume were substantially larger than those generated from flares or observed in the outflow from the region; on the basis of characteristics of individual flare emissions in the area, it is not possible that this source was associated with a single “rogue” flare. If included, it would have increased the average emission rate for the data set by ~10%. No other open burning plumes near this scale were observed, and generally, agricultural activity, including burns and field work with tractors, appeared to be very limited on the basis of assessments made by scientists flying on the aircraft.

The largest uncertainty is in SP2 calibration, which has been tied to ambient rBC sensitivity at the level of 15%.¹³ On the basis of the sensitivities noted upon determination of mixed layer height above ground level, average enhanced concentration, and wind speed from the data, we conservatively estimate their uncertainties at 10% each, with an additional 10% to reflect uncertainty in the uniformity of the vertically mixed rBC concentration. Uncertainties associated with the wind angle and length of transect integration are negligible in this analysis. Summing the systematic sources in quadrature provides an overall relative systematic uncertainty estimate in the measured rBC emission rate from the measured sources of 25%. The statistical uncertainty in the determination, as shown in [Table 1](#), is relatively small, only 8%, reflecting good consistency between estimates from different days and wind directions and providing confidence that the measurements do a good job covering the hatched area of [Figure 1](#) and rejecting significant biases from other sources. After assumption of constant emission rates throughout the day and night, implying that diurnal emissions associated with agricultural activity and other anthropogenic sources are unimportant here, the data lead to an overall estimate of rBC emissions for the sampled portion of the North Dakota Bakken region of 1400 ± 360 t/year. To the extent that daily activities associated with non-oil/gas sector activity do wane at night, these contributions are overestimated.

The measurements bound the possible emission rate from associated gas flaring. To this end, we pair the state estimate of associated gas flaring for May 2014 in the region¹ to the total rBC emission rate that we measured here, scaled down by 20% to estimate gas emissions only from the wells in the hatched area of [Figure 1](#). This generates an upper limit on the emission factor from flaring: 0.57 ± 0.14 g of rBC/(m³ of gas flared) (at STP).

The microphysical state of the rBC emitted specifically by flaring, and generally from all sources in the region, was determined. [Figure S2](#) presents mass size distributions of rBC observed (1) under nascent conditions produced by individual flares and sampled within minutes of emission and (2) in the outflows used to produce the F_{rBC} estimate (excluding the single outflow strongly influenced by open burning). The flare distributions were corrected to remove background air contributions concurrently sampled. The rBC mass median diameters average 166 ± 2 nm in the outflow (excepting the transect strongly influenced by open burning), which is larger than the rBC produced in U.S. metropolises,¹⁴ and is more consistent with uncontrolled biomass burning rBC emissions.¹⁵ This is consistent with substantial contributions to the total rBC emissions from flaring, which, when specifically analyzed, was associated with rBC with a mass median diameter of 192 ± 6 nm. However, unlike in uncontrolled biomass burning, the rBC generated by flares was not associated with optically detectable (by the SP2) amounts of non-rBC material, and without accumulation-mode rBC-free aerosols. This indicates that the flares produce nearly pure rBC that, on the basis of the work of Bond et al.,² exerts a positive climate forcing. The rBC-containing particles exported from the basin showed very similar characteristics, indicating that there was no substantial secondary production of aerosol materials condensing or coagulating with the rBC on time scales of hours and supporting our assumption that open burning, which typically produces and thickly coats rBC¹⁵ and copious amounts of organic carbon aerosol, did not contribute substantially to the net emissions during the observations.

The most recent inventories of BC emissions from the Bakken region of North Dakota are provided by the Environmental Protection Agency's National Emissions Inventory Database (EPA NEI), which in 2013 released an inventory appropriate for 2011 emissions (NEI-2011).¹⁶ The inventory includes oil and gas production sources but associates no EC with them in the Bakken, and hence obviously underestimates them; ~70% of the NEI EC emissions are attributed to off-road diesel emissions from agricultural activities (tractors), with ~15% each from agricultural open burning and on-road sources. The May EC emission rate in the NEI is 800 t/year over the hatched area of [Figure 1](#), a factor of 2 less than we observed in 2014. Bakken oil (gas) production increased by a factor of 2.5 (2.9) between May 2011 (appropriate for the NEI estimate) and May 2014 (appropriate for the observations here). Flaring increased by a factor of 3.3 over this time.¹ Only limited agricultural activities were observed during the flights, so if oil/gas production-related sources are in fact the dominant emitters in this season, this would suggest that NEI estimates were reasonably accurate in 2011 but misapportioned emission sources. On the other hand, estimates of BC produced by gas flaring may be biased high. The GAINS model¹⁷ has an emission factor of 1.6 g of rBC/(m³ of gas flared) (STP), which is a factor of 2.6 higher than the upper limit generated here. A more recent laboratory estimate of flaring emission factors,¹⁸ which also was based on laser-induced incandescence measurements, produced a reduced estimate of 0.51 g of rBC/(m³ of gas flared); this was referenced as an estimate of flaring that was still consistent with Arctic flaring being significant for climate.⁴ This value is also consistent with our upper limit. As we do not have measurements in other fields, it is not clear how well our

estimate will translate to flaring conditions in the rest of the world.

Total anthropogenic and natural North American BC emissions were estimated in the year 2000 at 380000 t/year,² hence, the total yearly rBC emissions estimated here, which are only partially due to the exceptional amount of gas flaring and oil/gas production activities in the Bakken (nearly 40% of the U.S. flaring total¹⁹), make up <1% of that total. It follows that lack of accounting for oil/gas production sources does not very significantly contribute to any large-scale underestimate of BC emissions or BC direct radiative forcing from North America.

On global scales, North America makes up less than 10% of total flaring.¹⁹ Thus, global-scale oil/gas production activities and associated flaring may produce significant amounts of BC, especially in the context of regional impacts.⁴

■ ASSOCIATED CONTENT

■ Supporting Information

The Supporting Information is available free of charge on the ACS Publications website at DOI: 10.1021/acs.estlett.5b00225.

Two figures and expanded technical discussion about the SP2 calibration and installation in the aircraft and the determination of mixing height (PDF)

■ AUTHOR INFORMATION

Corresponding Author

*E-mail: Joshua.p.schwarz@noaa.gov.

Author Contributions

The manuscript was written through contributions of all authors. All authors have given approval to the final version of the manuscript. J.P.S. wrote the primary manuscript. J.P.S., J.S.H., J.M.K., and J.P. analyzed data. J.P.S. and J.S.H. shared responsibility for the instrument. M.L.S. and J.P. contributed to operating the instrument on the aircraft. S.M. contributed modeling and inventory calculations. E.A.K., T.B.R., and C.S. contributed to project organization, flight planning, and logistics.

Notes

The authors declare no competing financial interest.

■ ACKNOWLEDGMENTS

We thank the pilots and crew of the NOAA Twin-Otter for their critical role in obtaining these measurements. This research was supported by NOAA's ESRL Chemical Sciences and Global Monitoring Divisions and by NASA Radiation Sciences and Upper Atmosphere Research Programs.

■ ABBREVIATIONS

BC, black carbon; SP2, single-particle soot photometer; VED, volume-equivalent diameter

■ REFERENCES

- (1) North Dakota Oil/Gas Production (<https://www.dmr.nd.gov/oilgas/stats/statisticsvw.asp>, accessed March 2015).
- (2) Bond, T. C.; Doherty, S. J.; Fahey, D. W.; Forster, P. M.; Berntsen, T.; DeAngelo, B. J.; Flanner, M. G.; Ghan, S.; Kärcher, B.; Koch, D.; Kinne, S.; Kondo, Y.; Quinn, P. K.; Sarofim, M. C.; Schultz, M. G.; Schulz, M.; Venkataraman, C.; Zhang, H.; Zhang, S.; Bellouin, N.; Guttikunda, S. K.; Hopke, P. K.; Jacobson, M. Z.; Kaiser, J. W.; Klimont, Z.; Lohmann, U.; Schwarz, J. P.; Shindell, D.; Storelvmo, T.; Warren, S. G.; Zender, C. S. Bounding the role of black carbon in the

climate system: A scientific assessment. *J. Geophys. Res. Atmospheres*. **2013**, *118* (11), 5380–5552.

- (3) Anenberg, S. C.; Schwartz, J.; Shindell, D.; Amann, M.; Faluvegi, G.; Klimont, Z.; Janssens-Maenhout, G.; Pozzoli, L.; Van Dingenen, R.; Vignati, E.; Emberson, L.; Muller, N. Z.; West, J. J.; Williams, M.; Demkine, V.; Hicks, W. K.; Kuylenstierna, J.; Raes, F.; Ramanathan, V. Global Air Quality and Health Co-benefits of Mitigating Near-Term Climate Change through Methane and Black Carbon Emission Controls. *Environ. Health Perspect.* **2012**, *120*, 831–839.

- (4) Stohl, A.; Klimont, Z.; Eckhardt, S.; Kupiainen, K.; Shevchenko, V. P.; Kopeikin, V. M.; Novigatsky, A. N. Black carbon in the Arctic: the underestimated role of gas flaring and residential combustion emissions. *Atmos. Chem. Phys.* **2013**, *13*, 8833–8855.

- (5) Schwarz, J. P.; Spackman, J. R.; Fahey, D. W.; Gao, R. S.; Lohmann, U.; Stier, P.; Watts, L. A.; Thomson, D. S.; Lack, D. A.; Pfister, L.; Mahoney, M. J.; Baumgardner, D.; Wilson, J. C.; Reeves, J. M. Coatings and their enhancement of black carbon light absorption in the tropical atmosphere. *J. Geophys. Res.* **2008**, *113* (D3), 2156–2202.

- (6) Schwarz, J. P.; Spackman, J. R.; Gao, R. S.; Perring, A. E.; Cross, E.; Onasch, T. B.; Ahern, A.; Wrobel, W.; Davidovits, P.; Olfert, J.; Dubey, M. K.; Mazzoleni, C.; Fahey, D. W. The detection efficiency of the single particle soot photometer. *Aerosol Sci. Technol.* **2010**, *44*, 612–628.

- (7) Gao, R. S.; Schwarz, J. P.; Kelly, K. K.; Fahey, D. W.; Watts, L. A.; Thompson, T. L.; Spackman, J. R.; Slowik, J. G.; Cross, E. S.; Han, J.-H.; Davidovits, P.; Onasch, T. B.; Worsnop, D. R. A novel method for estimating light scattering properties of soot aerosols using a modified single particle soot photometer. *Aerosol Sci. Technol.* **2007**, *41*, 125–135.

- (8) Baumgardner, D.; Popovicheva, O.; Allan, J.; Bernardoni, V.; Cao, J.; Cavalli, F.; Cozic, J.; Diapouli, E.; Eleftheriadis, K.; Genberg, P. J.; Gonzalez, C.; Gysel, M.; John, A.; Kirchstetter, T. W.; Kuhlbusch, T. A. J.; Laborde, M.; Lack, D.; Müller, T.; Niessner, R.; Petzold, A.; Piazzalunga, A.; Putaud, J. P.; Schwarz, J. P.; Sheridan, P.; Subramanian, R.; Swietlicki, E.; Valli, G.; Vecchi, R.; Viana, M. Soot Reference Materials for instrument calibration and intercomparisons: a workshop summary with recommendations. *Atmos. Meas. Tech.* **2012**, *5*, 1869–1887.

- (9) Petzold, A.; Ogren, J. A.; Fiebig, M.; Laj, P.; Li, S.-M.; Baltensperger, U.; Holzer-Popp, T.; Kinne, S.; Pappalardo, G.; Sugimoto, N.; Wehrli, C.; Wiedensohler, A.; Zhang, X.-Y. Recommendations for reporting “black carbon” measurements. *Atmos. Chem. Phys.* **2013**, *13*, 8365–8379.

- (10) Kondo, Y.; Sahu, L.; Moteki, N.; Khan, F.; Takegawa, N.; Liu, X.; Koike, M.; Miyakawa, T. Consistency and traceability of black carbon measurements made by laser-induced incandescence, thermal-optical transmittance, and filter-based photo-absorption techniques. *Aerosol Sci. Technol.* **2011**, *45*, 295–312.

- (11) Karion, A.; Sweeney, C.; Pétron, G.; Frost, G.; Hardesty, R. M.; Kofler, J.; Miller, B. R.; Newberger, T.; Wolter, S.; Banta, R.; Brewer, A.; Dlugokencky, E.; Lang, P.; Montzka, S. A.; Schnell, R.; Tans, P.; Trainer, M.; Zamora, R.; Conley, S. Methane emissions estimate from airborne measurements over a western United States natural gas field. *Geophys. Res. Lett.* **2013**, *40*, 4393–4397.

- (12) Peischl, J.; Ryerson, T. B.; Aikin, K. C.; de Gouw, J. A.; Gilman, J. B.; Holloway, J. S.; Lerner, B. M.; Nadkarni, R.; Neuman, J. A.; Nowak, J. B.; Trainer, M.; Warneke, C.; Parrish, D. D. Quantifying atmospheric methane emissions from the Haynesville, Fayetteville, and northeastern Marcellus shale gas production regions. *J. Geophys. Res. Atmos.* **2015**, *120*, 2119–2139.

- (13) Gysel, M.; Laborde, M.; Olfert, J. S.; Subramanian, R.; Gröhn, A. J. Effective density of Aquadag and fullerene soot black carbon reference materials used for SP2 calibration. *Atmos. Meas. Tech.* **2011**, *4*, 2851–2858.

- (14) Metcalf, A. R.; Craven, J. S.; Ensberg, J. J.; Brioude, J.; Angevine, W.; Sorooshian, A.; Duong, H. T.; Jonsson, J. J.; Flagan, R. C.; Seinfeld, J. H. Black carbon aerosol over the Los Angeles Basin during CalNex. *J. Geophys. Res.* **2012**, *117*, D21.

(15) Schwarz, J. P.; Gao, R. S.; Spackman, J. R.; Watts, L. A.; Thomson, D. S.; Fahey, D. W.; Ryerson, T. B.; Peischl, T.; Holloway, J. S.; Trainer, M.; Frost, G. J.; Baynard, T.; Lack, D. A.; de Gouw, J. A.; Warneke, C.; Del Negro, L. A. Measurement of the mixing state, mass, and optical size of individual black carbon particles in urban and biomass burning emissions. *Geophys. Res. Lett.* **2008**, *35*, L13810.

(16) Ahmadov, R.; McKeen, S.; Trainer, M.; Banta, R.; Brewer, A.; Brown, S.; Edwards, P. M.; de Gouw, J. A.; Frost, G. J.; Gilman, J.; Helmig, D.; Johnson, B.; Karion, A.; Koss, A.; Langford, A.; Lerner, A.; Olson, J.; Oltmans, S.; Peischl, J.; Petron, G.; Pichugina, Y.; Roberts, J. M.; Ryerson, T.; Schnell, R.; Senff, C.; Sweeney, C.; Thompson, C.; Veres, P. R.; Warneke, C.; Wild, R.; Williams, E. J.; Yuan, B.; Zamora, R. Understanding high wintertime ozone pollution events in an oil- and natural gas-producing region of the western US. *Atmos. Chem. Phys.* **2015**, *15*, 411–429.

(17) Amann, M.; Bertok, I.; Borken-Kleefeld, J.; Cofala, J.; Heyes, C.; Höglund-Isaksson, L.; Klimont, Z.; Nguyen, B.; Posch, M.; Rafaj, P.; Sandler, R.; Schöpp, W.; Wagner, F.; Winiwarter, W. Cost-effective control of air quality and greenhouse gasses in Europe: modelin and policy applications. *Environ. Mod. Software* **2011**, *26*, 1489–1501.

(18) McEwen, J. D. N.; Johnson, M. R. Black carbon particulate matter emission factors for buoyancy driven associate gas flares. *J. Air Waste Manage. Assoc.* **2012**, *62* (3), 307–321.

(19) Global Gas Flaring Reduction Partnership (<http://www.worldbank.org/en/programs/gasflaringreduction>, accessed May, 2015).

Exhibit 33

Emissions of Black Carbon from Flaring in the Bakken Oil and Gas Fields

New NOAA-led study measures "soot" from North Dakota flares

WEDNESDAY, SEPTEMBER 9, 2015

In the lonely reaches of northwestern North Dakota and across the border into Saskatchewan, the vast Bakken oil field hosts extensive activities to extract both crude oil and natural gas. Business is booming—production increased by 30 percent between May 2013 and May 2014. More than a quarter of the total gas produced from the Bakken operations can't be processed fast enough, though, and the common industry practice is to “flare” it—burn it off as it is vented to the atmosphere. Jutting 30 feet upward like enormous lit matchsticks, the flares pose a new question for atmospheric scientists: What do the flares put into the air? A new NOAA-led study has produced the first direct measurements of how much black carbon—a major component of airborne particles that are commonly referred to as “soot”—is emitted by the Bakken flaring operations.

The answer? “The flaring releases about 4 tons of black carbon a day, which hasn't been previously accounted for,” said Joshua Schwarz, a research scientist at NOAA and lead author of the study, published online September 8 in ***Environmental Science & Technology Letters***. “Fortunately, this amount is not significant for global climate because it is less than 1 percent of all the black carbon emitted in North America.”

Researchers from NOAA, the Cooperative Institute for Research in Environmental Sciences (CIRES) at the University of Colorado Boulder and the University of Michigan measured the emissions of black carbon during six flights of the NOAA Twin Otter research aircraft in May 2014. On board was the NOAA “Single Particle Soot Photometer,” an instrument that measures black carbon atmospheric concentration and microphysical properties. Black carbon is a product of incomplete combustion of fossil fuels and biomass, and its absorption properties make it a warming influence on climate. It is also harmful to human health when inhaled.

In the six flights, the research aircraft traversed the Bakken region during periods of steady high winds, sampling to get a “background” reading of the black carbon levels and then across the Bakken to measure the increases in black carbon resulting from the flaring operations. Researchers were able to use their data to calculate the black carbon emission rate for the region and estimate the amounts coming from the oil and gas production operations, primarily flaring.

The bottom line from the new study? Assuming the May 2014 measurement period was representative of yearly operations, the researchers find that an upper limit of 1400 ± 360 tons of black carbon are emitted each year from the flares at the Bakken region. Total emissions of black carbon in North America were estimated to be 380,000 tons per year in 2000.

The new study’s findings are likely indicative of North America, because about 40 percent of the total flaring that occurs in the U.S. is in the Bakken region. However, the authors note that on the global scale, North America makes up less than 10 percent of the total flaring, and they caution that the results may be different in other regions of the world.

Image: Flares burn at sunset in the Bakken oil and gas fields in North Dakota. Jeff Peischl/CIRES and NOAA

Authors of “Black Carbon Emissions from the Bakken Oil and Gas Development Region” in ***Environmental Science & Technology Letters***, published online September 8, include NOAA’s Joshua P. Schwarz and Thomas B. Ryerson; John S. Holloway, Joseph M. Katich, Stuart McKeen, Colm Sweeney, and Jeff Peischl from CIRES and NOAA; and Eric A. Kort and Mackenzie L. Smith from the University of Michigan.

contacts

Joshua Schwarz

NOAA lead author

Joshua.P.Schwarz@noaa.gov

303-497-4637

Monica Allen NOAA public affairs

monica.allen@noaa.gov

301-734-1123

Katy Human CIRES communications

kathleen.human@colorado.edu

303-735-0196

Exhibit 34

PRACTICE BRIDGE

Single-blind inter-comparison of methane detection technologies – results from the Stanford/EDF Mobile Monitoring Challenge

Arvind P. Ravikumar*, Sindhu Sreedhara†, Jingfan Wang†, Jacob Englander†‡, Daniel Roda-Stuart†§, Clay Bell¶, Daniel Zimmerle¶, David Lyon¶, Isabel Mogstad¶, Ben Ratner¶ and Adam R. Brandt†

Methane leakage regulations in the US and Canada have spurred the development of new technologies that promise faster and cheaper leak detection for the oil and natural gas industry. Here, we report results from the Stanford/EDF Mobile Monitoring Challenge – the first independent assessment of 10 vehicle-, drone-, and plane-based mobile leak detection technologies. Using single-blind controlled release tests at two locations, we analyze the ability of mobile technologies to detect, localize, and quantify methane emissions. We find that the technologies are generally effective at detecting leaks, with 6 of the 10 technologies correctly detecting over 90% of test scenarios (true positive plus true negative rate). All technologies demonstrated pad-level localization of leaks, while 6 of the 10 technologies could assign a leak to the specific piece of equipment in at least 50% of test scenarios. All systems tested here will require secondary inspection to identify leak locations for repair; thus, mobile leak detection technologies can act as a complement, and not a substitute, for currently used optical gas imaging systems. In general, emissions quantification needs improvement as most technologies were only able to generally provide order of magnitude emissions estimates. Improvements to quantification algorithms, reducing false positive detection rates, and identifying early applications will be critical for deployment at scale. Even as this study provides the first independent verification of the performance of mobile technologies, it only represents the first step in the road to demonstrating that these technologies will provide emissions reductions that are equivalent to existing regulatory approaches.

Keywords: Methane emissions; Technology; Oil and gas; Leak Detection and Repair; Policy

1. Introduction

The recent Intergovernmental Panel on Climate Change (IPCC) special report on global warming of 1.5°C highlighted the importance of reducing short-lived greenhouse gases like methane (Intergovernmental Panel on Climate Change, 2018). Methane, a major component of natural gas, has a global warming potential that is 36 times that of carbon dioxide over a 100-year period (Myhre, et al., 2013), and even higher over shorter time periods (Etminan, Myhre, Highwood, & Shine, 2016). Furthermore, methane

emissions contribute to sea-level rise over much longer timescales than their atmospheric lifetimes (Zickfeld, Solomon, & Gilford, 2017). These consequences are troubling given that official methane emissions inventory in the US and Canada have been found to be systematically underestimated (Alvarez, et al., 2018; Johnson, Tyner, Conley, Schwietzke, & Zavala-Araiza, 2017).

Recently, Canada and U.S. states such as Colorado and California implemented regulations to reduce fugitive emissions from the oil and gas industry (Environment and Climate Change Canada, 2018; Colorado Department of Public Health and Environment, 2014). A major component of these regulations is periodic leak detection and repair (LDAR) surveys conducted using established methods like U.S. Environmental Protection Agency (EPA) Method-21 or optical gas imaging (OGI) technologies.

There are two primary challenges to effective methane emissions reductions. First, cost-effectiveness is a critical feature for emission mitigation considering the large spatial extent of oil and gas facilities. OGI-based LDAR surveys, while anecdotally found to be effective (Keating

* Harrisburg University of Science and Technology, Harrisburg, Pennsylvania, US

† Stanford University, Stanford, California, US

‡ California Air Resources Board, Sacramento, California, US

§ Alphataraxia Management, Los Angeles, California, US

¶ Colorado State University Energy Institute, Fort Collins, Colorado, US

¶ Environmental Defense Fund, Washington DC, US

Corresponding author: Arvind P. Ravikumar
(aravikumar@harrisburgu.edu)

Research Inc., 2016), are time-consuming – a crew of 2 people can typically visit 4–6 well pads per day, depending on distance between sites. Conducting multiple OGI-based surveys every year at large numbers of facilities or visiting sparsely distributed sites could be costly, especially when low gas prices reduce the economic benefits of increased gas recovery. Furthermore, OGI-based leak surveys are dependent on operator experience and weather conditions (Ravikumar, Wang, McGuire, Bell, Zimmerle, & Brandt, 2018; Ravikumar, Wang, & Brandt, 2017).

Second, methane emissions are highly stochastic. Many recent studies have demonstrated the influence of super-emitters' on overall methane emissions (Brandt, Heath, & Cooley, 2016). These super-emitters – a small fraction of all emission points (top 5%) that contribute over 50% of total emissions – are caused by abnormal or otherwise unintentional process conditions like equipment malfunction, failure, or operator error (Zavala-Araiza, et al., 2017). Because of the outsized contribution of super-emitters, finding and repairing these anomalous emitters as quickly as possible is key to effective methane reductions.

To address these two challenges, the solution to methane leakage detection must be: (1) faster and more cost-effective on a dollars per site basis than OGI-based leak detection, and (2) performed much more frequently or continuously.

One class of technologies that aims to meet these challenges are mobile methane detectors (Fox, Barchyn, Risk, Ravikumar, & Hugenholtz, 2019). Many new mobile sensor platforms have been developed in recent years that promise faster and more cost-effective methane leak detection. These have been shown to detect methane emissions at various spatial scales and detection thresholds. For example, truck-based measurements in British Columbia have been used to better characterize facility-level and regional methane emissions (Atherton, et al., 2017). Several aircraft- and helicopter-based measurement campaigns in the US and Canada have expanded our understanding of methane emissions and revealed widespread underreporting in official inventories (Englander, Brandt, Conley, Lyon, & Jackson, 2018; Lyon, Alvarez, Zavala-Araiza, Brandt, Jackson, & Hamburg, 2016; Conley, Franco, Faloona, Blake, Peischl, & Ryerson, 2016; Frankenberg, et al., 2016; Yuan, et al., 2015; Johnson, Tyner, Conley, Schwietzke, & Zavala-Araiza, 2017). Recent studies have also demonstrated the use of UAVs to quantify methane emissions (Golston, et al., 2018; Nathan, et al., 2015; Barchyn, et al., 2017). Satellite data are often used to assess regional and global scale methane emissions (Turner, Frankenberg, Wennberg, & Jacob, 2017; Jacob, et al., 2016). Despite promising initial results, there has been no systematic testing of mobile leak detection technologies for applications in LDAR programs. The "methane observation networks with innovative technology to obtain reductions" (MONITOR) program developed by ARPA-E (U.S. Advanced Research Projects Agency (ARPA-E), 2014) has performed the most comprehensive controlled test of new methane detection technologies based on specific cost and performance targets, although these technologies are largely designed for continuous stationary deployment. Similarly, the Methane Detectors Challenge organized by the EDF in partnership with

industry tested continuous monitoring sources for methane leak detection (Southwest Research Institute, 2015).

In this paper, we report results from the Stanford/Environmental Defense Fund (EDF) Mobile Monitoring Challenge (MMC). The MMC was an open study that called for participants to take part in a single-blind, independently administered controlled release study. Section 2 gives an overview of the MMC methods including selection process, participating technologies, and test scenarios. Section 3 describes metrics used to assess the performance of the technologies. Section 4 provides results from each of the teams that participated in the MMC, and section 5 discusses the implications of this work to methane mitigation. Detailed test-related data and further analysis of team performance is provided in the supplementary information (S.I.).

2. Methods

2.1. Team selection

The MMC invited technologists to apply by submitting information on their organization, sensor technical specifications, and commercial characteristics (see S.I. for application form). The project website was advertised widely and remained open for applications for 65 days. The MMC received 25 applications from technologists based in 5 countries. An industry advisory board including members of major oil and gas companies was created to provide industry insights into desirable features of methane detection systems. Scientists and project managers from Stanford and EDF, as well as the industry advisory board, reviewed and scored the applications separately, then gathered in person to discuss the applications and select the final list of participants (see S.I. section 1 and Table 1). Selection criteria included scientific soundness, applicability to oil and gas facilities, and path to commercialization. Eleven organizations developing 12 technologies were selected to participate in the MMC – these included 3 truck-, 3 plane-, and 6 drone-based platforms. Due to technical and logistical challenges, two selected teams – Kairos Aerospace and Bluefield Technologies – did not participate in the field trials. After selection, authors (A.P.R. and I.M.) conducted one-on-one phone interviews with the science team of each technology to understand technology features and limitations. Teams were then assigned to one of three testing weeks based on their self-reported methane detection limits. A summary of the technologies selected as part of this study is given in Table 1 (also see S.I. SM_Table 1 for technical specifications). The tests in this study represents an independent assessment of the performance of methane leak detection technologies as would be observed by a regulator or site operator. As such, the participating teams did not have any interaction with or knowledge of the scientific team's analysis of their performance after the field tests.

2.2. Test locations and controlled releases

Two test locations were chosen for the MMC. Two weeks of releases were performed at the Methane Emissions Technology Evaluation Center (METEC), a Department of Energy funded controlled release facility in Fort Collins, CO. Release rates of total gas (87% CH₄, see S.I. section 2) at the METEC facility were in the 0–15 standard cubic feet per

Table 1: Summary of the technologies participating in the Stanford/EDF Mobile Monitoring Challenge. DOI: <https://doi.org/10.1525/elementa.373.t1>

Company	Platform Type	Sensor Type/Species Measured	Survey Method	Survey Speed ^a (mph)	Survey Height (m)
ABB/ULC Robotics	Drone	Cavity-enhanced laser absorption spectroscopy – Methane	Modified raster scan (wind responsive)	2–5	5–10 m
Advisian	Helicopter	Laser absorption spectroscopy – methane/ethane	Upwind/Downwind transects with sample tube	2–5	15–20 m
Aeris Technologies	Vehicle	Laser absorption spectroscopy – methane, ethane, water-vapor	Fence-line around equipment groups, facility	~10	1–2 m
Baker Hughes (GE)	Drone	Laser absorption spectroscopy – methane	Concentric circles around equipment	~5	5–10 m
Ball Aerospace	Plane	Airborne differential LIDAR – methane	Fly-overs (multiple passes)	~115	~1000 m
Heath Consultants Inc.	Vehicle	Off-axis integrated cavity output spectroscopy – methane, ethane	Fence-line around equipment groups, facility	~10	~1–2 m
Picarro	Drone and Vehicle	Cavity ringdown spectroscopy – methane, ethane, water-vapor	Upwind/Downwind transects	2–5	5–10 m
Seek Ops Inc.	Drone	Laser absorption spectroscopy – methane	Raster scan, with flux plane mapping	2–5	1–3 m
U Calgary	Vehicle	Open-path laser spectroscopy – methane	Fence-line and highway-based screening	~10 (fence-line) 30–50 (highway)	2–3 m
U Calgary and Ventus Geospatial	Drone (fixed-wing)	Open-path laser spectroscopy – methane	Multiple downwind plume transects	30–40	28–124 m

^aSome technologies were limited in their speed due to speed-limits at the METEC test-site (10 mph).

hour (scfh) range (0–0.25 kg CH₄/h). One week of releases were performed at a facility owned by Rawhide Leasing near Sacramento, CA. Test rates at the Sacramento facility spanned 0–1500 scfh (0–26 kg CH₄/h). Not all releases could be performed at METEC because some teams reported emissions detection limits that were too large for the emissions capability for the equipment and permitting in place at METEC (see S.I. section 2).

Teams were grouped based on self-reported detection thresholds – grouping together teams with similar detection limits ensures that tests are not too facile (for example, only leaks significantly larger than detection limits) nor too difficult (test leaks significantly smaller than detection limits). The final test dates and grouping are shown in S.I. All tests were conducted in a single blind fashion – only authors A.P.R., C.B., and A.R.B. were aware of the actual leak rates and saw leak rates during the test process. All technology teams and other members on the project did not have access to the test scenarios until after the tests were completed. Approximately 3 months after testing was completed, after all teams reported final results to Stanford scientists, the true leak rates were given to the teams for their own use in further technology development.

The blinding of the leakage results could in theory be broken by audible sound or odor from the emission point. Because of the low release volumes, no Stanford staff noted discernable noise of emission while touring sites. For safety reasons, both sites release odorized gas which contains mercaptan compounds. This resulted in frequent odors at both sites, which shifted with the

winds and would be most detectable when the team members were downwind from the release point (either due to the team moving with the vehicle or due to wind shifts). Given the complexity of the release patterns, their frequent temporal changes (every 10 min) and possibility of multiple release points, we do not expect the odors to provide consistent patterns that could be used by teams to break the blind. Furthermore, real oil and gas facilities frequency have odors associated with non-methane compounds in the raw gas, analogous to the test scenario here.

Methane Emissions Technology Evaluation Center (METEC), Fort Collins, CO. METEC is an ARPA-E funded controlled release test site for evaluating new methane emissions detection technologies (see **Figure 1(a)**). The site contains equipment typically found at natural gas production facilities such as wellheads, separators, and tank batteries, organized across 5 clusters of equipment analogous to well-pads (see S.I. section 2). The pads vary in complexity –two of the pads had 1 wellhead, 1 separator, and 1 tank each. Other pads had multiple equipment of the same group, such as 5 wellheads on pad 4. Each team was assigned a pad for initial testing and were rotated across pads periodically to ensure all teams tested on all pads. Each piece of equipment has multiple leak points fashioned out of 0.64 cm (¼ in.) diameter steel tubing – the tubing is well concealed to mimic realistic leak sources such as connectors and flanges. Natural gas (86–88 vol% methane, 8–10 vol% ethane, 2–4 vol% trace gases, with odorant) is sourced from a centrally located tank at 172 bar (2500 psi), with flow controlled by a combination of

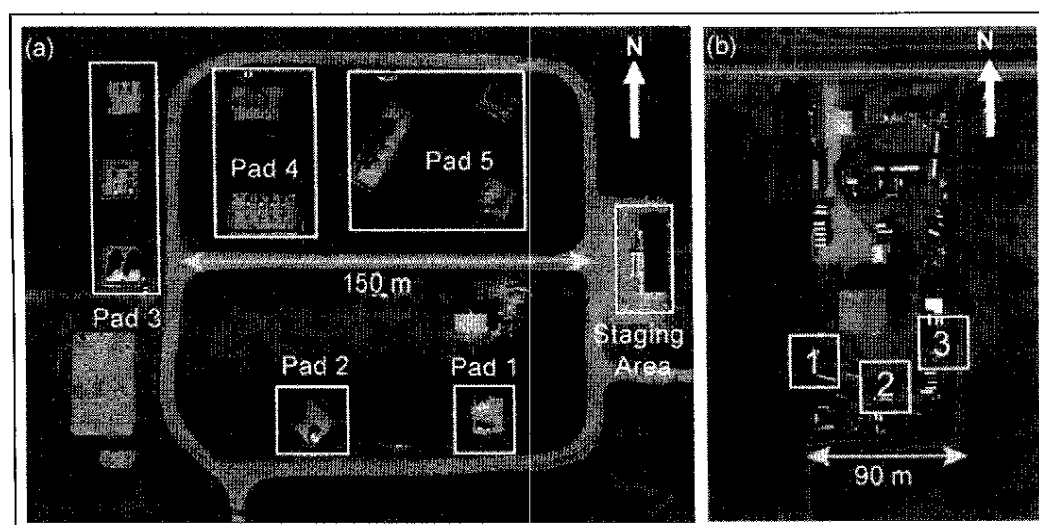


Figure 1: Google Earth image of Stanford/EDF Mobile Monitoring Challenge test locations. (a) METEC facility in Fort Collins, CO showing the pad configurations 1 through 5 and the staging area, **(b)** Rawhide Leasing facility near Sacramento, CA showing the approximate leak locations denoted 1, 2, and 3. The red circle shows the location of an anomalous non-test intermittent methane source. DOI: <https://doi.org/10.1525/elementa.373.f1>

pressure regulators and choked-flow orifices fitted with flow meters. During these tests, flow rates ranged from 0 to about 15 scfh. In addition, the site also included a 3-axis sonic anemometer that collected 1 minute-averaged meteorological data at ~3 m above the ground. The wind data from this instrument is later used to analyze the effect of intra-pad interference during testing (see S.I. section 5 and 6).

Rawhide Leasing Gas Yard, Sacramento, CA. Controlled release experiments at the Sacramento sites consisted of 3 individual sources separated by 30–60 m (see **Figure 1(b)**, and S.I. section 2). The sources consisted of a 2 m elevated stack of 2.54 cm diameter with test flow rates ranging from 50 scfh (0.87 kg CH₄/h) to about 1500 scfh (26 kg CH₄/h). Each of the sources were individually metered using a Sierra Instruments QuadraTherm 740i thermal mass flow meters with an accuracy of $\pm 0.75\%$ of full-scale reading. Natural gas (91 vol% methane, 6 vol% ethane, 3 vol% trace gases) was sourced from a pressurized tank at 2500 psi and stepped down to 50 psi with a regulator before passing through the flow meters. In addition to flow rates, the mass flow meters also monitored gas temperature along the line. Because over 90% of the flow rates were relatively small, being lower than 400 scfh (< 7 kg CH₄/h), we did not experience issues with Joule Thompson cooling effect (Maric, 2005). To allow for effective plume development through the atmosphere for aerial detection, leaks tested at this facility included a 3-minute buffer zone before and after each test period. The pre-test buffer allows the plume to develop while the post-test buffer lets the plume clear the area before the next test to avoid plume-overlap interference. This test site had other methane emissions not part of the controlled release test that were picked up by the technologies tested here (red circle in **Figure 1b**). The teams performed appropriate analysis to remove the effect of the co-located emissions whenever possible.

Test scenarios. We developed a series of test protocols of increasing complexity to assess the performance of mobile leak detection technologies. These tests were designed to assess the ability of technologies to locate and detect leaks, quantify flow rates, resolve multiple leaks that are closely spaced, and do it all within a specified time limit. The test protocols were similar at METEC and Sacramento test locations but varied in complexity (see S.I. section 3 and SM_Table 3). The teams could use as little or as much time as needed within the maximum allotted time for each test. We chose not to time individual teams separately and instead opted for “maximum time allowed” for two reasons: (a) vehicle speeds at both test sites were limited to 10 mph, artificially impacting measurement time for trucks, and (b) test sites are not the same as actively producing well sites and therefore, measurement times here might not be representative of field performance. While some teams stopped after detecting the leak within 2–4 minutes of a timed test, other teams used the entire test duration to improve their localization and quantification precision.

As multiple teams were measuring leaks simultaneously at METEC, study author (A.P.R.) worked in real-time to adjust leak locations across the 5 pads to minimize interference between pads. Leaks were preferentially placed downwind of non-leaks to minimize the amount of methane blowing from leaking sites to non-leaking sites. In addition, participants could drive between leak locations on different pads to sample both upwind and downwind methane data. Real-time monitoring of wind conditions by METEC personnel were used to assign leak configurations across the five pads for each test scenario that would minimize interference. Because teams rotated, and wind conditions changed, each team was given a mix of leak and non-leak observations (generally 50% leaks and 50% non-leaks). In S.I. (section 5 and 6) we present results from cleaning reported data of possible interference, but

present baseline results below. This is done by excluding any test scenarios that had a reasonable possibility of interference from upwind emission sources (see S.I. section 5 for more details on exclusion criteria). To be clear, interference is likely at oil and gas facilities either due to co-located emissions from the same pad or downwind emissions from a different pad. Whether this impacts technology performance is important to understanding the robustness of the algorithms used by the technologies to interpret raw data.

2.3. Performance metrics

A set of common metrics were developed to account for the variety in the sensors used, mobile platforms, survey protocols, analysis algorithms, and reporting parameters. These metrics included – (a) leak detection probability, (b) detection and localization, and (c) quantification accuracy. These are briefly described below.

Leak detection probability: Leak detection probability varies as a function of leak size for each technology. Leak detection probabilities are critical inputs to natural gas field simulators such as the Fugitive Emissions Abatement Simulation Toolkit (FEAST) that can help compare new detection technologies with established methods (Kemp, Ravikumar, & Brandt, 2016). Furthermore, developing estimates of detection threshold will assist in direct comparisons with currently used OGI technologies such as the FLIR GF-320 cameras. In this study, for technologies tested at METEC, we group leak sizes into 5 bins: <1, 1–3, 3–5, 5–8, and >8 scfh, and determine the fraction of test scenarios in each bin that was detected. For technologies tested in Sacramento, CA, the bin sizes were: <150, 150–300, 300–450, 450–600, and >600 scfh. All test scenarios of both leaks and non-leaks (zero tests) are combined into a true/false matrix chart. Four results are possible – a true positive (TP) result is recorded when a team correctly identifies an actual leak; a true negative (TN) occurs when a team correctly identifies a zero-leak test as not containing a leak; a false positive (FP) occurs when a team mis-identifies a zero-leak scenario as a leak; and a false negative (FN) result occurs when a team wrongly characterizes a leak as a zero-leak scenario.

Detection and localization: TP results are grouped into three levels of localization accuracy – level 1, 2, and 3. While some teams reported GPS coordinates that would make exact displacement calculations between actual and measured leak locations possible (i.e., m of offset between expected and actual location), numerous teams specified the equipment type or specific piece of equipment where emissions were detected. We chose this three-level metric to harmonize the different types of location information reported by the teams. All three levels of leak localization will require a secondary inspection to identify the leaking component or the correct leaking equipment for further repair.

Level-1: The team correctly identifies the leaking equipment. In scenarios with multiple equipment of the same group (e.g., 5 wellheads), the teams should also have identified the correct equipment number in that group. This indicates equipment-level attribution ability – for example, a team correctly reporting a leak on wellhead 4 on Pad 4, and corresponds to location accuracy within ~1–4

m. Although the correct equipment has been identified in Level-1 type leaks, a repair crew may still require a method like handheld Method-21, OGI, or bubble test to identify the leaking component.

Level-2: The team correctly identifies the leak equipment group but does not identify (or misidentifies) the equipment number when multiple equipment of the same group is present. For example, a team reporting a leak on wellhead 2 on Pad 4, when wellhead 4 was the actual leak location. Level-2 detection signifies some attributional ability, with effectiveness determined by the spatial density of equipment as well as resolution capabilities of the technology. Level-2 detection corresponds to location accuracy within ~4–10 m. There were no level-2 type leaks at the Sacramento test site because it contained only 3 isolated leak sources and did not have any group sources present. All tests results from the Sacramento site were identified as Level-1 or Level-3 detects. A Level-2 detection requires the operator to first identify the leaking equipment and component using a Method-21 or OGI-based sensor before repairs.

Level-3: The team correctly identifies a leak, but misidentifies the equipment group – for example, a team reporting a leak on separator 2 on Pad 4, when wellhead 4 on Pad 4 was the actual leak location. Teams that did not report any specific location data were automatically assigned Level 3 detection. This level translates to pad-level detection ability (~10+ m) and can be considered as a proxy for screening type technologies. A secondary ground team with a handheld device would be required to identify specific leak location before repairs can occur.

Finally, we also analyze results across equipment type – wellheads, separators, and tanks at METEC, and sources 1, 2, and 3 in California. This will show differences in performance that are affected by the height of the leaking equipment, a critical metric for truck and drone-based systems.

Quantification: Teams were asked to quantify emissions and report estimated flow rates for a subset of the test scenarios. Some teams also quantified emissions in scenarios where it was not required, and these results are scored as well. Quantification performance is shown as a parity chart between actual and estimated leak rates, with error bars if reported by teams. The best-fit linear regression between measured and actual volumes and the 95% confidence interval around the slope is reported.

We choose the charitable interpretation of reported data in the case of ambiguity. For example, consider a scenario where we tested detection and quantification of 2 closely spaced leaks on a separator group, and the team reported one quantification measurement for a separator leak without specifying the number of leaks. We interpreted this result as the team ‘detecting’ both leaks without resolving leak equipment, resulting in 2 level-2 detections. Furthermore, the quantification result would be compared to the combined flux rate of both leaks.

3. Results of the Mobile Monitoring Challenge

This section describes detailed results for participating team. Team performance is presented in alphabetical order. A few caveats should be noted:

- The sample sizes in different tests varies across teams because of the random nature of assigning test scenarios to teams, varying wind directions, robustness of technologies to high winds, and differences in preparation time across the technologies.
- The performance of all technologies is affected by weather conditions to varying degrees. We present data below from all test scenarios, irrespective of weather conditions. S.I. contains detailed analysis of team performance as a function of inter-pad interference.
- The suitability of a given technology for methane leak detection depends not only on the performance of the technologies themselves, but also on parameters such as facility type, and infrastructure density.

3.1. ABB/ULC Robotics

ABB deployed a UAV-mounted methane-only sensor based on cavity enhanced laser absorption spectroscopy. In addition to gas concentration values, the UAV collected GPS coordinates and wind speed using an on-board anemometer.

Figure 2(a) shows the binary detection results of the ABB system. TP rate is 77% ($n = 43$ of 56), all at level-3 localization, indicating detection effectiveness at the pad level. The average leak rate of the 18 (23%) FN indications was 2.4 scfh. FP rate is 22% ($n = 10$ of 45). A majority of these false positive (60%) occurred when multiple leaks were tested, indicating potential issues with leak resolution algorithms.

Figure 2(b) shows the detection probability of the technology as a function of leak-size. Detection probability varies from <30% for leaks <1 scfh, to 100% for leaks >8 scfh. The 53% detection probability for leaks smaller than 3 scfh partially explains the average false negative rate of 2.4 scfh. Re-testing of this technology only at higher leak rates would likely result in improved TP rates.

Figure 2(c) shows the quantification parity chart. The slope of the best-fit line was 0.025, indicating no correlation with the actual leak rate ($R^2 = 0.01$, Pearson's $\rho = 0.02$). The average difference between the actual

and measured leak rate was +2.8 scfh (95% C.I. [1.1, 4.5], $n = 28$). This underestimation was especially severe for leaks larger than 5 scfh, with a mean actual leak rate of 7.4 scfh, and the corresponding average measured leak rate being 3.1 scfh.

3.2. Advisian (Worley Parsons)

Advisian technology employed a Vapor-55 helicopter UAV outfitted with a laser spectroscopy-based methane-ethane sensor. The sample inlet was suspended about 50 ft below the helicopter through an inlet tube pulled behind the helicopter. In addition to gas concentration, the UAV collects GPS coordinates and meteorological data. This team provided two results for each test scenario – one that was immediately available based on 3-dimensional plots of concentration, and the other based on off-site data analysis performed on data uploaded to the cloud. Below we have used the off-site analysis results.

Figure 3(a) shows the TP rate for detection was 94% ($n = 36$), with the level-1, level-2, and level-3 localization at 47%, 25%, and 22%, respectively. The nearly 50% level-1 localization demonstrates equipment-level leak detection capability. However, 10 of the 17 level-2 and level-3 leak detections occurred during the multiple leaks per pad test scenarios, indicating challenges with distinguishing closely-spaced leaks. Across equipment types, the leak detection effectiveness was 90% ($n = 10$) for wellheads, 100% ($n = 24$) for separators, and 50% ($n = 2$) for tanks. The difference between tanks and wellheads/separators was not statistically significant due to the small sample size. The FP rate was 7% ($n = 2$ out of 29).

Figure 3(b) shows that the 100% detection probability cut-off is approximately 3 scfh.

Figure 3(c) shows the quantification parity chart for the sensor, with the slope of best-fit linear regression being 2.7. The error bars shown were directly reported by the team. The average difference between the actual and measured leak rate is -12.7 scfh (95% C.I. [-20.6, -4.8], $n = 33$), representing an average overestimation by approximately 3.5 times the average controlled release rate (3.64 scfh).

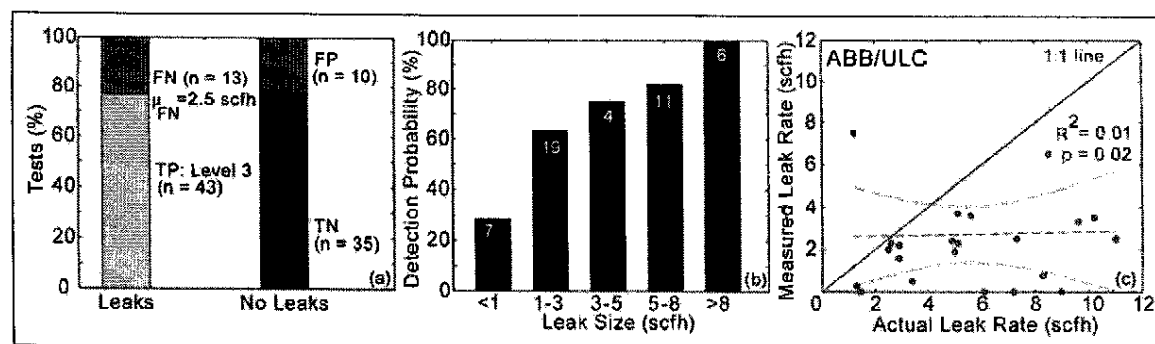


Figure 2: Performance results of ABB (ASEA Brown Boveri)/ULC Robotics in the Stanford/EDF Mobile Monitoring Challenge. (a) Binary detection characteristics of the technology, disaggregated by the level of true positive detection, (b) Leak detection probability across different leak size range, and (c) quantification parity chart between actual and measured leak rates. (TP: True Positive, FP: False Positive, TN: True Negative, FN: False Negative). DOI: <https://doi.org/10.1525/elementa.373.f2>

3.3. Aeris Technologies

Aeris Technologies uses a mid-infrared laser spectroscopy-based sensor mounted on a ground vehicle to detect methane, ethane, and water-vapor. In addition to gas concentrations, the system also measures meteorological data and GPS coordinates.

Figure 4(a) shows the detection characteristics for Aeris. Out of 52 total leaks, TP rate was 88%, with 50% at level-1, 15% at level-2, and 23% at level-3 localization. Six leaks were misidentified as zero leaks (FN), with mean FN leak rate of 1.5 scfh. Three of the six FN observations occurred during the multiple leaks per pad test, indicating challenges in spatial resolution of closely located emissions sources. Notably, there is a difference in detection effectiveness between equipment types: wellheads (TP = 87%, $n = 15$) and separators (TP = 97%, $n = 32$) had very high success rates, while, tanks had lower success rates (TP = 40%, $n = 5$). This suggest a possible challenge for measuring from taller equipment from a vehicle-based sensor and would point to the need for a wider sampling path to

allow more time for groundward dispersion of higher leaks.

Out of the 48 zero leaks tested, the FP rate was 15% ($n = 7$). Of the FP detections quantified (5/7), the average quantified FP leak rate was 0.5 scfh – over 19 times smaller than average measured leak rate of 9.6 scfh for actual leaks. This indicates that false positives were an issue near the detection limits of the technology, as seen in the detection probability curve **Figure 4(b)**.

Figure 4(c) shows the quantification parity chart for Aeris. The slope of the best-fit regression line is 3, indicating overestimation. The average difference between the actual and measured rate was –6.5 scfh, with the 95% C.I. ranging from –10.2 to –2.3 scfh. Five large overestimates (>30 scfh) in quantification are not shown in **Figure 4(c)** for clarity. However, these data points are included in our statistical analysis and are not arbitrarily discarded while calculating the R^2 and ρ coefficients. Removing these from the statistical analysis increases R^2 and ρ coefficients to 0.32 and 0.55, respectively.

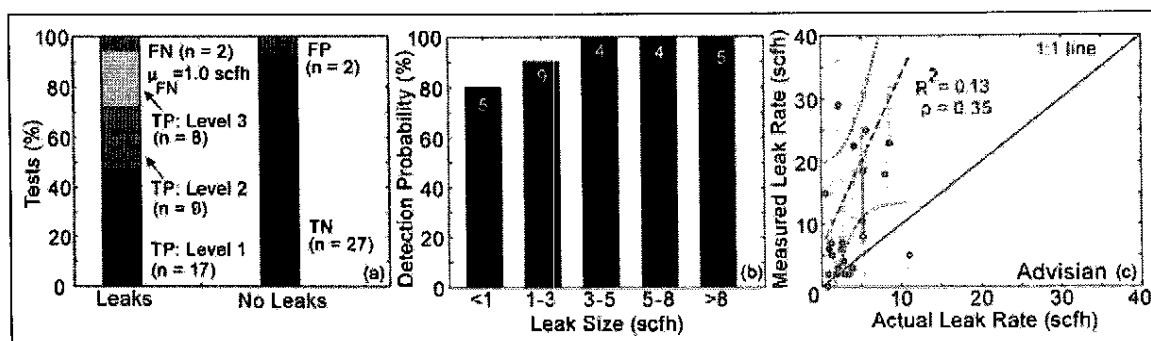


Figure 3: Performance results of Advisian (Worley Parsons Group) in the Stanford/EDF Mobile Monitoring Challenge. (a) Binary detection characteristics of the technology, disaggregated by the level of true positive detection, (b) Leak detection probability across different leak size range, and (c) quantification parity chart between actual and measured leak rates. (TP: True Positive, FP: False Positive, TN: True Negative, FN: False Negative). DOI: <https://doi.org/10.1525/elementa.373.f3>

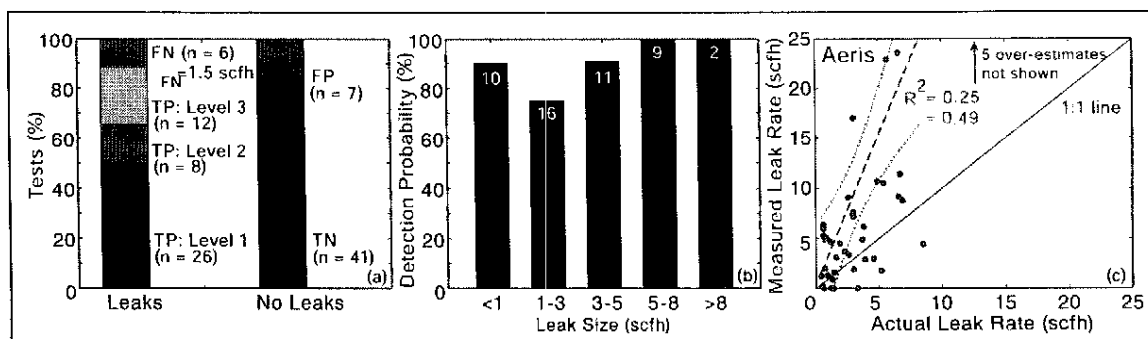


Figure 4: Performance results of Aeris Technologies in the Stanford/EDF Mobile Monitoring Challenge. (a) Binary detection characteristics of the technology, disaggregated by the level of true positive detection, (b) Leak detection probability across different leak size range, and (c) quantification parity chart between actual and measured leak rates. 5 large over-estimates in the data are not shown in (c) for clarity but are included in calculating best-fit lines. (TP: True Positive, FP: False Positive, TN: True Negative, FN: False Negative). DOI: <https://doi.org/10.1525/elementa.373.f4>

3.4. Baker Hughes (GE)

BHGE operated an UAV-mounted methane-only sensor based on absorption spectroscopy. The sensor collects single point measurements of methane concentration at 2 Hz frequency along with location information through an on-board GPS. Leaks are analyzed separately by combining with weather parameters from the ground anemometer data made available to the team.

Figure 5(a) shows the detection characteristics of the UAV-mounted sensor. TP rate is 68% ($n = 39$ of 57). Approximately half the detected leaks – 20 out of 39 – were level-3 localization, indicating pad-level attribution. Mean FN leak rate is 2.5 scfh, which is lower than the 6 scfh detection limit as described by the team prior to testing. FP rate of 71% (32 of 45) is high, indicating a need to improve processing algorithms to reduce false positive detection.

Figure 5(b) shows the detection probability charts for the technology. For leaks below 3 scfh, the detection probability is about 50%, aligning with team reported detection limits. BHGE reliably detected leaks greater than 8 scfh with 100% detection probability.

Figure 5(c) shows the quantification parity chart. Best-fit regression line has slope of 0.05, indicating under-estimation and lack of sensitivity to leak size. The mean measured leak rate was 1.2 scfh, corresponding to an average error of +2.2 scfh (95% C.I. [1.4, 3.0], $n = 57$) – the measured rates were only 35% of the actual leak rates.

3.5. Ball Aerospace

Ball Aerospace tested a methane-only sensor based on airborne differential absorption LIDAR mounted on a single-engine Cessna T206. The sensor samples data at 10 kHz and collects path-integrated methane concentration data in a 'push-broom' approach with a spatial resolution of about 2 m on the ground. Meteorological data from nearby ground weather station is integrated with sensor data to develop quantitative flux estimates. The airplane flew at 2800 ft altitude, and the controlled release tests were conducted at the Sacramento, CA site between 21–25 May 2018.

Figure 6(a) shows the detection characteristics of the Ball aerospace team. Out of 50 total leaks that were tested, TP rate is 74% at level-1 localization, demonstrating the

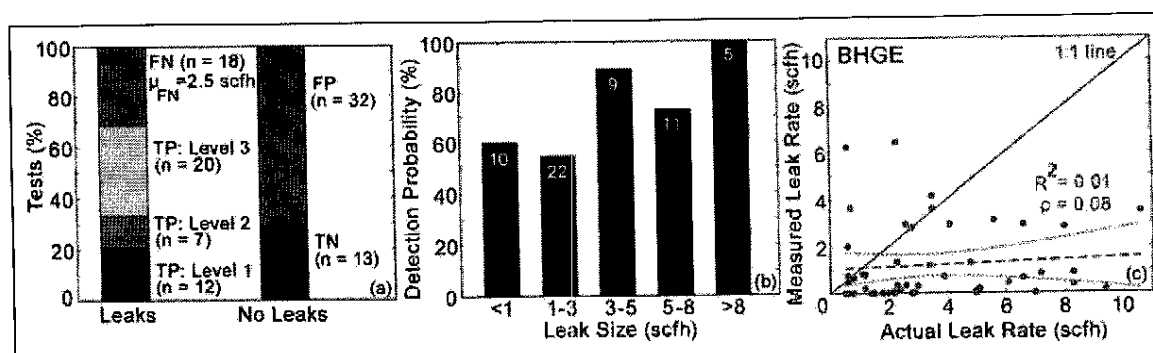


Figure 5: Performance results of Baker Hughes (General Electric) (BHGE) in the Stanford/EDF Mobile Monitoring Challenge. (a) Binary detection characteristics of the technology, disaggregated by the level of true positive detection, (b) Leak detection probability across different leak size range, and (c) quantification parity chart between actual and measured leak rates. (TP: True Positive, FP: False Positive, TN: True Negative, FN: False Negative). DOI: <https://doi.org/10.1525/elementa.373.f5>

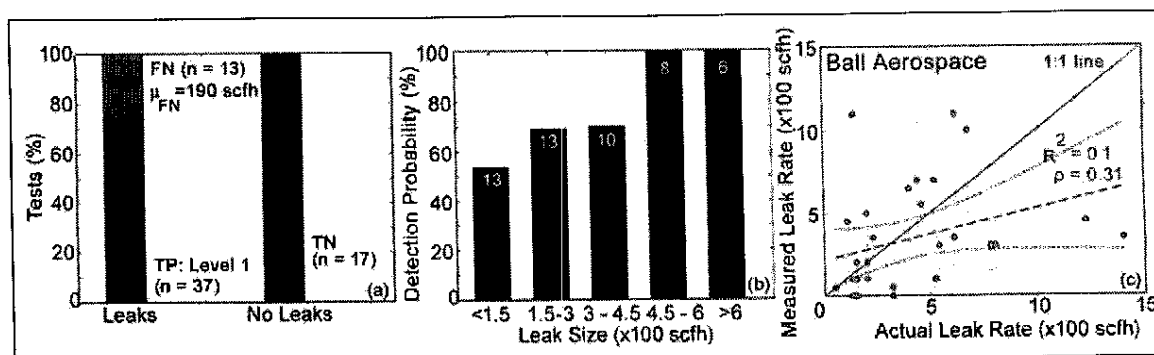


Figure 6: Performance results of Ball Aerospace in the Stanford/EDF Mobile Monitoring Challenge. (a) Binary detection characteristics of the technology, disaggregated by the level of true positive detection, (b) Leak detection probability across different leak size range, and (c) quantification parity chart between actual and measured leak rates. (TP: True Positive, FP: False Positive, TN: True Negative, FN: False Negative). DOI: <https://doi.org/10.1525/elementa.373.f6>

source attribution ability of the aircraft-mounted sensor. FN rate is 26% with mean FN rate of 190 scfh. This technology did not detect any FPs ($n = 17$). While the detection effectiveness at source 1 (west) and source 2 (south) were 88% and 80%, respectively, the effectiveness at source 3 (east) was only 46% ($n = 13$). The reason for this discrepancy is not well understood.

The detection probability plot (see **Figure 6(b)**) shows a threshold around 450 scfh. Leaks greater than 450 scfh had 100% probability of detection, while leaks smaller than 450 scfh had an average detection probability of about 64%. The lower detection effectiveness for leaks smaller than 200 scfh also explains the observed mean FN rate (190 scfh, see **Figure 6(a)**).

Figure 6(c) shows the quantification parity chart, with a best-fit linear regression slope of 0.32. The error bars are based on the teams' reports. The average error between actual and measured leak rate was +58 scfh (95% C.I. [-79, 196], $n = 32$), indicating an underestimation of the actual leak rate by ~15%. However, the confidence interval for the average error includes 0.

The effectiveness of airplane-based detection is dependent on the number of passes over the facility. In this study, the Ball Aerospace team averaged 4 passes during the 10-minute tests and 7 passes during the 15-minute tests that required quantification in addition to detection.

3.6. Heath Consultants Inc.

Heath Consultants Inc. tested the Mobile Guard – a vehicle-based leak detection system – that uses off-axis integrated cavity output spectroscopy to detect methane and ethane emissions. In addition to the analyzer, the truck also collected GPS and weather data using an on-board anemometer.

Figure 7(a) shows the detection characteristics of the truck-based measurement system. Out of a total of 92 leaks tested, Heath identified 86 at least partially (levels 1, 2, or 3), resulting in a FN rate of 6.5%. The average leak rate for the false negative tests was 1.8 scfh. 75 of the 86 detected leaks, or 82%, were in the level 1 or level 2 category – the technology identified the correct equipment

group for the leak source the vast majority of the time. In addition to the true positive results, Heath had a false positive rate of 25.6%, with 11 of the 43 zeros incorrectly identified as leaks. This rate was affected by the unusually windy conditions during the week of testing (see S.I. section 5). The mean wind speed during testing was over 13 mph, affecting detection and complicating analysis of raw concentration data. 9 out of 11 false positive detections for Heath occurred during the multiple leaks per pad test scenario, indicating potential challenges in resolving multiple leak sources from spatial concentration data.

Figure 7(b) shows the detection probability curves for Heath as a function of leak size range. This technology has high sensitivity, detecting leaks that are smaller than 1 scfh with approximately 90% success rate. No statistically significant difference in ability to detect leaks across different equipment types exists.

Figure 7(c) shows the quantification parity chart including both single-leak and multi-leak measurements. The slope of the best-fit linear regression line is 0.44 with larger leaks generally underestimated. The overall mis-estimation was skewed negatively (toward underestimation) but not statistically significant from 0 (95% C.I. [-1.4, 0.23], $n = 23$).

3.7. Picarro Inc.

Picarro tested a hybrid drone and vehicle-based methane, ethane, and water-vapor sensor based on optical absorption using cavity ringdown spectroscopy. The sensor was deployed on the ground in a vehicle while the gas inlet for the system was mounted on an unmanned aerial vehicle (UAV). This inlet is tethered to the ground-based sensor using a 150 ft long inlet tube. In addition to pollutant concentrations, the sensor also measured wind speed and GPS coordinates at approximately 1 Hz frequency.

Figure 8(a) shows the detection characteristics of Picarro's drone-based system. A TP rate of 92% (59/64) was achieved at level-2 and level-3 localization, demonstrating detection effectiveness at the pad-level. The average leak rate of the FN measurements – 5 out of the 64 tests – was 3.2 scfh. All tank-related leaks were correctly

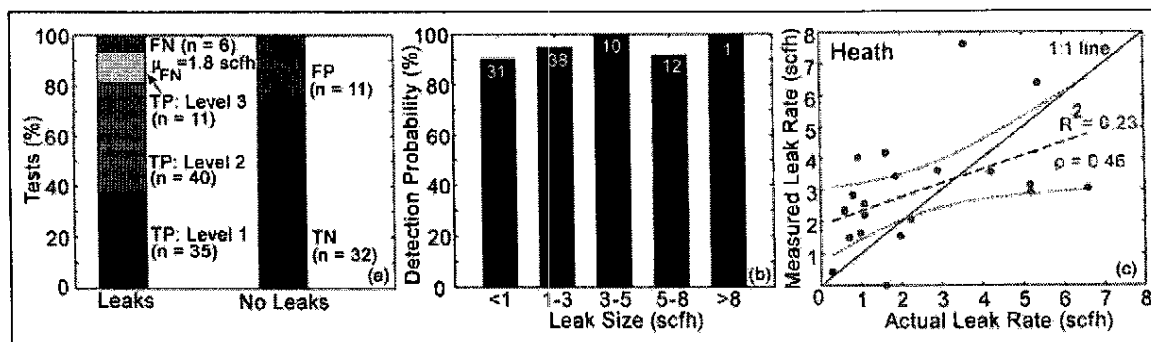


Figure 7: Performance results of Heath Consultants in the Stanford/EDF Mobile Monitoring Challenge. (a) Binary detection characteristics of the technology, disaggregated by the level of true positive detection, (b) Leak detection probability across different leak size range; the numbers on bars refer to sample size in each bin, and (c) quantification parity chart between actual and measured leak rates. (TP: True Positive, FP: False Positive, TN: True Negative, FN: False Negative). DOI: <https://doi.org/10.1525/elementa.373.f7>

identified ($n = 6$), showing success with leaks at height (difference is not statistically significant due to small sample size). A FP rate of 39% was found (9/23).

The level-3 leaks, all identified during the multiple leaks per pad test, point to limited ability to attribute sources at the equipment-group level. However, it was also during the multiple leaks per pad test that this technology tested 8 of the 9 false positive results in this study. This performance indicates suitability at screening pad-level emissions, while also demonstrating the need for improvement in algorithms for source attribution under complex emissions scenarios. The UAV system was not tested on one of the days (April 11th, 2018) because of winds gusting over 23 mph.

Figure 8(b) shows the detection probability curve for Picarro. There is no statistically significant difference in detection between the different leak rates. A high leak detection probability at small leak rates (<1 scfh) points to the underlying sensor's high sensitivity. **Figure 8(c)** shows the quantification parity for a sample size of 86 leaks (all leaks were quantified by Picarro). The error bars in **Figure 8(c)** are 70% confidence intervals as reported by Picarro. The slope of the regression line is 0.36, driven

by underestimation of leaks at larger leak rates (>6 scfh), while smaller leaks are generally overestimated. The average difference between the actual leak rate and the measured leak rate was -0.89 scfh, with a 95% confidence interval between -1.8 scfh and 0.01 scfh.

3.8. Seek Ops Inc.

Seek Ops Inc. tested a methane-only, continuous in-situ monitoring sensor based on laser absorption spectroscopy mounted on a UAV platform. The drone measured methane concentration and GPS coordinates, while wind is measured using a custom ground station on the site erected by the team.

Figure 9(a) shows the detection characteristics of the drone-mounted sensor. This technology had a 100% TP rate ($n = 63$), with a majority of the leaks (68%) detected at the level-1 scenario. The remaining emissions were equally split (16% each) between level-2 and level-3 detection scenarios. Most level-3 scenario for Seek Ops occurred on pads 1 and 2, where the specific leak location was ambiguous because of the heat map of emission covering more than one equipment. These aggregate statistics also

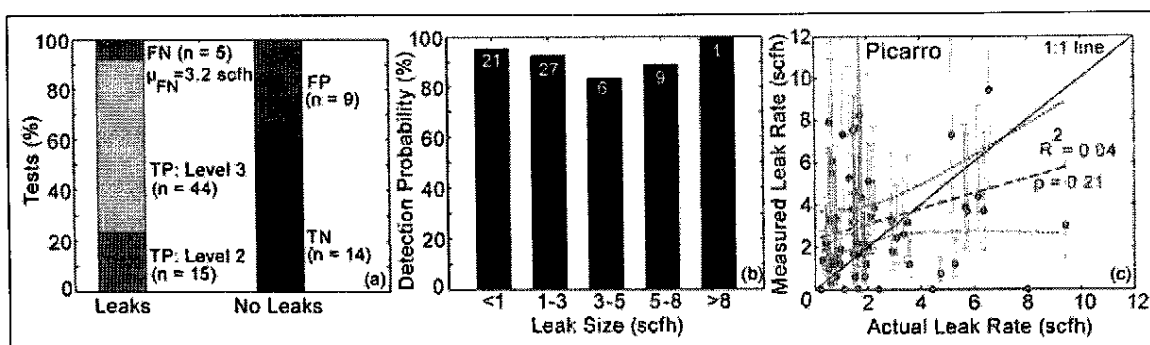


Figure 8: Performance results of Picarro Inc. in the Stanford/EDF Mobile Monitoring Challenge. (a) Binary detection characteristics of the technology, disaggregated by the level of true positive detection, (b) Leak detection probability across different leak size range, and (c) quantification parity chart between actual and measured leak rates. (TP: True Positive, FP: False Positive, TN: True Negative, FN: False Negative). DOI: <https://doi.org/10.1525/elementa.373.f8>

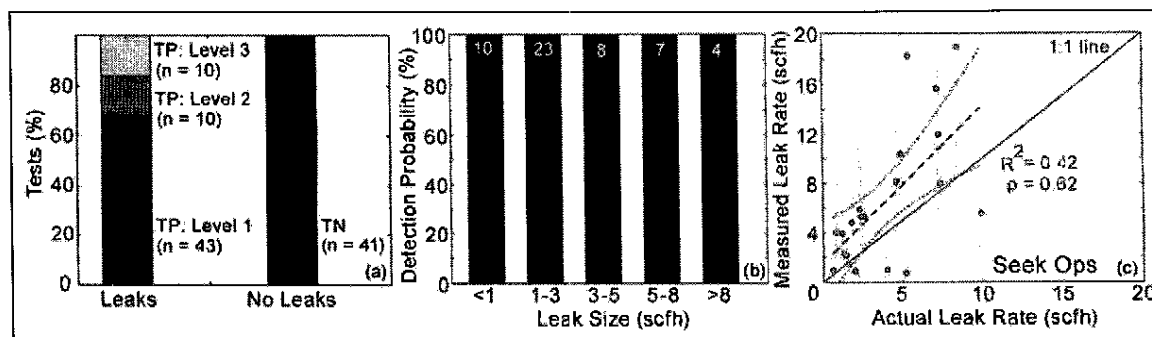


Figure 9: Performance results of Seek Ops Inc. in the Stanford/EDF Mobile Monitoring Challenge. (a) Binary detection characteristics of the technology, disaggregated by the level of true positive detection, (b) Leak detection probability across different leak size range, and (c) quantification parity chart between actual and measured leak rates. (TP: True Positive, FP: False Positive, TN: True Negative, FN: False Negative). DOI: <https://doi.org/10.1525/elementa.373.f9>

include results from the multiple leaks per pad scenarios, demonstrating the ability of Seek Ops algorithms to distinguish multiple closely-spaced emissions sources. The team did not have any FP detection. **Figure 9(b)** shows detection of 100% in all leak classes.

Figure 9(c) shows the quantification parity chart, with the error bars as directly reported by Seek Ops. The slope of the regression line is 1.27, suggesting overestimation of measured flux rates. The average difference between actual and measured leak rates is -2.6 scfh, with a 95% confidence interval between -4.3 and -0.8 scfh ($n = 63$), suggesting intercept (rather than slope) bias towards overestimation of leak rates.

3.9. University of Calgary (UC)

The University of Calgary (UC) team deployed two different technologies – a vehicle-based methane-only sensor, and a fixed-wing drone-based sensor. Both these technologies were tested between May 21–25 2018 near Sacramento, CA. We only include results from the truck-based system here, due to small number of flights with the fixed-wing drone. Results from the drone are presented in S.I. section 4.

The vehicle-based platform is fitted with a roof-mounted, methane-only open-path laser absorption sensor (LICOR LI-7700) that works on the principle of wavelength modulation spectroscopy, a 3D anemometer, and a vehicle position and orientation system. The platform, designed for both fence-line type measurements as well as fast-screening mode from public roads, collects data from all on-board instruments at 10 Hz.

Figure 10(a) shows the detection characteristics of the UC truck-based platform. TP rate is 94%, with $n = 55$ leaks (71%) at level-1 localization, and $n = 18$ leaks (23%) at level-3 localization. 15 of the 18 level-3 detects were from either source 1 (west) or source 2 (south) – interference from the non-test methane emissions from the site under appropriate wind conditions could have contributed to mis-identification. Mean FN flow rate is 121 scfh. A high FP rate (60%) could partly be due to interfering emissions sources from the front of the site.

Figure 10(b) shows the detection probability curve as a function of leak size. Leaks above 450 scfh have a 100% detection probability, even though all leaks are detected at the 80% level or higher. The lowest detection probability (82%) for leaks less than 150 scfh is consistent with the average FN flow rate of 121 scfh. The differences in detection probability across the range of leak sizes considered are not statistically significant.

Figure 10(c) shows the quantification parity chart of the technology, with the slope of the best-fit regression line being 0.4, indicating some underestimation of reported emissions. One reason for the underreporting could be attributed to data processing – the team subtracted the influence of the non-test emission at site by estimating its leak rate. However, the intermittent nature of the non-test leak could have resulted in an overestimation (instantaneous rate > average rate) thereby underestimating test scenario emissions. The average error between the actual and measured leak rate was 185 scfh (95% C.I. [137, 234], $n = 73$), confirming the over-estimation seen in the best-fit regression line.

4. Discussion

Table 2 summarizes the performance of these technologies along parameters chosen to highlight the collective capabilities of mobile systems as well as potential challenges ahead. All technologies are effective at detecting leaks, with 8 of the 9 tested technologies demonstrating a true positive leak rate of at least 75%. More importantly, 5 of 9 technologies show a near perfect true positive detection rate of 90% or higher – this shows the ability of technologies to detect leaks as small as 1 scfh. Despite this, the source attribution capability – denoted by the fraction of leaks detected at level-1 or level-2 (equipment-group level attribution) – varies significantly from 0% to 84%. Technologies such as ABB/ULC Robotics, Picarro, and BHGE largely confine their detection to pad-level attribution – leak repair and mitigation will require a complementary technology to identify emitting equipment and component. For technologies with high level-1 and level-2 detection capabilities, an OGI or similar

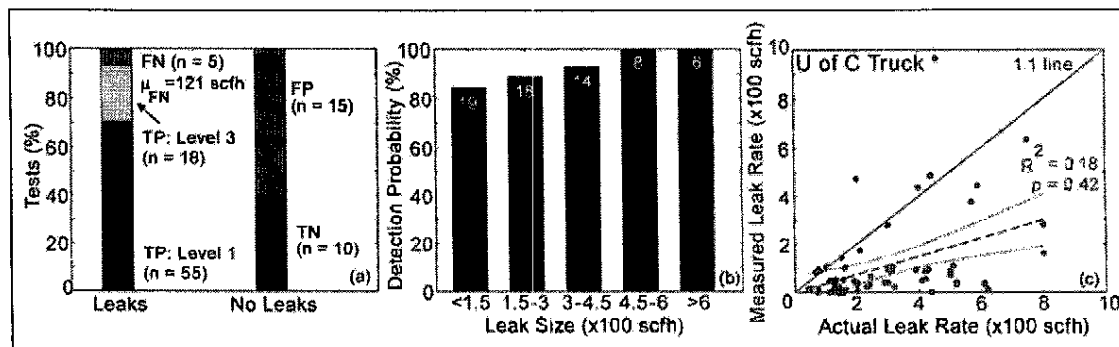


Figure 10: Performance results of University of Calgary (Truck) in the Stanford/EDF Mobile Monitoring Challenge. (a) Binary detection characteristics of the technology, disaggregated by the level of true positive detection, (b) Leak detection probability across different leak size range, and (c) quantification parity chart between actual and measured leak rates. (TP: True Positive, FP: False Positive, TN: True Negative, FN: False Negative). DOI: <https://doi.org/10.1525/elementa.373.f10>

Table 2: Summary of performance of the 9 technologies tested in the Stanford/EDF Mobile Monitoring Challenge. DOI: <https://doi.org/10.1525/elementa.373.t2>

Technology	Technology Type	Detection Effectiveness		False Positive Rate (%)	Detection Limit (leak rate where detection probability is 100%, scfh)	Quantification Accuracy ($\frac{\text{Measured}}{\text{Actual}}$, % tests)	
		True Positive (% all levels)	True Positive (Levels 1–2(%))			0.5 – 2x*	0.1 – 10x* O(M)
ABB/ULC Robotics	Drone	77	0	22	≥8	30	78
Advisian	Drone	94	72	7	3–5	25	79
Aeris Technologies	Truck	88	65	15	5–8	38	79
Baker Hughes (GE)	Drone	68	33	71	≥8	24	54
Ball Aerospace	Plane	76	76	0	450–600	53	83
Heath Consultants	Truck	93	82	26	≥8	48	95
Picarro	Drone sampling	92	23	39	≥8	45	92
Seek Ops Inc.	Drone	100	84	0	≤1	36	100
U. Calgary (Truck)	Truck	94	71	60	450–600	18	74

* Fraction of tests where the measured emission rates are within (a) 0.5–2 times, and (b) 0.1–10 times of the actual emission rate.

technology may still be required to identify the leaking component and initiate repairs.

The false positive rate is an important indication of a system's ability to differentiate methane signal from noise. Methane is often present at elevated concentrations at oil and gas facilities, and the ability to distinguish natural variability from an emissions source is critical to effective mitigation. This is especially important for technologies that have small leak detection thresholds. Three technologies in this study had false positives rates lower than 10%, four more in the 15–40% range, and two technologies with false positive rates greater 50%. The high false positive rate in some of the technologies occurred despite a high leak detection rate. This indicates that sensor algorithms that process raw concentration data play an important role in the success and failure rate of these technologies. A combination of high sensitivity and ineffective algorithms can lead to high false positive rates because of an inability to clearly distinguish leak signal from background methane noise. Technologists should carefully consider the needs of the application – trade-offs between high sensitivity, high false positives, and quantification may be acceptable in some applications (rapid detection of 'super-emitters'), but unacceptable in others (quantifying mitigation potential, inventory). For technologies tested at the California site, the presence of non-test methane emissions from the site could have contributed to the high false positive rate for the University of Calgary vehicle-based technology.

All the technologies tested at METEC had detection limits lower than 10 scfh – in **Table 2**, we define the detection

limit as the leak rate beyond which the probability of detection is 100% under test conditions. Four of the technologies had a detection limit of at least 8 scfh, while two others were in the 3–8 scfh range. Because SeekOps identified all the leaks, we estimate that their detection limit is lower than 1 scfh. These numbers are comparable to the detection limits of OGI-based leak detection under ideal weather conditions (Ravikumar, Wang, McGuire, Bell, Zimmerle, & Brandt, 2018). Ball Aerospace's aerial system and University of Calgary's truck-based screening system have detection limits in the 450–600 scfh range – these rates are comparable to the 90th percentile of component-level emission rates found at oil and gas facilities (Brandt, Heath, & Cooley, 2016).

In general, quantification performance needs improvement. Most quantification efforts had appreciable errors in average leak rate or slope (or both). This is due to a fundamental issue: quantification of leakage rates from detected concentrations in downwind plumes is a challenging "inverse problem" that is a well-known hurdle in a number of scientific fields. Furthermore, typical plume inversion algorithms may require longer averaging time than the economics of mobile solutions would support. Some quantification results were sufficiently correlated with actual leak sizes that the resulting size estimates might be useful in a simple 3-class binning approach (i.e., small/medium/large to prioritize leak fixes). **Table 2** estimates the accuracy of quantification using two metrics – one, fraction of tests where measured emissions rates are between 0.5x and 2x of the actual emission rate, and two, fraction of tests where measured emission rates are within

an order of magnitude (0.1 – 10x) of the actual emission rate. Only Ball Aerospace estimated leaks within 0.5 – 2x of the actual leak rate in more than 50% of the tests. The overall performance on this metric ranged from a low of 18% to a high of 53%. This performance improves when considering an order of magnitude accuracy level – 8 of the 9 technologies estimated leak sizes to within an order of magnitude of the actual leak rate in at least 74% of test scenarios. In particular, Seek Ops, Heath Technologies Inc., and Picarro Inc. achieved an order of magnitude accuracy in 100%, 95%, and 92% of test scenarios, respectively. In general, the Pearson's coefficient (ρ) was larger than the linear regression coefficient (R^2), indicating that technologies are better at quantifying larger leaks compared to smaller leaks. Finally, the importance of quantification also depends on the application – rapid detection of large emissions sources for effective methane mitigation might not require accurate quantification.

Performance of the technologies are affected not only by inherent sensor capabilities but also factors such as environmental conditions, survey protocol, and facility characteristics. For example, technologies that use a suspended sample inlet (Advisian) or a tethered sample tube (Picarro Inc.) might face additional challenges in the presence of nearby power lines or taller equipment. An important source of error, given our test configuration, is inter-pad interference from wind-borne dispersion of leaks. To account for this, we analyzed the performance of teams tested at METEC under two scenarios – weak and strong interference (see S.I. section 5 and 6). These two analyses sought to discard test results based on a set of criteria established to identify potential interference issues in leak detection. We found that under both weak and strong interference scenarios, the fraction of tests correctly identified (TPs and TNs) were not statistically different from base-case scenario where all tests were included. This suggests that whatever differences in performance that were observed between the teams did not arise from inter-pad interference.

Some technologies would be well served by re-testing at higher leak rates (>10 scfh). The combined testing format followed here requires supplying a range of leak sizes to satisfy multiple technologies at the same time. More detailed one-on-one testing could allow improved analysis of minimum detection rates and effectiveness. For example, BHGE performed well in the class of leaks >8 scfh and could be re-tested with more samples in that regime. This is especially important considering that a recent study of emissions in the Marcellus shale found that the average emission rate at the pad-level was 5.5 kg/h, corresponding to ~350 scfh (Caulton, et al., 2019). However, these are pad-level estimates, and component-level emissions can be significantly smaller – testing at the METEC facility between 0–15 scfh therefore provides a reasonable test of performance for technologies that detect emissions component-level detection. Conversely, testing at the Sacramento test location with emission rates in the 0–1500 scfh is well suited for technologies that detect aggregated pad-level emissions.

While no single technology can satisfy all the requirements for leak detection and quantification across the

natural gas supply chain, the results demonstrated here provide regulators and the industry with a range of options. There are technologies with strengths in survey speed that are suitable for leak detection along inter-state transmission pipelines, while technologies with high pad-level (but not equipment-level) detection effectiveness indicate potential use as a screening-technology to cover large areas. With potential improvements to algorithms that transform raw concentration data into actionable information, these technologies could become prominent tools to mitigate methane emissions.

A number of practicalities emerged in 3 weeks of testing that are relevant to any attempt to extrapolate these results to field conditions. First: drone technologies tested in this study are still immature, resulting in labor intensity, frequent battery recharge requirements, grounding due to winds, and substantial ground crew effort. Ground-based systems like the truck-mounted Heath and Aeris technologies experienced few of these issues and so have practical advantages that are not represented in above tables. At the same time, drone-based systems can be effective in quantifying emissions from taller equipment and during calm atmospheric conditions where plumes do not disperse but accumulate around the leak source – these conditions pose difficulty for truck-based systems where the plume lofts into the atmosphere and do not intersect the truck-based sensor. Second, drone-based technologies required accommodations that may be difficult to implement in real-world surveys: Advisian and Picarro dangled sample tubes from drones that has the potential to get tangled with equipment or nearby power lines, while SeekOps had a ground technician dedicated to traffic management and avoiding collisions due to the low-flying technique. The employed deployment methods may cause practical difficulties in labor cost and survey time with usage of the technology but will hopefully be solved by technology development.

Even as this study provides the first controlled and independent verification of the performance of mobile leak detection technologies, this is only one step in the road to demonstrating that these technologies will provide emissions reductions that are equivalent to traditional OGI-based methods. Demonstrating equivalence with OGI will require more testing and assessing the performance of these technologies under specific survey protocols (Ravikumar, & Brandt, 2017). Whether the emissions reductions from monthly truck-based screening surveys, for example, are equivalent to emissions reductions from semi-annual OGI-based LDAR survey can be answered through a statistical simulations (for example, using the FEAST simulation platform) (Kemp, Ravikumar, & Brandt, 2016) as well as pilot testing these technologies at oil and gas facilities with co-occurring OGI studies (Fox, et al., 2019). Clearly, the next frontier in mobile methane emissions mitigation is to develop standardized protocols to demonstrate technology equivalence for use across large geographic areas.

It is critical to remember that these results apply to the technologies that are in active development. Many of the systems tested here have undergone changes to both hardware and software since they were tested for this

study. It is a rapidly evolving field and stakeholders should always look for the most recent data to make decisions on deployment and regulatory acceptance.

Supplemental files

The supplemental files for this article can be found as follows:

- **Text S1.** Single-blind inter-comparison of methane detection technologies – Results from the Stanford/EDF mobile monitoring challenge. DOI: <https://doi.org/10.1525/elementa.373.s1>
- **Section 1.** Selection process.
- **Section 2.** Test locations and site configurations.
- **Section 3.** Test protocols.
- **Section 4.** Results from the University of Calgary drone system.
- **Section 5.** Interference analysis: methods.
- **Section 6.** Interference analysis: results.
- **Appendix A.** Stanford/EDF Mobile Monitoring Challenge Application Form. DOI: <https://doi.org/10.1525/elementa.373.s2>
- **Data S1.** MMCRResults_Heath. DOI: <https://doi.org/10.1525/elementa.373.s3>
- **Data S2.** MMCRResults_Picarro. DOI: <https://doi.org/10.1525/elementa.373.s4>
- **Data S3.** MMCRResults_ABB_ULC. DOI: <https://doi.org/10.1525/elementa.373.s5>
- **Data S4.** MMCRResults_Advisian. DOI: <https://doi.org/10.1525/elementa.373.s6>
- **Data S5.** MMCRResults_Aeris. DOI: <https://doi.org/10.1525/elementa.373.s7>
- **Data S6.** MMCRResults_BHGE. DOI: <https://doi.org/10.1525/elementa.373.s8>
- **Data S7.** MMCRResults_SeekOps. DOI: <https://doi.org/10.1525/elementa.373.s9>
- **Data S8.** MMCRResults_BallAerospace. DOI: <https://doi.org/10.1525/elementa.373.s10>
- **Data S9.** MMCRResults_UofCTruck. DOI: <https://doi.org/10.1525/elementa.373.s11>
- **Data S10.** MMCRResults_UofCDrone. DOI: <https://doi.org/10.1525/elementa.373.s12>
- **Data S11.** MMC_WeakInterferenceAnalysis. DOI: <https://doi.org/10.1525/elementa.373.s13>
- **Data S12.** MMC_StrongInterferenceAnalysis. DOI: <https://doi.org/10.1525/elementa.373.s14>

Acknowledgements

We appreciate Mike McGuire (formerly with Colorado State University) for his assistance with conducting the field tests at METEC. We also thank the members of the industry advisory board for providing valuable insight on the needs of leak detection at oil and gas facilities, as well as helping the scientific team to understand the commercial viability of the applicants. The industry advisory board included experts from Exxon-Mobil, Schlumberger, Noble Energy, Shell, Equinor, and PG&E. A.P.R. would especially like to thank Nuance Chocolate Inc. (Fort Collins, CO) and the Fat Tire Brewing Company for providing much needed respite after long days in the field.

Funding information

The authors acknowledge funding from the Stanford Natural Gas Initiative and the Environmental Defense Fund.

Competing interests

The authors have no competing interests to declare.

Author contributions

- Substantial contributions to conception and design: APR, ARB
- Acquisition of data: APR, SS, JW, JE, DR, CB
- Analysis and interpretation of data: APR, ARB, SS, DL, DZ, IM, BR
- Drafting the article or revising it critically for important intellectual content: APR, ARB, SS, DZ, IM, BR
- Final approval of the version to be published: All authors

References

- Alvarez, RA, Zavala-Araiza, D, Lyon, DR, Allen, DT, Barkley, ZR, Brandt, AR, Davis, KJ, Herndon, SC, Jacob, DJ, Karion, A, Kort, EA, Lamb, BK, Lauvaux, T, Maasakkers, JD, Marchese, AJ, Omara, M, Pacala, SW, Peischl, J, Robinson, AL, Shepson, PB, Sweeney, C, Townsend-Small, A, Wofsy, SC and Hamburg, SP. 2018. Assessment of methane emissions from the U.S. oil and gas supply chain. *Science* **361**: 186–188. DOI: <https://doi.org/10.1126/science.aar7204>
- Atherton, E, Risk, D, Fougere, C, Lavoie, M, Marshall, A, Werring, J, Williams, JP and Minions, C. 2017. Mobile measurements of methane emissions from natural gas developments in northeastern British Columbia, Canada. *Atmos. Chem. Phys.* **17**: 12405–12420. DOI: <https://doi.org/10.5194/acp-17-12405-2017>
- Barchyn, T, Hugenholtz, C, Myshak, C and Bauer, J. 2017. A UAV-based system for detecting natural gas leaks. *J. Unmanned Vehicle Systems* **6**: 18–30. DOI: <https://doi.org/10.1139/juvs-2017-0018>
- Brandt, A, Heath, G and Cooley, D. 2016. Methane leaks from natural gas systems follow extreme distributions. *Environ. Sci. Technol.* **50**: 12512–12520. DOI: <https://doi.org/10.1021/acs.est.6b04303>
- Caulton, DR, Lu, JM, Lane, HM, Buchholz, B, Fitts, JP, Golston, LM, Guo, X, Li, Q, McSpiritt, J, Pan, D, Wendt, L, Bou-Zeid, E and Zondlo, MA. 2019. Importance of superemitter natural gas well pads in the Marcellus shale. *Environmental Science & Technology* **53**(9): 4747–4754. DOI: <https://doi.org/10.1021/acs.est.8b06965>
- Colorado Department of Public Health and Environment. 2014. Regulation Number 7: Control of Ozone via Ozone Precursors and Control of Hydrocarbons via Oil and Gas Emissions. 5 CCR 1001-9. Denver.
- Conley, S, Franco, G, Faloona, I, Blake, DR, Peischl, J and Ryerson, TB. 2016. Methane emissions from the 2015 Aliso Canyon blowout in Los Angeles, CA. *Science*. DOI: <https://doi.org/10.1126/science.aaf2348>

- Englander, J, Brandt, A, Conley, S, Lyon, D and Jackson, R. 2018. Aerial Interyear Comparison and Quantification of Methane Emissions Persistence in the Bakken Formation of North Dakota, USA. *Environ. Sci. Technol.* **52**: 8947–8953. DOI: <https://doi.org/10.1021/acs.est.8b01665>
- Environment and Climate Change Canada. 2018. Regulations Respecting Reduction in the Release of Methane and Certain Volatile Organic Compounds (Upstream Oil and Gas Sector). SOR, 2018-66.
- Etminan, M, Myhre, G, Highwood, E and Shine, K. 2016. Radiative forcing of carbon dioxide, methane and nitrous oxide: A significant revision of the methane radiative forcing. *Geophys. Res. Lett.* **43**: 12614–12623. DOI: <https://doi.org/10.1002/2016GL071930>
- Fox, T, Barchyn, T, Risk, D, Ravikumar, A and Hugenholtz, C. 2019. A review of close-range and screening technologies for mitigating fugitive methane emissions in upstream oil and gas. *Environmental Research Letters* **14**(5): 053002. DOI: <https://doi.org/10.1088/1748-9326/ab0cc3>
- Fox, TA, Ravikumar, AP, Hugenholtz, CH, Zimmerle, D, Barchyn, TE, Johnson, MR, Lyon, D and Taylor, T. 2019. A methane emissions reduction equivalence framework for alternative leak detection and repair programs. *Elem. Sci. Anth.* **7**(1): 30. DOI: <https://doi.org/10.1525/elementa.369>
- Frankenberg, C, Thorpe, AK, Thompson, DR, Hulley, G, Kort, EA, Vance, N, Borchardt, J, Krings, T, Gerilowski, K, Sweeney, C, Conley, S, Bue, BD, Aubrey, AD, Hook, S and Green, RO. 2016. Airborne methane remote measurements reveal heavy-tail flux distribution in Four Corners region. *Proc. Natl. Acad. Sciences*. DOI: <https://doi.org/10.1073/pnas.1605617113>
- Golston, LM, Aubut, NF, Frish, MB, Yang, S, Talbot, RW, Gretencord, C, McSpirt, J and Zondlo, MA. 2018. Natural gas fugitive leak detection using an unmanned aerial vehicle: localization and quantification of emission rate. *Atmosphere* **9**(9): 333. DOI: <https://doi.org/10.3390/atmos9090333>
- Intergovernmental Panel on Climate Change. 2018. *Global Warming of 1.5 C*. New York, NY: United Nations.
- Jacob, DJ, Turner, AJ, Maasakkers, JD, Sheng, J, Sun, K, Liu, X, Chance, K, Aben, I, McKeever, J and Frankenberg, C. 2016. Satellite observations of atmospheric methane and their value for quantifying methane emissions. *Atmos. Chem. Phys.* **16**: 14371–14396. DOI: <https://doi.org/10.5194/acp-16-14371-2016>
- Johnson, MR, Tyner, DR, Conley, S, Schwietzke, S and Zavala-Araiza, D. 2017. Comparisons of Airborne Measurements and Inventory Estimates of Methane Emissions in the Alberta Upstream Oil and Gas Sector. *Environ. Sci. Tech.* **51**: 13008–13017. DOI: <https://doi.org/10.1021/acs.est.7b03525>
- Keating Research Inc. 2016. *The Colorado case study on methane emissions: conversations with the oil and gas industry*. Telluride, CO.
- Kemp, C, Ravikumar, A and Brandt, A. 2016. Comparing natural gas leakage detection technologies using an open-source virtual gas field simulator. *Environ. Sci. Technol.* **50**: 104–115. DOI: <https://doi.org/10.1021/acs.est.5b06068>
- Lyon, D, Alvarez, R, Zavala-Araiza, D, Brandt, A, Jackson, R and Hamburg, S. 2016. Aerial surveys of elevated hydrocarbon emissions from oil and gas production sites. *Environ. Sci. Technol.* **50**: 4877–4886. DOI: <https://doi.org/10.1021/acs.est.6b00705>
- Maric, I. 2005. The Joule-Thomson effect in natural gas flow-rate measurements. *Flow Meas. Instrum.* **16**: 387–395. DOI: <https://doi.org/10.1016/j.flowmeasinst.2005.04.006>
- Myhre, G, Shindell, D, Breon, F, Collins, W, Fuglestad, J, Huang, J, Koch, D, Lamarque, J, Lee, D, Mendoza, B, Nakajima, T, Robock, A, Stephens, G, Takemura, T, Zhang, H, Aamaas, B, Boucher, O, Dalsoren, SB, Daniel, JS, Forster, P, Granier, C, Haigh, J, Hodnebrog, O, Kaplan, JO, Marston, G, Nielsen, CJ, O'Neill, BC, Peters, GP, Pongratz, J, Prather, M, Ramaswamy, V, Raphael, R, Rotstayn, L, Smith, SJ, Stevenson, D, Vernier, J, Wild, O and Young, P. 2013. Anthropogenic and Natural Radiative Forcing. In *Climate Change 2013: The Physical Science Basis. Contribution of Working Group I to the Fifth Assessment Report of the Intergovernmental Panel on Climate Change*, 1–44. New York: Cambridge University Press.
- Nathan, BJ, Golston, LM, O'Brien, AS, Ross, K, Harrison, WA, Tao, L, Lary, DJ, Johnson, DR, Covington, AN, Clark, NN and Zondlo, MA. 2015. Near-field characterization of methane emission variability from a compressor station using a model aircraft. *Environmental Science & Technology* **49**(13): 7896–7903. DOI: <https://doi.org/10.1021/acs.est.5b00705>
- Ravikumar, A and Brandt, A. 2017. Designing better methane mitigation policies: the challenge of distributed small sources in the natural gas sector. *Env. Res. Lett.* **12**: 040023. DOI: <https://doi.org/10.1088/1748-9326/aa6791>
- Ravikumar, A, Wang, J and Brandt, A. 2017. Are optical gas imaging techniques effective for methane leak detection? *Environ. Sci. Technol.* **51**: 718–724. DOI: <https://doi.org/10.1021/acs.est.6b03906>
- Ravikumar, A, Wang, J, McGuire, M, Bell, C, Zimmerle, D and Brandt, A. 2018. “Good versus Good Enough?” Empirical Tests of Methane Leak Detection Sensitivity of a Commercial Infrared Camera. *Environ. Sci. Technol.* **52**: 2368–2374. DOI: <https://doi.org/10.1021/acs.est.7b04945>
- Southwest Research Institute. 2015. *Testing of methane detection systems – Phase 2*. Washington, DC: Environmental Defense Fund.
- Turner, A, Frankenberg, C, Wennberg, P and Jacob, D. 2017. Ambiguity in the causes for decadal trends in atmospheric methane and hydroxyl. *Proc. Natl. Acad. Sciences* **114**: 5367–5372. DOI: <https://doi.org/10.1073/pnas.1616020114>

- U.S. Advanced Research Projects Agency (ARPA-E).** 2014. *Methane Observation Networks with Innovative Technology to Obtain Reductions*. Washington, DC.
- Yuan, B, Kaser, L, Karl, T, Graus, M, Peischl, J, Campos, TL, Shertz, S, Apel, EC, Hornbrook, RS, Hills, A, Gilman, JB, Lerner, BM, Warneke, C, Flocke, FM, Ryerson, TB, Guenther, AB and de Gouw, JA.** 2015. Airborne flux measurements of methane and volatile organic compounds over the Haynesville and Marcellus shale gas production regions. *J. Geophys. Res. Atmos.* **120**: 6271–6289. DOI: <https://doi.org/10.1002/2015JD023242>
- Zavala-Araiza, D, Alvarez, RA, Lyon, DR, Allen, DT, Marchese, AJ, Zimmerle, DJ and Hamburg, SP.** 2017. Super-emitters in natural gas infrastructure are caused by abnormal process conditions. *Nature Communications* **8**: 1–10. DOI: <https://doi.org/10.1038/ncomms14012>
- Zickfeld, K, Solomon, S and Gilford, D.** 2017. Centuries of thermal sea-level rise due to anthropogenic emissions of short-lived greenhouse gases. *Proc. Natl. Acad. Sciences* **114**: 657–662. DOI: <https://doi.org/10.1073/pnas.1612066114>

How to cite this article: Ravikumar, AP, Sreedhara, S, Wang, J, Englander, J, Roda-Stuart, D, Bell, C, Zimmerle, D, Lyon, D, Mogstad, I, Ratner, B and Brandt, AR. 2019. Single-blind inter-comparison of methane detection technologies – results from the Stanford/EDF Mobile Monitoring Challenge. *Elem Sci Anth*, 7: 37. DOI: <https://doi.org/10.1525/elementa.373>

Domain Editor-in-Chief: Detlev Helmig, Institute of Alpine and Arctic Research, University of Colorado Boulder, US

Guest Editor: Brian Lamb, Washington State University, US

Knowledge Domain: Atmospheric Science

Part of an *Elementa* Forum: Oil and Natural Gas Development: Air Quality, Climate Science, and Policy

Submitted: 16 April 2019 **Accepted:** 19 August 2019 **Published:** 10 September 2019

Copyright: © 2019 The Author(s). This is an open-access article distributed under the terms of the Creative Commons Attribution 4.0 International License (CC-BY 4.0), which permits unrestricted use, distribution, and reproduction in any medium, provided the original author and source are credited. See <http://creativecommons.org/licenses/by/4.0/>



Elem Sci Anth is a peer-reviewed open access journal published by University of California Press.

OPEN ACCESS

Exhibit 35

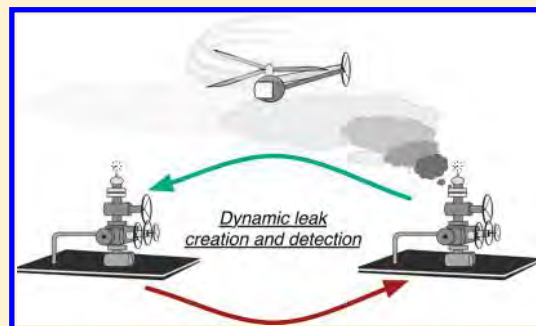
Comparing Natural Gas Leakage Detection Technologies Using an Open-Source “Virtual Gas Field” Simulator

Chandler E. Kemp, Arvind P. Ravikumar, and Adam R. Brandt*

Department of Energy Resources Engineering, Stanford University, 367 Panama Street, Stanford, California 94305, United States

S Supporting Information

ABSTRACT: We present a tool for modeling the performance of methane leak detection and repair programs that can be used to evaluate the effectiveness of detection technologies and proposed mitigation policies. The tool uses a two-state Markov model to simulate the evolution of methane leakage from an artificial natural gas field. Leaks are created stochastically, drawing from the current understanding of the frequency and size distributions at production facilities. Various leak detection and repair programs can be simulated to determine the rate at which each would identify and repair leaks. Integrating the methane leakage over time enables a meaningful comparison between technologies, using both economic and environmental metrics. We simulate four existing or proposed detection technologies: flame ionization detection, manual infrared camera, automated infrared drone, and distributed detectors. Comparing these four technologies, we found that over 80% of simulated leakage could be mitigated with a positive net present value, although the maximum benefit is realized by selectively targeting larger leaks. Our results show that low-cost leak detection programs can rely on high-cost technology, as long as it is applied in a way that allows for rapid detection of large leaks. Any strategy to reduce leakage should require a careful consideration of the differences between low-cost technologies and low-cost programs.



INTRODUCTION

Fugitive methane (CH_4) emissions from the natural gas system are an important source of anthropogenic greenhouse gases (GHGs),¹ representing $\approx 25\%$ of U.S. CH_4 emissions. In extreme cases, fugitive emissions could offset the climate benefits of switching from other fossil fuels to natural gas.^{2,3} Leak detection and repair (LDAR) programs aim to reduce fugitive CH_4 emissions while providing additional revenue to natural gas producers from the sale of recovered gas. LDAR is an area of active research, and many proposed LDAR concepts rely heavily on new technologies, including constant monitoring of gas wells with high-precision methane sensors,^{4,5} automated surveys of natural gas fields based on infrared (IR) camera technology,⁶ or remote sensing of methane plumes using aircraft or satellites.^{7,8}

While many LDAR concepts and technologies have been studied in the literature, less work has been performed to rigorously compare different proposed LDAR programs regarding their effectiveness. For example, which LDAR technology has the most potential to reduce the cost of CH_4 mitigation, or how important is labor minimization in driving cost reductions from a new LDAR concept? Rigorously comparing proposed LDAR programs requires a model of leakage from a gas facility as well as a model of how a LDAR program would detect any given leak. Such a model must be able to accurately simulate the evolution of leakage through time under various proposed and implemented LDAR programs. This model must also include all major costs of

LDAR programs, such as labor and technology costs. Because no such model currently exists, we developed the Fugitive Emissions Abatement Simulation Toolkit (FEAST) model to explore the effect of various LDAR programs on long-term leakage rates.

In FEAST, CH_4 leaks in a computer-simulated gas field are generated dynamically as the simulation proceeds. Dependent upon the LDAR program under study, the repair rate is calculated using a physics-based model: the concentration of methane downwind of every leak is simulated using a Gaussian plume model, and the specifications of a particular LDAR program are applied to the simulated plume to determine whether or not it is detected. LDAR programs in FEAST are represented by a combination of technology parameters (e.g., survey sensitivity) and implementation parameters (e.g., survey frequency). Given a LDAR program, FEAST finds and fixes leaks appropriately. Integrating the leakage rate through time yields the total amount of lost gas under a particular LDAR program. From assignment of a value to the lost gas and estimation of the cost of maintaining the LDAR program, FEAST estimates the economic value of the LDAR program in net present value (NPV) terms and LDAR program environmental benefits.

Received: December 11, 2015

Revised: March 23, 2016

Accepted: March 23, 2016

Published: March 23, 2016

In this paper, FEAST is applied to four conceptual LDAR programs. We first describe the FEAST methodology and LDAR program representations. We then compare our simplified LDAR programs to illustrate their strengths, weaknesses, potential for improvement, and relative value. We conclude with a description of future directions for research.

METHODOLOGY

FEAST is an open-source model programmed in the MATLAB computing environment.⁹ FEAST model code and documentation are made open source as the [Supporting Information](#) and, thus, can be downloaded and used as desired by the reader.

Markov Model. FEAST simulates leakage from a natural gas field by modeling every potential leaking component in the field using a two-state Markov process: a component may either be in the “leaking” state or in the “robust” state. The simulation time period is broken into discrete time steps, and every component, whether leaking or not, is given a probability of changing state in a given time step. This probability depends upon the LDAR program being simulated and the behavior of the natural gas infrastructure. Note that Markov processes (by definition) do not depend upon behavior history, while in reality, there is some evidence that the probability of leakage from a component depends upon its type and age.^{10–13} This is considered further in the [Results and Discussion](#). With more experimental and statistical data, future versions of FEAST could be implemented using higher order Markov chains.

The FEAST Markov model is implemented in three basic steps: gas field initialization, dynamic simulation, and results storage (see [Figure 1](#)).

Gas Field Initialization. The initial condition is defined by the number and size of leaks distributed throughout the natural gas field as well as physical characteristics of the gas field that affect the performance of LDAR programs. Physical characteristics include distance between wells, number of potentially leaking components per well, and area at each wellsite that must be searched for leaks.

Several publicly available data sets exist that characterize the leakage from existing gas fields ([Table 1](#)). As shown in [Table 1](#), the Fort Worth air quality study¹⁴ (henceforth FWAQS) offers the largest sample of leaks that is publicly available. We calculate the average number of leaks per well found in the FWAQS (≈ 6) and apply a truncated normal distribution about this average, approximated to the nearest integer, to initialize leaks in FEAST. FEAST then randomly draws the size of each leak from the leaks found in the FWAQS, which have a heavy-tailed size distribution (i.e., log-normal like; large leaks are proportionally more impactful than would be expected in a simple Gaussian size distribution). The result is a randomly generated set of leaks that is statistically similar to the empirical FWAQS data. FEAST can also use other leak size distributions, provided information from a user. It should be emphasized here that there is growing evidence^{15,16} of highly skewed leak size distribution in the natural gas infrastructure. The leak sizes used in this model, derived from the FWAQS, represent one such heavy-tailed distribution.

The distance between wells, number of components per well, and other physical features were chosen to be within the range of values found for U.S. natural gas fields (see [Table S3.1](#) and [section S3.2.2](#) of the [Supporting Information](#)).

Atmospheric Conditions. The performance of LDAR programs depends upon the environmental conditions surrounding the gas field, such as the wind speed and

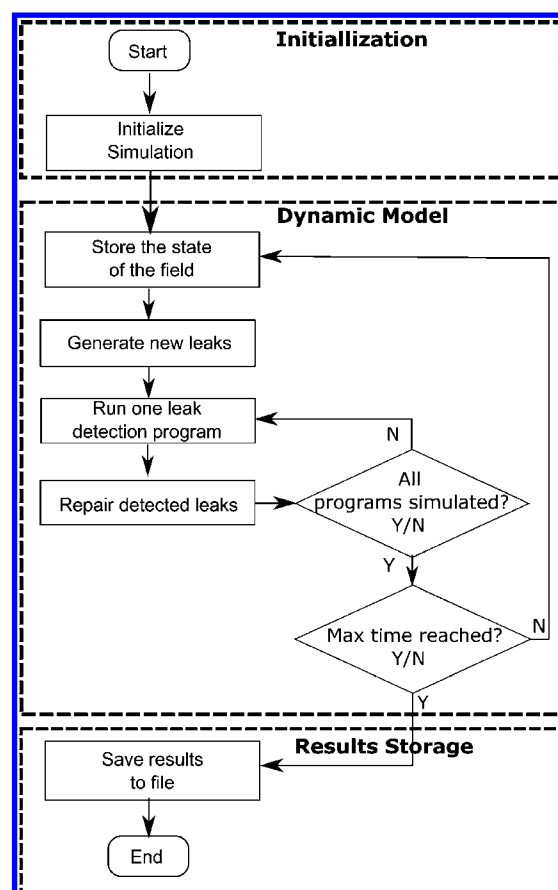


Figure 1. Flowchart of the FEAST model structure.

atmospheric stability. The wind speed is chosen from an empirical distribution suggested by the Advanced Research Projects Agency-Energy (ARPA-E) in the recent Methane Observation Networks with Innovative Technology to Obtain Reductions (MONITOR) challenge.⁴ For each time step, one wind speed is selected from this data set at random. The wind direction is chosen from a second empirical wind data set collected at Fort Worth.²¹ Once the wind speed has been selected, the stability class is chosen at random with equal probability from the realistic classes associated with that wind speed.²² See [section S3.3](#) of the [Supporting Information](#) for more details. In the absence of site-specific information, the ARPA-E wind speed distribution can be used as a template wind profile near production facilities. Users of this model can input appropriate data sets specific to the infrastructure being studied. It should be noted that meteorological conditions, such as atmospheric conditions, time of day, etc., can play a significant role in detection capability for different technologies. While these can be included in the technology modeling, the results presented in this paper assume daytime operation for all technologies.

Dynamic Simulation. At each time step, a small fraction of components in the robust state are changed to the leaking state to emulate a non-zero leak production rate. No published studies were found that directly estimate the leak production rate; however, it is possible to use two existing studies to estimate the rate of leak generation.

First, the Carbon Limits data set¹⁷ (henceforth CL) provides one means for estimating the leak production rate. CL reports data from thousands of wells, suggesting that, within the first

Table 1. Summary of Results from Leakage Studies of Natural Gas Production Facilities

name	year	detection method	number of wells	number of leaks	leaks per well
Carbon Limits ^{17 a}	2014	IR ^b camera	≈5300	NR	NR
Fort Worth ^{14 c}	2011	FID ^d /IR camera	1138	2126 ^e	≈2
Allen et al. ¹⁸	2013	IR camera	292	769	≈2.6
Kuo ¹⁹	2012	spectroscopy	172	59	≈0.3
API 4589 ²⁰	1993	FID	82	1513	≈18
Fernandez ¹¹	2006	bubble test	12	132	11

^aCarbon Limits reported the number of well sites and well batteries surveyed. We estimate the number of wells by assuming an average of three wells per survey in the well sites and well batteries category. There were 39 505 leaks recorded in all facilities. ^bIR = infrared. ^cAll components were surveyed with an IR camera. A total of 10% were also surveyed with a FID. ^dFID = flame ionization detector. ^eData on the number of wells and leaks can be found in the Government of Fort Worth, TX website <http://fortworthtexas.gov/gaswells/air-quality-study/final>. Site-specific data can be found in Appendix 3-B: Emissions calculations workbook of the Fort Worth, TX Air Quality Study.¹⁴

year after a leak survey is completed, the average natural gas well battery emits 1.8 tons of volatile organic compounds (tVOC). The associated methane leak creation rate is calculated on the basis of the following four assumptions: (1) Leakage that persists after the LDAR survey is negligible (i.e., leaks that are found in a LDAR survey are fixed). (2) The rate of leakage increases linearly throughout the year. (3) CH₄ and volatile organic compounds (VOCs) mole fractions are consistent with the average values reported by technical documents.²⁰ (4) The number of leaks repaired between LDAR surveys is negligible.

Using these assumptions, we derive eq 1 for the leak creation rate, where E_{VOC} is the estimated total VOC emissions between surveys, Δt is the length of time between surveys (1 year, in this case), and $m_{\text{CH}_4}/m_{\text{VOC}}$ is the mass ratio of CH₄ emissions to VOC emissions (see section SA.2 of the Supporting Information for the method used to estimate $m_{\text{CH}_4}/m_{\text{VOC}}$). According to eq 1, the CL data suggest a leak creation rate of 3.8×10^{-4} g of CH₄/s per well per day.

$$R_l = \frac{2E_{\text{VOC}}}{\Delta t^2} \frac{m_{\text{CH}_4}}{m_{\text{VOC}}} \quad (1)$$

Alternatively, FWAQS data¹⁴ can be used to estimate the leak production rate. On the basis of the assumption that the rate of leakage increased linearly from zero when the facility was first built, the leak creation rate in the Barnett shale region can be estimated by dividing the total leakage rate in the FWAQS study by the average age of gas wells. This gives a leak production rate of 1.8×10^{-4} g/s per well per day or ≈50% of the CL value. FEAST defaults to the average value of 2.6×10^{-4} g/s per well per day. There are many possible explanations for the discrepancy between the two results reported above, including different types of infrastructure, different facility age, different regulations, or different management practices in the two regions studied. As noted below, more work is needed to generate better estimates of the leak detection rate. To compensate for the lack of reliable data on leak production rates across the U.S. infrastructure, we have used a range from 1.8×10^{-4} to 3.8×10^{-4} g/s per well per day in the sensitivity analysis. Because the model is open-source, these values could be replaced with a more representative generation rate for a particular set of gas wells.

The probability of a component switching from the robust to the leaking state during a time step of duration δt is given by eq 2, where R_l is the leakage creation rate (g/s per well per day), $N_{c/w}$ is the number of components per well, and μ_1 is the average leak size (g/s).

$$P_{R,L} = \frac{R_l}{N_{c/w}\mu_1} \delta t \quad (2)$$

At each time step every robust component is given the probability $P_{R,L}$ to begin leaking. Components that begin leaking have leakage rates drawn from FWAQS empirical data, as during initialization.

Choosing a $P_{R,L}$ that is constant through time implies that the quality of gas infrastructure and maintenance does not change during the simulation. It does not imply that the leakage increases linearly through time. On the contrary, the stochastic nature of FEAST allows for a different number of leaks to be introduced at every time step and the size of each created leak is chosen randomly, independent of $P_{R,L}$. Super-emitters are extremely large but rare leaks in the FWAQS, and their frequency in FEAST follows the FWAQS distribution. When FEAST happens to generate a super-emitter, a significant discontinuity occurs in the total field leakage, just as the total leakage from a real gas field suddenly increases if a tank hatch cover is accidentally left open. Over sufficiently long time scales, these discontinuities can be averaged out and the total leakage will increase approximately linearly if $P_{R,L}$ is constant (and repairs are neglected). A small modification to the Markov model can allow for a variable $P_{R,L}$ if a change in the leak production rate is expected. We explore one such scenario in the Results and Discussion.

LDAR Programs. A LDAR program in FEAST includes the combination of an applied LDAR technology and a LDAR implementation. Technology parameters include factors such as detector costs and sensitivities, while implementation parameters include factors such as frequency of surveys or repair practices. The probability that a leaking component switches to the robust state ($P_{L,R}$) in a given time step requires a model of the LDAR program being evaluated. By definition

$$P_{L,R} = P_{L,R}^{\text{null}} + P_{L,R}^{\text{LDAR}} \quad (3)$$

By default, all LDAR simulations include a “null LDAR program”, which contributes $P_{L,R}^{\text{null}}$ to the probability of detecting a leak. In the scenarios below, $P_{L,R}^{\text{null}} N_L^i = P_{R,L} N_R^i$, where N_L^i and N_R^i are the initial number of leaking and robust components, respectively. That is, the background rate of leak creation multiplied by the number of robust components equals the rate of leak detection multiplied by the number of leaking components without LDAR, and therefore, the number of leaks is in steady state over long-time Markov simulation. Adding a LDAR program on top of the null program increases the value of $P_{L,R}$ by adding additional probability of finding and fixing leaks $P_{L,R}^{\text{LDAR}}$, such that a new, lower steady-state leakage

Table 2. Notable Parameter Settings in the Base Case and Extreme Sensitivity Cases^a

symbol	name	units	base case	high savings	low savings
Markov Model					
R_l	leak production rate	g/s per well per day	2.6×10^{-4}	5.2×10^{-4}	1.3×10^{-4}
	leak size data source		FWAQS ¹⁴		Allen ¹⁸
C_g	gas price	\$/mcf	5	8	3
R_{RD}	real discount rate	% per year	8	5	10
A	aging factor		1	2	
FID					
C_{cap}	total capital	\$	35000	20000	50000
λ	lifetime	years	10	20	5
R_S	survey speed	components/hour	150	300	75
T_{SI}	survey interval	days	100	200	50
T_{SU}	setup time	hours	0.5		
DD					
$C_{detector}$	cost per detector	\$	500	200	1000
$N_{s/W}$	detectors per well		4	2	8
T_{LI}	repair interval	days	50	25	100
T_{setup}	setup time	hours	0.5		
Φ_{min}	minimum concentration	g/m ³	10^{-2}	10^{-3}	10^{-1}
MIR					
C_{cap}	capital cost	\$	120000	60000	240000
λ	lifetime	years	10	5	20
R_S	survey speed	components/hour	500	1000	250
Γ_{min}	minimum concentration path	m-g/m ³	0.4	0.2	2
$F_{PD,min}$	minimum fraction of pixels above Γ_{min} for detection	%	10	20	5
T_{SI}	survey interval	days	100	200	50
T_{SU}	setup time	hours	0.5		
AIR					
C_{cap}	total capital cost	\$	193000	100000	300000
$F_{PD,min}$	minimum fraction of pixels above Γ_{min} for detection	%	10	5	20
Γ_{min}	minimum concentration path	m-g/m ³	0.4	0.2	2
T_{SI}	survey interval	days	14	7	28
v_S	survey speed	m/s	5	10	2.5
Z_{cam}	camera height	m	20	10	40
λ	lifetime	years	3	6	1.5

^aSee the Supporting Information for a complete list of Markov model and LDAR program specifications.

rate is reached. Changing the settings of the null program allows the user to explore scenarios in which the background prevalence of leaks increases as the facility ages (i.e., $P_{L,R}^{null}N_L^i < P_{R,L}N_R^j$).

Four simplified example LDAR programs are simulated here. These LDAR programs include the following: (1) Flame ionization detector (FID): Manual application of a flame ionization detector technology, after which components with a local CH₄ concentration above a threshold are replaced. The FID technology is the “default” first pass detection technology used in many historical studies. (2) Distributed detector (DD): Methane detectors are placed at intervals along the dominant downwind direction characteristic of the location and alert repair crews when local concentrations at a detector exceed a threshold detection limit. After leaks are detected, repairs are performed at a set repair interval. (3) Manual infrared (MIR): A manual infrared imaging method, wherein an operator uses an IR camera to visualize methane plumes and tags components to be fixed. A manual IR technique is another very commonly applied LDAR method. (4) Automated infrared (AIR): An automated infrared technique where an IR-equipped aircraft flies over natural gas sites and detects leaks from their IR signature. After leaks are detected, images of each leak are sent to repair crews to facilitate repair.

The most important parameters for each LDAR program are given in Table 2. See Tables S3.5–S3.8 of the Supporting Information for full details of LDAR parameters and default settings for each LDAR program.

In the FID survey method, all leaks are found and repaired at each time step when a survey occurs. Therefore, $P_{L,R}^{LDAR} = 0$ at all time steps, except at the time step of a survey when $P_{L,R}^{LDAR} = 1$. Such a detection certainty is justified because the underlying data set used in FEAST was obtained using a FID-based leak detection program.

FEAST uses a Gaussian plume model to compute $P_{L,R}^{LDAR}$ for the DD, MIR, and AIR programs. Such a model accounts for the buoyancy of emitted gas and reflection of the plume off the ground. The effect of an atmospheric inversion is not considered because we are interested in the behavior of plumes within a few tens of meters of the ground. The concentration Φ (g/m³) downwind of the plume is given by

$$\Phi = \frac{Q}{2\pi\sigma_y(x)\sigma_z(x)} \exp\left(-\frac{(y-y_0)^2}{2\sigma_y^2(x)}\right) \left[\exp\left(-\frac{(z-z_M(x))^2}{2\sigma_z^2(x)}\right) + \exp\left(-\frac{(z+z_M(x))^2}{2\sigma_z^2(x)}\right) \right] \quad (4)$$

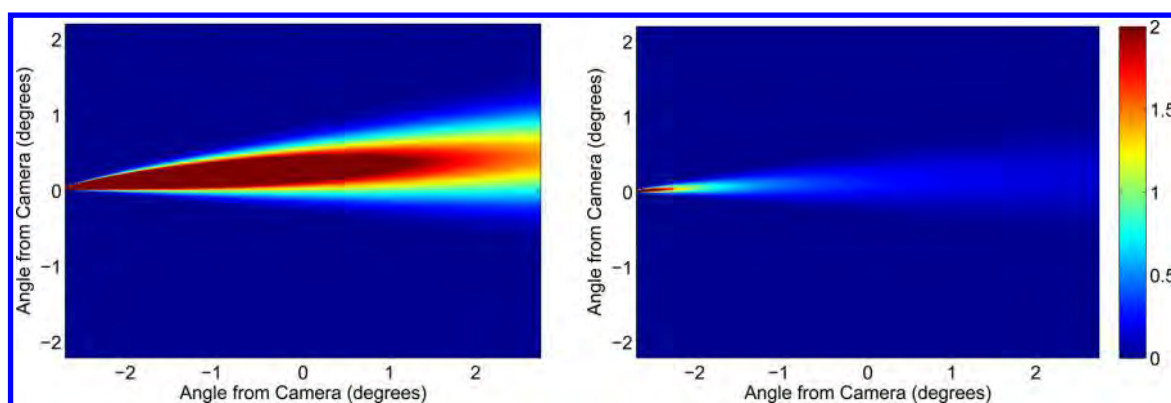


Figure 2. Simulated concentration path length profile of natural gas leaks of (left) 1.5 g/s and (right) 0.15 g/s, at a wind speed of 2 m/s and stability class C. Leaks are imaged by a camera 30 m to the side of the leak source. The color bar indicates the signal-to-noise ratio as imaged by the IR camera.

where x , y , and z are the coordinates at which the concentration is to be calculated (m): x is measured downwind of the leak, z is the vertical displacement from the ground, y_0 is the position of the leak source in the y direction. Q is the leak flux (g/s), and u is the wind speed (m/s). σ_y and σ_z are the standard deviation of the plume concentration (m), extracted using linear interpolation to published curves^{22–24} based on the atmospheric stability class. Finally, z_M is the vertical position of the middle of the plume as a function of x . z_M accounts for the plume buoyancy and follows the methodology suggested by Beychok (see section S2.3 of the Supporting Information).²⁵

The DD, MIR, and AIR programs use the Gaussian plume model in different ways. For the DD detector, the concentration of methane at the location of the plume is compared to a predefined detection threshold. If the concentration is greater than the threshold, the leak is detected. The probability that the concentration exceeds the detection threshold depends upon the size of the leak, the location of the leak relative to the detector, and atmospheric conditions. The location of the leaks are chosen randomly within a pad area definition. Various placement patterns of DD sensors are explored in prior work.²⁶

The detection threshold for the IR camera methods requires that a minimum fraction of the camera pixels be above a minimum concentration path length.²⁷ The signal in each pixel is estimated by numerically integrating the concentration calculated by the Gaussian plume model along the path imaged by each pixel according to eq 5, where α is an implied constant in the detection criteria and Λ is the path imaged by a pixel.

$$\text{signal} = \alpha \int_{\Lambda} \Phi(x(s), y(s), z(s)) \, ds \quad (5)$$

A simulation of this concentration path length, as seen by an IR camera 30 m to the side of the leak source, for two different leak rates, using the Gaussian plume model is shown in Figure 2.

Economic Analysis. The Markov model generates a time series of leakage associated with each simulated LDAR technology. Assigning a value to the gas saved by a LDAR program in comparison to a status quo simulation (in this case, the null LDAR program) enables a NPV analysis of each modeled LDAR program and an estimate of the CH₄ emitted.

We use a standard NPV analysis to compare the economic value of various LDAR programs. The NPV is calculated according to eq 6, where Z_t is the set of all time steps, $V_L(t_i)$ is

the value of the leakage lost during the i th time step, and C is the cost of running the LDAR program in the i th time step. R_{RD} is the real discount rate (8%).

$$\text{NPV} = \sum_{i \in Z_t} (V_L(t_i) - C(t_i)) \left(\frac{1}{1 + R_{RD}} \right)^{t_i} \quad (6)$$

The price of natural gas for base-case analysis is fixed at \$5/mcf over the entire simulation period, while a range from \$3 to 8/mcf is used for sensitivity analysis. The cost of fixing leaks is drawn at random from a comprehensive list of over 1600 leaks from a 2006 United States Environmental Protection Agency (U.S. EPA) study,¹¹ with costs adjusted for inflation. There was no correlation between the measured leak magnitudes in that study and the estimated costs to fix each leak (see Figure S3.14 of the Supporting Information), thereby justifying randomly selecting costs. It should be noted that the NPV analysis performed here is only representative and is best used as a tool to compare various LDAR technologies in terms of its cost-effectiveness instead of absolute dollar terms. Further refinement of this model would need to incorporate enterprise-level information regarding capital structures and specific characteristics of the business model in use.

RESULTS AND DISCUSSION

A FEAST scenario is defined by the user-defined settings, inputs, and underlying data set provided to FEAST. We refer to the results generated by running FEAST once as one realization of a particular scenario. Because FEAST is stochastic, results will change each time FEAST runs a particular scenario. Numerous realizations must be analyzed to understand the implications of a particular scenario.

Figure 3 shows the leakage time series of a single realization of the default scenario in FEAST for different LDAR programs, including the null program and a no-repair program. While the time-series change in total leakage will be different for each realization because of the stochastic nature of the model, the general trends in Figure 3 are characteristic of the LDAR programs. This simulation covers a 10 year time period; therefore, the number of evaluation periods is large, and steady-state behavior is always reached. The gas saved over the duration of the simulation by a particular LDAR program is the area between the null program time series and the LDAR program time series.

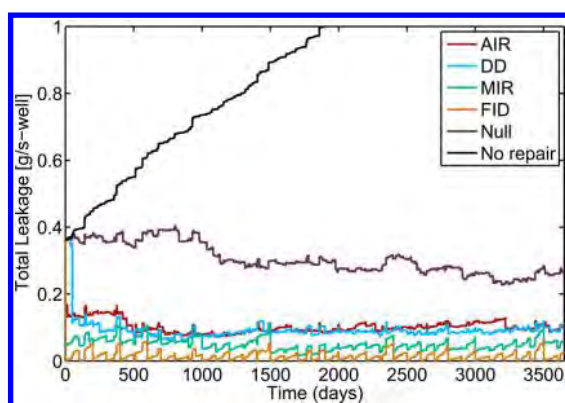


Figure 3. Time series of a single realization of the default scenario in FEAST for the four different LDAR programs, including the null and no-repair programs. In the no-repair case, the total leakage doubles within a few years, while it reaches a steady state in every other case. The null repair scenario fixes the majority of the leaks compared to the no-repair scenario, and therefore, any marginal advantage of the LDAR programs is calculated when compared to the null scenario.

The null LDAR program is intended to emulate repairs that occur in the field without any explicit LDAR program and is set in this scenario as noted above ($P_{L,R}N_L^i = P_{R,L}N_R^i$). These null program repairs may occur during routine maintenance or upgrades to equipment. We suggest that the null program be used to represent the status quo, although users can choose their own baseline. The no-repair program never removes any leaks from the gas field, and the leakage increases indefinitely ($P_{L,R} = 0$). Because the null scenario repairs the majority of the leaks compared to a no-repair scenario, it is only instructive to compare any marginal advantages of a LDAR program to the null scenario (i.e., no-repair results are not used to calculate LDAR benefits below).

There are two types of variability in FEAST: the variability in the mean behavior between different scenarios and the stochastic variability between realizations. Figure 4 illustrates both of these types of variability. The left panel shows the difference in the mean behavior of the LDAR programs, broken down into cost and benefit components. We can see that the labor cost (a major component of “finding cost”) dominates in some technologies (e.g., FID), while the capital cost dominates in others (e.g., DD). The error bars represent the standard error in the estimate of the mean NPV as a result of the limited sample size employed here. The standard error was computed as

$$\sigma_{\mu} = \frac{\sigma_s}{\sqrt{N}} \quad (7)$$

where σ_{μ} is the expected standard deviation of the mean in similar samples, σ_s is the sample standard deviation, and N is the number of samples (realizations). In this work, $N = 100$ for each scenario. The variation between stochastic realizations is shown in the right panel of Figure 4. We see that, while the variation between realizations is large, the technologies are different enough that clear trends can be discerned. Considering the median NPV for all realizations, the AIR, DD, and MIR LDAR programs have a positive NPV across the range of inter-realization variability. In comparison to these technologies, the intensive labor costs for a FID-based LDAR program results in a negative median NPV.

Perhaps the most instructive results from FEAST are illustrated by varying scenario settings, as shown in a tornado

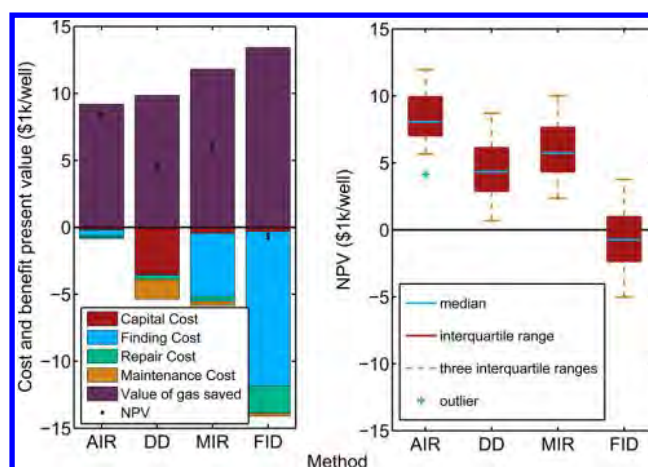


Figure 4. (Left) Variability in the mean behavior between different scenarios of the various LDAR programs shown as a cost versus benefit diagram. Note that the distribution of costs between capital, labor, repairs, and maintenance are dependent upon the technology and methodology adopted in the LDAR program. For example, while the cost of implementing a DD program is dominated by the cost of the detectors, the FID program effectively depends only upon labor costs. (Right) Stochastic variability between different realizations of a scenario for different LDAR programs. While the variation exceeds 50% of the mean in some cases, clear trends can be observed: the FID program, highly dependent upon labor cost, has a significantly lower NPV compared to other LDAR programs.

diagram in Figure 5. The settings used to generate these sensitivity cases are given in Table 2. They were chosen to represent the realistic range of values for each parameter. Note that simulating fields within the realistic range of leak production rates given available data result in enormous variability between scenarios. Clearly, improved data to quantify the leak production rate of gas fields would mitigate the primary driver of uncertainty in FEAST.

One of the base case assumptions in FEAST is a constant leak production rate. Some evidence suggests that gas infrastructure is likely to produce leaks at a greater rate as it ages, although little data exist to quantify this effect in natural gas wells.^{10–13} We allow for a variable leak production rate in one sensitivity case: the leak production rate increases linearly from 2.6×10^{-4} g/s per well per day to twice its value over the 10 year simulation period. It can be clearly seen from Figure 5 that any additional increase in the baseline leak creation rate only increases the value of the LDAR programs.

Each LDAR program has unique characteristics that can be adjusted in FEAST to explore their effects. The FID program can be greatly improved by reducing the time required to complete surveys and decreasing the frequency of surveys from the default case. This is because the baseline FID cost is dominated by the labor cost of this slow technology. This result is intuitive because the FID program has no trouble finding leaks and labor is the primary cost of the FID program; reducing the frequency of surveys reduces labor costs more than it decreases gas savings.

In either IR camera program, improving the sensitivity of each camera pixel to methane increases the value of the LDAR programs. However, the results are less sensitive to the number of pixels that must be above the detection limit. Only the MIR program is sensitive to the survey time and survey interval of the program, while the value of the AIR program is largely independent of these factors. In fact, the AIR program is only

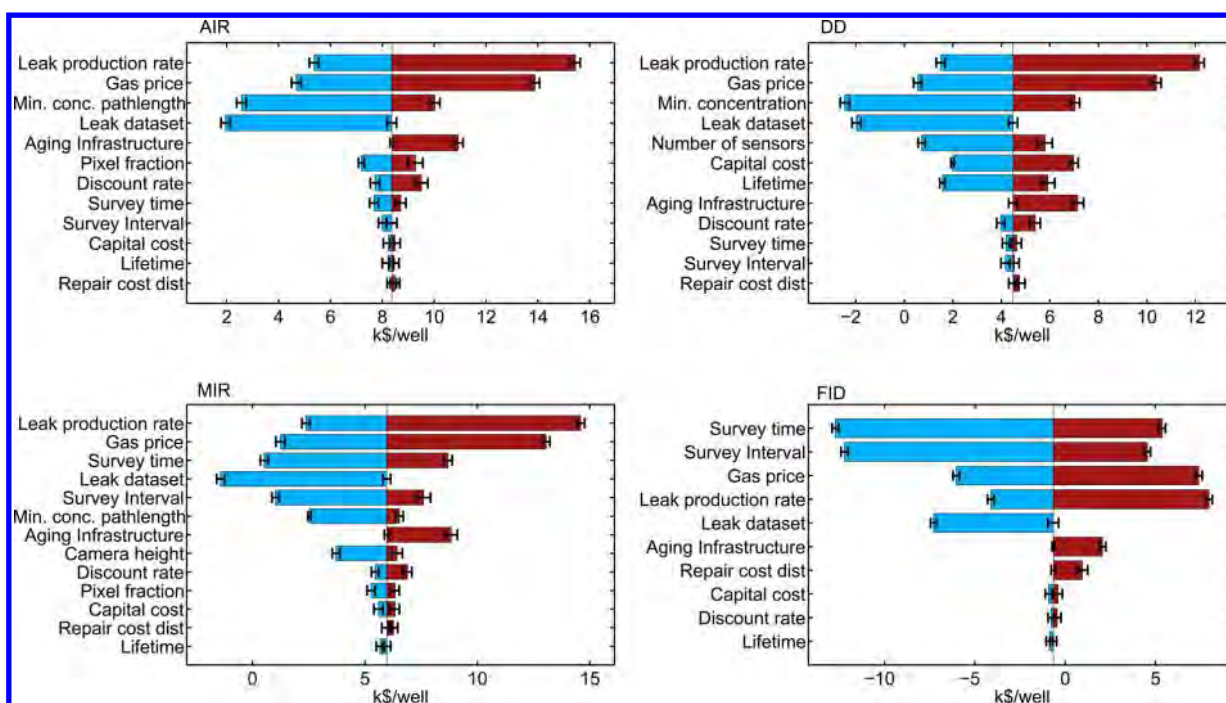


Figure 5. Sensitivity of the NPV of the four simulated LDAR programs to various parameters of the natural gas field, detection technology, and survey procedures. It should be noted that extrinsic factors such as the leak production rate and gas price play an out-sized role in determining the NPV of various LDAR programs. In the case of FID, which has significantly lower NPV than other LDAR programs, we see that reducing the intervals of leak detection will result in a greater cost reduction compared to the reduction in gas savings.

sensitive to properties that affect the number and size of leaks that it detects. This is because the amortized operating costs of the AIR program are very small in comparison to the amount of gas that it detects, as a result of the fact that the automated airborne system can visit a large number of wells per unit time. Reducing the amount of gas detected by 20% has a greater effect on the cash flow of the AIR program than doubling its operating expenses.

The DD program shares many traits with the AIR program: it benefits from changes that increase the number of leaks detected and is insensitive to the survey interval and survey time required to pinpoint the location of leaks. However, the distributed detector program is the only program simulated that is significantly sensitive to the capital cost of the equipment. A distributed detector program requires detectors to be placed at every well, while a single piece of survey equipment for a FID, MIR, or AIR program can service hundreds or even thousands of gas wells, depending upon the survey frequency and time for each survey. Low-sensitivity methane detectors can have extremely low capital costs on the order of \$1, but detectors with parts per billion (ppb) scale sensitivity can cost \$10 000–100 000. In the base case, we simulated an intermediate detector with a cost of \$500 and a sensitivity of 15 ppm.

Notwithstanding the sources of variability in results outlined above, the absolute values computed with FEAST are encouraging. We found that the MIR, AIR, and DD programs are likely to have positive NPVs. Under most scenarios we considered, the AIR program has the greatest NPV, ranging up to \$15 000 per well over a 10 year period in the best case sensitivity scenario (see Figure 5).

The most speculative of these scenarios is perhaps the AIR program. Some AIR assumptions may ultimately prove unrealistic. However, the basic characteristics of the program that make it cost-effective are instructive: it allows for high-

speed servicing of wells and only identifies relatively large leaks. Sacrificing some sensitivity for speed allows for the majority of leakage to be found (when using realistic heavy-tailed leak size distributions) while greatly reducing operating costs and reducing the cost of fixing small leaks with small gas savings. With these factors included, the capital cost of a drone and high-performance IR camera system (estimated at \$193 000 for the purposes of this example) proved to be largely immaterial to the project NPV. This clearly shows that there is a significant divergence between low-cost LDAR technologies (“cheap detectors”) and low-cost LDAR programs (“cheap detection”). Low-cost LDAR programs can in fact rely on highly sophisticated and high-cost technology, as long as this technology is applied in a way that allows for rapid scanning and robust detection of large leaks. The end member of such a technology spectrum would be a high-resolution satellite-based system, which would have very high capital costs but could, in principle, detect leaks across a wide swath of the Earth’s surface each day.

One of the big challenges in the methane leakage problem is its magnitude; the vast variety in the infrastructure and skewed leak size distribution makes direct measurements and subsequent extrapolation costly (i.e., large sample sizes are needed). Considering the costs associated with implementing leak detection programs, it becomes vitally important to develop tools to help businesses develop cost-effective strategies. FEAST is general enough to allow for businesses and others to tailor the model to specific sites/conditions as they see fit. The results presented here should not be taken as definitive but more as an example of the various possibilities available to users.

We emphasize that the economic analysis of various LDAR programs presented here is only indicative of general trends and should not be interpreted as a definitive analysis of the

cost/benefit ratio for a given technology. Also, FEAST NPV calculations are operator-centric: they take into account the additional revenue from the sale of recovered gas in its cost/benefit analysis but neglect other important effects, such as the social cost of carbon, a future carbon tax or carbon trading market, health benefits associated with the reduction of VOCs, and the avoided costs of climate change adaptation. In proposing new regulations to reduce methane emissions from the U.S. oil and natural gas industry by 40–45% from 2012 levels in 2025, the U.S. EPA has estimated net climate benefits alone at \$120–150 million.²⁸ Adding benefits accrued from reductions in health effects related to fine particle pollution, ozone, and air toxics and improvements in visibility would only incentivize support for a strong methane mitigation policy, resulting in a much higher social NPV for various LDAR programs.

■ ASSOCIATED CONTENT

■ Supporting Information

The Supporting Information is available free of charge on the ACS Publications website at DOI: 10.1021/acs.est.5b06068.

Simulation code in MATLAB (ZIP)

technical documentation and user guide (PDF)

■ AUTHOR INFORMATION

Corresponding Author

*Telephone: +1-650-724-8251. Fax: +1-650-725-2099. E-mail: abrandt@stanford.edu.

Notes

The authors declare no competing financial interest.

■ REFERENCES

- (1) United States Environmental Protection Agency (U.S. EPA). *Inventory of U.S. Greenhouse Gas Emissions and Sinks: 1990–2012*; U.S. EPA: Washington, D.C., 2014.
- (2) Alvarez, R. A.; Pacala, S. W.; Winebrake, J. J.; Chameides, W. L.; Hamburg, S. P. Greater focus needed on methane leakage from natural gas infrastructure. *Proc. Natl. Acad. Sci. U. S. A.* **2012**, *109*, 6435–6440.
- (3) Brandt, A.; Heath, G. A.; Kort, E. A.; O'Sullivan, F.; Petron, G.; Jordaan, S. M.; Tans, P.; Wilcox, J.; Gopstein, A. M.; Arent, D.; Wofsy, S.; Brown, N. J.; Bradley, R.; Stucky, G. D.; Eardley, D.; Harriss, R. Methane Leaks from North American Natural Gas Systems. *Science* **2014**, *343*, 733–735.
- (4) Advanced Research Projects Agency-Energy (ARPA-E). *Methane Observation Networks with Innovative Technology to Obtain Reductions (MONITOR)*; ARPA-E: Washington, D.C., 2014; http://arpa-e.energy.gov/sites/default/files/documents/files/MONITOR%20and%20DELTA%20Project%20Descriptions_Final_12.15.14.pdf.
- (5) Environmental Defense Fund (EDF). *Methane Detectors Challenge*; EDF: Washington, D.C., 2015; <https://www.edf.org/energy/natural-gas-policy/methane-detectors-challenge>.
- (6) Rebellion Photonics. 2015; <http://rebellionphotonics.com/>.
- (7) Kort, E.; Frankenberg, C.; Costigan, K. R.; Lindenmaier, R.; Dubey, M. K.; Wunch, D. Four corners: The largest US methane anomaly viewed from space. *Geophys. Res. Lett.* **2014**, *41*, 6898–6903.
- (8) KairosAerospace. <http://kairosaerospace.com/>.
- (9) Mathworks, Inc., *MATLAB, Version 2015b*; Mathworks, Inc.: Natick, MA, 2015.
- (10) Gallagher, M. E.; Down, A.; Ackley, R. C.; Zhao, K.; Phillips, N.; Jackson, R. B. Natural Gas Pipeline Replacement Programs Reduce Methane Leaks and Improve Consumer Safety. *Environ. Sci. Technol. Lett.* **2015**, *2*, 286–291.
- (11) Fernandez, R. *Cost Effective Directed Inspection and Maintenance Control Opportunities at Five Gas Processing Plants and Upstream Gathering Compressor Stations and Well Sites*; United States Environmental Protection Agency (U.S. EPA): Washington, D.C., 2006.
- (12) Jackson, R. B.; Down, A.; Phillips, N. G.; Ackley, R. C.; Cook, C. W.; Plata, D. L.; Zhao, K. Natural gas pipeline leaks across Washington, DC. *Environ. Sci. Technol.* **2014**, *48*, 2051–8.
- (13) Phillips, N. G.; Ackley, R.; Crosson, E. R.; Down, A.; Hutyrá, L. R.; Brondfield, M.; Karr, J. D.; Zhao, K.; Jackson, R. B. Mapping urban pipeline leaks: Methane leaks across Boston. *Environ. Pollut.* **2013**, *173*, 1–4.
- (14) City of Fort Worth. *Natural Gas Air Quality Study*; City of Fort Worth: Fort Worth, TX, 2011; <http://fortworthtexas.gov/gaswells/air-quality-study/final/>.
- (15) Lyon, D. R.; Zavala-Araiza, D.; Alvarez, R. A.; Harriss, R.; Palacios, V.; Lan, X.; Talbot, R.; Lavoie, T.; Shepson, P.; Yacovitch, T. I.; et al. Constructing a spatially resolved methane emission inventory for the Barnett Shale region. *Environ. Sci. Technol.* **2015**, *49*, 8147–8157.
- (16) Brandt, A. R.; et al. Energy and environment. Methane leaks from North American natural gas systems. *Science (Washington, DC, U. S.)* **2014**, *343*, 733–735.
- (17) Saunier, S. *Quantifying Cost-effectiveness of Systematic Leak Detection and Repair Programs Using Infrared Cameras*; Carbon Limits: Oslo, Norway, 2014; http://www.carbonlimits.no/wp-content/uploads/2015/06/Carbon_Limits_LDAR.pdf.
- (18) Allen, D.; Torres, V. M.; Thomas, J.; Sullivan, D. W.; Harrison, M.; Hendler, A.; Herndon, S. C.; Kolb, C. E.; Fraser, M. P.; Hill, A. D.; Lamb, B.; Miskimins, J.; Sawyer, R.; Seinfeld, J. Measurements of methane emissions at natural gas production sites in the United States. *Proc. Natl. Acad. Sci. U. S. A.* **2013**, *110*, 17768–17773.
- (19) Kuo, J. *Estimation of Methane Emissions from the California Natural Gas System*; California Energy Commission: Fullerton, CA, 2012; <http://www.energy.ca.gov/2014publications/CEC-500-2014-072/CEC-500-2014-072.pdf>.
- (20) Bourke, J.; Mire, K.; Newsom, V.; Pike, M.; Ramanan, R.; Shah, A.; Strong, J.; Tixier, C.; Yang, J. *Fugitive Hydrocarbon Emissions from Oil and Gas Production Operations*; American Petroleum Institute (API): Washington, D.C., 1993; 4589.
- (21) National Oceanic and Atmospheric Administration (NOAA). *National Weather Service Forecast Office Dallas/Fort Worth, TX Climate Data*; NOAA: Silver Spring, MD, 2014; <http://www.srh.noaa.gov/fwd/?n=dfwclimo>.
- (22) Seinfeld, J.; Pandis, S. *Atmospheric Chemistry and Physics*, 2nd ed.; John Wiley and Sons, Inc.: Hoboken, NJ, 2006.
- (23) Pasquill, F. The estimation of the dispersion of windborne material. *Meteorol. Mag.* **1961**, *90*, 33–49.
- (24) Gifford, F. A. Use of Routine Meteorological Observations for Estimating Atmospheric Dispersion. *Nucl. Saf.* **1961**, *2*, 47–51.
- (25) Beychok, M. *Fundamentals of Stack Gas Dispersion*, 4th ed.; Milton R. Beychok: Irvine, CA, 2005.
- (26) Kemp, C. A Simulation Method for Methane Leak Detection and Repair Technologies. Master's Thesis, Stanford University, Stanford, CA, 2015.
- (27) Benson, R. G.; Panek, J. A.; Drayton, P. Direct Measurements of Minimum Detectable Vapor Concentrations Using Passive Infrared Optical Imaging Systems. *Proceedings of the 101st Annual Conference & Exhibition (ACE) Meeting of the Air and Waste Management Association*; Portland, OR, June 24–27, 2008; Paper 1025.
- (28) United States Environmental Protection Agency (U.S. EPA). *Oil and Natural Gas Sector: Emission Standards for New and Modified Sources*. *Fed. Regist.*, 2015, *80*, 56593–56698.

Exhibit 36

With Initial Data Showing Permian Flaring on the Rise Again, New Survey Finds 1 in 10 Flares Malfunctioning or Unlit, Venting Unburned Methane into the Air

Persistent emissions problem requires urgent action by industry, regulators

July 22, 2020

Stacy MacDiarmid, (512) 691-3439, smacdiarmid@edf.org

Matt McGee, (512) 691-3478, mmcgee@edf.org

(AUSTIN, TX) A [new aerial survey](#) reveals that the percentage of malfunctioning flares at oil and gas facilities across the Permian region remains stubbornly high, at the same time that preliminary analysis of federal satellite data shows flaring activity in the basin is on the rise. Together the results suggest that one of the industry's biggest challenges in the basin is poised for resurgence.

Researchers with Environmental Defense Fund's [PermianMAP](#) initiative found that more than one in every 10 flares surveyed in June were either unlit — [venting uncombusted methane](#) straight to the atmosphere — or only partially burning the gas they were releasing. This is consistent with [two surveys](#) done before the price crash. Meanwhile EDF scientists evaluating data from the National Oceanic and Atmospheric Administration's VIIRS satellite instrument say that Permian flaring is on the rebound, with [June volume up 50%](#) after a steep slide from February through May.

One of the largest oilfields on Earth, the Permian straddles Texas and New Mexico, neither of which has historically regulated flaring effectively.

"Malfunctioning and unlit flares are a longstanding problem for the industry and one of the largest sources of methane emissions in the Permian," said EDF scientist [David Lyon](#). "The fact that we have not seen any improvement in flare performance over three separate surveys tells us that industry and regulators need to get much more serious about the problem. The best solution is to eliminate routine flaring altogether."

According to [other satellite data](#), Permian operators sent 280 billion cubic feet of gas worth about \$420 million up their flare stacks in 2019 — more than enough to supply every home in Texas. Historically, Texas and New Mexico have not made flaring or methane a regulatory priority. But policymakers in both states now have important opportunities to institute critical safeguards.

“It’s troubling to see methane pollution from flares persist at the same time it appears flaring activity is on the rise again,” said [Jon Goldstein](#), EDF director of regulatory and legislative affairs. “This data underscores the need for New Mexico’s oil and gas regulators to implement rules that comprehensively address methane waste and pollution. The drafts released this week are a good start, but must be strengthened to close critical loopholes.”

Drafts of the two New Mexico rules can be found [here](#) and [here](#). Photos, video, a map and other images for media are available [here](#).

Methane is a potent greenhouse gas, human sources of which are responsible for more than a quarter of the warming we’re experiencing today. It’s also the main ingredient in natural gas. When methane escapes into the atmosphere, it has over 80 times the warming power of carbon dioxide over the first 20 years.

Although flaring waste and localized emissions are a familiar problem by now, [EDF’s helicopter surveys](#) are the first effort ever to assess the methane emissions associated with flaring in the region. It is the latest product of EDF’s [year-long PermianMAP initiative](#) to measure methane emissions using aircraft, stationary towers and ground-based mobile sensors.

The survey results come on the heels of [satellite data](#) released earlier this year showing total oil and gas methane emissions in the Permian are more than two times higher than federal inventories indicate.

###

Environmental Defense Fund ([edf.org](#)), a leading international nonprofit organization, creates transformational solutions to the most serious environmental problems. EDF links science, economics, law and innovative private-sector partnerships. Connect with us on [EDF Voices](#), [Twitter](#) and [Facebook](#).

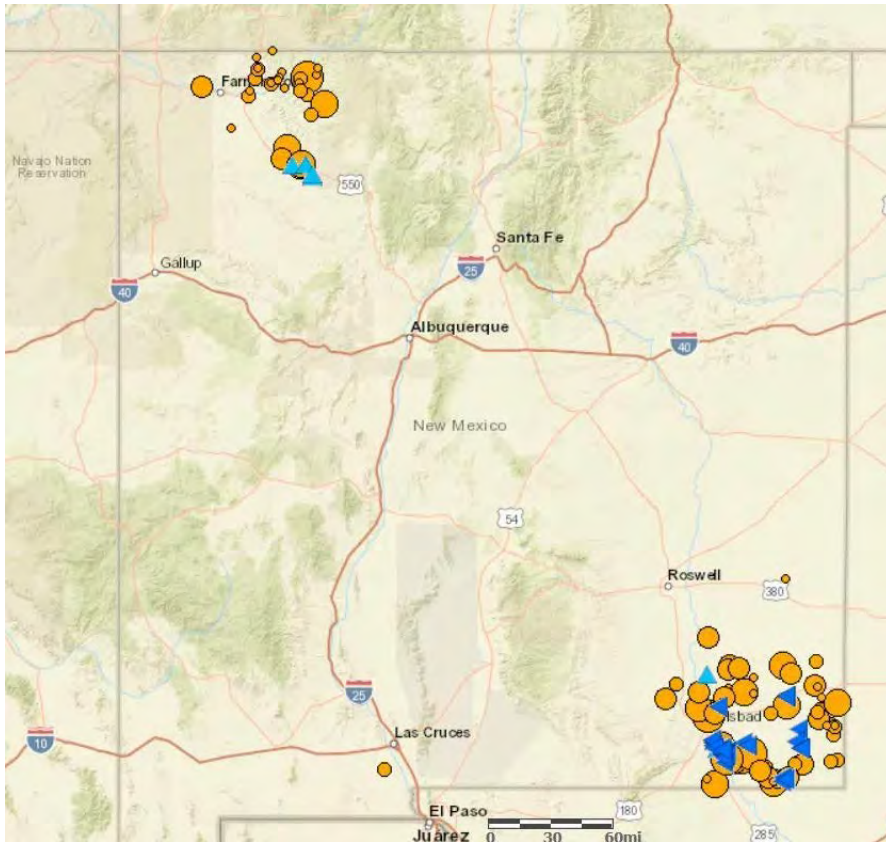
Exhibit 37

ENVIRONMENTAL PROJECT

January 16, 2020

NMED discovers more potential methane emission violations

By Kendra Chamberlain



NMED

The New Mexico Environment Department maintains an interactive online map of methane and other air pollutants. Source: NMED

The New Mexico Environment Department (NMED) announced more possible emission violations produced by oil and gas operations around the state. The department said it acquired video footage collected by citizens using forward-looking infrared (FLIR) cameras documenting methane and other air contaminants. NMED believes the emissions depicted in the video footage are “potential violations of existing state permits or regulations,” the department said in a statement.

RELATED: NMED issues first round of violation notices for methane emissions in Permian Basin (<https://nmpoliticalreport.com/2019/11/05/nmed-issues-first-round-of-violation-notices-for-methane-emissions-in-permian-basin/>)

NMED is sending written notices to oil and gas operators about the emissions. Oil and gas producers will have 14 days to correct the issues. If those issues are not corrected within that time frame, NMED said it may launch an investigation or initiate civil enforcement of the violations, which could include assessing monetary penalties to producers who are in violation.

The FLIR footage has been uploaded to the state's [online interactive methane map](https://gis.web.env.nm.gov/oem/?map=methane) (<https://gis.web.env.nm.gov/oem/?map=methane>). The map also contains FLIR footage documenting “significant emissions” collected during two recent flyover compliance inspections conducted by NMED and the EPA.



Emissions captured by Earthworks using a forward-looking infrared camera. Source: Earthworks

During two flyover compliance inspections in September and October 2019, officials identified and documented emissions leaks from flares, tanks and other types of oil and gas equipment. Officials found 111 of over 5,300 storage tanks were emitting methane and other pollutants, and 13 of the 530 flares observed were unlit and emitting methane.

NMED said the department is now reviewing that footage to determine if any violations had taken place.

“The Department is addressing oil and natural gas emissions through innovative compliance assurance measures today as we invest in methane regulations for tomorrow,” said NMED Cabinet Secretary James Kenney in a statement. “The emissions documented in many of these videos are unacceptable to this Department and pose significant health and safety risks to New Mexico communities and employees of these companies.”

RELATED: [Guv. announces ‘data refinery’ to track methane emissions by satellite](https://nmpoliticalreport.com/2019/09/19/guv-announces-data-refinery-to-track-methane-emissions-by-satellite/)

(<https://nmpoliticalreport.com/2019/09/19/guv-announces-data-refinery-to-track-methane-emissions-by-satellite/>).

Environmental group Earthworks praised NMED for enforcing emissions rules in oil and gas activity in the state.


Earthworks’ Colorado and New Mexico field advocate Nathalie Eddy said NMED’s notices “suggest that New Mexico is putting the public interest ahead of — or at least on equal footing with — the oil and gas industry’s pursuit of profits.”


“NMED’s enforcement letters recognize that New Mexicans living with oil and gas production — involuntarily and continuously monitoring it — are important allies in protecting their own health & environment from oil and gas pollution,” Eddy said. “Today’s news is a concrete validation that community and community-advocate complaints are a vital tool to reign in dangerous oil and gas pollution.”


The New Mexico Oil and Gas Association (NMOGA) is supportive of NMED’s efforts to enforce emissions compliance among oil and gas producers.


“We are constantly working to reduce our emissions and environmental impacts, and data collected by the EPA shows that we’re making progress while continuing to produce more oil and natural gas,” NMOGA spokesperson Robert McEntyre told *NM Political Report* in an email. “While operators strive to fully comply with the law, we respect the role NMED plays to ensure a fair and level playing field for the industry.”

Share this:

 (<https://nmpoliticalreport.com/2020/01/16/nmed-discovers-more-potential-methane-emission-violations/?share=facebook&nb=1>)

 (<https://nmpoliticalreport.com/2020/01/16/nmed-discovers-more-potential-methane-emission-violations/?share=twitter&nb=1>)

 (<https://nmpoliticalreport.com/2020/01/16/nmed-discovers-more-potential-methane-emission-violations/#print>)

 More (#)

Related



([https://nmpoliticalreport.com/2019/11/05/nmed-issues-first-round-of-violation-](https://nmpoliticalreport.com/2019/11/05/nmed-issues-first-round-of-violation-notice-for-methane-emissions-in-permian-basin/)

[issues-first-round-of-violation-
notices-for-methane-
emissions-in-permian-basin/](https://nmpoliticalreport.com/2019/11/05/nmed-issues-first-round-of-violation-notice-for-methane-emissions-in-permian-basin/)).

**NMED issues first
round of violation
notices for methane
emissions in
Permian Basin**

([https://nmpoliticalreport.com/2019/11/05/nmed-](https://nmpoliticalreport.com/2019/11/05/nmed-issues-first-round-of-violation-notice-for-methane-emissions-in-permian-basin/)

November 5, 2019

In "Environmental Project"

[methane-rulemaking-
progresses-questions-about-
exemptions-linger/](https://nmpoliticalreport.com/2020/11/11/as-methane-rulemaking-progresses-questions-about-exemptions-linger/)).

**As methane
rulemaking
progresses,
questions about
exemptions linger**

([https://nmpoliticalreport.com/2020/11/11/as-](https://nmpoliticalreport.com/2020/11/11/as-methane-rulemaking-progresses-questions-about-exemptions-linger/)

November 11, 2020

In "Environmental Project"

[says-it-cannot-deny-oil-and-
gas-permits-due-to-ozone-
concerns/](https://nmpoliticalreport.com/2020/08/25/nmed-says-it-cannot-deny-oil-and-gas-permits-due-to-ozone-concerns/)).

**NMED says it
cannot deny oil and
gas permits due to
ozone concerns**

([https://nmpoliticalreport.com/2020/08/25/nmed-](https://nmpoliticalreport.com/2020/08/25/nmed-says-it-cannot-deny-oil-and-gas-permits-due-to-ozone-concerns/)

and-gas-permits-due-to-
ozone-concerns/)

August 25, 2020

In "Environmental Project"

Exhibit 38

ENVIRONMENTAL STUDIES

Quantifying methane emissions from the largest oil-producing basin in the United States from space

Yuzhong Zhang^{1,2,3,4*}, Ritesh Gautam^{2*}, Sudhanshu Pandey⁵, Mark Omara², Joannes D. Maasakkers⁵, Pankaj Sadavarte^{5,6}, David Lyon², Hannah Nesser¹, Melissa P. Sulprizio¹, Daniel J. Varon¹, Ruixiong Zhang^{7,8}, Sander Houweling^{5,9}, Daniel Zavala-Araiza^{2,10}, Ramon A. Alvarez², Alba Lorente⁵, Steven P. Hamburg², Ilse Aben⁵, Daniel J. Jacob¹

Using new satellite observations and atmospheric inverse modeling, we report methane emissions from the Permian Basin, which is among the world's most prolific oil-producing regions and accounts for >30% of total U.S. oil production. Based on satellite measurements from May 2018 to March 2019, Permian methane emissions from oil and natural gas production are estimated to be $2.7 \pm 0.5 \text{ Tg a}^{-1}$, representing the largest methane flux ever reported from a U.S. oil/gas-producing region and are more than two times higher than bottom-up inventory-based estimates. This magnitude of emissions is 3.7% of the gross gas extracted in the Permian, i.e., ~60% higher than the national average leakage rate. The high methane leakage rate is likely contributed by extensive venting and flaring, resulting from insufficient infrastructure to process and transport natural gas. This work demonstrates a high-resolution satellite data-based atmospheric inversion framework, providing a robust top-down analytical tool for quantifying and evaluating subregional methane emissions.

INTRODUCTION

Methane is a potent greenhouse gas with a relatively short average atmospheric residence time of about a decade and is also a precursor of tropospheric ozone (1). The emission-based radiative forcing for methane (including effects on tropospheric ozone and stratospheric water vapor) is 0.97 W m^{-2} since preindustrial times, which is about 60% of that for CO_2 (2). Roughly a third of the contemporary anthropogenic methane emissions come from the fossil fuel energy sector worldwide (oil, natural gas, and coal) (~100 to 180 Tg a^{-1}) (3, 4, 5). Curbing anthropogenic methane emissions, including those from the oil/gas sector, is considered an effective strategy to slow the rate of near-term climate warming (1). However, the rapid increase in oil and natural gas (O/G) production in the United States since around 2005, driven primarily by hydraulic fracturing and horizontal drilling, has led to major concerns about increasing methane emissions and adverse climate impacts (6). By upscaling data collected from field measurements in some of the largest O/G production basins in the United States, Alvarez *et al.* (7) estimated 13 Tg annual methane emissions from the national O/G supply chain for 2015, which is 60% higher than the official estimates by the U.S. Environmental Protection Agency (EPA) (8). The largest discrepancy was found in the O/G production segment where the estimate by Alvarez *et al.* (7) (7.6 Tg a^{-1}) was more than two times that by EPA, which relies on inventory-based estimates (3.5 Tg a^{-1}) (8).

While field measurements provide in-depth information about a particular site or area, it is often challenging to expand the measurement capacity to observe a diverse set of targets distributed globally over longer periods of time. Additional challenges exist for areas that are difficult to access for technical or proprietary reasons. On the other hand, global satellite observations of column atmospheric methane offer a unique vantage point to identify emission hot spots and quantify regional emissions (9). Using data from Scanning Imaging Absorption spectroMeter for Atmospheric CHartography (SCIAMACHY) satellite observations averaged between 2003 and 2009, Kort *et al.* (10) found large anomalous methane levels from the Four Corners region in the United States, with total methane emissions associated with natural gas, coal, and coalbed sources estimated as $0.59 \pm 0.08 \text{ Tg a}^{-1}$. While the SCIAMACHY data were fairly limited in spatial resolution ($30 \text{ km} \times 60 \text{ km}$) and measurement precision [30 parts per billion in volume or (ppbv)] (9), it was the first time that satellite observations were used to quantify a dense O/G-related methane emission hot spot. This finding also led to several dedicated airborne studies to better understand methane sources in the region (11, 12), which reported methane fluxes comparable to the satellite-based estimate (10).

Here, we demonstrate and exploit the capability of a recent space-borne sensor, the Tropospheric Monitoring Instrument (TROPOMI), to map atmospheric methane enhancements in the United States and quantify emissions from the Permian Basin (Fig. 1), which has become one of the world's most prolific oil-producing regions in recent years due to advances in drilling technologies. Located in New Mexico and Texas in a region of $\sim 400 \text{ km} \times 400 \text{ km}$, Permian is currently the largest oil-producing basin in the United States. In 2018, the Permian Basin produced $5.5 \times 10^5 \text{ m}^3$ (or 3.5 million barrels) of crude oil and $3.2 \times 10^8 \text{ m}^3$ (or 11 billion feet^3) of natural gas every day (~30 and ~10% of the U.S. national totals, respectively), which was 4 and 2.5 times their corresponding levels in 2007 (around the time of SCIAMACHY observations) (Fig. 2) (13). While the surging production in the Permian Basin and its importance in the U.S. oil boom during the last decade have been widely covered in mass

¹School of Engineering and Applied Sciences, Harvard University, Cambridge, MA 02138, USA. ²Environmental Defense Fund, Washington, DC 20009, USA. ³School of Engineering, Westlake University, Hangzhou, Zhejiang Province, China. ⁴Institute of Advanced Technology, Westlake Institute for Advanced Study, Hangzhou, Zhejiang Province, China. ⁵SRON Netherlands Institute for Space Research, Utrecht, Netherlands. ⁶TNO, Department of Climate, Air and Sustainability, Utrecht, Netherlands. ⁷School of Earth and Atmospheric Sciences, Georgia Institute of Technology, Atlanta, GA 30332, USA. ⁸ClimaCell Inc., 280 Summer Street Floor 8, Boston, MA 02210, USA. ⁹Department of Earth Sciences, Vrije Universiteit Amsterdam, Amsterdam, Netherlands. ¹⁰Institute for Marine and Atmospheric Research Utrecht (IMAU), Utrecht University, Utrecht, Netherlands.

*Corresponding author. Email: zhangyuzhong@westlake.edu.cn (Y.Z.); rgautam@edf.org (R.G.)

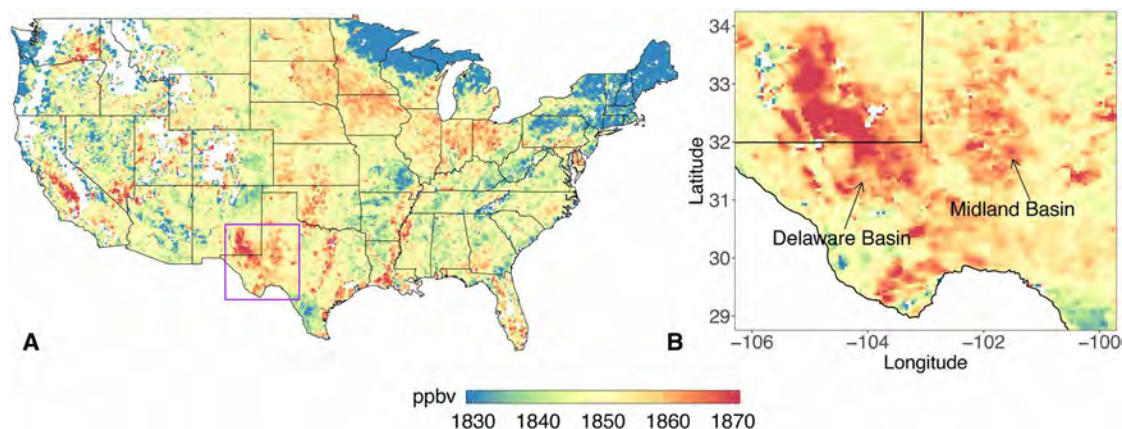


Fig. 1. Satellite observations of the Permian methane anomaly. TROPOMI satellite data derived elevation-corrected column methane mixing ratio for (A) the conterminous United States and (B) the Permian Basin containing the Delaware and Midland sub-basins. White shading represents missing data. Purple boundary in (A) indicates the study domain encompassing the Permian Basin. Methane averages are computed from monthly means of TROPOMI measurements during May 2018 and March 2019.

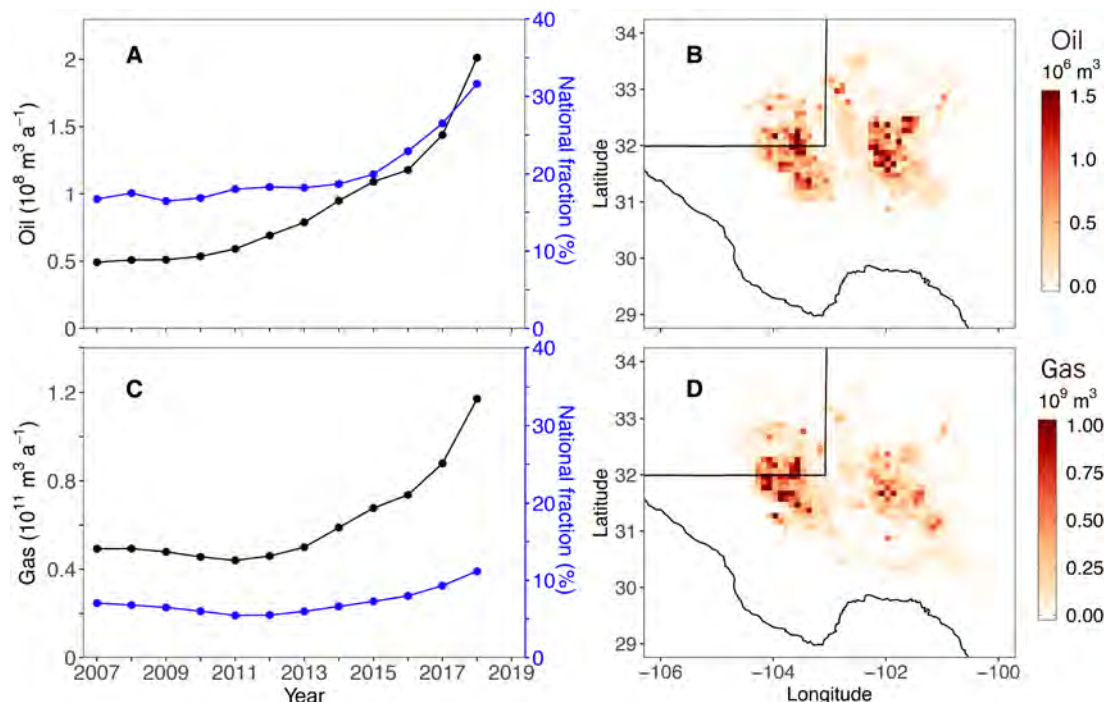


Fig. 2. Oil and gas production in the Permian Basin. (A and C) Time series of annual O/G production in black and the corresponding fractions of total U.S. production in blue [data from the Drilling Productivity Report by EIA (13)]. (B and D) Spatial distribution of oil and gas production for 2018 [data from Enverus Drillinginfo (50)]. Oil production includes both crude and condensate production. Gas production represents gross (before processing) gas production.

media (14), the scale of associated methane emissions from this critical O/G basin is unknown, despite reports of increased flaring and venting activity (15).

Using 11 months of recent data acquired by TROPOMI during 2018–2019, we focus on the distinct methane concentration anomaly over the Permian Basin and quantify the associated methane emissions with a state-of-the-art atmospheric inverse modeling framework. TROPOMI was launched in October 2017 onboard the European Space Agency's Sentinel-5P satellite and provides column atmospheric methane measurements with higher spatial resolution ($7 \text{ km} \times 7 \text{ km}$ at nadir) and precision (0.6%) than was previously available (16), providing near-daily global coverage with its large 2600-km-wide

swath (17). Our integrated satellite-based approach provides new insights into the dynamic landscape of O/G-related methane emissions in the United States and should pave the way forward toward routine quantification, monitoring, and evaluation of methane emissions from source regions distributed globally.

RESULTS

Satellite observations of the Permian methane anomaly

Figure 1A shows a map of column-averaged dry-air methane mixing ratio over the conterminous United States, retrieved from TROPOMI measurements, with correction for the topography effect (denoted

as XCH_4^t ; see Materials and Methods). The data are averaged from May 2018 to March 2019. Substantial enhancements of XCH_4^t relative to the surrounding background, up to ~ 30 ppbv, are found over the Permian Basin, indicating strong methane emissions. Other notable enhancements are observed in California's central valley, coastal Southeast, and the Mississippi River Valley, likely associated with anthropogenic (agriculture, dairy) and natural (wetland) sources. The elevated methane levels in central California were also seen earlier in the SCIAMACHY analysis (10).

The methane enhancements over the Permian Basin show a characteristic two-branch pattern, which aligns with the two major O/G production sub-basins, the Delaware basin to the west and the Midland basin to the east (Fig. 1B). The enhancement over the Delaware basin, where extensive new exploitation has taken place during the last 5 years (18) (fig. S1), is larger than that over the Midland basin (Fig. 1B). Intensive O/G production activity in these two sub-basins is also captured by satellite observations of radiant heat from gas flaring [Fig. 3A; nighttime observations by the Visible Infrared Imaging Radiometer Suite (VIIRS)] and NO_2 tropospheric column densities (Fig. 3B; daytime observations by TROPOMI). Flaring is a common practice in O/G operations to burn off unwanted or excess gas, and NO_2 is a gaseous pollutant released during gas flaring and other combustion activities in O/G fields (19, 20). On the basis of measurements by the VIIRS instrument onboard the Suomi National Polar-orbiting Partnership satellite, we estimate an average flaring rate of 5.9 ± 1.2 billion $\text{m}^3 \text{a}^{-1}$ during the period of this study, about 4.6% of the gross gas production (see text S1). A fourfold increase in flaring intensity since 2012, observed by the VIIRS instrument, is indicative of the rapid growth in O/G production across the Permian Basin (fig. S1).

Methane emission quantification

We quantify the methane emission rate from the Permian Basin and its spatial distribution with atmospheric inverse modeling, which optimizes spatially resolved methane emission rates by drawing information from TROPOMI observations and the prior emission estimate following the Bayesian rule. The inversion seeks to optimize monthly methane emission rates resolved at $0.25^\circ \times 0.3125^\circ$ horizontal resolution in a study domain containing the Permian Basin and the surrounding region (29° – 34°N , 100° – 106°W). The solution to the

optimization is found analytically with closed-form characterization of the error statistics (3). An atmospheric transport model (a nested version of GEOS-Chem over North America with a $0.25^\circ \times 0.3125^\circ$ horizontal resolution) (21) is used as the forward model to relate atmospheric methane columns with ground-level emissions in the study domain and the contributions from outside the domain. The optimization by the inversion significantly reduces the observation-model mismatch with decreased root mean square error (prior, 23 ppbv; posterior, 14 ppbv) and increased correlation (R ; prior, 0.30; posterior, 0.62) (fig. S2). See Materials and Methods for more details about the configurations of the inverse modeling including error accounting and prior information.

When aggregating monthly spatially resolved posterior emissions to the basin-level annual average, we find a methane emission flux of $2.9 \pm 0.5 \text{ Tg a}^{-1}$ from the Permian Basin (30° – 34°N , 101° – 105°W) (Fig. 4A; see Materials and Methods for the uncertainty analysis). This estimate is more than a factor of 2 larger than the bottom-up estimate based on an extrapolation of EPA greenhouse gas inventory data (EI_{BU} , 1.2 Tg a^{-1} ; see Materials and Methods) (Fig. 4A), suggesting that current methane emissions in the Permian are under-represented in national bottom-up emission inventories (22). Our inversion result is in close agreement with a basin-level estimate based on extrapolation of limited ground-based site-level measurements in the Permian (EI_{ME} , 2.8 Tg a^{-1}) (Fig. 4A). It should be noted that these site-level measurements were primarily conducted in the New Mexico portion of the Permian Basin and covered only a

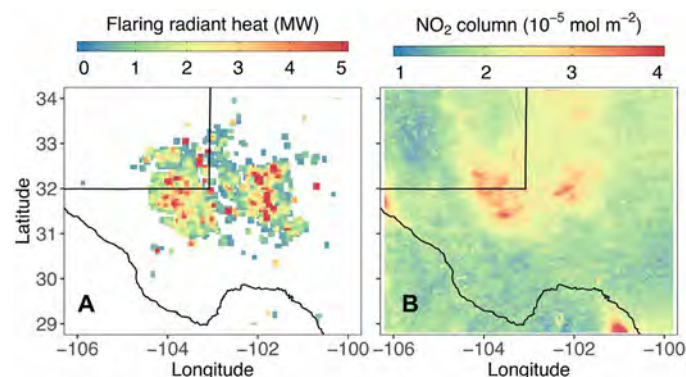


Fig. 3. Satellite observations of gas flaring radiant heat and NO_2 tropospheric column density over the Permian Basin. (A) Gas flaring radiant heat is the annual average of 2018 measured by the VIIRS satellite instrument, and (B) NO_2 tropospheric column density is the 3-month average (June, July, and August of 2018) measured by the TROPOMI instrument, indicating colocated hot spots over the Delaware and Midland sub-basins.

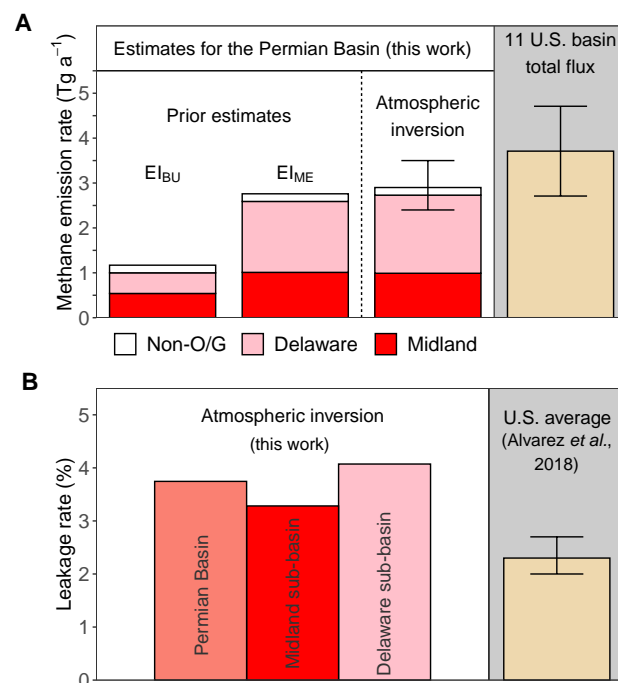


Fig. 4. Methane emission quantification for the Permian Basin. (A) Annual methane emissions from the Permian Basin from two prior emission inventories (EI_{BU} and EI_{ME}), and TROPOMI satellite data-based atmospheric inversion and a mass balance method. The breakdown for Delaware, Midland, and non-O/G sources is shown in pink, red, and white for EI_{BU} , EI_{ME} , and atmospheric inversion, respectively. The estimate for the Permian Basin is compared with total emissions from 11 U.S. basins reported in literature (7, 24, 25) (table S1). (B) Leakage rates for the Permian Basin and two sub-basins, in comparison with the average leakage reported for the entire United States (7).

small fraction of production sites (see Materials and Methods and text S2). As a comparison, we also apply a fast mass balance method following Buchwitz *et al.* (23) to estimate basin-level emissions, which yields an annual mean emission rate of $3.2 \pm 2.0 \text{ Tg a}^{-1}$ for the Permian Basin. This result is consistent with that derived from a full atmospheric inversion. Despite the large uncertainty of the mass balance method, this data-driven approach provides an independent estimate of emissions derived primarily using TROPOMI data (see text S3 for more discussion).

Removing the non-O/G sources (0.2 Tg a^{-1}) from the total flux obtained via the inversion (2.9 Tg a^{-1}), we estimate the methane emissions related to O/G activity to be 2.7 Tg a^{-1} in the Permian Basin. Put in the context of national emissions, this value is approximately one quarter of total emissions from all U.S. oil and gas production areas in 2015 (10.9 Tg a^{-1} , including emissions from production, gathering, and processing, which largely occur in the production areas) (7). Our estimated emission rate for the Permian is significantly higher than those reported in the literature for other major U.S. O/G-producing basins. Table S1 summarizes methane emission estimates for 11 U.S. basins (7, 24, 25) from previous aircraft-based studies [i.e., Haynesville (24, 26), Barnett (24, 27), Northeast Pennsylvania (26, 28), Southwest Pennsylvania (25), San Juan (12), Fayetteville (26, 29), Bakken (24, 30), Uinta (31), Weld (32), West Arkoma (26), Eagle Ford (24), and the Denver Basin (24)]. Our estimate for the Permian (2.7 Tg a^{-1}) is about a factor of 4 higher than the largest methane emissions from these previously reported O/G basins [i.e., Eagle Ford, 0.73 Tg a^{-1} (24)] and is even comparable to the 11-basin sum (3.7 Tg a^{-1}) (Fig. 4A and table S1). This comparison with recent literature indicates that the Permian Basin is likely the largest observed methane-emitting O/G basin in the United States and a substantial contributor to national O/G-related emissions.

Distribution of methane emissions

High-resolution observations from TROPOMI enable us to resolve methane emissions at an unprecedented spatial and temporal resolution, relative to the previous generation of satellite instruments such as the Greenhouse gases Observing SATellite (GOSAT) and SCIAMACHY (9). Figure 5 presents the spatial distribution of methane emissions in the Permian Basin at about a quarter-degree resolution derived from our atmospheric inversion. Compared to the prior inventory El_{BU} , our inversion finds larger methane emissions near the center of the Delaware and Midland sub-basins. Sensitivity inversions further show that this spatial pattern is robust against prior emissions of varied magnitudes and distributions (fig. S3), demonstrating that it is primarily informed by satellite observations.

The spatial distribution of methane emissions derived from inversion is closely correlated with that of gross gas production ($R = 0.78$), but to a lesser degree with that of oil production ($R = 0.53$) and that of the well number density ($R = 0.31$) (fig. S4). Similarly, when we sum up the O/G-related emissions for two sub-basins, the ratio of methane emissions between Delaware and Midland ($1.7/1.0 \text{ Tg a}^{-1} = 1.7$) is closest to the ratio of gas production (1.4), compared to that of oil production (1.0) and well number density (0.7). Because unconventional wells tend to have much higher production per well than conventional wells (33), the dependence of methane emissions on gross gas production rather than the well number density suggests that unconventional wells and infrastructure associated with these wells (e.g., gathering stations), which have been developed recently, are likely the major methane emitters in the Permian Basin.

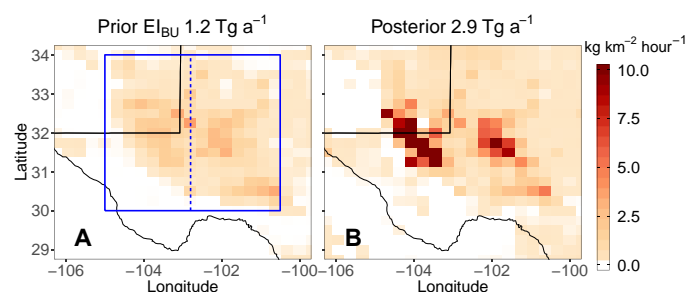


Fig. 5. Spatial distribution of methane emission rates in the Permian Basin. (A) Bottom-up emission inventory El_{BU} extrapolated from EPA greenhouse gas inventory data (prior). (B) TROPOMI observation-derived emissions using Bayesian atmospheric inverse modeling (posterior). The prior and posterior basin-total emissions, indicated on top of the figure, are computed over the area enclosed by the solid blue boundary, with contributions from two sub-basins, the Delaware (left of the dashed line) and Midland (right of the dashed line).

In addition to the spatial distribution, our monthly inversion also provides information about the temporal variation of methane emissions during the 11 months of observation (fig. S5). Although the inversion's ability to resolve the spatial distribution of emissions varies from month to month because of uneven monthly sampling of TROPOMI (fig. S5), our inversion ensemble (table S2 and fig. S5) generally results in consistent monthly basin-level emission estimates (see also uncertainty analysis in Materials and Methods). We speculate that high emissions in December 2018 may be related to a very low in-basin gas price toward the end of 2018, resulting from insufficient gas gathering and transmission capacity in the Permian Basin (33,34). That said, we do not find an apparent increasing trend in methane emissions, although natural gas production from the Permian Basin increased steadily by $\sim 20\%$ during the overlapping 11-month period (fig. S6). Further investigation is required to delineate factors controlling the temporal variations of O/G-related methane emissions.

DISCUSSION

Using an inverse analysis of TROPOMI satellite observations, we estimate a total methane flux of $2.9 \pm 0.5 \text{ Tg a}^{-1}$ in the Permian Basin, with 2.7 Tg a^{-1} coming from O/G-related activity. Methane losses of this magnitude represent a waste of an important resource; for instance, this is enough natural gas to supply 7 million households in the state of Texas (35). Moreover, the 2.7 Tg a^{-1} methane emitted in Permian results in the same radiative forcing as $\sim 260 \text{ Tg a}^{-1} \text{ CO}_2$ over a 20-year time horizon ($86 \text{ Tg CO}_2 \text{ a}^{-1}$ over a 100-year time horizon) (global warming potential of 96 for 20 years and 32 for 100 years) (7, 36), about the same as annual CO_2 emissions from the entire U.S. residential sector ($290 \text{ Tg CO}_2 \text{ a}^{-1}$ in 2017) (22).

Our estimate (2.7 Tg a^{-1}) equates to a production-normalized ($73 \text{ Tg CH}_4 \text{ a}^{-1}$, derived from $127 \text{ billion m}^3 \text{ a}^{-1}$ natural gas production during the study period using 80% methane content by volume) emission rate (or methane leakage rate) of $3.7 \pm 0.7\%$, which is $\sim 60\%$ higher than the national average of $2.3 \pm 0.3\%$ (7) (Fig. 4B). The leakage rate is even higher for the rapidly developing Delaware sub-basin (4.1%). Comparable high leakage rates have also been reported in other oil production-focused basins such as the Bakken (24) (table S1), but these basins produce much lower natural gas than the Permian Basin does. Previous studies summarized in table

S1 show an inverse relationship between the basin-level leakage rate and gas production (24); however, the Permian Basin is an outlier with high oil production, high gas production, and a high leakage rate.

Overall, the high leakage rate in the Permian Basin appears to be associated with insufficient infrastructure for natural gas gathering, processing, and transportation (34, 37), leading to extensive venting and flaring (Fig. 3), which contributes to high methane emissions. The greater profitability of oil production contributes to a lack of investment in natural gas takeaway capacity, which, in turn, has resulted in excessive supply of associated gas and a very low in-basin gas price in the Permian (34). In addition, with the rescinding of U.S. federal requirements on gas capture and fugitive emissions in 2018, current regulations on O/G methane emissions in the Permian Basin are less stringent at both federal and state levels (see text S4). All these factors may increase the incentive for operators to vent and flare their product. On the other hand, the higher-than-average leakage rate in the Permian Basin implies an opportunity to reduce methane emissions in this rapidly growing oil and gas-producing region, through better design, effective management, regulation, and infrastructure development.

MATERIALS AND METHODS

TROPOMI methane observations

We use daily column-averaged dry air column methane mixing ratio (XCH_4) data retrieved from TROPOMI measurements (38) between May 2018 and March 2019. TROPOMI, onboard the polar-orbiting Sentinel-5 Precursor satellite, is a push-broom imaging spectrometer that provides near-daily global coverage with a swath width of 2600 km and a nadir ground pixel size of $7 \text{ km} \times 7 \text{ km}$ at approximately 13:30 local overpass time (17). The retrieval algorithm accounts for the “full physics” of the light path by simultaneously inferring methane concentrations and physical scattering properties, using the oxygen A-band in the near infrared (NIR) and the methane absorption band in the short-wave infrared (SWIR) (39). Only high-quality XCH_4 measurements retrieved under cloud-free conditions are used in this study (as indicated by the retrieval quality assurance flags in TROPOMI data product). These measurements are filtered for solar zenith angle ($<70^\circ$), low viewing zenith angle ($<60^\circ$), smooth topography (1 SD of surface elevation $<80 \text{ m}$ within 5-km radius), and low aerosol load (aerosol optical thickness <0.3 in NIR) (40).

The TROPOMI XCH_4 product is further corrected for any known retrieval biases (40). The errors in the TROPOMI XCH_4 measurements have been assessed against GOSAT XCH_4 data (38) and were found to correlate with surface albedo. A global bias correction linearly dependent on surface albedo was then derived and applied to the TROPOMI data (40). This bias-corrected TROPOMI XCH_4 product is used in this study. Negligible correlation of errors with other retrieved parameters (e.g., aerosol optical thickness) was found in the assessment. Validation with independent ground-based measurements from the Total Column Carbon Observing Network shows that the bias-corrected TROPOMI XCH_4 has a bias of $-4.3 \pm 7.4 \text{ ppbv}$, improved upon the uncorrected XCH_4 product ($-12 \pm 11.5 \text{ ppbv}$) (40). In addition, we also examine the correlation between bias-corrected XCH_4 and other retrieved parameters for the subset of TROPOMI data over the domain of this study. We find no correlation with albedo ($R^2 = 0.00$) and a negligible correlation with aerosol optical thickness ($R^2 = 0.07$), supporting the idea that the XCH_4 enhancement over the Permian Basin (Fig. 1B) is robust.

Figure S7A shows the average XCH_4 over the conterminous United States and the Permian Basin between May 2018 and March 2019 before the topographical correction. We derive the elevation-corrected methane column (XCH_4^t) shown in Fig. 1 by applying a third-order polynomial correction fitted over the U.S. domain following Kort *et al.* (10). The mass balance method uses the elevation-corrected data (XCH_4^t) for emission quantification, while the inversion method uses XCH_4 (bias-corrected) directly obtained from the data product, because the topography effect is taken care of by the atmospheric transport model.

Atmospheric inverse modeling

We perform an inverse analysis of TROPOMI observations to derive optimized estimation of monthly methane emissions at $0.25^\circ \times 0.3125^\circ$ horizontal resolution in the Permian Basin. Quantification of emissions at this combination of relatively high spatial and temporal resolution, not achievable with previous generations of satellite observations such as from GOSAT or SCIAMACHY, is enabled by higher-resolution TROPOMI satellite observations (41). Figure S7B shows that the Permian Basin is well sampled by TROPOMI during the study period, likely because of frequent cloud-free conditions in the region. A total of ~200,000 TROPOMI XCH_4 retrievals within the study domain ($29^\circ\text{--}34^\circ\text{N}$, $100^\circ\text{--}106^\circ\text{W}$) between May 2018 and March 2019 are used for the inversion.

Let \mathbf{x} be the state vector that we seek to optimize through inversion, including a gridded ensemble of methane emissions and an additional element representing the regional model bias in XCH_4 . The regional model bias term (a monthly scalar uniform over the inversion domain) is necessary to account for spatially uniform biases caused by imperfect lateral boundary condition and emission errors outside the study domain. The inversion solves for an optimal estimate of \mathbf{x} by minimizing the following cost function

$$J(\mathbf{x}) = (\mathbf{x} - \mathbf{x}_A)^T \mathbf{S}_A^{-1} (\mathbf{x} - \mathbf{x}_A) + (\mathbf{y} - \mathbf{K}\mathbf{x})^T \mathbf{S}_O^{-1} (\mathbf{y} - \mathbf{K}\mathbf{x}) \quad (1)$$

where TROPOMI XCH_4 observations are assembled in \mathbf{y} , \mathbf{x}_A is the prior estimate of \mathbf{x} , \mathbf{S}_A is the prior error covariance matrix, \mathbf{S}_O is the observational error covariance matrix, and \mathbf{K} is the Jacobian matrix describing the sensitivity of XCH_4 to emissions and the regional model bias ($\partial\mathbf{y}/\partial\mathbf{x}$).

Minimization of Eq. 1 at $\nabla_{\mathbf{x}} J(\mathbf{x}) = 0$ yields the posterior estimation ($\hat{\mathbf{x}}$), the posterior error covariance matrix ($\hat{\mathbf{S}}$), and the averaging kernel matrix (\mathbf{A}) (42)

$$\hat{\mathbf{x}} = \mathbf{x}_A + \mathbf{S}_A \mathbf{K}^T (\mathbf{K} \mathbf{S}_A \mathbf{K}^T + \mathbf{S}_O)^{-1} (\mathbf{y} - \mathbf{K} \mathbf{x}_A) \quad (2)$$

$$\hat{\mathbf{S}} = (\mathbf{K}^T \mathbf{S}_O^{-1} \mathbf{K} + \mathbf{S}_A^{-1})^{-1} \quad (3)$$

$$\mathbf{A} = \mathbf{I}_n - \hat{\mathbf{S}} \mathbf{S}_A^{-1} \quad (4)$$

Here, \mathbf{I}_n is an identity matrix where n is the dimension of the state vector \mathbf{x} . The trace of \mathbf{A} , often called as the degrees of freedom for signal (DOFS), quantifies the number of pieces of information constraining the n -dimensional state vector.

To solve for Eqs. 2 to 4, the prior estimate (\mathbf{x}_A) for gridded methane emissions is required. Using different sources of information, we create two gridded emission inventories for the study region: one based on bottom-up information (EI_{BU}) and the other based on extrapolation

of ground-based site-level measurements (EI_{ME}) (see below for descriptions of the inventories). Both emission inventories are time invariant. We use EI_{BU} as the prior estimate in the base inversion, while we use EI_{ME} in a sensitivity inversion to evaluate the impact of the prior estimate ($PI_{EI_{ME}}$; see table S2). We perform further evaluations using prior emissions constructed by disaggregating the total O/G-related emission flux from EI_{BU} with varied spatial proxies (i.e., well count, $PI_{EI_{well}}$, natural gas production, $PI_{EI_{gas}}$, and oil production, $PI_{EI_{oil}}$) (table S2 and fig. S3).

The difference between the EI_{BU} and EI_{ME} (Fig. 5A and fig. S3A) measures the uncertainty of our prior knowledge, and we thus specify prior errors (S_A) for emissions as the absolute difference between EI_{BU} and EI_{ME} . We also specify the prior error for the regional model XCH_4 bias as 10 ppbv. To test the sensitivity to prior errors, we perturb S_A in two sensitivity inversions by doubling ($PE \times 2$) or halving ($PE \times 0.5$) prior errors (table S2). S_O is constructed with the residual error method (43), which results in an error averaged at ~ 11 ppbv. Both S_O and S_A are taken to be diagonal matrices. We also perform a sensitivity inversion to test the impact of error correlations with off-diagonal terms specified following Cusworth *et al.* (44) (OE_Cor; see table S2).

A nested version of the GEOS-Chem chemical transport model (12.1.0) is used as the forward model in the inversion to link XCH_4 to surface emissions. To account for the vertical sensitivity of the satellite instrument, we compute simulated XCH_4 by applying TROPOMI averaging kernels to simulated methane vertical profiles. We construct the Jacobian matrix K , column by column, with simulations perturbing each state vector element independently. The simulations are performed over North America and adjacent oceans driven by GEOS-FP-assimilated meteorological data from the NASA Global Modeling and Assimilation Office on a $0.25^\circ \times 0.3125^\circ$ horizontal grid and 47 vertical layers (~ 30 layers in the troposphere) (21). The boundary conditions for the nested-grid simulation are from a $4^\circ \times 5^\circ$ global simulation from May 2018 to March 2019 driven by GEOS-FP meteorological fields. Note that methane emissions and sinks used in this simulation are optimized with previous-year (2010–2017) GOSAT satellite data following Maasakkers *et al.* (3). Such generated boundary conditions may be biased (i.e., unable to capture the growth of global methane concentrations; see fig. S9), and we account for it by introducing a monthly regional model bias term in the inversion. The retrieved regional model biases may vary with the extent of the inversion domain. To test this sensitivity, we also perform an inversion with a larger spatial domain (27° – 36° N, 98° – 108° W) (Bg_Large; see table S2).

Inversion uncertainty

The posterior error covariance matrix (\hat{S} , Eq. 2) and averaging kernel matrix (A , Eq. 3) evaluate the uncertainty of an inversion solution given inversion parameters (e.g., S_A , S_O , forward model). Figure S5 shows monthly posterior errors for basin-level emissions (derived from \hat{S}) and corresponding DOFS (trace of A) from our base inversion. Overall, the posterior errors for basin-level emissions are $<5\%$ of the estimated emission flux, and the DOFS are between 5 and 30 for the monthly inversion, indicating that the TROPOMI data are able to constrain basin-level methane emissions and partially resolve the spatial distribution on a monthly basis. The monthly variations in the posterior error and DOFS are mainly driven by uneven data coverage from TROPOMI sampling. For example, poor data coverage

in November 2018 results in a large posterior error and a small DOFS (fig. S5).

We also perform an ensemble of sensitivity inversions by perturbing the configurations and parameters in the base inversion (table S2), aiming to characterize the uncertainties resulting from assumptions made in the inversion not captured by the analytical posterior error. Our results show that all these sensitivity inversions lead to consistent basin-level emission estimates. Annual mean fluxes from sensitivity inversions are within 0.5 Tg a^{-1} of that from our base inversion (table S2), with general agreement in monthly variations as well (fig. S5). Because the uncertainty resulting from sensitivity inversions are significantly larger than that deduced from posterior error covariance matrix (fig. S5), we report the uncertainty of our basin-level emission estimate (0.5 Tg a^{-1}) as half of the range from the inversion ensemble (2.4 to 3.4 Tg a^{-1}).

Furthermore, to assess the uncertainty due to model transport, we compare hourly GEOS-FP 10-m wind speed against measurements at the Midland Airport (MAF) in the Permian Basin during the period of May 2018 and March 2019. Airport wind measurements are not assimilated in the GEOS-FP reanalysis (45), so these observations are independent. We find that the GEOS-FP 10-m wind speed compares well with the airport measurements in both daytime and nighttime (fig. S8), with mean biases of less than 6% in the mean wind speed. We conclude that errors in the model wind fields are unlikely to be a major source of error in the inversion.

We introduced a regional model bias term in monthly inversions to correct for regional background biases in simulated methane concentrations, which result mainly from imperfect boundary conditions. To check our estimate for this regional bias term, we sample the model simulation to compare with independent observations, i.e., surface measurements at the Mauna Loa Observatory (MLO; a Pacific free tropospheric site upwind of the North American continent) (46), tower measurements at Moody, Texas (WKT) (47), and aircraft measurements offshore Corpus Christi, Texas (TGC) (48). The latter two sites are geographically much closer to the Permian Basin (~ 400 km from WKT and ~ 700 km from TGC) than MLO, but can be affected by local emissions that are not optimized in our inversion. Our results show that the model simulation, when corrected with monthly regional model biases (derived from monthly inversions over the Permian Basin), is able to capture the observed monthly variation in methane concentrations, notably the sharp increase from August to October 2018 in MLO and WKT observations (fig. S9), supporting that it is necessary to optimize the regional model bias in the inversion. Better agreement is observed at MLO and TGC compared to WKT (fig. S9), likely because WKT is located closer to local sources that are not fully optimized in the inversion. Overall, most of the differences between the prior simulation and TROPOMI observations can be explained by the regional model biases, except for the mismatch in the vicinity of the Permian Basin (fig. S2). We further perform a sensitivity inversion with a varied spatial domain (Bg_Large). Compared to the base inversion, Bg_Large results in a lower regional methane background (by 3 ppbv on average) and a higher methane emission flux (3.4 Tg a^{-1}) (table S2 and fig. S5), reflecting the error correlation between regional methane biases and methane emissions.

In addition, we note that the inversion cannot fully explain the methane enhancement extending outside the Delaware Basin in the northwest direction (near 33° N, 105° W), although the inversion overall substantially improves the agreement between observations

and model simulations (fig. S2). While our investigations do not attribute an obvious source of emissions causing the northwestern enhancement (whether oil/gas or other sources), the basin-level O/G emission estimates presented here are robust if this enhancement is caused by non-O/G sources, but are conservative if it is caused by O/G sources.

Emission inventory based on bottom-up information

We create a bottom-up methane emission estimate (EI_{BU}) for the study domain starting from the gridded version of the EPA anthropogenic greenhouse gas emission inventory for 2012 (49). Maasakkers *et al.* (49) developed a procedure to spatially and temporally allocate the national sectorial methane emissions reported in the U.S. Inventory of Greenhouse Gas Emissions and Sinks (GHGI) by U.S. EPA on a $0.1^\circ \times 0.1^\circ$ grid, using various databases at the state, county, local, and point-source level. The emission inventory includes methane emissions from agriculture, coal mining, natural gas systems, petroleum (oil) systems, waste, and other minor anthropogenic sources.

To reflect the intensifying exploitation activity in recent years in the Permian Basin, we then make an extrapolation of the methane emissions from the oil and gas production sector, using 2018 Enverus Drillinginfo data on well count, well completion, and production (50). To account for the changes in the national average emission factors, we further scale the subsectorial production emissions using the ratio between the latest GHGI (22) and a previous GHGI that Maasakkers *et al.* (49) was based on (51) for 2013 emissions. The updates result in total methane emissions of 1.2 Tg a^{-1} in the Permian Basin (blue box in Fig. 5A), with 1.0 Tg a^{-1} coming from O/G-related emissions and the remainder mainly from agriculture. We use this updated gridded emission inventory (EI_{BU}) as the prior emission estimate for the inversion. The resulting emissions inventory dataset (EI_{BU} inventory) is publicly available for our study region encompassing the entire Permian Basin (<https://doi.org/10.7910/DVN/NWQGHU>).

Emission inventory based on site-level emission measurements

An alternative prior estimation of methane emissions is obtained by extrapolating ground-based methane emission measurements from a limited sample of oil and gas production sites in the Permian Basin (primarily in the New Mexico portion of the basin) during July and August 2018 (52). The measurements found a wide range of site-level emission rates, which appear to be associated with the complexity of infrastructure, and were classified into emission rates for simple (with only wellheads and/or pump jacks) versus complex sites (also with storage tanks and/or compressors). Extrapolating these site-level emission rates to the entire Permian gave a basin-level methane emission rate of 2.3 Tg a^{-1} from O/G production. Additional emissions from compressor stations and processing plants are estimated to be 0.22 and 0.14 Tg a^{-1} , respectively, using activity data from Enverus Drillinginfo's midstream infrastructure dataset, facility-level emission factors from literature (53, 54), and blowdown event emission factors from GHGI (22). We then disaggregate the basin-level O/G-related emissions to a $0.1^\circ \times 0.1^\circ$ grid by the spatial distribution of gas production (Fig. 2D). To complete the inventory, non-O/G anthropogenic methane emissions (0.2 Tg a^{-1}) are taken from EI_{BU} . This emission inventory (EI_{ME}), based primarily on extrapolation of limited site-level measurements, provides an alternative prior estimate for the inversion and is used to test the sensitivity of the results to the choice of prior information (fig. S3). See text S2 for detailed infor-

mation regarding the site-level measurements and the extrapolation procedure. The resulting emissions inventory dataset (EI_{ME} inventory) is publicly available for our study region encompassing the entire Permian Basin (<https://doi.org/10.7910/DVN/NWQGHU>).

SUPPLEMENTARY MATERIALS

Supplementary material for this article is available at <http://advances.sciencemag.org/cgi/content/full/6/17/eaaz5120/DC1>

REFERENCES AND NOTES

1. D. Shindell, J. C. I. Kuylenstierna, E. Vignati, R. van Dingenen, M. Amann, Z. Klimont, S. C. Anenberg, N. Muller, G. Janssens-Maenhout, F. Raes, J. Schwartz, G. Faluvegi, L. Pozzoli, K. Kupiainen, L. Höglund-Isaksson, L. Emberson, D. Streets, V. Ramanathan, K. Hicks, N. T. K. Oanh, G. Milly, M. Williams, V. Demkina, D. Fowler, Simultaneously mitigating near-term climate change and improving human health and food security. *Science* **335**, 183–189 (2012).
2. G. Myhre, D. Shindell, F.-M. Bréon, W. Collins, J. Fuglestad, J. Huang, D. Koch, J.-F. Lamarque, D. Lee, B. Mendoza, T. Nakajima, A. Robock, G. Stephens, T. Takemura, H. Zhang, Anthropogenic and natural radiative forcing, in *Climate Change 2013: The Physical Science Basis. Contribution of Working Group I to the Fifth Assessment Report of the Intergovernmental Panel on Climate Change*, T. F. Stocker, D. Qin, G.-K. Plattner, M. Tignor, S. K. Allen, J. Boschung, A. Nuares, Y. Xia, V. Bex, P. M. Midgley, Eds. (Cambridge Univ. Press, 2013), pp. 659–740.
3. J. D. Maasakkers, D. J. Jacob, M. P. Sulprizio, T. R. Scarpelli, H. Nesser, J.-X. Sheng, Y. Zhang, M. Hersher, A. A. Bloom, K. W. Bowman, J. R. Worden, G. Janssens-Maenhout, R. J. Parker, Global distribution of methane emissions, emission trends, and OH concentrations and trends inferred from an inversion of GOSAT satellite data for 2010–2015. *Atmos. Chem. Phys.* **19**, 7859–7881 (2019).
4. S. Schwietzke, O. A. Sherwood, L. M. P. Bruhwiler, J. B. Miller, G. Etiope, E. J. Dlugokencky, S. E. Michel, V. A. Arling, B. H. Vaughn, J. W. C. White, P. P. Tans, Upward revision of global fossil fuel methane emissions based on isotope database. *Nature* **538**, 88–91 (2016).
5. B. Hmiel, V. V. Petrenko, M. N. Dyonisius, C. Buizert, A. M. Smith, P. F. Place, C. Harth, R. Beaudette, Q. Hua, B. Yang, I. Vimont, S. E. Michel, J. P. Severinghaus, D. Etheridge, T. Bromley, J. Schmitt, X. Fain, R. F. Weiss, E. Dlugokencky, Preindustrial $^{14}\text{CH}_4$ indicates greater anthropogenic fossil CH_4 emissions. *Nature* **578**, 409–412 (2020).
6. R. A. Alvarez, S. W. Pacala, J. J. Winebrake, W. L. Chameides, S. P. Hamburg, Greater focus needed on methane leakage from natural gas infrastructure. *Proc. Natl. Acad. Sci. U.S.A.* **109**, 6435–6440 (2012).
7. R. A. Alvarez, D. Zavala-Araiza, D. R. Lyon, D. T. Allen, Z. R. Barkley, A. R. Brandt, K. J. Davis, S. C. Herndon, D. J. Jacob, A. Karion, E. A. Kort, B. K. Lamb, T. Lauvaux, J. D. Maasakkers, A. J. Marchese, M. Omara, S. W. Pacala, J. Peischl, A. L. Robinson, P. B. Shepson, C. Sweeney, A. Townsend-Small, S. C. Wofsy, S. P. Hamburg, Assessment of methane emissions from the U.S. oil and gas supply chain. *Science* **361**, 186–188 (2018).
8. EPA, Inventory of US greenhouse gas emissions and sinks: 1990–2015 (2017); <https://www.epa.gov/ghgemissions/inventory-us-greenhouse-gas-emissions-and-sinks-1990-2015>.
9. D. J. Jacob, A. J. Turner, J. D. Maasakkers, J. Sheng, K. Sun, X. Liu, K. Chance, I. Aben, J. McKeever, C. Frankenberg, Satellite observations of atmospheric methane and their value for quantifying methane emissions. *Atmos. Chem. Phys.* **16**, 14371–14396 (2016).
10. E. A. Kort, C. Frankenberg, K. R. Costigan, R. Lindenmaier, M. K. Dubey, D. Wunch, Four corners: The largest US methane anomaly viewed from space. *Geophys. Res. Lett.* **41**, 6898–6903 (2014).
11. C. Frankenberg, A. K. Thorpe, D. R. Thompson, G. Hulley, E. A. Kort, N. Vance, J. Borchardt, T. Krings, K. Gerilowski, C. Sweeney, S. Conley, B. D. Bue, A. D. Aubrey, S. Hook, R. O. Green, Airborne methane remote measurements reveal heavy-tail flux distribution in Four Corners region. *Proc. Natl. Acad. Sci. U.S.A.* **113**, 9734–9739 (2016).
12. M. L. Smith, A. Gvakharia, E. A. Kort, C. Sweeney, S. A. Conley, I. Faloona, T. Newberger, R. Schnell, S. Schwietzke, S. Wolter, Airborne quantification of methane emissions over the four corners region. *Environ. Sci. Technol.* **51**, 5832–5837 (2017).
13. EIA, Drilling productivity report; <https://www.eia.gov/petroleum/drilling/> [accessed 1 May 2019].
14. C. Krauss, "The 'monster' Texas oil field that made the U.S. a star in the world market," *New York Times*, 2019.
15. K. A. Willyard, G. W. Schade, Flaring in two Texas shale areas: Comparison of bottom-up with top-down volume estimates for 2012 to 2015. *Sci. Total Environ.* **691**, 243–251 (2019).
16. SRON, S5P Mission Performance Centre Methane [L2__CH4__] Readme, S5P-MPC-SRON-PRF-CH4, V01.03.02 (2019).

17. J. P. Veeffkind, I. Aben, K. McMullan, H. Förster, J. de Vries, G. Otter, J. Claas, H. J. Eskes, J. F. de Haan, Q. Kleipool, M. van Weele, O. Hasekamp, R. Hoogeveen, J. Landgraf, R. Snel, P. Tol, P. Ingmann, R. Voors, B. Kruizinga, R. Vink, H. Visser, P. F. Levelt, TROPOMI on the ESA Sentinel-5 Precursor: A GMES mission for global observations of the atmospheric composition for climate, air quality and ozone layer applications. *Remote Sens. Environ.* **120**, 70–83 (2012).
18. EIA, The Wolfcamp play has been key to Permian Basin oil and natural gas production growth (2018); <https://www.eia.gov/todayinenergy/detail.php?id=37532#tab1> [accessed 18 August 2019].
19. Y. Zhang, R. Gautam, D. Zavala-Araiza, D. J. Jacob, R. Zhang, L. Zhu, J.-X. Sheng, T. Scarpelli, Satellite-observed changes in Mexico's offshore gas flaring activity linked to oil/gas regulations. *Geophys. Res. Lett.* **46**, 1879–1888 (2019).
20. B. N. Duncan, L. N. Lamsal, A. M. Thompson, Y. Yoshida, Z. Lu, D. G. Streets, M. M. Hurwitz, K. E. Pickering, A space-based, high-resolution view of notable changes in urban NO_x pollution around the world (2005–2014). *J. Geophys. Res. Atmos.* **121**, 976–996 (2016).
21. J. X. Sheng, D. J. Jacob, A. J. Turner, J. D. Maasakkers, M. P. Sulprizio, A. A. Bloom, A. E. Andrews, D. Wunch, High-resolution inversion of methane emissions in the Southeast US using SEAC⁴RS aircraft observations of atmospheric methane: Anthropogenic and wetland sources. *Atmos. Chem. Phys.* **18**, 6483–6491 (2018).
22. EPA, Inventory of US greenhouse gas emissions and sinks: 1990–2017 (2019); <https://www.epa.gov/ghgemissions/inventory-us-greenhouse-gas-emissions-and-sinks-1990-2017>.
23. M. Buchwitz, O. Schneising, M. Reuter, J. Heymann, S. Krautwurst, H. Bovensmann, J. P. Burrows, H. Boesch, R. J. Parker, P. Somkuti, R. G. Detmers, O. P. Hasekamp, I. Aben, A. Butz, C. Frankenberg, A. J. Turner, Satellite-derived methane hotspot emission estimates using a fast data-driven method. *Atmos. Chem. Phys.* **17**, 5751–5774 (2017).
24. J. Peischl, S. J. Eilerman, J. A. Neuman, K. C. Aikin, J. de Gouw, J. B. Gilman, S. C. Herndon, R. Nadkarni, M. Trainer, C. Warneke, T. B. Ryerson, Quantifying methane and ethane emissions to the atmosphere from Central and Western U.S. oil and natural gas production regions. *J. Geophys. Res. Atmos.* **123**, 7725–7740 (2018).
25. X. Ren, D. L. Hall, T. Vinciguerra, S. E. Benish, P. R. Stratton, D. Ahn, J. R. Hansford, M. D. Cohen, S. Sahu, H. He, C. Grimes, J. D. Fuentes, P. B. Shepson, R. J. Salawitch, S. H. Ehrman, R. R. Dickerson, Methane emissions from the Marcellus Shale in Southwestern Pennsylvania and Northern West Virginia based on airborne measurements. *J. Geophys. Res. Atmos.* **124**, 1862–1878 (2019).
26. J. Peischl, T. B. Ryerson, K. C. Aikin, J. A. de Gouw, J. B. Gilman, J. S. Holloway, B. M. Lerner, R. Nadkarni, J. A. Neuman, J. B. Nowak, M. Trainer, C. Warneke, D. D. Parrish, Quantifying atmospheric methane emissions from the Haynesville, Fayetteville, and northeastern Marcellus shale gas production regions. *J. Geophys. Res. Atmos.* **120**, 2119–2139 (2015).
27. A. Karion, C. Sweeney, E. A. Kort, P. B. Shepson, A. Brewer, M. Cambaliza, S. A. Conley, K. Davis, A. Deng, M. Hardesty, S. C. Herndon, T. Lauvaux, T. Lavoie, D. Lyon, T. Newberger, G. Pétron, C. Rella, M. Smith, S. Wolter, T. I. Yacovitch, P. Tans, Aircraft-based estimate of total methane emissions from the Barnett Shale region. *Environ. Sci. Technol.* **49**, 8124–8131 (2015).
28. Z. R. Barkley, T. Lauvaux, K. J. Davis, A. Deng, N. L. Miles, S. J. Richardson, Y. Cao, C. Sweeney, A. Karion, M. K. Smith, E. A. Kort, S. Schwietzke, T. Murphy, G. Cervone, D. Martins, J. D. Maasakkers, Quantifying methane emissions from natural gas production in north-eastern Pennsylvania. *Atmos. Chem. Phys.* **17**, 13941–13966 (2017).
29. S. Schwietzke, G. Pétron, S. Conley, C. Pickering, I. Mielke-Maday, E. J. Dlugokencky, P. P. Tans, T. Vaughn, C. Bell, D. Zimmerle, S. Wolter, C. W. King, A. B. White, T. Coleman, L. Bianco, R. C. Schnell, Improved mechanistic understanding of natural gas methane emissions from spatially resolved aircraft measurements. *Environ. Sci. Technol.* **51**, 7286–7294 (2017).
30. J. Peischl, A. Karion, C. Sweeney, E. A. Kort, M. L. Smith, A. R. Brandt, T. Yeskoo, K. C. Aikin, S. A. Conley, A. Gvakharia, M. Trainer, S. Wolter, T. B. Ryerson, Quantifying atmospheric methane emissions from oil and natural gas production in the Bakken shale region of North Dakota. *J. Geophys. Res. Atmos.* **121**, 6101–6111 (2016).
31. A. Karion, C. Sweeney, G. Pétron, G. Frost, R. Michael Hardesty, J. Kofler, B. R. Miller, T. Newberger, S. Wolter, R. Banta, A. Brewer, E. Dlugokencky, P. Lang, S. A. Montzka, R. Schnell, P. Tans, M. Trainer, R. Zamora, S. Conley, Methane emissions estimate from airborne measurements over a western United States natural gas field. *Geophys. Res. Lett.* **40**, 4393–4397 (2013).
32. G. Pétron, A. Karion, C. Sweeney, B. R. Miller, S. A. Montzka, G. J. Frost, M. Trainer, P. Tans, A. Andrews, J. Kofler, D. Helmig, D. Guenther, E. Dlugokencky, P. Lang, T. Newberger, S. Wolter, B. Hall, P. Novelli, A. Brewer, S. Conley, M. Hardesty, R. Banta, A. White, D. Noone, D. Wolfe, R. Schnell, A new look at methane and nonmethane hydrocarbon emissions from oil and natural gas operations in the Colorado Denver-Julesburg Basin. *J. Geophys. Res. Atmos.* **119**, 6836–6852 (2014).
33. M. Omara, M. R. Sullivan, X. Li, R. Subramanian, A. L. Robinson, A. A. Presto, Methane emissions from conventional and unconventional natural gas production sites in the marcellus shale basin. *Environ. Sci. Technol.* **50**, 2099–2107 (2016).
34. RBN Energy, "Hell In Texas—Permian gas takeaway headed for capacity wall," RBN Energy Drill Down Report (2018).
35. EIA, Natural gas consumption by end use; https://www.eia.gov/dnav/ng/ng_cons_sum_dcu_STX_a.htm. [accessed 20 August 2019].
36. M. Etminan, G. Myhre, E. J. Highwood, K. P. Shine, Radiative forcing of carbon dioxide, methane, and nitrous oxide: A significant revision of the methane radiative forcing. *Geophys. Res. Lett.* **43**, 12,614–12,623 (2016).
37. T. Curtis, B. Montalbano, *The Permian Basin Produces Gas, Too—Permian Basin Oil and Gas Production Growth: A Case Study for Gas Infrastructure Needs in the U.S.* (Energy Policy Research Foundation Inc., 2018).
38. H. Hu, J. Landgraf, R. Detmers, T. Borsdorff, J. A. de Brugh, I. Aben, A. Butz, O. Hasekamp, Toward global mapping of methane with TROPOMI: First results and intersatellite comparison to GOSAT. *Geophys. Res. Lett.* **45**, 3682–3689 (2018).
39. H. Hu, O. Hasekamp, A. Butz, A. Galli, J. Landgraf, J. A. de Brugh, T. Borsdorff, R. Scheepmaker, I. Aben, The operational methane retrieval algorithm for TROPOMI. *Atmos. Meas. Tech.* **9**, 5423–5440 (2016).
40. O. Hasekamp, A. Lorente, H. Hu, A. Butz, J. A. de Brugh, J. Landgraf, "Algorithm theoretical baseline document for Sentinel-5 Precursor methane retrieval (issue 1.10), SRON-S5P-LEV2-RP-001" (SRON, 2019).
41. J.-X. Sheng, D. J. Jacob, J. D. Maasakkers, Y. Zhang, M. P. Sulprizio, Comparative analysis of low-Earth orbit (TROPOMI) and geostationary (GeoCARB, GEO-CAPE) satellite instruments for constraining methane emissions on fine regional scales: Application to the Southeast US. *Atmos. Meas. Tech.* **11**, 6379–6388 (2018).
42. G. P. Brasseur, D. J. Jacob, *Modeling of Atmospheric Chemistry* (Cambridge Univ. Press, 2017).
43. C. L. Heald, D. J. Jacob, D. B. A. Jones, P. I. Palmer, J. A. Logan, D. G. Streets, G. W. Sachse, J. C. Gille, R. N. Hoffman, T. Nehrkorn, Comparative inverse analysis of satellite (MOPITT) and aircraft (TRACE-P) observations to estimate Asian sources of carbon monoxide. *J. Geophys. Res. Atmos.* **109**, D23306 (2004).
44. D. H. Cusworth, D. J. Jacob, J.-X. Sheng, J. Benmergui, A. J. Turner, J. Brandman, L. White, C. A. Randles, Detecting high-emitting methane sources in oil/gas fields using satellite observations. *Atmos. Chem. Phys.* **18**, 16885–16896 (2018).
45. M. M. Rienecker, M. J. Suarez, R. Todling, J. Bacmeister, L. Takacs, H.-C. Liu, W. Gu, M. Sienkiewicz, R. D. Koster, R. Gelaro, I. Stajner, J. E. Nielsen, "The GEOS-5 data assimilation system—Documentation of versions 5.0.1, 5.1.0, and 5.2.0" (NASA Tech. Rep. NASA/TM-2008-104606, NASA, 2008), vol. 27, 118 pp.; <https://gmao.gsfc.nasa.gov/pubs/docs/Rienecker369.pdf>.
46. E. J. Dlugokencky, A. M. Crotwell, P. M. Lang, J. W. Mund, M. E. Rhodes, Atmospheric methane dry air mole fractions from quasi-continuous measurements at Barrow, Alaska and Mauna Loa, Hawaii, 1986–2017, version: 2019-06-21; ftp://aftp.cmdl.noaa.gov/data/trace_gases/ch4/in-situ/surface/ (2018).
47. A. E. Andrews, J. D. Kofler, M. E. Trudeau, J. C. Williams, D. H. Neff, K. A. Masarie, D. Y. Chao, D. R. Kitzis, P. C. Novelli, C. L. Zhao, E. J. Dlugokencky, P. M. Lang, M. J. Crotwell, M. L. Fischer, M. J. Parker, J. T. Lee, D. D. Baumann, A. R. Desai, C. O. Stanier, S. F. J. De Wekker, D. E. Wolfe, J. W. Munger, P. P. Tans, CO₂, CO, and CH₄ measurements from tall towers in the NOAA Earth System Research Laboratory's Global Greenhouse Gas Reference Network: Instrumentation, uncertainty analysis, and recommendations for future high-accuracy greenhouse gas monitoring efforts. *Atmos. Meas. Tech.* **7**, 647–687 (2014).
48. C. Sweeney, A. Karion, S. Wolter, T. Newberger, D. Guenther, J. A. Higgs, A. E. Andrews, P. M. Lang, D. Neff, E. Dlugokencky, J. B. Miller, S. A. Montzka, B. R. Miller, K. A. Masarie, S. C. Biraud, P. C. Novelli, M. Crotwell, A. M. Crotwell, K. Thoning, P. P. Tans, Seasonal climatology of CO₂ across North America from aircraft measurements in the NOAA/ESRL Global Greenhouse Gas Reference Network. *J. Geophys. Res. Atmos.* **120**, 5155–5190 (2015).
49. J. D. Maasakkers, D. J. Jacob, M. P. Sulprizio, A. J. Turner, M. Weitz, T. Wirth, C. Hight, M. DeFigueiredo, M. Desai, R. Schmeltz, L. Hockstad, A. A. Bloom, K. W. Bowman, S. Jeong, M. L. Fischer, Gridded national inventory of U.S. methane emissions. *Environ. Sci. Technol.* **50**, 13123–13133 (2016).
50. Enverus DrillingInfo, DI Desktop (2019); didesktop.com.
51. EPA, Inventory of US greenhouse gas emissions and sinks: 1990–2014 (2016); <https://www.epa.gov/ghgemissions/inventory-us-greenhouse-gas-emissions-and-sinks-1990-2014>.
52. EDF, New Mexico oil & gas data (2019); <https://www.edf.org/nm-oil-gas/> [accessed 18 August 2019].
53. A. J. Marchese, T. L. Vaughn, D. J. Zimmerle, D. M. Martinez, L. L. Williams, A. L. Robinson, A. L. Mitchell, R. Subramanian, D. S. Tkacik, J. R. Roscioli, S. C. Herndon, Methane emissions from United States natural gas gathering and processing. *Environ. Sci. Technol.* **49**, 10718–10727 (2015).
54. A. L. Mitchell, D. S. Tkacik, J. R. Roscioli, S. C. Herndon, T. I. Yacovitch, D. M. Martinez, T. L. Vaughn, L. L. Williams, M. R. Sullivan, C. Floerchinger, M. Omara, R. Subramanian, D. Zimmerle, A. J. Marchese, A. L. Robinson, Measurements of methane emissions

- from natural gas gathering facilities and processing plants: Measurement results. *Environ. Sci. Technol.* **49**, 3219–3227 (2015).
55. C. Elvidge, M. Zhizhin, K. Baugh, F.-C. Hsu, T. Ghosh, Methods for global survey of natural gas flaring from visible infrared imaging radiometer suite data. *Energies* **9**, 14 (2016).
 56. A. M. Robertson, R. Edie, D. Snare, J. Soltis, R. A. Field, M. D. Burkhart, C. S. Bell, D. Zimmerle, S. M. Murphy, Variation in methane emission rates from well pads in four oil and gas basins with contrasting production volumes and compositions. *Environ. Sci. Technol.* **51**, 8832–8840 (2017).
 57. D. Zavala-Araiza, D. R. Lyon, R. A. Alvarez, K. J. Davis, R. Harriss, S. C. Herndon, A. Karion, E. A. Kort, B. K. Lamb, X. Lan, A. J. Marchese, S. W. Pacala, A. L. Robinson, P. B. Shepson, C. Sweeney, R. Talbot, A. Townsend-Small, T. I. Yacovitch, D. J. Zimmerle, S. P. Hamburg, Reconciling divergent estimates of oil and gas methane emissions. *Proc. Natl. Acad. Sci. U.S.A.* **112**, 15597–15602 (2015).
- Acknowledgments:** We thank the team that realized the TROPOMI instrument and its data products, consisting of the partnership between Airbus Defense and Space Netherlands, KNMI, SRON, and TNO, commissioned by NSO and ESA. Sentinel-5 Precursor is part of the EU Copernicus program, and Copernicus Sentinel data 2018–2019 have been used. We acknowledge the provision of publicly available VIIRS night-fire data. We also acknowledge NOAA Earth System Research Laboratory's Global Greenhouse Gas Reference Network for providing methane measurements at MLO, WKT, and TGC. **Funding:** This work was supported by the Kravis Scientific Research Fund, the Robertson Foundation, GALEs project (#15597) by the Dutch Technology Foundation STW, and the TROPOMI national program through NSO. Y.Z. was funded by the Kravis Fellowship through EDF and by Harvard University. P.S. and S.P. are funded through the GALEs project (#15597) by the Dutch Technology Foundation STW, which is part of the Netherlands Organization for Scientific Research (NWO). A.L. acknowledges funding from the TROPOMI national program through NSO. R.G., M.O., D.L., D.Z.-A., R.A.A., and S.P.H. were funded by the Robertson Foundation. D.J.J. was funded by the NASA Carbon Monitoring System. **Author contributions:** Y.Z. and R.G. led the study and wrote the manuscript with inputs from all coauthors; Y.Z. performed inversion simulations, carried out sensitivity experiments, and interpreted results with inputs from D.J.J.; S.P., P.S., S.H., A.L., and I.A. analyzed TROPOMI data and provided mass balance calculations; J.D.M. provided bottom-up inventory data analysis; M.O., D.L., D.Z.-A., R.A.A., and S.P.H. provided field measurement-based inventory data analysis; H.N. and M.P.S. contributed to setting up the nested GEOS-Chem simulation; D.J.V. evaluated GEOS-FP wind data; Y.Z. and R.Z. analyzed VIIRS radiant heat and TROPOMI NO₂ data; all authors provided scientific inputs during the analysis and reviewed and commented on the manuscript. **Competing interests:** The authors declare that they have no competing interests. **Data and materials availability:** All data needed to evaluate the conclusions in the paper are present in the paper and/or the Supplementary Materials. Spatially resolved methane emission estimates over the Permian Basin from this study (El_{BU}, El_{ME}, and the posterior estimate from atmospheric inverse modeling) can be accessed through <https://doi.org/10.7910/DVN/NWQGHU>. TROPOMI data are available through <https://scihub.copernicus.eu/>. VIIRS radiant heat data are available through https://eogdata.mines.edu/download_viirs_fire.html. The GEOS-Chem model is available at <https://doi.org/10.5281/zenodo.1553349>. Additional data related to this paper may be requested from the authors.
- Submitted 16 September 2019
Accepted 19 March 2020
Published 22 April 2020
10.1126/sciadv.aaz5120
- Citation:** Y. Zhang, R. Gautam, S. Pandey, M. Omara, J. D. Maasackers, P. Sadavarte, D. Lyon, H. Nesser, M. P. Sulprizio, D. J. Varon, R. Zhang, S. Houweling, D. Zavala-Araiza, R. A. Alvarez, A. Lorente, S. P. Hamburg, I. Aben, D. J. Jacob, Quantifying methane emissions from the largest oil-producing basin in the United States from space. *Sci. Adv.* **6**, eaaz5120 (2020).

Quantifying methane emissions from the largest oil-producing basin in the United States from space

Yuzhong Zhang, Ritesh Gautam, Sudhanshu Pandey, Mark Omara, Joannes D. Maasakkers, Pankaj Sadavarte, David Lyon, Hannah Nesser, Melissa P. Sulprizio, Daniel J. Varon, Ruixiong Zhang, Sander Houweling, Daniel Zavala-Araiza, Ramon A. Alvarez, Alba Lorente, Steven P. Hamburg, Ilse Aben and Daniel J. Jacob

Sci Adv **6** (17), eaaz5120.
DOI: 10.1126/sciadv.aaz5120

ARTICLE TOOLS

<http://advances.sciencemag.org/content/6/17/eaaz5120>

SUPPLEMENTARY MATERIALS

<http://advances.sciencemag.org/content/suppl/2020/04/20/6.17.eaaz5120.DC1>

REFERENCES

This article cites 40 articles, 5 of which you can access for free
<http://advances.sciencemag.org/content/6/17/eaaz5120#BIBL>

PERMISSIONS

<http://www.sciencemag.org/help/reprints-and-permissions>

Use of this article is subject to the [Terms of Service](#)

Science Advances (ISSN 2375-2548) is published by the American Association for the Advancement of Science, 1200 New York Avenue NW, Washington, DC 20005. The title *Science Advances* is a registered trademark of AAAS.

Copyright © 2020 The Authors, some rights reserved; exclusive licensee American Association for the Advancement of Science. No claim to original U.S. Government Works. Distributed under a Creative Commons Attribution NonCommercial License 4.0 (CC BY-NC).

Exhibit 39

DEPARTMENT OF PUBLIC HEALTH AND ENVIRONMENT

Air Quality Control Commission

REGULATION NUMBER 7

**CONTROL OF OZONE VIA OZONE PRECURSORS AND CONTROL OF HYDROCARBONS VIA OIL
AND GAS EMISSIONS
(EMISSIONS OF VOLATILE ORGANIC COMPOUNDS AND NITROGEN OXIDES)**

5 CCR 1001-9

[Editor's Notes follow the text of the rules at the end of this CCR Document.]

Outline of Regulation

PART A Applicability and General Provisions

- I. Applicability
- II. General Provisions

Appendix A Colorado Ozone Nonattainment or Attainment Maintenance Areas

PART B Storage, Transfer, and Disposal of Volatile Organic Compounds and Petroleum Liquids
and Petroleum Processing and Refining

- I. General Requirements for Storage and Transfer of Volatile Organic Compounds
- II. Storage of Highly Volatile Organic Compounds
- III. Disposal of Volatile Organic Compounds
- IV. Storage and Transfer of Petroleum Liquid
- V. Crude Oil
- VI. Petroleum Processing and Refining
- VII. Control of Volatile Organic Compound Leaks from Vapor Collection Systems and Vapor
Control Systems Located at Gasoline Terminals, Gasoline Bulk Plants, and Gasoline
Dispensing Facilities

Appendix B Criteria for Control of Vapors from Gasoline Transfer to Storage Tanks

Appendix C Criteria for Control of Vapors from Gasoline Transfer at Bulk Plants

PART C Surface Coating, Solvents, Asphalt, Graphic Arts and Printing, and Pharmaceuticals

- I. Surface Coating Operations
- II. Solvent Use

III.	Use of Cutback Asphalt
IV.	Graphic Arts and Printing
V.	Pharmaceutical Synthesis
Appendix D	Minimum Cooling Capacities for Refrigerated Freeboard Chillers on Vapor Degreasers
Appendix E	Emission Limit Conversion Procedure
PART D	Oil and Natural Gas Operations
I.	Volatile Organic Compound Emissions from Oil and Gas Operations
II.	(State Only) Statewide Controls for Oil and Gas Operations
III.	(State Only) Natural Gas-Actuated Pneumatic Controllers Associated with Oil and Gas Operations
IV.	(State Only) Control of Emissions from the Natural Gas Transmission and Storage Segment
V.	(State Only) Oil and Natural Gas Operations Emissions Inventory
VI.	(State Only) Oil and Natural Gas Pre-Production and Early-Production Operations
PART E	Combustion Equipment and Major Source RACT
I.	Control of Emissions from Engines
II.	Control of Emissions from Stationary and Portable Combustion Equipment in the 8-Hour Ozone Control Area
III.	Control of Emissions from Specific Major Sources of VOC and/or NO _x in the 8-Hour Ozone Control Area
IV.	Control of Emissions from Breweries in the 8-hour Ozone Control Area
PART F	Statements of Basis, Specific Statutory Authority and Purpose

Pursuant to Colorado Revised Statutes Section 24-4-103 (12.5), materials incorporated by reference are available for public inspection during normal business hours, or copies may be obtained at a reasonable cost from the Air Quality Control Commission (the Commission), 4300 Cherry Creek Drive South, Denver, Colorado 80246-1530. The material incorporated by reference is also available through the United States Government Printing Office, online at www.govinfo.gov. Materials incorporated by reference are those editions in existence as of the date indicated and do not include any later amendments.

PART A Applicability and General Provisions

I. Applicability

I.A.

I.A.1. The provisions of this regulation shall apply as follows:

PART D Oil and Natural Gas Operations

I. Volatile Organic Compound Emissions from Oil and Gas Operations

I.A. Applicability

I.A.1. Except as provided in Section I.A.2., this section applies to oil and gas operations that collect, store, or handle hydrocarbon liquids or produced water in the 8-hour Ozone Control Area (State Only: or any ozone nonattainment or attainment/maintenance area) and that are located at or upstream of a natural gas plant.

I.A.2. Oil refineries are not subject to Section I.

I.B. Definitions specific to Section I.

I.B.1. “Affected Operations” means oil and gas exploration and production operations, natural gas compressor stations and natural gas drip stations, to which Section I. applies.

I.B.2. “Air Pollution Control Equipment”, as used in Section I., means a combustion device or vapor recovery unit. Air pollution control equipment also means alternative emissions control equipment, pollution prevention devices, and processes that comply with the requirements of Section I.D.4. that are approved by the Division.

I.B.3. “Approved Instrument Monitoring Method” means an infra-red camera, EPA Method 21, or other instrument based monitoring method or program approved in accordance with Section I.L.8. If an owner or operator elects to use Division approved continuous emission monitoring, the Division may approve a streamlined inspection, recordkeeping, and reporting program for such operations.

I.B.4. “Atmospheric Storage Tanks or Atmospheric Condensate Storage Tanks” means a type of condensate storage tank that vents, or is designed to vent, to the atmosphere.

I.B.5. “Auto-Igniter” means a device which will automatically attempt to relight the pilot flame in the combustion chamber of a control device in order to combust volatile organic compound emissions.

I.B.6. “Calendar Week” means a week beginning with Sunday and ending with Saturday.

I.B.7. “Commencement of operation” means when a source first conducts the activity that it was designed and permitted for. In addition, for oil and gas well production facilities, commencement of operation is the date any permanent production equipment is in use and product is consistently flowing to sales lines, gathering lines, or storage tanks from the first producing well at the stationary source, but no later than end of well completion operations (including flowback).

I.B.8. “Condensate Storage Tank” means any tank or series of tanks that store condensate and are either manifolded together or are located at the same well pad.

I.B.9. “Centrifugal Compressor” means any machine used for raising the pressure of natural gas by drawing in low pressure natural gas and discharging significantly higher pressure natural gas by means of mechanical rotating vanes or impellers. Screw, sliding vane, and liquid ring compressors are not centrifugal compressors.

I.B.10. “Component” means each pump seal, flange, pressure relief device (including thief hatches or other openings on a controlled storage tank), connector, and valve that

necessary, the Division may require use of an alternative emission factor that complies with Section I.C.2.b.(iii).

I.C.2.b.(ii) (State Only) For storage tanks at natural gas compressor stations and natural gas drip stations, the source must use a site-specific volatile organic compound emission factor established pursuant to Section I.C.2.b.(iii). If the Division has reason to believe that the site-specific emission factor is no longer representative, or if it deems it otherwise necessary, the Division may require use of an alternative emission factor that complies with Section I.C.2.b.(iii).

I.C.2.b.(iii) (State Only) Establishment of or Updating Approved Emission Factors

I.C.2.b.(iii)(A) (State Only) The Division may require the source to develop and/or use a more recent default basin-specific or site-specific volatile organic compound emission factor pursuant to Section I.C.2.b., if such emission factor would be more reliable or accurate.

I.C.2.b.(iii)(B) (State Only) For storage tanks at oil and gas exploration and production operations, the source may use a site-specific volatile organic compound emission factor for which the Division has no objection, and which is based on collection and analysis of a representative sample of hydrocarbon liquids or produced water pursuant to a test method approved by the Division.

I.C.2.b.(iii)(C) (State Only) For storage tanks at natural gas compressor stations and natural gas drip stations, a source may use a volatile organic compound emissions factor that was used for reporting emissions from the source on APENs filed on or before February 28, 2003, or an alternative site-specific volatile organic compound emission factor established pursuant to Section I.C.2.b.

I.C.2.b.(iii)(D) (State Only) A default basin-specific volatile organic compound emissions factor must be one for which the Division has no objection, and which is based on collection and analysis of a representative sample of hydrocarbon liquids or produced water or an alternative method, pursuant to a test method approved by the Division, except as otherwise provided in I.C.2.b.(i).

I.C.2.b.(iii)(E) (State Only) A site-specific volatile organic compound emissions factor must be one for which the Division has no objection, and which is based on collection and analysis of a representative sample of hydrocarbon liquids or produced water pursuant to a test method approved by the Division.

I.D. Storage Tank Emission Controls

I.D.1. System-Wide Control Strategy for Condensate Storage Tanks

I.D.1.a. Beginning May 1, 2011, through April 30, 2020, owners and operators of all atmospheric condensate storage tanks that emit greater than or equal to two tons

per year of actual uncontrolled volatile organic compounds must employ air pollution control equipment to reduce emissions of volatile organic compounds from atmospheric condensate storage tanks by 90% from uncontrolled actual emissions on a calendar weekly basis May 1 through September 30 and 70% from uncontrolled actual emissions on a calendar monthly basis during October 1 through April 30.

Emission reductions are not required for each and every unit, but instead shall be based on overall reductions in uncontrolled actual emissions from all the atmospheric condensate storage tanks associated with the affected operations for which the owner or operator filed, or was required to file, an APEN pursuant to Regulation Number 3, Part A, due to either having exceeded reporting thresholds or retrofitting with air pollution control equipment in order to comply with the system-wide control strategy.

I.D.1.b. The system-wide control strategy does not apply to natural gas-processing plants subject to Section I.G. or qualifying natural gas compressor stations subject to Section I.I.

I.D.1.c. The system-wide control strategy does not apply to any owner or operator where the APENs for all of the atmospheric condensate storage tanks associated with the affected operations owned or operated by such person in calendar year 2019 or January 1, 2020, through April 30, 2020, reflect a total of less than 30 tons-per-year of actual uncontrolled emissions of VOCs in the 8-Hour Ozone Control Area.

I.D.2. New and Modified Condensate Tanks

I.D.2.a. Beginning February 1, 2009, through March 1, 2020, owners or operators of any new or modified atmospheric condensate storage tank at exploration and production sites shall collect and control emissions by routing emissions to and operating air pollution control equipment pursuant to Section I.D. The air pollution control equipment shall have a control efficiency of at least 95%, and shall control volatile organic compounds during the first 90 calendar days after commencement of operation of the storage tank, or after the well was re-completed, re-fractured or otherwise stimulated. The air pollution control equipment and associated monitoring equipment required pursuant to Section I.C.1. may be removed after the first 90 calendar days as long as the source can demonstrate compliance with the applicable system-wide standard.

I.D.3. Storage Tank Control Strategy

I.D.3.a. Applicability

I.D.3.a.(i) Owners or operators of storage tanks with uncontrolled actual emissions of VOCs equal to or greater than four (4) tons per year based on a rolling twelve-month total must collect and control emissions from each storage tank by routing emissions to and operating air pollution control equipment that achieves a VOC control efficiency of 95%. If a combustion device is used, it must have a design destruction efficiency of at least 98% for VOC, except where the combustion device has been authorized by permit prior to March 1, 2020.

I.D.3.a.(ii) (State Only) Owners or operators of storage tanks with uncontrolled actual emissions of VOCs equal to or greater than two (2)

tons per year based on a rolling twelve-month total and not subject to Section I.D.3.a.(i) must collect and control emissions from each storage tank by routing emissions to and operating air pollution control equipment that achieves a VOC control efficiency of 95%. If a combustion device is used, it must have a design destruction efficiency of at least 98% for VOC, except where the combustion device has been authorized by permit prior to March 1, 2020.

I.D.3.b. Compliance Deadlines

- I.D.3.b.(i) A storage tank subject to Section I.D.3.a.(i) and constructed on or after March 1, 2020, must be in compliance by commencement of operation of that storage tank.
- I.D.3.b.(ii) (State Only) A storage tank subject to Section I.D.3.a.(ii) and constructed on or after March 1, 2020, must be in compliance by commencement of operation of that storage tank.
- I.D.3.b.(iii) A storage tank subject to Section I.D.3.a.(i) and constructed before March 1, 2020, must be in compliance by May 1, 2020, or by commencement of operation of the storage tank, whichever comes later.
- I.D.3.b.(iv) (State Only) A storage tank subject to Section I.D.3.a.(ii) and constructed before March 1, 2020, must be in compliance by May 1, 2020, or by commencement of operation of the storage tank, whichever comes later.
- I.D.3.b.(v) A storage tank subject to Section I.D.3.a.(i) and not otherwise subject to Sections I.D.3.b.(i). or I.D.3.b.(iii) that increases uncontrolled actual emissions to four (4) tons per year VOC or more on a rolling twelve-month basis after March 1, 2020, must be in compliance within sixty (60) days of the first day of the month after which the storage tank VOC emissions exceeded four (4) tons per year on a rolling twelve-month basis.
- I.D.3.b.(vi) (State Only) A storage tank subject to Section I.D.3.a.(ii) and not otherwise subject to Sections I.D.3.b.(ii) or I.D.3.b.(iv) that increases uncontrolled actual emissions to two (2) tons per year VOC based on a rolling twelve-month basis after March 1, 2020, must be in compliance within sixty (60) days of the first day of the month after which the storage tank VOC emissions exceeded two (2) tons per year on a rolling twelve-month basis.
- I.D.3.b.(vii) If air pollution control equipment is not installed by the applicable compliance date in Sections I.D.3.b.(iii) or I.D.3.b.(v), compliance with Section I.D.3.a.(i) may alternatively be demonstrated by shutting in all wells producing into that storage tank by the date in Sections I.D.3.b.(iii) or I.D.3.b.(v) so long as production does not resume from any such well until the air pollution control equipment is installed and operational.
- I.D.3.b.(viii) (State Only) If air pollution control equipment is not installed by the applicable compliance date in Sections I.D.3.b.(iv) or I.D.3.b.(vi), compliance with Section I.D.3.a.(ii) may alternatively be demonstrated by shutting in all wells producing into that storage tank by the date in Sections I.D.3.b.(iv) or I.D.3.b.(vi) so long as production does not resume

from any such well until the air pollution control equipment is installed and operational.

I.D.3.b.(ix) This Section I.D.3. does not apply to storage tanks at natural gas-processing plants subject to Section I.G. or qualifying natural gas compressor stations subject to Section I.I.

I.D.4. Alternative emissions control equipment and pollution prevention devices and processes installed and implemented after June 1, 2004, shall qualify as air pollution control equipment, and may be used in lieu of, or in combination with, combustion devices and/or vapor recovery units to achieve the emission reductions required by this Section I.D., if the following conditions are met:

I.D.4.a. The owner or operator obtains a construction permit authorizing such use of the alternative emissions control equipment or pollution prevention device or process. The proposal for such equipment, device or process shall comply with all regulatory provisions for construction permit applications and shall include the following:

I.D.4.a.(i) A description of the equipment, device or process;

I.D.4.a.(ii) A description of where, when and how the equipment, device or process will be used;

I.D.4.a.(iii) The claimed control efficiency and supporting documentation adequate to demonstrate such control efficiency;

I.D.4.a.(iv) An adequate method for measuring actual control efficiency; and

I.D.4.a.(v) Description of the records and reports that will be generated to adequately track emission reductions and implementation and operation of the equipment, device or process, and a description of how such matters will be reflected in the records and reports required by Section I.F.

I.D.4.b. Public notice of the application is provided pursuant to Regulation Number 3, Part B, Section III.C.4.

I.D.4.c. EPA approves the proposal. The Division shall transmit a copy of the permit application and any other materials provided by the applicant, all public comments, all Division responses and the Division's permit to EPA Region 8. If EPA fails to approve or disapprove the proposal within 45 days of receipt of these materials, EPA shall be deemed to have approved the proposal.

I.E. Monitoring of Storage Tanks and Air Pollution Control Equipment

I.E.1. Applicability

I.E.1.a. The owner or operator of any storage tank that is being controlled pursuant to this Section I. (except storage tanks subject to Section I.D.3.a.(ii)).

I.E.1.b. (State Only) The owner or operator of any storage tank subject to Section I.D.3.a.(ii).

I.E.2. Monitoring Requirements

II. (State Only) Statewide Controls for Oil and Gas Operations

II.A. (State Only) Definitions

- II.A.1. "Air Pollution Control Equipment," as used in this Section II., means a combustion device or vapor recovery unit. Air pollution control equipment also means alternative emissions control equipment and pollution prevention devices and processes intended to reduce uncontrolled actual emissions that comply with the requirements of Section II.B.2.e.
- II.A.2. "Approved Instrument Monitoring Method," means an infra-red camera, EPA Method 21, or other Division approved instrument based monitoring method or program. If an owner or operator elects to use Division approved continuous emission monitoring, the Division may approve a streamlined inspection and reporting program for such operations.
- II.A.3. "Auto-Igniter" means a device which will automatically attempt to relight the pilot flame in the combustion chamber of a control device in order to combust VOC emissions.
- II.A.4. "Centrifugal Compressor" means any machine used for raising the pressure of natural gas by drawing in low pressure natural gas and discharging significantly higher pressure natural gas by means of mechanical rotating vanes or impellers. Screw, sliding vane, and liquid ring compressors are not centrifugal compressors.
- II.A.5. "Class II Disposal Well Facility" means a facility that injects underground fluids which are brought to the surface in connection with natural gas storage operations or oil or natural gas production and that may be commingled with waste waters from gas plants which are an integral part of production operations, unless those waters are classified as a hazardous waste at the time of injection. Class II disposal well facilities do not include wells which inject fluids for enhanced recovery of oil or natural gas or for storage of hydrocarbons which are liquid at standard temperature and pressure.
- II.A.6. "Commencement of operation" means when a source first conducts the activity that it was designed and permitted for. In addition, for oil and gas well production facilities, commencement of operation is the date any permanent production equipment is in use and product is consistently flowing to sales lines, gathering lines, or storage tanks from the first producing well at the stationary source, but no later than end of well completion operations (including flowback).
- II.A.7. "Component" means each pump seal, flange, pressure relief device (including thief hatches or other openings on a controlled storage tank), connector, and valve that contains or contacts a process stream with hydrocarbons, except for components in process streams consisting of glycol, amine, produced water, or methanol.
- II.A.8. "Connector" means flanged, screwed, or other joined fittings used to connect two pipes or a pipe and a piece of process equipment or that close an opening in a pipe that could be connected to another pipe. Joined fittings welded completely around the circumference of the interface are not considered connectors.
- II.A.9. "Dump Valve" means a liquid-control valve in a separator that controls liquid level within the separator vessel.
- II.A.10. "Dump Event" means the opening of a dump valve allowing liquid to flow from a separator equipped with a dump valve to a storage tank.

is subject to 40 CFR Part 60, Subpart OOOO (February 23, 2014) on that date or thereafter. The measurement of accumulated hours of operation (26,000) or months elapsed (36) begins on January 1, 2015.

- II.B.4. Oil refineries are not subject to Section II.
- II.B.5. Glycol natural gas dehydrators that are subject to an emissions control requirement in a federal maximum achievable control technology ("MACT") standard under 40 CFR Part 63 (December 17, 2006), a Best Available Control Technology ("BACT") limit, or a New Source Performance Standard ("NSPS") under 40 CFR Part 60 (December 17, 2006) are not subject to Section II., except for the leak detection and repair requirements in Section II.E.
- II.C. Emission reduction from storage tanks at oil and gas exploration and production operations, Class II disposal well facilities, well production facilities, natural gas compressor stations, and natural gas processing plants.
 - II.C.1. Control and monitoring requirements for storage tanks
 - II.C.1.a. (State Only) Beginning May 1, 2008, owners or operators of all storage tanks storing condensate with uncontrolled actual emissions of VOCs equal to or greater than twenty (20) tons per year based on a rolling twelve-month total must collect and control emissions from each storage tank by routing emissions to and operating air pollution control equipment that has a control efficiency of at least 95% for VOCs.
 - II.C.1.b. (State Only) Owners or operators of storage tanks with uncontrolled actual emissions of VOCs equal to or greater than six (6) tons per year based on a rolling twelve-month total must collect and control emissions from each storage tank by routing emissions to and operating air pollution control equipment that achieves a hydrocarbon control efficiency of 95%. If a combustion device is used, it must have a design destruction efficiency of at least 98% for hydrocarbons, except where the combustion device has been authorized by permit prior to May 1, 2014.
 - II.C.1.b.(i) (State Only) Control requirements of Section II.C.1.b. must be achieved in accordance with the following schedule:
 - II.C.1.b.(i)(A) A storage tank constructed on or after May 1, 2014, must be in compliance within ninety (90) days of the date that the storage tank commences operation.
 - II.C.1.b.(i)(B) A storage tank constructed before May 1, 2014, must be in compliance by May 1, 2015.
 - II.C.1.b.(i)(C) A storage tank not otherwise subject to Sections II.C.1.b.(i)(A) or II.C.1.b.(i)(B) that increases uncontrolled actual emissions to six (6) tons per year VOC or more on a rolling twelve-month basis after May 1, 2014, must be in compliance within sixty (60) days of discovery of the emissions increase.
 - II.C.1.b.(ii). Control requirements within ninety (90) days of commencement of operation.

II.C.1.b.(ii)(A) Beginning May 1, 2014, through March 1, 2020, owners or operators of storage tanks at well production facilities must collect and control emissions by routing emissions to operating air pollution control equipment during the first ninety (90) calendar days after commencement of operation. The air pollution control equipment must achieve a hydrocarbon control efficiency of 95%. If a combustion device is used, it must have a design destruction efficiency of at least 98% for hydrocarbons. This control requirement does not apply to storage tanks that are projected to have emissions less than 1.5 tons of VOC during the first ninety (90) days after commencement of operation.

II.C.1.b.(ii)(B) The air pollution control equipment and any associated monitoring equipment required pursuant to Section II.C.1.c.(i) may be removed at any time after the first ninety (90) calendar days as long as the source can demonstrate that uncontrolled actual emissions from the storage tank will be below the threshold in Section II.C.1.b.

II.C.1.c. (State Only) Owners or operators of storage tanks with uncontrolled actual emissions of VOCs equal to or greater than two (2) tons per year based on a rolling twelve-month total must collect and control emissions from each storage tank by routing emissions to and operating air pollution control equipment that achieves a hydrocarbon control efficiency of 95%. If a combustion device is used, it must have a design destruction efficiency of at least 98% for hydrocarbons, except where the combustion device has been authorized by permit prior to March 1, 2020.

II.C.1.c.(i) Control requirements of Section II.C.1.c. must be achieved in accordance with the following schedule

II.C.1.c.(i)(A) A storage tank constructed on or after March 1, 2020, must be in compliance by commencement of operation of that storage tank.

II.C.1.c.(i)(B) A storage tank constructed before March 1, 2020, that is not already controlled under Sections I.D. or II.C.1.b. must be in compliance by May 1, 2021.

II.C.1.c.(i)(C) A storage tank not otherwise subject to Sections II.C.1.c.(i)(A) or II.C.1.c.(i)(B) that increases uncontrolled actual emissions above the applicable threshold in Section II.C.1.c.(i)(B) after the applicable date in Section II.C.1.c.(i)(B) must be in compliance within sixty (60) days of the first day of the month after which the storage tank emissions exceeded the applicable threshold based on a rolling twelve-month basis.

II.C.1.c.(ii) If air pollution control equipment is not installed by the applicable compliance date in Sections II.C.1.c.(i)(A), II.C.1.c.(i)(B), or II.C.1.c.(i)(C), compliance with Section II.C.1.c. may alternatively be demonstrated by shutting in all wells producing into that storage tank by the date in Sections II.C.1.c.(i)(A), II.C.1.c.(i)(B), or II.C.1.c.(i)(C) so long as production does not resume from any such well until the air pollution control equipment is installed and operational.

II.C.1.c.(iii) Owners or operators of storage tanks for which the use of air pollution control equipment would be technically infeasible without supplemental fuel may apply to the Division for an exemption from the control requirements of Section II.C.1.c. Such request must include documentation demonstrating the infeasibility of the air pollution control equipment. The applicability of this exemption does not relieve owners or operators of compliance with the storage tank monitoring requirements of Section II.C.1.d.

II.C.1.d. (State Only) Beginning May 1, 2014, or the applicable compliance date in Sections II.C.1.b.(i) or II.C.1.c.(i), whichever comes later, owners or operators of storage tanks subject to Section II.C.1. must conduct audio, visual, olfactory (AVO) and additional visual inspections of the storage tank and any associated equipment (e.g., separator, air pollution control equipment, or other pressure reducing equipment) at the same frequency as liquids are loaded out from the storage tank. These inspections are not required more frequently than every seven (7) days but must be conducted at least every thirty-one (31) days. Monitoring is not required for storage tanks or associated equipment that are unsafe, difficult, or inaccessible to monitor, as defined in Section II.C.1.e. The additional visual inspections must include, at a minimum

II.C.1.d.(i) Visual inspection of any thief hatch, pressure relief valve, or other access point to ensure that they are closed and properly sealed.

II.C.1.d.(ii) Visual inspection or monitoring of the air pollution control equipment to ensure that it is operating, including that the pilot light is lit on combustion devices used as air pollution control equipment.

II.C.1.d.(iii) If a combustion device is used, visual inspection of the auto-igniter and valves for piping of gas to the pilot light to ensure they are functioning properly.

II.C.1.d.(iv) Visual inspection of the air pollution control equipment to ensure that the valves for the piping from the storage tank to the air pollution control equipment are open.

II.C.1.d.(v) If a combustion device is used, inspection of the device for the presence or absence of smoke. If smoke is observed, either the equipment must be immediately shut-in to investigate the potential cause for smoke and perform repairs, as necessary, or EPA Method 22 must be conducted to determine whether visible emissions are present for a period of at least one (1) minute in fifteen (15) minutes.

II.C.1.d.(vi) Beginning May 1, 2020, or the applicable compliance date in Section II.C.1.c.(i), whichever comes later, visual observation of the dump valve(s) of the last separator(s) before the storage tank(s) to ensure the dump valve is free of debris and not stuck open. The owner or operator is not required to observe the actuation of the dump valve during this inspection; however, if a dump event occurs during the inspection, the owner or operator must confirm proper operation of the valve.

II.C.1.d.(vii) Beginning May 1, 2020, or the applicable compliance date in Section II.C.1.c.(i), whichever comes later, a check for the presence of liquids in liquid knockout vessels that do not drain automatically, underground lines, and aboveground piping.

II.C.1.d.(vii)(A) For liquid knockout vessels for which a procedure exists to check liquid level, check for the presence of liquids. If liquids are present above the low level indication point, drain liquids.

II.C.1.d.(vii)(B) For liquid knockout vessels for which no procedure exists to check liquid level, drain liquids.

II.C.1.d.(vii)(C) For underground lines and aboveground piping that is not sloped to a liquid knockout or tank and for which a procedure exists to check for the presence of liquids accumulation, check for the presence of liquids and drain liquids as needed.

II.C.1.d.(vii)(D) For underground lines and aboveground piping that is not sloped to a liquid knockout vessel or tank and for which no written procedure exists to check for the presence of liquids accumulation, drain liquids quarterly.

II.C.1.e. (State Only) If storage tanks or associated equipment is unsafe, difficult, or inaccessible to monitor, the owner or operator is not required to monitor such equipment until it becomes feasible to do so.

II.C.1.e.(i) Difficult to monitor means it cannot be monitored without elevating the monitoring personnel more than two meters above a supported surface or is unable to be reached via a wheeled scissor-lift or hydraulic type scaffold that allows access up to 7.6 meters (25 feet) above the ground.

II.C.1.e.(ii) Unsafe to monitor means it cannot be monitored without exposing monitoring personnel to an immediate danger as a consequence of completing the monitoring.

II.C.1.e.(iii) Inaccessible to monitor means buried, insulated, or obstructed by equipment or piping that prevents access by monitoring personnel.

II.C.2. (State Only) Capture and monitoring requirements for storage tanks that are fitted with air pollution control equipment as required by Sections I.D. or II.C.1.

II.C.2.a. Owners or operators of storage tanks must route all hydrocarbon emissions to air pollution control equipment, and must operate without venting hydrocarbon emissions from the thief hatch (or other access point to the tank) or pressure relief device during normal operation, unless venting is reasonably required for maintenance, gauging (unless the use of a storage tank measurement system is required pursuant to and the operator complies with Section II.C.4.), or safety of personnel and equipment. Compliance must be achieved in accordance with the schedule in Section II.C.2.b.(ii).

II.C.2.a.(i) Venting is emissions from a controlled storage tank thief hatch, pressure relief device, or other access point to the storage tank, which:

II.C.2.a.(i)(A) Are primarily the result of over-pressurization, whether related to design, operation, or maintenance; or

II.C.2.a.(i)(B) Are the result of an open, unlatched, or visibly unseated pressure relief device (e.g., thief hatch or pressure relief valve),

- V.C.2.u. Produced water storage tanks.
- V.C.2.v. Produced water loadout.
- V.C.2.w. Reciprocating compressor leaks or vents, aggregated per facility.
- V.C.2.x. Separators (e.g., two-phase separators, three-phase separators, high/low pressure separators, heater-treaters, vapor recovery towers, etc.).
- V.C.2.y. Stationary combustion turbines.
- V.C.2.z. Stationary compression ignition internal combustion engines.
- V.C.2.aa. Stationary spark ignition internal combustion engines.
- V.C.2.bb. Temporary completion and/or workover equipment (e.g., tanks).
- V.C.2.cc. Thermal oxidizing units, where not otherwise reported in the emissions of another emissions source category.
- V.C.2.dd. Well completions (includes flowback).
- V.C.2.ee. Well workovers.
- V.C.2.ff. Wellhead bradenhead.

VI. (State Only) Oil and Natural Gas Pre-Production and Early Production Operations

VI.A. Definitions

- VI.A.1. "Commencement of operation" means when a source first conducts the activity that it was designed and permitted for. In addition, for oil and gas well production facilities, commencement of operation is the date any permanent production equipment is in use and product is consistently flowing to sales lines, gathering lines, or storage tanks from the first producing well at the stationary source, but no later than end of well completion operations (including flowback).
- VI.A.2. "Drill-out" means the process of removing the plugs placed during hydraulic fracturing or refracturing. Drill-out ends after the removal of all stage plugs and the initial wellbore clean-up.
- VI.A.3. "Drilling" or "drilled" means the process to bore a hole to create a well for oil and/or natural gas production.
- VI.A.4. "Flowback" means the process of allowing fluids and entrained solids to flow from a well following stimulation, either in preparation for a subsequent phase of treatment or in preparation for cleanup and placing the well into production. The term flowback also means the fluids and entrained solids flowing from a well after drilling or hydraulic fracturing or refracturing. Flowback ends when all temporary flowback equipment is removed from service. Flowback does not include drill-out.
- VI.A.5. "Flowback vessel" means a vessel that contains flowback.
- VI.A.6. "Hydraulic fracturing" means the process of directing pressurized fluids containing any combination of water, proppant, and any added chemicals to penetrate tight formations,

VI.C.3. Owners or operators must notify the Division and the local government with jurisdiction over the location of the operations, using the contact provided in Section VI.C.1.b.(iv), within forty-eight (48) hours of responsive action(s) taken as a result of recorded values in excess of the response level.

VI.D. Emission reduction from pre-production flowback vessels

VI.D.1. Control

VI.D.1.a. Owners or operators of a well with flowback that begins on or after May 1, 2021, must collect and control emissions from each flowback vessel on and after the date flowback is routed to the flowback vessel by routing emissions to and operating air pollution control equipment that achieves a hydrocarbon control efficiency of at least 95%. If a combustion device is used, it must have a design destruction efficiency of at least 98% for hydrocarbons.

VI.D.1.a.(i) Owners or operators must use enclosed, vapor-tight flowback vessels.

VI.D.1.a.(ii) Flowback vessels must be inspected, tested, and refurbished where necessary to ensure the flowback vessel is vapor-tight prior to receiving flowback.

VI.D.1.a.(iii) Owners or operators must use a tank measurement system to determine the quantity of liquids in the flowback vessel(s).

VI.D.1.a.(iii)(A) Thief hatches or other access points to the flowback vessel must remain closed and latched during activities to determine the quantity of liquids in the flowback vessel(s).

VI.D.1.a.(iii)(B) Opening the thief hatch or other access point if required to inspect, test, or calibrate the tank measurement system or to add biocides or chemicals is not a violation of Section VI.D.1.a.(ii)(A).

VI.D.1.a.(iv) Combustion devices used during pre-production operations must be enclosed, have no visible emissions during normal operation, and be designed so that an observer, by means of visual observation from the outside of the enclosed combustion device, or by other means approved by the Division, determine whether it is operating properly.

VI.D.1.a.(iv)(A) Combustion devices must be equipped with an operational auto-igniter upon installation of the combustion device.

VI.D.2. Monitoring

VI.D.2.a. Owners or operators of a well with flowback that begins on or after May 1, 2021, must conduct daily visual inspections of the flowback vessel and any associated equipment.

VI.D.2.a.(i) Visual inspection of any thief hatch, pressure relief valve, or other access point to ensure that they are closed and properly seated.

- VI.D.2.a.(ii) Visual inspection or monitoring of the air pollution control equipment to ensure that it is operating.
- VI.D.2.a.(iii) Visual inspection of the air pollution control equipment to ensure that the valves for the piping from the flowback vessel to the air pollution control equipment are open.
- VI.D.2.a.(iv) If a combustion device is used, visual inspection of the auto-igniter and valves for piping of gas to the pilot light to ensure they are functioning properly.
- VI.D.2.a.(v) If a combustion device is used, inspection of the device for the presence or absence of smoke. If smoke is observed, either the equipment must be immediately shut-in to investigate the potential cause for smoke and perform repairs, as necessary, or EPA Method 22 must be conducted to determine whether visible emissions are present for a period of at least one (1) minute in fifteen (15) minutes.

VI.D.3. Recordkeeping

- VI.D.3.a. The owner or operator of each flowback vessel subject to Section VI.D.1. must maintain records for a period of two (2) years and make them available to the Division upon request, including
 - VI.D.3.a.(i) The API number of the well and the associated facility location, including latitude and longitude coordinates.
 - VI.D.3.a.(ii) The date and time of the onset of flowback.
 - VI.D.3.a.(iii) The date and time the flowback vessels were permanently disconnected, if applicable.
 - VI.D.3.a.(iii) The date and duration of any period where the air pollution control equipment is not operating.
 - VI.D.3.a.(iv) Records of the inspections required in Section VI.D.2. including the time and date of each inspection, a description of any problems observed, a description and date of any corrective action(s) taken, and the name of the employee or third party performing corrective action(s).
 - VI.D.3.a.(v) Where a combustion device is used, the date and result of any EPA Method 22 test or investigation pursuant to Section VI.D.2.a.(v).

PART E Combustion Equipment and Major Source RACT

I. Control of Emissions from Engines

I.A. Requirements for new and existing engines.

- I.A.1. The owner or operator of any natural gas-fired stationary or portable reciprocating internal combustion engine with a manufacturer's design rate greater than 500 horsepower commencing operations in the 8-hour Ozone Control Area on or after June 1, 2004 shall employ air pollution control technology to control emissions, as provided in Section I.B.

Exhibit 40

**ENVIRONMENTAL IMPACT PREVENTION
900 SERIES**

901. GENERAL STANDARDS

903. VENTING OR FLARING NATURAL GAS

Venting and Flaring of natural gas represent waste of an important energy resource and pose safety and environmental risks. Venting and Flaring, except as specifically allowed in this Rule 903, are prohibited.

a. Notice to Local Governments and Emergency Responders.

- (1) **Prior Notice.** As soon as practicable prior to, but no later than two hours before, any planned Flaring of natural gas allowed pursuant to this Rule 903, Operators will provide verbal, written, or electronic notice to the Relevant and Proximate Local Governments and to the local emergency response authorities.
- (2) **Subsequent Notice.** In the event of Flaring due to an Upset Condition, Operators will provide verbal, or electronic notice as soon as possible, but no later than 12 hours, to the Relevant and Proximate Local Governments and to the local emergency response authorities.
- (3) **Waiver.** Relevant and Proximate Local Governments and local emergency response authorities may waive their right to notice under this Rule 903.a at any time, pursuant to Rule 302.f.(1).A.
- (4) **Recordkeeping.** Operators will maintain records of notice provided pursuant to this Rule 903.a, and provide the records to the Director upon request.

b. Emissions During Drilling Operations.

- (1) Operators will capture or combust gas downstream of the mud-gas separator using best drilling practices while maintaining safe operating conditions.
- (2) If capturing or combusting gas would pose safety risks to onsite personnel, Operators may Vent and will provide verbal notification to the Director within 12 hours and submit a Form 4, Sundry Notice within 7 days. The Operator need not seek a formal variance pursuant to Rule 502. A Form 23, Well Control Report may also be required if the criteria in Rule 428.c are met. If Venting pursuant to this Rule 903.b.(2) exceeds 24 hours, the Operator will seek the Director's approval to continue Venting.
- (3) Combustors will be located a minimum of 100 feet from the nearest surface hole location and enclosed.

c. Emissions During Completion Operations.

- (1) **Reduced Emission Completions Practices.** Operators will adhere to reduced emission completion practices as specified in 40 C.F.R. § 60.5375a, as incorporated by reference in Rule 901.b, on all newly Completed and re-completed oil and gas Wells regardless of whether the Well is hydraulically fractured, unless otherwise specified in this Rule 903.c.
- (2) **Flowback Vessels.** Operators will enclose all Flowback vessels and adhere to the AQCC Regulation No. 7 standards for emission reduction from pre-production Flowback vessels as specified in 5 C.C.R. § 1001-9:D.VI.D, as incorporated by reference in Rule 901.b.

(3) Operators may Flare gas during completion operations with specific written approval from the Director under any of the following circumstances:

- A.** The Operator obtains the Director's approval to Flare through an approved gas capture plan pursuant to Rule 903.e;
- B.** The Operator submits, and the Director approves, a Form 4 allowing the Operator to Flare gas that would otherwise not be permitted pursuant to Rule 903.c.
 - i.** On the Form 4 the Operator will explain why Flaring is necessary to Complete the Well, and will protect and minimize adverse impacts to public health, safety, welfare, the environment, and wildlife resources.
 - ii.** On the Form 4 the Operator will estimate anticipated Flaring volume and duration.
 - iii.** On the Form 4 the Operator will explain its plan to connect the facility to a Gathering Line or otherwise utilize the gas in the future.
 - iv.** The Director may approve a Form 4 requesting permission to Flare during completion if the Director determines that the Flaring is necessary to Complete the Well and will protect and minimize adverse impacts to public health, safety, welfare, the environment, and wildlife resources; or
- C.** The Operator may direct gas to an emission control device and combust the gas if necessary to ensure safety or during an Upset Condition for a period not to exceed 24 cumulative hours. If Flaring pursuant to this Rule 903.c.(3).C exceeds 24 hours, the Operator will seek the Director's approval to continue Flaring. Within 7 days of the Flaring event, the Operator will submit a Form 4 reporting the Upset Condition or safety issues that resulted in the Flaring event and include the estimated volume of gas Flared.

d. Emissions During Production.

- (1)** After the Commencement of Production Operations at an Oil and Gas Location, Venting or Flaring of natural gas produced from any Completed Well is prohibited except under the following circumstances:
- A.** Gas Flared or Vented during an Upset Condition is allowed for a period necessary to address the upset, not to exceed 24 cumulative hours. Operators will maintain records of the date, cause, estimated volume of gas Flared or Vented, and duration of each Upset Condition resulting in Flaring or Venting, and will make such records available to the Director upon request.
 - B.** Gas Vented during and as part of active and required maintenance and repair activity, including pipeline pigging, as long as the Venting is not prohibited by AQCC Regulation No. 7, 5 C.C.R. § 1001-9, as incorporated by reference in Rule 901.b. Operators will use operational best practices to minimize Venting during maintenance and repair activity.
 - C.** If approved by the Director on a Gas Capture Plan pursuant to Rule 903.e, gas Flared during a Production Evaluation or Productivity Test for a period not to exceed 60 days.
 - D.** Gas Vented during a Bradenhead test pursuant to Rule 419.
 - E.** Any event of Well liquids unloading, as long as the Well liquids unloading employs best management practices to minimize hydrocarbon emissions as required by the AQCC

Regulation No. 7, 5 C.C.R. § 1001-9, as incorporated by reference in Rule 901.b. Operators will capture or Flare gas escaping into the air during liquids unloading if the escape of the gas poses a risk to public health, safety, or welfare due to the risk of a fire, explosion, or inhalation. Pursuant to Rule 405.s, all Well liquids unloading, including swabbing, will be reported to the Director. The Operator will submit a Form 42, Field Operations Notice – Notice of Well Liquids Unloading, no less than:

- i. 48 hours prior to conducting Well liquids unloading; or
 - ii. As soon as possible prior to conducting Well liquids unloading if 48 hours notice would require an alternative or extended Well liquids unloading practice that increases emissions.
 - F. Flaring or Venting approved pursuant to Rule 903.d.(3) or on a Form 4 prior to January 15, 2021.
- (2) For any instance of Venting or Flaring permitted pursuant to Rules 903.d.(1).A–E for a period that exceeds 8 consecutive or 24 cumulative hours, the Operator will submit a Form 4 reporting:
- A. The estimated or measured volume and content of gas Vented or Flared;
 - B. Gas analysis of the gas Vented or Flared, including hydrogen sulfide;
 - C. Explanation, rationale, and cause for the Venting or Flaring event; and
 - D. A description of any operational best practices used to minimize Venting during maintenance and repair activity.
- (3) At Wells that have Commenced Production Operations prior to January 15, 2021 and that are Venting or Flaring natural gas because they are not connected to a natural gas Gathering Line or putting the natural gas to beneficial use, the Operator may request permission from the Director to Flare or Vent by submitting a gas capture plan via a Form 4 no later than the date the Operator's previously approved Form 4 expires and in no case later than January 15, 2022. If an Operator loses access to a Gathering Line after January 15, 2021, the Operator will submit a gas capture plan via a Form 4 within 30 days of losing the Gathering Line access. The Operator may not Flare or Vent pursuant to this Rule 903.d.(3) unless and until the Director approves the Form 4. The Director may approve a one-time request to Flare or Vent for a period not to exceed 12 months, if the Director determines that Flaring or Venting is necessary to produce the Well, will minimize waste, and will protect and minimize adverse impacts to public health, safety, welfare, the environment, and wildlife resources. For any such Form 4 submitted prior to January 15, 2022, the Director will not approve the one-time request to Flare or Vent to any date after January 15, 2022. The gas capture plan on the Form 4 will describe:
- A. The estimated volume and content of the gas to be Flared or Vented;
 - B. Gas analysis including hydrogen sulfide for the subject Well;
 - C. For requests based on lack of available infrastructure, the Operator will state why the Well cannot be connected to infrastructure;
 - D. When the Well(s) will be connected to infrastructure, why the Operator commenced production of the Well before infrastructure was available, and whether the mineral Owner will be compensated for the Vented or Flared gas; and

- E. Options for using the gas instead of Flaring or Venting, including to generate electricity, gas processing to recover natural gas liquids, or other options for using the gas.

(4) Measurement and Reporting.

- A. Operators will measure the volume of all gas Vented, Flared, or used at an Oil and Gas Location by direct measurement or by estimating the volume of gas Vented, Flared or used. The volume of gas Vented, Flared, or used will be reported on a per Well basis on the Form 7, Operator's Monthly Report of Operations.
- B. Operators will notify all mineral Owners of the volume of oil and gas that is Vented, Flared, or used on-lease. Operators will maintain records of such notice and provide the records to the Director upon request.

- (5)** All Flared gas will be combusted in an enclosed device equipped with an auto-igniter or continuous pilot light and a design destruction efficiency of at least 98% for hydrocarbons.

(6) Pits.

e. Gas Capture Plans.

(1) Gas Capture Plan Submission.

- A. On a Form 2A, Oil and Gas Location Assessment the Operator will commit to connecting to a gathering system by the Commencement of Production Operations, or submit a gas capture plan as an attachment to their Form 2A, pursuant to Rule 304.c.(12).
- B. Gas capture plans will demonstrate compliance with the requirements of Rules 903.b–d and include the following information:
 - i. A description and map of the location of the closest or contracted natural gas gathering system or point of sale.
 - ii. The name of the company operating the closest or contracted natural gas gathering system.
 - iii. The Operator's plan for connecting their facility to a natural gas gathering system or otherwise putting gas to beneficial use, including:
 - aa. Discussion of potential rights of way issues;
 - bb. Construction schedules;
 - cc. Date of availability of the gas Gathering Line;
 - dd. Whether the nearest or contracted gas gathering system has capacity to accept the anticipated gas to be produced at the location at the time of application; and
 - ee. Options for beneficial use of natural gas that are alternatives to Flaring during production operations prior to connection to gas Gathering Lines, including, but not limited to: onsite use, natural gas liquid processing, electrical power generation, gas to liquid, reinjection for enhanced oil recovery, or other options.

- iv. For a Wildcat (Exploratory) Well or if the Operator anticipates conducting a Production Evaluation or Productivity Test, a description of the planned Production Evaluation or Productivity Test and any issues related to the Operator's ability to connect to a gas Gathering Line.
 - v. Any anticipated safety risks that will require the Operator to allow gas to escape, rather than being captured or combusted during drilling operations, pursuant to Rule 903.b.(2).
 - vi. A description of operational best practices that will be used to minimize Venting during active and planned maintenance allowed pursuant to Rule 903.d.(1).B.
 - vii. Procedures the Operator will employ to reduce the frequency of Well liquids unloading events.
 - viii. Anticipated volumes of liquids and gas production and a description of how separation equipment will be sized to optimize gas capture.
- (2) **Verification.** Operators will verify that their facility has been connected to a gathering line by submitting a Form 10, Certificate of Clearance pursuant to Rule 219.
- (3) **Compliance.** If an Operator does not connect its facility to a gathering line or otherwise put gas to beneficial use as described in the Operator's Form 2A or gas capture plan, the Director may require the Operator to shut in a Well until it is connected to a Gathering Line or the gas is put to beneficial use. The Operator may request a Commission hearing pursuant to Rule 503.g.(10), however, the Well will remain shut in until the Commission's hearing occurs.

Exhibit 41

Projecting the Temporal Evolution of Methane Emissions from Oil and Gas Production Sites

Felipe J. Cardoso-Saldaña and David T. Allen*



Cite This: *Environ. Sci. Technol.* 2020, 54, 14172–14181



Read Online

ACCESS |



Metrics & More

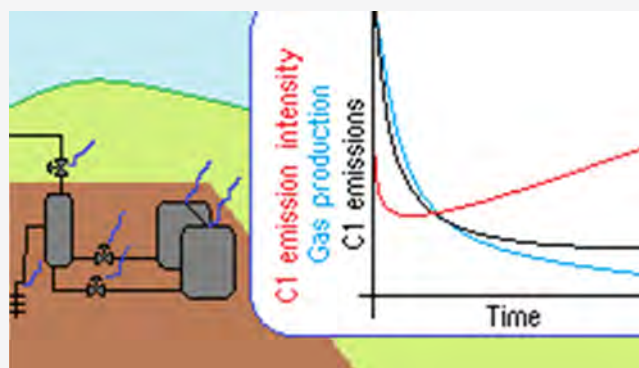


Article Recommendations



Supporting Information

ABSTRACT: Many recent studies have reported methane emissions from oil and gas production regions, often reporting results as a methane emission intensity (methane emitted as a percentage of natural gas produced or methane produced). Almost all of these studies have been instantaneous snapshots of methane emissions; however, total methane emissions from a production site and the methane emission intensity would be expected to evolve over time. A detailed site-level methane emission estimation model is used to estimate the temporal evolution of methane emissions and the methane emission intensity for a variety of well configurations with and without emission mitigation measures in place. The general pattern predicted is that total emissions decrease over time as production declines. Methane emission intensity shows complex behavior because production-dependent emissions decline at different rates and some emissions do not decline over time. Prototypical uncontrolled wet gas wells can have approximately half of their emissions over a 10 year period occur in the first year; instantaneous wellsite methane emission intensities range over a factor of 3 (0.62–2.00%) in the same period, with a 10 year production weighted-average lifecycle methane emission intensity of 0.79%. Including emission control in the form of a flare can decrease the average lifecycle methane emission intensity to 0.23%. Emissions from liquid unloadings, which are observed in subsets of wells, can increase the lifecycle methane emission intensity by up to a factor of 2–3, between 1.2 and 2.3%, depending on the characteristics of the unloadings. Emissions from well completion flowbacks raise the average lifecycle methane emission intensity from 0.79 to 0.81% for flowbacks with emission controls; for flowbacks with uncontrolled emissions, lifecycle methane emissions increase to 1.26%. Dry gas and oil wells show qualitatively similar temporal behavior but different absolute emission rates.



INTRODUCTION

Methane is a greenhouse gas with a global warming potential 28–34 times higher than carbon dioxide over a 100 year period.¹ Anthropogenic sources represent around 60% of methane emissions on a global scale, and fossil fuel production and use account for approximately one-third of the anthropogenic methane emissions,² with most of the emissions from fossil fuels coming from natural gas supply chains. Of the methane emissions attributed to natural gas supply chains, between 40 and 60% have been attributed to production sites,^{3,4} and a significant amount of data has been collected on methane emissions from production sites.

Sampling has been done on individual components or processes occurring on production sites,^{5–7} downwind of production sites,^{8,9–12} and using an aircraft to sample emissions from production sites.^{13,14} While these studies sampled emissions from wells with diverse characteristics [location, gas-to-oil ratio (GOR), age of wells, etc.], the measurements have only captured a snapshot of emissions and have not tracked the evolution of emissions in time as the wells aged. Because the production of natural gas is projected to

continue for decades,¹⁵ it will be important to be able to project how emissions will evolve as wells age.

Most of the new production in the United States is from low-permeability reservoirs, and production from these reservoirs is characterized by having a fast falloff in the production of hydrocarbons,¹⁶ with production falling to 50–80% of the initial level during the first year.^{17,18} To the extent that emissions scale with production or change as the operational practices at wells change in response to decreasing production, emissions at wellsites are also expected to change over time. Some sources of emissions, such as flashing from storage tanks, would be expected to scale nearly directly with the production and would be projected to decline as wells age.

Received: May 12, 2020

Revised: October 13, 2020

Accepted: October 13, 2020

Published: October 27, 2020



ACS Publications

© 2020 American Chemical Society

14172

<https://dx.doi.org/10.1021/acs.est.0c03049>
Environ. Sci. Technol. 2020, 54, 14172–14181

Other activities resulting in emissions, such as liquid unloadings, may increase as wells age. These time-varying emissions will vary from region to region, depending on the reservoir characteristics and types of equipment at sites. A systematic understanding of the temporal evolution of emissions from wellsites is lacking.

Most of the limited understanding of how emission rates might change at production sites over time has been focused on leaks. Kemp et al.¹⁹ developed a model [(the fugitive emissions abatement simulation toolkit (FEAST))] that generates a time series of methane emissions from leaks at an ensemble of production sites over many years of well operation, where leaks randomly appear and disappear over time. In the FEAST model, the effect of leak detection and repair (LDAR) programs on emission reduction can be assessed by assuming a success rate in identifying leaks and a success rate in repairing leaks.^{19,20} While this type of model begins to address the temporal evolution of emissions for leaks, data from a variety of sources indicate that leaks constitute only a small fraction of total emissions at production sites. For example, leaks represented 13 and 7% of the methane emissions at production sites based on estimates for the year 2013 in the Barnett Shale and Eagle Ford Shale production regions, respectively.^{21,22} At a national level, leaks accounted for 16% of methane emissions of the production segment of oil and gas systems, based on 2018 data from the Environmental Protection Agency (EPA) Greenhouse Gas Reporting Program²³ and 7% of methane emissions in the production sector of petroleum systems in 2017, based on the EPA's Inventory of U.S. Greenhouse Gas Emissions and Sinks.²⁴

More comprehensive data on the temporal evolution of methane emissions from production sites are limited. Englander et al.²⁵ analyzed methane emissions from production sites in the Bakken that were surveyed for 2 consecutive years with an infrared camera from a helicopter and reported that sites with detected emissions during the first year were far more likely to be emitting in the second year than would be expected by chance, but the reasons and sources for this persistency were unknown. Johnson et al.²⁶ reported the results of six discrete measurements of all emissions at a single production site in the Marcellus Shale, with dry gas characteristics, taken over a period of 2 years and found temporal variation that is largely driven by emissions from water tank flashing.

While these temporal studies provide some guidance on expected emission variation over time in limited situations, an overall assessment of the temporal pattern of wellsite emissions is not available for a variety of wells with different characteristics. This paper will map the predicted temporal evolution of methane emissions for each source on prototypical wellsites and the temporal evolution of the ratio of methane emissions to natural gas production (methane emission intensity) on a volumetric basis. The methane emission intensity evolution over time will be compared to a production weighted-average of the methane emission intensity over a 10 year well lifetime. The methane emission intensity averaged over a decade of simulated operation is used to illustrate the importance of the early stages of a well's operation, when total production is the highest, in determining the total projected emissions. The time integrated intensity also illustrates the importance of certain types of operations, such as liquid unloadings, in determining total projected emissions. Future work will analyze the changes in emissions

and methane emission intensity with respect to time for wells aggregated over entire production basins, based on historical production and activity data.

METHODOLOGY

The development of site-scale emission time series involves generating prototypical well configurations, which include the specification of wellstream compositions, production decay curves, equipment types, equipment emission rates, operational practices, and the effects of emission mitigation methods. A flow diagram showing how prototypical sites are constructed is shown in Figure S1. Emissions included originate from water flashing, condensate flashing, leaks, pneumatic controllers, and chemical injection pumps. Production sites can also have emissions originating from dehydrators and compressors; however, the number of dehydrators per well and compressors per well across basins in the United States, based on US EPA GHGRP 2018 data,²³ are 0.012 and 0.044 (Table S1), respectively. Thus, emissions from these two sources are not included in this analysis of individual wells; however, their emissions should be included when ensembles of multiple wells are simulated. The wellsite specifications and the calculations used to estimate emissions from each source type are described in the following sections. All prototypical production sites are assumed to have one well and are modeled for a period of 3600 days (~10 years) starting from the onset of production.

Production Decay Curves. Wells in basins with low permeability experience a rapid decrease in production, followed by a period of slower decrease in production. This behavior is typically characterized by fitting empirical production data to exponential or hyperbolic decline curves to generate production decay curves. In this work, production decay curves are taken from the US Energy Information Administration (EIA),²⁷ for production representative of the Eagle Ford Shale, which includes oil, wet gas, and dry gas decays. Decay curves from the EIA are hyperbolic and are of the form

$$Q_t = Q_i / (1 + b * D_i * t)^{1/b} \quad (1)$$

where Q_t is the production in month t , Q_i is the initial production rate, D_i is the initial decline rate, t is the time in months, and b is the degree of curvature of the decay rate. Production decay curves from the EIA are subdivided into productivity categories: wells among the top 15% in production for the Eagle Ford Shale, wells among the middle 70% in production, and wells among the bottom 15% in production. These categories of decay based on production are referred to as "top decay", "middle decay", and "bottom decay", respectively. The parameters for the decay curves used to create site configurations are provided in Table S2.

Wells with hydrocarbon production tend to produce water as a byproduct. Water production follows a similar decay behavior as hydrocarbons. Water decay curves are not available from the EIA, or from other studies in the Eagle Ford Shale, to the authors' knowledge. Thus, water decay rates are taken from Bai et al.²⁸ which reports water decay curves for wells in the Denver-Julesburg basin. Bai et al.²⁸ divided the production of water into three periods: initial flowback from fracturing, with high water production during the first days of production, followed by a transition period, and finally a produced water

period. Parameters for this hyperbolic decay are given in Table S3.

Production decay curves lead to estimates of bulk hydrocarbon production rates over time as standard cubic feet of natural gas or barrels of condensate produced. However, to estimate methane emissions, it is necessary to speciate the bulk hydrocarbons into individual species and to estimate the GORs. In oil and gas production facilities, a mixture of hydrocarbons and water coming out of the wellhead is sent to separators, which split the mixture into a produced gas stream, a liquid hydrocarbon stream, and a water stream,²¹ each with a characteristic composition; the water and condensate streams are further sent to atmospheric storage tanks releasing emissions. This process is modeled using the Peng–Robinson equation-of-state (PR-EOS) and Henry's law, starting from a wellstream composition, in order to find the compositions of individual species in the produced gas, the hydrocarbon liquid stream leaving the separator, the water stream leaving the separator, the mass of emissions flashed per barrel produced in the atmospheric tanks, and GORs.²² Four different types of wellstream compositions, which span a wide range of hydrocarbon types encountered in oil and gas production basins, were modeled. The produced hydrocarbon types are referred to as black oil, volatile oil, wet gas, and dry gas (Table S4). It is assumed that separators achieve thermodynamic equilibrium at all points of time in the well's lifetime. On wells simulated with an oil decay curve (volatile oil and black oil compositions), the oil production is determined directly from the decay curve, while the gas production is calculated by multiplying the oil production by the GOR. On the other hand, for wells simulated with a natural gas decay curve (wet gas and dry gas compositions), the gas production is determined directly from the decay curve, while the liquid hydrocarbon production is calculated by dividing the gas production by the GOR.

In some jurisdictions, the reported produced gas of a particular well needs to include the salable produced gas plus any emissions occurring on the production site, which can include emissions not only from the condensate and water flashing but also from leaks or other fugitive sources.²⁹ On the other hand, the hydrocarbon liquid production is estimated under standard conditions, representative of the condensate remaining in the stock-tank after flashing at atmospheric pressure. In this work, the quantity of produced gas is assumed to include both salable gas and emissions and is the amount calculated directly with a gas decline curve or indirectly with an oil decline curve and its GOR.

Change in Composition versus Time. Within reservoirs, most oil and gas are stored in kerogen, an organic portion of rock mass.³⁰ The kerogen contains pores where hydrocarbons are stored either in the pore spaces of the rock ("free gas") or adsorbed onto the pore walls. In conventional reservoirs, most of the hydrocarbons exist as free gas and flow from the pores to the wellbore to surface production facilities. However, in unconventional reservoirs, a large fraction of hydrocarbons (20–85%) is adsorbed onto the walls,³⁰ requiring hydraulic fracturing to artificially create fractures in the rock that allow hydrocarbon flow.

The primary driver of change in composition in unconventional reservoirs is believed to be absorption: as the pressure decreases due to depletion of the reservoir, gas which is adsorbed onto the walls desorbs to the bulk and flows to the wellhead,³¹ changing the composition reaching the wellhead.³²

However, complex behavior can originate because of the small pores acting as a molecular sieve for large molecules, only allowing the small molecules to flow³⁰ and because individual components have different mobilities; for example, methane is more mobile than ethane and propane.³³ Pressure decline in the reservoir altering the thermodynamic equilibrium of hydrocarbons can also lead to hydrocarbon composition variability as a function of time, as is the case for conventional reservoirs.

Rigorously determining the compositional change in the produced hydrocarbons as a function of time, accounting for complexities in unconventional reservoir behavior, is beyond the scope of this work. Thus, the approach is to use empirical data to account for the temporal evolution of composition. Hyperbolic functions are fitted to changes in the molar fraction of individual species with respect to their initial molar fraction using data reported by Freeman et al.³⁴ to model the changes in the composition of individual species and is applied to all hydrocarbon types (wet gas, dry gas, volatile oil, and black oil). The overall pattern is an increase in the fraction of methane in produced gas over time (see the [Supporting Information](#) sections S.2.2 and S.3.1). The results are reported both assuming a constant composition throughout the well's lifetime and a changing composition.

Emissions from Condensate and Water Flashing. The PR-EOS thermodynamic model is used to calculate the compositions of the condensate stream leaving the separator and going to atmospheric storage tanks and is also used to perform a flash calculation at atmospheric pressure simulating the flashing in the condensate tank. The flash under atmospheric conditions leads to an estimate of methane emitted per barrel of condensate produced, which can then be coupled with the production time series of liquid hydrocarbons to construct a time series of emissions from condensate tank flashing. Henry's law is used to estimate the methane emissions per barrel of water produced and is coupled with water production calculated with the decay curve to construct a time series of emissions from water flashing. The operating conditions (temperature and pressure) of the wellsite separators affect the amount of methane present in the liquid streams exiting the separator, which then flash in atmospheric pressure storage tanks and release emissions. Details on operating conditions selected are shown in the [Supporting Information](#) section S.2.3.

Scenarios with mitigation of emissions from the condensate and water flashing were included by assuming that flaring reduces emissions by 98%. While measurements of methane destruction removal efficiency at flares on production sites have reported median efficiencies lower³⁵ (~97%) and higher³⁶ (>99.97%) than this value, 98% is selected given that this value is commonly used by operators when reporting emissions. It is assumed that when there is control on tanks, both the water and condensate tanks will share the same control device if there is both water and condensate production. Installation of high- and low-pressure separators in series, rather than a single separator, is also included as an emission mitigation strategy.³⁷ Well configurations with two separators are used for wet gas and oil production, while dry gas is assumed to have only one separator as methane emissions from water tanks are generally much lower than from condensate tanks.

Pneumatic Devices. Emissions from pneumatic devices are due to pneumatic controllers and pneumatic chemical

injection pumps. The prototypical wellsites presented in this work are assumed to have one chemical injection pump, one wellhead pneumatic controller, and pneumatic controllers on separators. For oil and wet gas wells, two pneumatic controllers on separators are assigned, while for dry gas wells one is assigned. In scenarios with two separators, an additional pneumatic controller is included. Emissions of pneumatic devices are assumed to be constant throughout the lifetime of the well. This assumption is made even though intermittent controllers might actuate less frequently as production declines, because studies have found that malfunctioning controllers account for the majority of emissions and emissions from malfunctioning controllers are not expected to correlate directly with numbers of actuations. Emission measurements for chemical injection pumps are taken from Allen et al.⁵ and are assumed to be constant. Mitigation scenarios assuming electrification of pneumatic devices are included; whenever electrification is used, emissions from pneumatic devices are set to zero.

Leaks. The methane emission rate from leaks at a production site is expected to change over time given that the number of leaks will vary as new leaks emerge, and leaks are fixed during LDAR programs or by operators detecting them during routine visits to the site. Little data are available on rates of leak generation and repair.²⁰ For simplicity, in this work, emissions from leaks are simulated assuming that the number of leaks and emission rates of individual leaks remain constant throughout the lifetime of the well. The number of leaks is randomly selected from a distribution of leaks per well observed at production sites by Allen et al.⁵ The emission rate is selected from the same distribution. It should be noted that this is a simple and limited way of modeling the contribution of leaks throughout the lifetime of the site, and it is based on extrapolating snapshots of emissions observed in field campaigns for a longer period of time. However, as a separate sensitivity analysis, time series generated by the FEAST model with and without LDAR programs are coupled with emissions rates from the other sources at production sites to analyze the effect of a temporally variable behavior of leak emission rates on the methane emission intensity (see the [Supporting Information](#) section S.3.5.5).

Completions/Refracturing/Recompletions. Well completions occur after a well has been drilled and before it is brought into production. Well completions remove fluids injected during hydraulic fracturing and are a source of methane emissions. Emissions from well completions occur before the start of production. Methane emissions from completions are analyzed with and without emission controls (reduced emission completions) using emission factors from the EPA of 40.6 Mg of methane per event for wells that do not perform reduced emission completions, 3.2 Mg of methane per completion for wells that have reduced emission completions, recovering gases, and 5.9 Mg of methane per event for wells that have reduced emission completions, flaring gases.³⁸ Completion emissions are also modeled with an emission factor of 124 Mg of methane per event for wells that have completions without controls, which is the average potential emission per event measured by Allen et al.⁵ EPA emission factors indicate the total methane emissions per event but not the potential emissions (methane that would have been emitted but is recovered or flared); however, potential emissions are required to estimate the total methane produced, which is used in the average lifecycle methane emission

intensity calculation, by adding the potential emissions to the methane produced during the production phase of the well. In all scenarios, it is assumed that the potential to emit is the average reported by Allen et al.⁵ of 124 Mg per event and is added to the methane produced during the production phase to estimate the total methane produced.

Refracturing might be used to stimulate a well after production has declined,³⁹ or the same vertical well bore might be used to access different source rocks at different depths (recompletion). Oruganti et al.³⁹ analyzed wells with refracturing in the Bakken and Eagle Ford Shale production regions and found that refracturing is usually performed within the first few years of a well's lifetime. Production after refracturing can be higher, equal to, or lower than the initial production of the well, and the decay could be faster or slower. In this work, scenarios with and without refracturing/recompletion are analyzed. When refracturing is assumed, the time when refracturing takes place is randomly selected from a distribution based on data from Oruganti et al.³⁹ in the Eagle Ford Shale (18.7 months, SD = 9.4 for oil wells; 27.6 months, SD = 15.8 for gas wells). It is assumed that the decay, level of production, and composition profile are the same as the original decline. Emission factors and duration for well refracturing are assumed to be the same as those for well completions.

Liquid Unloadings. As the gas moves out of the reservoir and ascends through the wellbore, its pressure decreases, causing condensation and forming liquid droplets. These droplets will continue to flow upward if the velocity of the fluid moving upward is higher than a critical velocity,⁴⁰ which is dependent on the density and surface tension of the fluid. If the velocity of the fluid is below the critical velocity, droplets will start accumulating in the wellbore leading to liquid loadings. As time progresses, production will decrease leading to a decrease in the velocity in the wellbore. Wellbore velocity falling below the critical velocity leads to the onset of liquid unloadings. After the onset, liquid unloadings will be required periodically to remove liquids from the wellbore. To construct a time series of emissions from liquid unloadings, it is necessary to first determine when the onset of liquid unloading occurs and then model the emissions from unloadings.

While there are models that allow prediction of the onset of liquid unloading by combining decline curves with wellbore models,⁴¹ a full characterization of the wellbore (diameters, lengths of vertical and lateral segments, and angles) is needed to generate accurate results. Here, the approach to predict the onset of liquid unloadings is based on randomly selecting the time of onset from a distribution based on empirical data, taken from Brito et al.⁴¹ (31.3 months average; 10.2 months SD).

The most common types of unloading for gas wells are as follows: manual unloading without a plunger (generally used when unloadings are infrequent), manual unloading with a plunger and automated unloading with a plunger (generally done when frequent unloadings are required).^{7,42} Here, various time series of emissions from liquid unloadings are constructed, and they all include a period without liquid unloadings followed by the onset of liquid unloadings after which emissions appear. During the period with liquid unloadings, a variety of scenarios for the selection of unloading methods are possible. In this work, the scenarios considered include (i) emissions from manual liquid unloadings only; (ii) manual liquid unloadings during a period equivalent to the

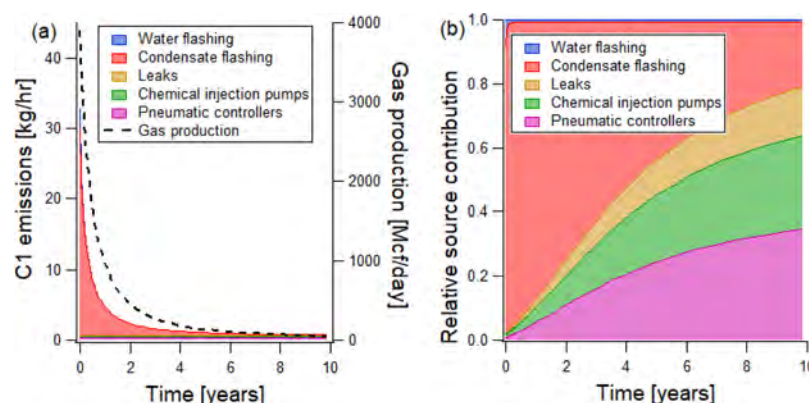


Figure 1. Time series of (a) absolute emissions and gas production and (b) relative contribution of emissions from a wet gas site. The time series assumes changes in the wellstream composition over time, no mitigation measures, and middle decay curves on the gas production.

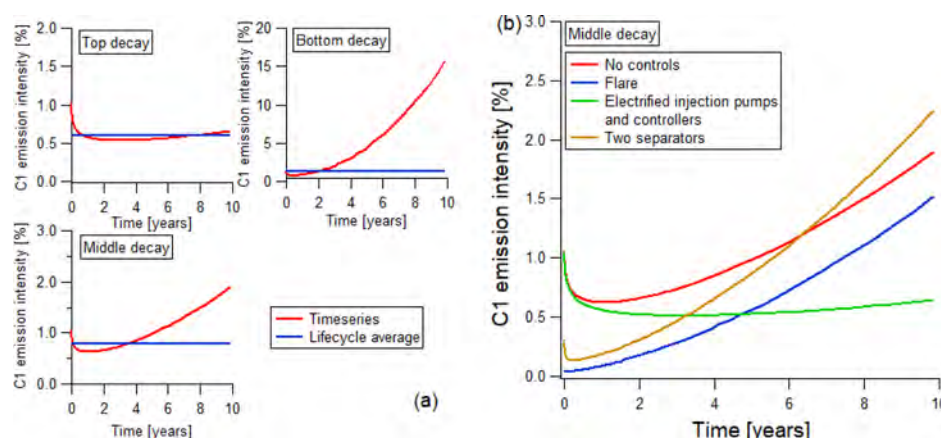


Figure 2. (a) Methane emission intensity time series and average lifecycle methane emission intensity for the wet gas composition modeled with top, middle, and bottom decay curves of gas production without mitigation strategies and assuming a change in the wellstream composition. (b) Methane emission intensity time series of the wet gas composition modeled with a middle decay curve of gas production under various mitigation scenarios and assuming a change in the wellstream composition.

time from the start of production to the onset time followed by automated unloadings; (iii) manual liquid unloadings during a period equivalent to twice the time from the start of production to the onset time followed by automated unloadings, and (iv) only automated unloadings. Additional details on how the time series of emissions from liquid unloadings are constructed are provided in the [Supporting Information](#) section S.3.7.

Techniques to prevent loading of the wellbore, such as adding tubing to the casing to delay the onset of liquid loading and adding a compressor that provides gas lift, foams, or pumps in the wellbore,⁴⁰ are not analyzed in this work, as they generally do not result in venting. Liquid loadings can also occur in oil wells, where the most common approach to unload the wellbore is the use of jack pumps. Unloading of oil wells is not analyzed in this work.

RESULTS

A time series of emissions during production (without emissions from completions, recompletions, and refracturing) and without episodic emissions (without emissions from liquid unloadings) for selected prototypical wet gas sites and prototypical dry gas sites, assuming changes in the wellstream composition, are reported in the following subsections. The temporal evolution of the methane emission intensity and how

it is affected by the various mitigation strategies are also reported. The results assuming a constant wellstream composition are reported in [Supporting Information](#) sections S.3.5.1 and S.3.5.2. The time series of prototypical volatile oil and prototypical black oil hydrocarbons are shown in the [Supporting Information](#) section S.3.5.3. Changes in the molar fraction of individual species with respect to their initial molar fraction, changes in the gas to oil ratio, and changes in the light alkane emission rates of the hydrocarbons modeled in this work are reported in the [Supporting Information](#) sections S.3.1–S.3.3, respectively. A summary of emissions from all the prototypical well configurations constructed for the production phase is reported in the [Supporting Information](#) section S.3.5.4. A sensitivity analysis of LDAR programs, based on the FEAST model, on methane emission intensity is reported in the [Supporting Information](#) section S.3.5.5. Emissions from completions and liquid unloadings are analyzed separately in following subsections and also in the [Supporting Information](#) sections S.3.6 and S.3.7.

Uncertainties in emission estimates are characterized using Monte Carlo simulations. Each wellsite simulation is performed 1000 times. In each instance of the Monte Carlo analysis, emissions from individual pieces of equipment (e.g., pneumatic controllers) are randomly selected from emission measurements. The uncertainty in the emission estimates is

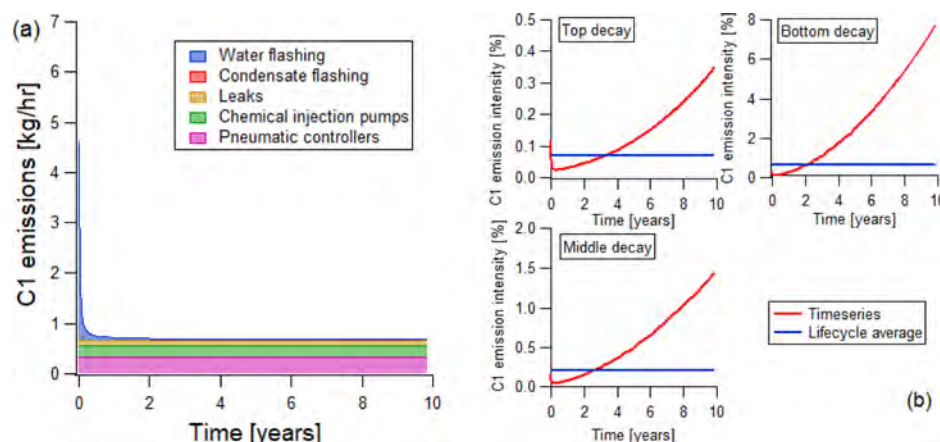


Figure 3. (a) Time series of absolute emissions from a dry gas site modeled with a middle decay curve on the gas production. (b) Methane emission intensity time series and average lifecycle methane emission intensity for the dry gas composition modeled with the top, middle, and bottom decay curves of gas production. All time series assume changes in the wellstream composition and no mitigation measures.

characterized by reporting the 2.5th and 97.5th percentiles of emissions.

Emission Time Series during Production. Wet Gas Sites. An emission time series of a prototypical production site with wet gas characteristics is shown in Figure 1. This time series represents a well modeled with a middle decay curve and changes in the wellstream composition over the lifetime of the well. No emission mitigation measures and no emissions from well completions, recompletions, or liquid unloadings are included, as they are analyzed later in this work. Emissions are the highest during the initial production, dominated by condensate flashing and water flashing (Figure 1a). During the first year, ~48% of emissions occurring throughout the 10 year production period are released; during the first two years, ~65% of the total emissions take place; and during the first half of the period, ~85% of the total emissions occur. As time progresses, emissions from condensate and water flashing decrease because of the decay in condensate and water production. As hydrocarbon and water production decrease, the relative source contribution of emissions from pneumatic controllers, chemical injection pumps, and leaks increase (Figure 1b), even though emissions from these sources remain constant. The 2.5th and 97.5th percentiles of emissions from all sources reported in Figure 1a are reported in the Supporting Information section S.3.5.1.

A common metric to characterize methane emissions from natural gas supply chains is the emission intensity.⁴³ The time series of methane emission intensity for the wet gas wells with the bottom, middle, and top decay curves are shown in Figure 2a, for scenarios where the wellstream composition is assumed to change as a function of time and without mitigation strategies implemented. Here, the methane emission intensity is reported as methane emissions divided by natural gas production, in volumetric units. A sensitivity analysis comparing various intensity metrics (methane emissions divided by methane produced and methane emissions divided by gas produced, on a mass basis) is provided in the Supporting Information section S.3.5.7. The methane emission intensity has a complex behavior, initially decreasing, then increasing. The decrease is because the wellstream composition is changing and because the water production, and thus, emissions from water flashing, are simulated with a more rapid decay than the gas production. As time progresses, the

production decreases and emissions from the condensate and water flashing decrease while those from chemical injection pumps, pneumatic devices, and leaks remain constant, leading to an increase in the methane emission intensity. The estimated methane emission intensity using a top decay curve is initially 1.02% and has a range of 0.53–1.02%. The integrated 10 year emissions are 0.60% of the integrated 10 year production (lifecycle average). The methane emission intensity estimated with a middle decay curve is initially 1.06% and has a range of 0.62–2.00% and a lifecycle average of 0.79%. The methane emission intensity estimated based on a bottom decay curve is initially 1.25% and has a range of 0.75–14.49% and an average lifecycle of 1.38%. These results illustrate that because most emissions occur early in the well's lifetime, the lifecycle methane emission intensity over 10 years is closer to the initial methane emission intensity than the final methane emission intensity.

Mitigation strategies affect the temporal profile of emissions, and thus, the temporal profile of the methane emission intensity. Figure 2b shows the effect of mitigation strategies implemented using the middle decay curve in a scenario with tank flash control, a scenario with electrified pneumatic devices, and a scenario with two separators instead of one; these results represent the cases where the composition of hydrocarbons is assumed to change as a function of time. Implementing electrification of the pneumatic devices leads to the greatest reductions in the methane emission intensity at later times in a well's life. Having two separators reduces the intensity early in the well's life but increases the emission intensity late in the 10 year period because of the addition of a pneumatic controller on the second separator. In contrast, adding a flare significantly reduces the methane emission intensity at all times. As studies measuring emissions from production sites suggest that some tank control systems are not able to handle the flashing emissions completely leading to emissions upstream of tank control units,^{44,45} a sensitivity analysis on emissions with thresholds on the emissions that can be controlled is provided in the Supporting Information section S.3.5.6.

Figure 2 suggests that the methane emission intensity changes as a function of time both under normal operating conditions and when mitigation strategies are implemented, thus this metric should be interpreted carefully if it is employed

Table 1. Lifecycle Average Methane Emission Intensity for Wet Gas and Dry Gas Hydrocarbons Modeled with the Medium Decay Curve, One Separator, with Pneumatic Devices, and Assuming That Composition Changes as a Function of Time under Various Completion Types^a

hydrocarbon modeled	lifecycle average methane emission intensity [C1/gas produced in vol %]				
	without including completion emissions	including completion that flares, EPA emission factor	including completion that recovers the gas, EPA emission factor	including completion that vents, EPA emission factor	including completion that vents, emission factor from ref. 26
wet gas no tank control	0.79 (0.53–1.63)	0.81 (0.55–1.64)	0.80 (0.54–1.63)	0.94 (0.68–1.77)	1.26 (1.00–2.10)
wet gas flare tank control	0.23 (0.10–0.97)	0.25 (0.12–0.98)	0.24 (0.11–0.97)	0.38 (0.25–1.12)	0.70 (0.58–1.44)
dry gas no tank control	0.21 (0.09–0.78)	0.23 (0.11–0.80)	0.22 (0.10–0.79)	0.35 (0.23–0.91)	0.63 (0.50–1.19)
dry gas flare tank control	0.20 (0.08–0.77)	0.22 (0.10–0.79)	0.21 (0.09–0.78)	0.34 (0.22–0.90)	0.62 (0.50–1.18)

^aThe 2.5th and 97.5th percentiles are shown in parenthesis.**Table 2. Lifecycle Average Methane Emission Intensity for Wet Gas and Dry Gas Hydrocarbons Modeled with the Medium Decay Curve, One Separator, without Emissions from Completions, with Pneumatic Devices, and Assuming That Composition Changes as a Function of Time under Various Scenarios of Liquid Unloading Time Series^a**

hydrocarbon modeled	lifecycle average methane emission intensity [C1/gas produced in vol %]				
	without including liquid unloadings	only manual liquid unloadings after onset	manual liquid unloadings for 2 times the length of period before onset, followed by automatic unloadings	manual liquid unloadings for the same time as the length of period before onset, followed by automatic unloadings	only automatic unloadings after onset
wet gas no tank control	0.79 (0.53–1.63)	1.22 (0.96–2.06)	1.40 (1.14–2.23)	1.90 (1.64–2.73)	2.28 (2.02–3.11)
wet gas flare tank control	0.23 (0.10–0.97)	0.66 (0.53–1.40)	0.84 (0.71–1.57)	1.34 (1.21–2.07)	1.72 (1.59–2.45)
dry gas no tank control	0.21 (0.09–0.78)	0.59 (0.46–1.15)	0.74 (0.62–1.30)	1.17 (1.05–1.74)	1.50 (1.38–2.06)
dry gas flare tank control	0.20 (0.08–0.77)	0.58 (0.46–1.14)	0.73 (0.61–1.29)	1.16 (1.04–1.73)	1.49 (1.37–2.05)

^aThe 2.5th and 97.5th percentiles are shown in parenthesis.

in assessing the performance of methane mitigation strategies. Further work is needed to determine a metric that better captures the reductions in emissions due to the implementation of mitigation strategies. Methane emission intensity calculated with the mean, 2.5th percentile, and 97.5th percentile of emissions from all sources of Figure 2 is reported in the Supporting Information section S.3.5.1.

Dry Gas. An emission time series of a production site with dry gas characteristics is shown in Figure 3a. This time series is constructed with a middle decay curve, assuming changes in the wellstream composition and without mitigation strategies. During the first year, 13% of the emissions in the 10 year period occur; during the first two years, 23% of the emissions; and during the first half, 53% of the emissions occur. The decay of water emissions on the dry gas site (Figure 3a) is faster than the decay in condensate emissions in the wet gas site (Figure 1a). While this general predicted pattern is expected to be reliable due to the relatively rapid decay of flowback water early in a well's life and a slower decay of produced formation water, the precise timing of the decay should be viewed with caution because of the limited data on water decay curves. The variability in emissions of the dry gas site is smaller than that of the wet gas site due to the lack of condensate tank flashing, which accounts for the majority of uncontrolled emissions in a wet gas site. The variability in emissions for the dry gas site is dominated by emissions from

water tank flashing, which is consistent with measurements at a single dry gas production site taken over a period of 2 years by Johnson et al.²⁶

The time series of the methane emission intensity in the dry gas site also has a complex behavior (Figure 3b). The emission intensity initially declines as emissions from water flashing decay faster than the natural gas production and because composition changes; however, it later increases as methane emissions decline less rapidly than production. The scenario modeled using a middle decay of gas production has an initial methane emission intensity of 0.16%, a range of 0.04–1.51%, and an average lifecycle methane emission intensity of 0.21%. The scenario modeled using a bottom decay curve of gas production has an initial methane emission intensity of 0.30%, a range of 0.09–7.91%, and an average lifecycle emission intensity of 0.67%. The scenario that uses a top decay curve has an initial methane emission intensity of 0.12%, a range of 0.02–0.34%, and an average lifecycle intensity of 0.07%. The methane emission intensity ranges and the average lifecycle methane emission intensity of the dry gas site are lower than those in the wet gas site. The mean, 2.5th and 97.5th percentiles of emissions from all sources of Figure 3 are reported in the Supporting Information section S.3.5.2.

Effect of Well Completions. Emissions from completions are episodic and have relatively large emission rates for a short period of time. Table 1 shows the increases in the average

lifecycle methane emission intensity when emissions from completions are included along with the emissions that are part of the production period (not including liquid unloadings). Completions with controls lead to a relatively small increase in the average lifecycle methane emission intensity compared to scenarios when emissions from completions are not considered. However, vented completions (no control) will have a significant impact on the lifecycle average methane emission intensity. The absolute value of the methane emission factor can increase by 0.02–0.15% when the EPA emission factor is used and up to 0.5% if the potential emissions reported by Allen et al.⁵ are used (more than doubling the 10 year average methane emission intensity in some cases of uncontrolled emissions). Scenarios of prototypical wells modeled with top and bottom decay curves are reported in the [Supporting Information](#) section S.3.6. For wells modeled with bottom decay, the effect of any completion on the methane emission intensity will be larger compared to medium or top decay because the lifecycle natural gas produced is lower.

Emission Time Series of Liquid Unloadings. [Table 2](#) shows the increase in the average lifecycle methane emission intensity when liquid unloadings are considered for selected scenarios (no completions included). Additional scenarios are included in the [Supporting Information](#) section S.3.7. Details of the increases in the emission intensity depend significantly on the assumptions made about the unloading frequency and type (see the [Supporting Information](#) section S.3.7), but as shown in [Table 2](#) for representative results, it is not unusual for unloadings to double a well's average lifecycle methane emission intensity, and increases of up to an order of magnitude are possible compared to cases without unloadings. However, these results should be viewed with caution. Overall, unloading emissions reported in the US Greenhouse Gas Inventory (GHGRI) represent a relatively small fraction of total upstream methane emissions because only a small fraction of wells has venting associated with liquid unloading. When these emissions occur, however, the analyses presented in this work indicate that liquid unloadings will have a significant impact on a given well's average lifecycle methane emission intensity.

■ IMPLICATIONS

The analyses presented in this article show that methane emissions and the methane emission intensity from a wellsite can change significantly and in complex ways over a well's lifetime as the production and operations change. Emissions from liquid unloading can have a particularly large impact on the total emissions and emission intensity, but these emissions do not occur on all wells. Reconciliations of emission estimates with atmospheric measurements at production sites should account for this evolution in wellsite behavior. The analyses also demonstrate that the commonly used methane emission intensity metrics will change over a well's lifetime and that a well's lifecycle methane emission intensity is generally dominated by the first few years of a well's life when emissions and production are the greatest. Changes in the methane emission intensity over time and the variation in absolute values of the intensity depending on how it is defined suggest that this metric should be used with caution.

■ ASSOCIATED CONTENT

Supporting Information

The Supporting Information is available free of charge at <https://pubs.acs.org/doi/10.1021/acs.est.0c03049>.

Detailed data on wellsite characteristics, additional simulation scenarios, and uncertainty estimates ([PDF](#))

■ AUTHOR INFORMATION

Corresponding Author

David T. Allen — Center for Energy and Environmental Resources, University of Texas at Austin, Austin, Texas 78758, United States; orcid.org/0000-0001-6646-8755; Phone: (512)-475-7842; Email: allen@che.utexas.edu

Author

Felipe J. Cardoso-Saldaña — Center for Energy and Environmental Resources, University of Texas at Austin, Austin, Texas 78758, United States; ExxonMobil Upstream Integrated Solutions, Spring, Texas 77389, United States; orcid.org/0000-0002-6359-8076

Complete contact information is available at: <https://pubs.acs.org/doi/10.1021/acs.est.0c03049>

Notes

This work was supported by ExxonMobil through its membership in The University of Texas at Austin Energy Institute. One of the authors (F.J.C.-S.) did an internship at ExxonMobil during the preparation of this manuscript and has accepted a full-time position at ExxonMobil. The other author (D.T.A.) has served as the chair of the Environmental Protection Agency's Science Advisory Board (2012–2015; in this role, he was a paid Special Governmental Employee); D.T.A. has current research support from the National Science Foundation, the Texas Commission on Environmental Quality, ExxonMobil Upstream Research Company, Pioneer Natural Resources, Environmental Defense Fund, and the Collaboratory to Advance Methane Science. D.T.A. has done work as a consultant for multiple companies in recent years, including British Petroleum, Eastern Research Group, ExxonMobil, KeyLogic, and SLR.

The authors declare no competing financial interest.

■ ACKNOWLEDGMENTS

Funding to perform the analyses reported here was provided by the ExxonMobil Upstream Research Company.

■ REFERENCES

- (1) IPCC. *Climate Change 2014: Synthesis Report. Contribution of Working Groups I, II and III to the Fifth Assessment Report of the Intergovernmental Panel on Climate Change*; Core Writing Team; Pachauri, R. K.; Meyer, L. A., Eds.; IPCC: Geneva, Switzerland, 2014; p 151.
- (2) National Academies of Sciences, Engineering, and Medicine. *Improving Characterization of Anthropogenic Methane Emissions in the United States*; The National Academies Press: Washington, DC, 2018.
- (3) U.S. Environmental Protection Agency (EPA). *Inventory of U.S. Greenhouse Gas Emissions and Sinks: 1990–2015* (EPA, 2017). www.epa.gov/ghgemissions/inventory-us-greenhouse-gas-emissions-and-sinks-1990-2015 Accessed on December 14th, 2019.
- (4) Alvarez, R. A.; Zavala-Araiza, D.; Lyon, D. R.; Allen, D. T.; Barkley, Z. R.; Brandt, A. R.; Davis, K. J.; Herndon, S. C.; Jacob, D. J.; Karion, A.; Kort, E. A.; Lamb, B. K.; Lauvaux, T.; Maasakkers, J. D.; Marchese, A. J.; Omara, M.; Pacala, S. W.; Peischl, J.; Robinson, A. L.;

- Shepson, P. B.; Sweeney, C.; Townsend-Small, A.; Wofsy, S. C.; Hamburg, S. P. Assessment of methane emissions from the U.S. oil and gas supply chain. *Science* **2018**, *361*, 186–188.
- (5) Allen, D. T.; Torres, V. M.; Thomas, J.; Sullivan, D. W.; Harrison, M.; Hendler, A.; Herndon, S. C.; Kolb, C. E.; Fraser, M. P.; Hill, A. D.; Lamb, B. K.; Miskimins, J.; Sawyer, R. F.; Seinfeld, J. H. Measurements of Methane Emissions at Natural Gas Production Sites in the United States. *Proc. Natl. Acad. Sci.* **2013**, *110*, 17768–17773.
- (6) Allen, D. T.; Pacsi, A. P.; Sullivan, D. W.; Zavala-Araiza, D.; Harrison, M.; Keen, K.; Fraser, M. P.; Daniel Hill, A.; Sawyer, R. F.; Seinfeld, J. H. Methane Emissions from Process Equipment at Natural Gas Production Sites in the United States: Pneumatic Controllers. *Environ. Sci. Technol.* **2015**, *49*, 633–640.
- (7) Allen, D. T.; Sullivan, D. W.; Zavala-Araiza, D.; Pacsi, A. P.; Harrison, M.; Keen, K.; Fraser, M. P.; Daniel Hill, A.; Lamb, B. K.; Sawyer, R. F.; Seinfeld, J. H. Methane Emissions from Process Equipment at Natural Gas Production Sites in the United States: Liquid Unloadings. *Environ. Sci. Technol.* **2015**, *49*, 641–648.
- (8) Yacovitch, T. I.; Herndon, S. C.; Roscioli, J. R.; Floerchinger, C.; McGovern, R. M.; Agnese, M.; Pétron, G.; Kofler, J.; Sweeney, C.; Karion, A.; Conley, S. A.; Kort, E. A.; Nähle, L.; Fischer, M.; Hildebrandt, L.; Koeth, J.; McManus, J. B.; Nelson, D. D.; Zahniser, M. S.; Kolb, C. E. Demonstration of an ethane spectrometer for methane source identification. *Environ. Sci. Technol.* **2014**, *48*, 8028–8034.
- (9) Yacovitch, T. I.; Herndon, S. C.; Pétron, G.; Kofler, J.; Lyon, D.; Zahniser, M. S.; Kolb, C. E. Mobile Laboratory Observations of Methane Emissions in the Barnett Shale Region. *Environ. Sci. Technol.* **2015**, *49*, 7889–7895.
- (10) Rella, C. W.; Tsai, T. R.; Botkin, C. G.; Crosson, E. R.; Steele, D. Measuring emissions from oil and natural gas well pads using the mobile flux plane technique. *Environ. Sci. Technol.* **2015**, *49*, 4742–4748.
- (11) Lan, X.; Talbot, R.; Laine, P.; Torres, A. Characterizing Fugitive Methane Emissions in the Barnett Shale Area Using a Mobile Laboratory. *Environ. Sci. Technol.* **2015**, *49*, 8139–8146.
- (12) Zavala-Araiza, D.; Herndon, S. C.; Roscioli, J. R.; Yacovitch, T. I.; Johnson, M. R.; Tyner, D. R.; Omara, M.; Knighton, B. Methane emissions from oil and gas production sites in Alberta, Canada. *Elem. Sci. Anth.* **2018**, *6*, 27.
- (13) Lyon, D. R.; Alvarez, R. A.; Zavala-Araiza, D.; Brandt, A. R.; Jackson, R. B.; Hamburg, S. P. Aerial Surveys of Elevated Hydrocarbon Emissions from Oil and Gas Production Sites. *Environ. Sci. Technol.* **2016**, *50*, 4877–4886.
- (14) Schwietzke, S.; Harrison, M.; Lauderdale, T.; Branson, K.; Conley, S.; George, F. C.; Jordan, D.; Jersey, G. R.; Zhang, C.; Mairs, H. L.; Pétron, G.; Schnell, R. C. Aerially guided leak detection and repair: A pilot field study for evaluating the potential of methane emission detection and cost-effectiveness. *J. Air Waste Manage. Assoc.* **2019**, *69*, 71–88.
- (15) International Energy Agency. *World Energy Outlook*, 2017.
- (16) Patzek, T. W.; Male, F.; Marder, M. From the Cover: Cozzarelli Prize Winner: Gas production in the Barnett Shale obeys a simple scaling theory. *Proc. Natl. Acad. Sci.* **2013**, *110*, 19731–19736.
- (17) Baihly, J. D.; Altman, R. M.; Malpani, R.; Luo, F. Shale gas production decline trend comparison over time and basins. *SPE Annual Technical Conference and Exhibition*; Society of Petroleum Engineers, 2010.
- (18) Wachtmeister, H.; Lund, L.; Aleklett, K.; Höök, M. Production decline curves of tight oil wells in eagle ford shale. *Nat. Resour. Res.* **2017**, *26*, 365–377.
- (19) Kemp, C. E.; Ravikumar, A. P.; Brandt, A. R. Comparing Natural Gas Leakage Detection Technologies Using an Open-Source “Virtual Gas Field” Simulator. *Environ. Sci. Technol.* **2016**, *50*, 4546–4553.
- (20) Ravikumar, A. P.; Brandt, A. R. Designing better methane mitigation policies: the challenge of distributed small sources in the natural gas sector. *Environ. Res. Lett.* **2017**, *12*, 044023.
- (21) Allen, D. T.; Cardoso-Saldaña, F. J.; Kimura, Y. Variability in Spatially and Temporally Resolved Emissions and Hydrocarbon Source Fingerprints for Oil and Gas Sources in Shale Gas Production Regions. *Environ. Sci. Technol.* **2017**, *51*, 12016–12026.
- (22) Cardoso-Saldaña, F. J.; Kimura, Y.; Stanley, P.; McGaughey, G.; Herndon, S. C.; Roscioli, J. R.; Yacovitch, T. I.; Allen, D. T. Use of Light Alkane Fingerprints in Attributing Emissions from Oil and Gas Production. *Environ. Sci. Technol.* **2019**, *53*, 5483–5492.
- (23) 2011–2018 GHGRP Industrial Profile. https://www.epa.gov/sites/production/files/2019-10/documents/subpart_w_2018_industrial_profile.pdf (accessed Dec 14, 2019).
- (24) U.S. Environmental Protection Agency (EPA). Inventory of U.S. Greenhouse Gas Emissions and Sinks: 1990–2017 (EPA, 2017). <https://www.epa.gov/sites/production/files/2019-04/documents/us-ghg-inventory-2019-main-text.pdf> (accessed Jan 29, 2020).
- (25) Englander, J. G.; Brandt, A. R.; Conley, S.; Lyon, D. R.; Jackson, R. B. Aerial Interyear Comparison and Quantification of Methane Emissions Persistence in the Bakken Formation of North Dakota, USA. *Environ. Sci. Technol.* **2018**, *52*, 8947–8953.
- (26) Johnson, D.; Heltzel, R.; Oliver, D. Temporal Variations in Methane Emissions from an Unconventional Well Site. *ACS Omega* **2019**, *4*, 3708–3715.
- (27) EIA. Oil and Gas Supply Module of the National Energy Modeling System: Model Documentation 2013, Appendix 2.c. 2013, [http://www.eia.gov/forecasts/aeo/nems/documentation/ogsm/pdf/m063\(2013\).pdf](http://www.eia.gov/forecasts/aeo/nems/documentation/ogsm/pdf/m063(2013).pdf) (accessed March 15, 2018).
- (28) Bai, B.; Carlson, K.; Prior, A.; Douglas, C. Sources of variability in flowback and produced water volumes from shale oil and gas wells. *J. Unconv. Oil Gas Resour.* **2015**, *12*, 1–5.
- (29) Texas Administrative Code Title 16 Part 1 Chapter 3 Rule 3.27: Gas to be Measured and Surface Commingling of Gas. [https://texreg.sos.state.tx.us/public/readtac\\$ext.TacPage?sl=R&app=9&p_dir=&p_rloc=&p_tloc=&p_ploc=&p_pg=1&p_tac=&ti=16&pt=1&ch=3&rl=27](https://texreg.sos.state.tx.us/public/readtac$ext.TacPage?sl=R&app=9&p_dir=&p_rloc=&p_tloc=&p_ploc=&p_pg=1&p_tac=&ti=16&pt=1&ch=3&rl=27) (accessed March 13, 2019).
- (30) Salama, A.; Amin, M. F. E.; Kumar, K.; Sun, S. Flow and transport in tight and shale formations: a review. *Geofluids* **2017**, *2017*, 4251209.
- (31) Li, D.; Zhang, L.; Wang, J. Y.; Lu, D. Composition-transient analysis in shale-gas reservoirs with consideration of multicomponent adsorption. *SPE J.* **2016**, *21*, 648–664.
- (32) Wu, H.; He, Y.; Qiao, R. Recovery of multicomponent shale gas from single nanopores. *Energy Fuels* **2017**, *31*, 7932–7940.
- (33) Li, D.; Zhang, L.; Lu, D. Effect of distinguishing apparent permeability on flowing gas composition, composition change and composition derivative in tight- and shale-gas reservoir. *J. Petrol. Sci. Eng.* **2015**, *128*, 107–114.
- (34) Freeman, C.; Moridis, G. J.; Michael, G. E.; Blasingame, T. A. Measurement, modeling, and diagnostics of flowing gas composition changes in shale gas wells. *SPE Latin America and Caribbean Petroleum Engineering Conference*; Society of Petroleum Engineers, 2012.
- (35) Gvakharia, A.; Kort, E. A.; Brandt, A.; Peischl, J.; Ryerson, T. B.; Schwarz, J. P.; Smith, M. L.; Sweeney, C. Methane, black carbon, and ethane emissions from natural gas flares in the Bakken Shale, North Dakota. *Environ. Sci. Technol.* **2017**, *51*, 5317–5325.
- (36) Caulton, D. R.; Shepson, P. B.; Cambaliza, M. O. L.; McCabe, D.; Baum, E.; Stirm, B. H. Methane destruction efficiency of natural gas flares associated with shale formation wells. *Environ. Sci. Technol.* **2014**, *48*, 9548–9554.
- (37) Porter, M. D.; Natili, R.; Strathman, A. Marcellus Shale Production Facility Emissions: Overcoming Challenges in the Liquids-Rich Area. *SPE Eastern Regional Meeting*; Society of Petroleum Engineers, 2016.
- (38) US Environmental Protection Agency. Inventory of U.S. Greenhouse Gas Emissions and Sinks 1990–2013: Revision to Hydraulically Fractured Gas Well Completions and Workovers Estimate. <https://www3.epa.gov/climatechange/pdfs/HF-Gas-well-completion-workover-update-memo-4-10-2015.pdf> (accessed Dec 10, 2019).

- (39) Oruganti, Y. D.; Mittal, R.; McBurney, C. J.; Garza, A. R. Re-fracturing in eagle ford and Bakken to increase reserves and generate incremental NPV: field study. *SPE Hydraulic Fracturing Technology Conference*; Society of Petroleum Engineers, 2015.
- (40) Lea, J. F., Jr; Rowlan, L. *Gas Well Deliquification*; Gulf Professional Publishing, 2019.
- (41) Brito, R.; Pereyra, E.; Sarica, C. A Novel Analysis to Detect When and Where Liquid Loading Occurs in Horizontal Gas Wells-Case Studies. *SPE North America Artificial Lift Conference and Exhibition*; Society of Petroleum Engineers, 2016.
- (42) Zaimes, G. G.; Littlefield, J. A.; Augustine, D. J.; Cooney, G.; Schwietzke, S.; George, F. C.; Lauderdale, T.; Skone, T. J. Characterizing Regional Methane Emissions from Natural Gas Liquid Unloading. *Environ. Sci. Technol.* **2019**, *53*, 4619–4629.
- (43) Alvarez, R. A.; Pacala, S. W.; Winebrake, J. J.; Chameides, W. L.; Hamburg, S. P. Greater focus needed on methane leakage from natural gas infrastructure. *Proc. Natl. Acad. Sci.* **2012**, *109*, 6435–6440.
- (44) Mansfield, M. L.; Lyman, S. N.; O'Neil, T.; Anderson, R.; Jones, C.; Tran, H.; Mathis, J.; Barickman, P.; Oswald, W.; LeBaron, B. Storage Tank Emissions Pilot Project (STEPP): Fugitive Organic Compound Emissions from Liquid Storage Tanks in the Uinta Basin. Vernal, Utah: Utah State University. 2017, available at <https://documents.deq.utah.gov/air-quality/planning/technical-analysis/DAQ-2017-009061.pdf> Accessed July 22nd, 2020.
- (45) Lyman, S. N.; Tran, T.; Mansfield, M. L.; Ravikumar, A. P. Aerial and ground-based optical gas imaging survey of Uinta Basin oil and gas wells. *Elementa* **2019**, *7*, 43.

Exhibit 42

Permian Methane Analysis Project

[Return to Home Page](#)



[View Operator Emissions](#)

[View Regional Emissions](#)

[Flaring Surveys](#)

[Submit a Response](#)

[Download Datasets](#)

Take a quick tour of this Operator Dashboard

[Project Methodology](#)

Explore the Map

EDF Study Area (measured to date)

Permian Basin

Filter by Measurement Area

- ☒ Show all areas
- ☐ Only show areas with one operator

Search by Survey Number

- ☐ 1 (Oct 2019 - May 2020)
- ☐ 2 (July 2020 - Sept 2020)
- ☐ 3 (Oct 2020 - Dec 2020)
- ☒ All surveys to date (aggregate view)

Search for Well API

Wells not searchable in all survey view

Search by Operator Ticker

Display all

Copyright © 2020 EDF

Select One or More Operators to Compare Emissions Data

ABRAXAS
PETROLEUM

ADMIRAL PERMIAN
RESOURCES

AMEREDEV LLC

APACHE
CORPORATION

ARCH OIL & GAS
LLC

ARMOR
PETROLEUM INC

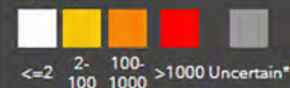
ATLANTIC
OPERATING II, LLC

BATTALION OIL
(HALCON
OPERATING CO
INC)

BETTIS BOYLE &
STOVALL

BLACKBEARD
OPERATING, LLC

Methane Emission Rate (kg/hr)



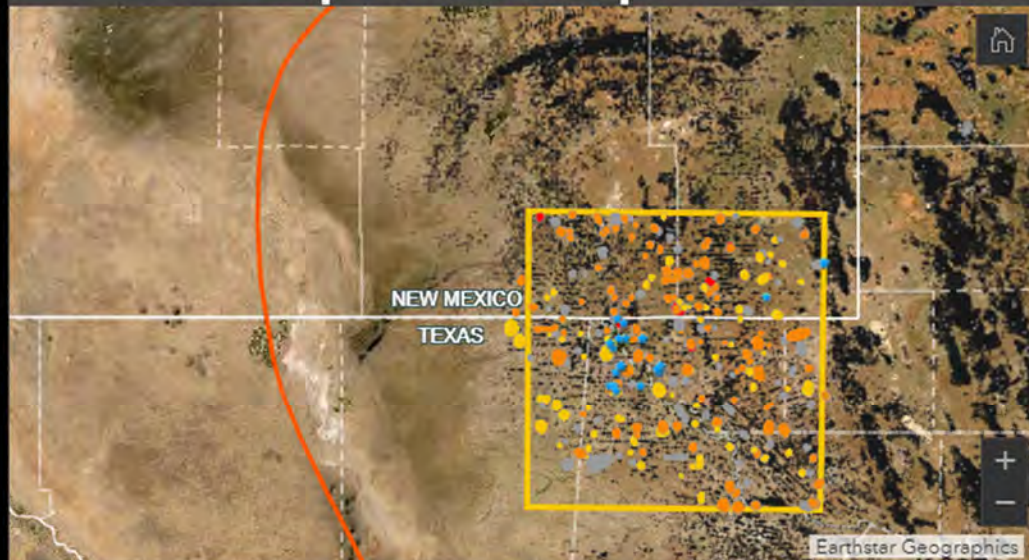
*Emissions are between zero and a variable detection limit. [Learn More](#)

Survey Type and Operator Responses

- ☐ Aerial Surveys
- ☐ Ground Surveys
- ☐ Surveys with Multiple Operators
- ☒ Operator Responses

Infrastructure

- ☐ Active Oil & Gas Wells
- ☐ Inactive/Plugged/Other Wells
- ☐ Processing Plants
- ☐ Tank Batteries



METHANE EMISSION EVENTS

Permian Methane Analysis Project

[Return to Home Page](#)



[View Operator Emissions](#)

[View Regional Emissions](#)

[Flaring Surveys](#)

[Submit a Response](#)

[Download Datasets](#)

Explore the Map

- ☒ EDF Study Area (measured to date)
- ☐ Permian Basin

Filter by Measurement Area

- ☒ Show all areas
- ☐ Only show areas with one operator

Search by Survey Number

- ☐ 1 (Oct 2019 - May 2020)
- ☐ 2 (July 2020 - Sept 2020)
- ☐ 3 (Oct 2020 - Dec 2020)
- ☒ All surveys to date (aggregate view)

Search for Well API

Wells not searchable in all survey view

Search by Operator Ticker

Display all

Copyright © 2020 EDF

Take a quick tour of this Operator Dashboard

[Project Methodology](#)

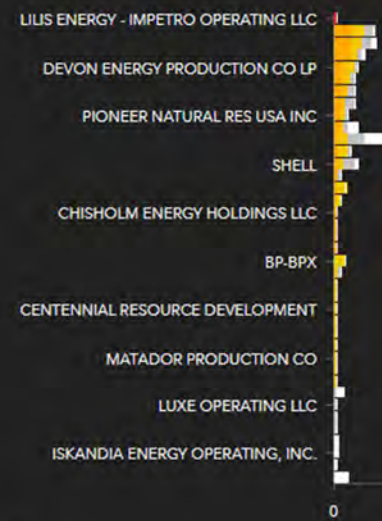
Select One or More Operators to Compare Emissions Data

ABRAXAS PETROLEUM
ADMIRAL PERMIAN RESOURCES
AMERDEV LLC
APACHE CORPORATION
ARCH OIL & GAS LLC
ARMOR PETROLEUM INC
ATLANTIC OPERATING II, LLC
BATTALION OIL (HALCON OPERATING CO INC)
BETTIS BOYLE & STOVALL
BLACKBEARD OPERATING, LLC
BP-BPX

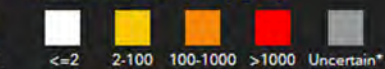
Methane Measurement Counts by Operator

These charts present the number of measurements taken for each operator, categorized by emission rate. The chart on the left shows those measurements that are attributable only to that operator. The chart on the right shows measurements attributable to that operator plus others (i.e. multiple operator measurement areas).

Single Operator Measurements

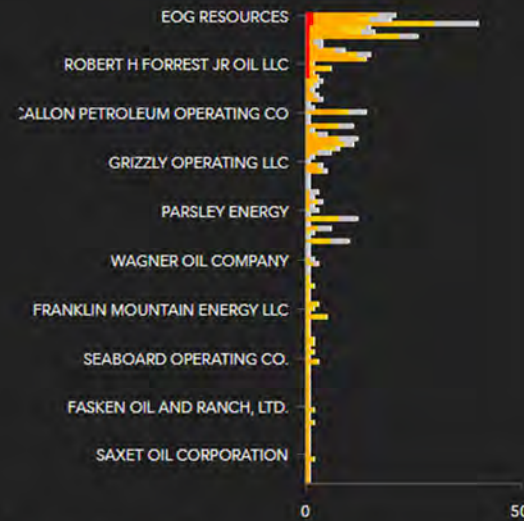


Methane Emission Rate (kg/hr)



*Aerial surveys cannot detect methane below ~40kg/hr [Learn More](#)

Multiple Operator Measurements



MEASUREMENT COUNTS BY OPERATOR

Permian Methane Analysis Project

[Return to Home Page](#)



[View Operator Emissions](#)

[View Regional Emissions](#)

[Flaring Surveys](#)

[Submit a Response](#)

[Download Datasets](#)

Explore the Map

- ☐ EDF Study Area (measured to date)
- ☐ Permian Basin

Filter by Measurement Area

- ☒ Show all areas
- ☐ Only show areas with one operator

Search by Survey Number

- ☐ 1 (Oct 2019 - May 2020)
- ☐ 2 (July 2020 - Sept 2020)
- ☐ 3 (Oct 2020 - Dec 2020)
- ☒ All surveys to date (aggregate view)

Search for Well API

Wells not searchable in all survey view

Search by Operator Ticker

Display all

Copyright © 2020 EDF

Take a quick tour of this Operator Dashboard

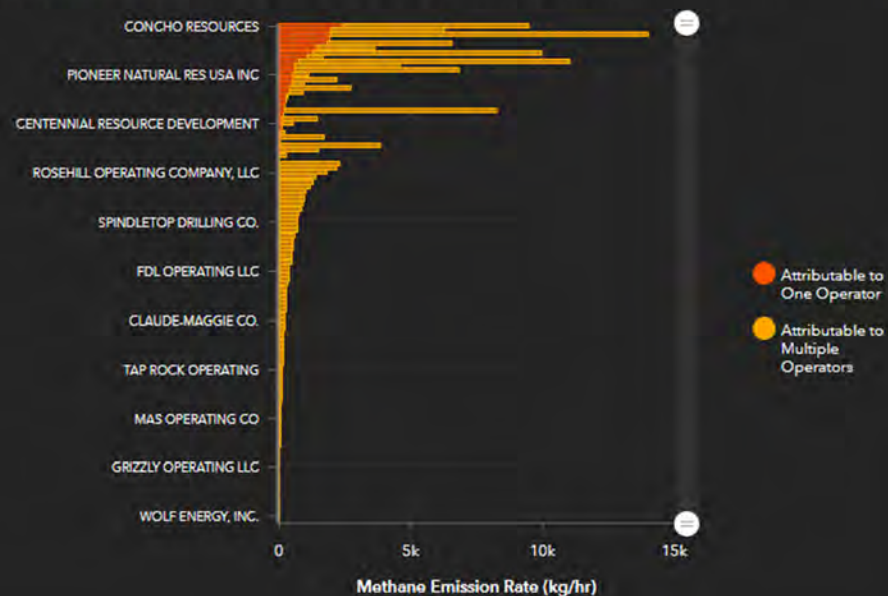
[Project Methodology](#)

Select One or More Operators to Compare Emissions Data

ABRAXAS PETROLEUM
ADMIRAL PERMIAN RESOURCES
AMERDEV LLC
APACHE CORPORATION
ARCH OIL & GAS LLC
ARMOR PETROLEUM INC
ATLANTIC OPERATING II, LLC
BATTALION OIL (HALCON OPERATING CO INC)
BETTIS BOYLE & STOVALL
BLACKBEARD OPERATING, LLC
BP-BPX

Methane Emission Rate by Operator

By default, all operators are sorted by emission rates attributable to one operator (highest sole operator emission rates at the top). Use the scroll bar (right) to navigate and see the individual operator names, or select a specific set of operators on the side-bar.



EMISSION RATES BY OPERATOR

Permian Methane Analysis Project

[Return to Home Page](#)



[View Operator Emissions](#)

[View Regional Emissions](#)

[Flaring Surveys](#)

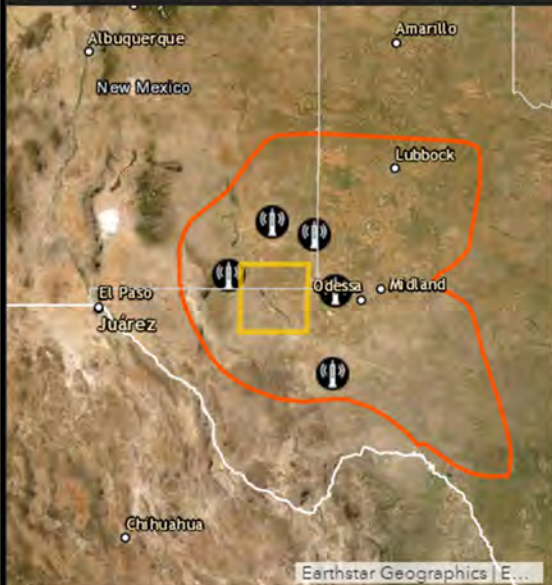
[Submit a Response](#)

[Download Datasets](#)

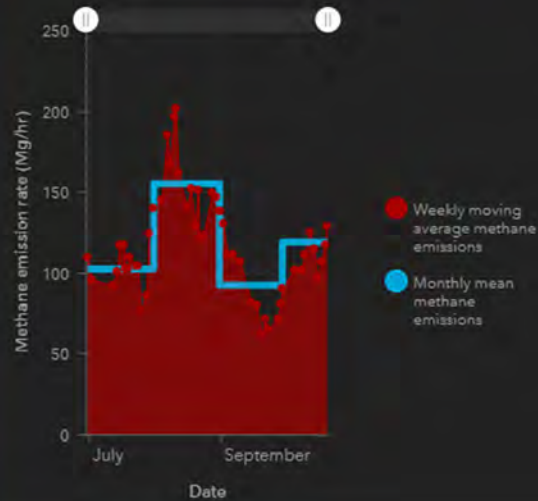
Regional Estimate of Permian Methane Emissions

About this view

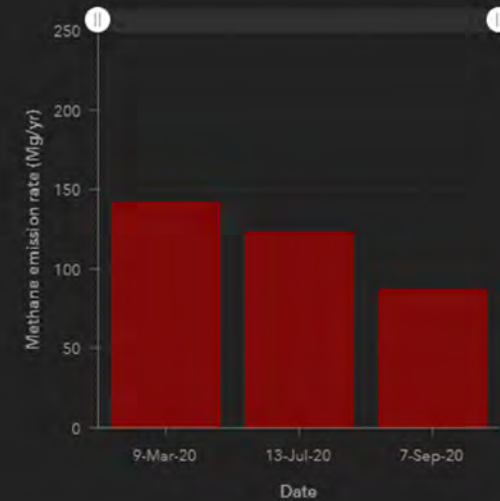
Regional emissions are measured in two ways: 1) From sensors installed on towers encircling the study area, monitored by Penn State researchers; 2) From regional mass balance flights operated by Scientific Aviation. Estimates are updated monthly. Read more about these [methods](#) and [download the data](#).



Tower-based estimates



Aircraft-based estimates



[CURRENT REGIONAL ESTIMATES](#)

[REGIONAL ESTIMATES AS OF MARCH 9th, 2020](#)

Permian Methane Analysis Project

[Return to Home Page](#)



[View Operator Emissions](#)

[View Regional Emissions](#)

[Flaring Surveys](#)

[Submit a Response](#)

[Download Datasets](#)

About this view

Helicopter surveys of the Delaware and Midland basins studied malfunctioning flares in 2020.

Four **random surveys** (in Feb., March, June, Nov.) consistently found roughly 5% of active flares to be unlit and venting methane to the atmosphere, while between 3-7% exhibited combustion issues.

A **supplementary systematic study** in June found about 25% of all active flares in a 400 km² area were unlit and venting methane.

In November, a **repeat study** surveyed 200 km² three times over a week to assess persistence. Approximately 60% of the malfunctioning flares were recorded to be operational at least one day during the course of the survey.

[Read more about our methodology.](#)

Select Flare Type

- ☒ All flares surveyed
- ☐ Combustion Issues
- ☐ Unlit and Venting
- ☐ Operational or Inactive

- Flares malfunctioning in 2 or more surveys
- Flares malfunctioning in 1 survey
- Operational or Inactive Flares
- Active Oil & Gas Wells
- EDF Flare Study Areas
- Permian Basin
- Systematic Study Area
- Repeat Study Area

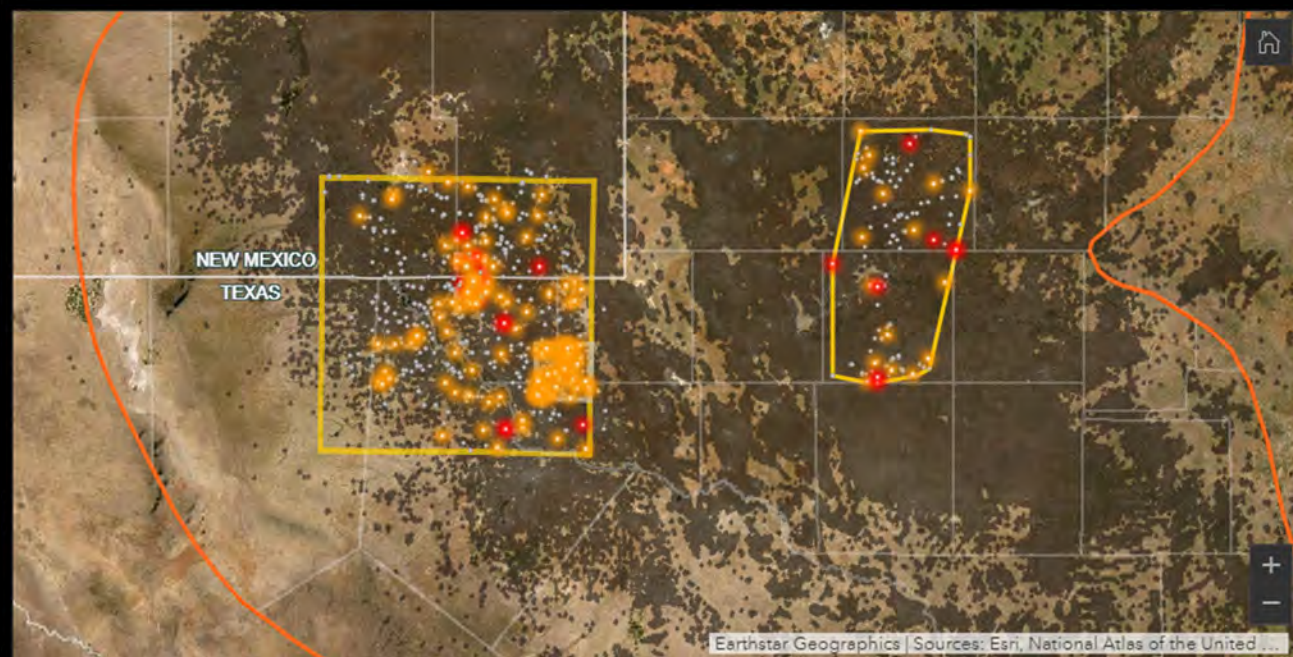


Exhibit 43

THOMAS MICHAEL ALEXANDER

1332 Landfall Drive
Wilmington, NC
(910)256-7814
(479)409-6495

EDUCATION

- * **University of Denver, Denver, Colorado**
Master of Arts, Environmental Policy and Management, completed all coursework, 1994
- * **South Dakota School of Mines and Technology, Rapid City, South Dakota**
Master of Science, Mining Engineering, 1981
Bachelor of Science, Mining Engineering, 1981
- * **Duke University, Durham, North Carolina**
Post-graduate work in chemistry and genetics, 1973
- * **Wake Forest University, Winston-Salem, North Carolina**
Bachelor of Arts, Psychology, 1973
Athletic Scholarship (golf), 1969-1973
- * **Oil & Gas Industry Courses**, including but not limited to reservoir, economics, production, drilling, safety, cementing, directional wells, hydraulic stimulation, conformance, facilities, pressure analysis.

RELEVANT WORK EXPERIENCE

Over 39 years of comprehensive technical, operational and HSE experience in the oil and gas industry; recognized as an industry expert in unconventional resource development.
Assisted in development of leading edge regulatory frameworks within Southwestern Energy, New Brunswick and North Carolina.
Exceptional understanding of varying social, economic, regulatory, and political interests.
Excellent experienced communicator with multiple levels of understanding.
Very comfortable with all forms of media, live and otherwise.
Demonstrated composure in the most difficult public relations situations.
Adept at building consensus amongst multiple stakeholders.

EMPLOYMENT HISTORY

- | | |
|---------------------|---|
| July 2016-present | Environmental Defense Fund – Technical/Regulatory Consultant
Assisting with several key projects involving underground natural gas storage, flaring/venting, conventional regulation reviews, underground gas storage in China, IOGCC regulatory project, Illinois and Oklahoma gas storage regulation comment, white paper covering HSE Management Systems, Risk Management, Emergency Response Planning, policy, process, procedure, corporate culture and water management. |
| Jan 2017-Mar 2018 | Independent Energy Standards Corporation - Consultant
Assisted in the development of rubrics to evaluate companies' HSE management systems, risk management programs, corporate culture, emergency response plans, upstream engineering and operations. Assisted as well in developing an HSE management system for IES itself. Helped evaluate IES clients in underground natural gas storage operations and upstream independent oil and gas operations in the mid-continent. |
| Oct. 2012-Apr. 2016 | Southwestern Energy Company – Vice President Health Safety & Environment
Managed staff of over 60 HSE professionals assisting full breadth of company operations. Worked closely with federal and state government and regulatory agencies to insure safe and responsible development of company's oil and natural gas assets. Led team efforts that reduced company and contractor injury rates by over |

50%. Managed all aspects of the cultural conversion to behavior based safety. Retired April 1, 2016.

- May 2010-Sep. 2012 **SWN Resources Canada – General Manager, New Brunswick, Canada**
Managed company's initial international exploration project covering 2.5 million acres. Worked closely with provincial government, regulators, First Nations, and the public on a daily basis. Delivered well over 100 presentations and consultations, including numerous media events (live television, radio, scrums, and print). Served on Board of Directors of the Canadian Society of Unconventional Resources. Served on Board of Atlantica Centre for Energy, and was Treasurer for newly-formed New Brunswick Oil and Natural Gas Association.
- Mar. 2007-Apr. 2010 **Southwestern Energy Company, Houston, Texas – Fayetteville Shale Completion Manager**
Managed a team of up to 75 professionals and was responsible for the completion of over 1200 horizontal wells. Annual completion budgets were in excess of \$500,000,000. Team coordinated activity with drilling, geology, geophysics, land, and production. Shared technical and operational expertise at numerous industry conferences. Served on initial committee that ultimately developed our Model Regulatory Framework.
- Apr. 2004-Feb. 2007 **Southwestern Energy Company – Team Lead Fayetteville Shale Project**
Promoted to Team Lead for Fayetteville Shale Project and managed multidisciplinary staff. Responsible for drilling, completion, and production of some 50 vertical and 90 horizontal wells during the initial phases of the project.
- Jan. 2001-Mar. 2004 **Southwestern Energy Company, Fayetteville, Arkansas – Staff and Senior Staff Production Engineer**
Reviewed well performance of over 200 wells. Prepared commingling of 90 to 100 wells and identified 40-50 candidates for artificial lift. Directed the field work to accomplish these installations and comminglings. Identified over 30 stimulation candidates, designed the refracs and supervised their execution. Responsible for the completion design and execution of over 20 new wells each year.
- Dec. 1997-Nov. 2000 **New Prospect Company, Fort Smith, Arkansas – Production/Reservoir Engineer**
Responsible for all production and reservoir aspects of over 200 wells, Consulted to Southwestern Energy 12/1998 – 12/2000 regarding production, operations, and artificial lift.
- Nov. 1996-Nov. 1997 **Oil and Gas Consulting Engineer, Fort Smith, Arkansas**
- June 1994-Nov. 1996 **Revere Corporation, Fort Smith, Arkansas – Operations/Engineering Manager**
Designed and executed all drilling, completion, and production, including artificial lift, recompletions, workovers, and safety and environmental concerns. Supervised and trained field and office personnel, provided expert testimony at state and local levels.
- Sep. 1989-Jun. 1994 **Habersham Energy Company, Englewood, Colorado – Vice President Operations**
Managed all phases of an independent operating oil and gas company. Supervised 8 employees, served on board of directors, executed the annual budget.
- Jul. 1998-Sept. 1989 **Southwest Operating, Incorporated, Tyler, Texas – President**
Acquired and invested in producing oil and gas properties.
- Aug.1984-Jul. 1988 **Altair Energy Corporation, Tyler, Texas – Senior Vice President Operations**
Involved in all phases of drilling, production, property acquisition and divestiture.
- Aug. 1981-Aug. 1984 **Schlumberger Offshore Services, Houston, Texas – Field and Sales Engineer**

Involved

Performed petrophysical logging services for offshore oil and gas companies.

personnel supervision, equipment logistics, nuclear sources and explosives control, log interpretation, electronic equipment maintenance, calibration, trouble-shooting and repairs. Sold logging products, petrophysical evaluations, and new technologies.

Mar. 1975-Jun. 1981

United States Air Force – B-52H Navigator and Radar Navigator

SAC B-52H crew member. Consistently rated top in class and operations in all phases of performance and training. Honorably discharged with the rank of Captain.